CONSEJO SUPERIOR DE INVESTIGACIONES CIENTÍFICAS
INSTITUTO DE CIENCIA DE MATERIALES DE MADRID
Departamento de Materiales para las Tecnologías de la Información

Doctoral Thesis

PIEZOELECTRIC MULTILAYER COMPOSITE THIN FILMS BASED ON $Pb(Mg_{1/3}Nb_{2/3})O_3$–$PbTiO_3$: PREPARATION AND CHARACTERIZATION

Author

Haitham El Hosiny Ali Mohammed

Supervisors:

Dr. Ricardo Jiménez Rioboó

Dr. Jesús Ricote Santamaría

UNIVERSIDAD AUTÓNOMA DE MADRID
Departamento de Física Aplicada

Madrid 2013

CONSEJO SUPERIOR DE INVESTIGACIONES CIENTÍFICAS
INSTITUTO DE CIENCIA DE MATERIALES DE MADRID
Departamento de Materiales para las Tecnologías de la Información

Doctoral Thesis

PIEZOELECTRIC MULTILAYER COMPOSITE THIN FILMS BASED ON $Pb(Mg_{1/3}Nb_{2/3})O_3$–$PbTiO_3$: PREPARATION AND CHARACTERIZATION

Author

HAITHAM EL HOSINY ALI MOHAMMED

Supervisors:

Dr. Ricardo Jiménez Rioboó

Dr. Jesús Ricote Santamaría

UNIVERSIDAD AUTÓNOMA DE MADRID
Departamento de Física Aplicada

Madrid, 2013

To my parents,
my daughter, and my wife
(Yasmin & Yasmin)

I would like to acknowledge the support of the Spanish Ministry of Science and Innovation (now Ministry of Economy and Competitiveness) for the FPI PhD grant (Reference BES-2008-010132). The work carried out in this thesis has been funded by the Spanish Project MAT2010-15365.

First of all I would like to thank my supervisors Dr. Ricardo Jiménez Rioboó and Dr. Jesús Ricote Santamaría for continual and valuable guidance during this work and for encouragements, support, help and supervision of my thesis. I have learned a lot from every discussion with them.

I would like to thank my tutor (Faculty of science-UAM university) Dr. Manuel Cervera Goy for interesting and helpful suggestions.

Deep thanks to Dra. Maria Lourdes Calzada for her continuous encouragement, suggestions and guidance to the preparation of thin films.

I would like to thank also Dra. Lorena Pardo and Dr. Miguel Algueró for their good words with me, for his sincere interest in the progress of my work.

I would like to thank Dr. J. Pérez de la Cruz and Dr. J. R. A. Fernandes of the Instituto de Engenharia de Sistemas e Computadores do Porto (INESC TEC) of Portugal for the measurement of the piezoelectric coefficients of the films by interferometry.

Deep thanks to my colleagues Dr. Iñigo Bretos and Dr. Harvey Amorín for their help and continuous encouragement, and for the many useful discussions, from which I learnt a lot. Also, thanks to Álvaro and Dulce.

I would like to thank, most sincerely, all the people in ICMM-CSIC and especially in the department of Materials for Information Technologies.

Many thanks to my parents (Ali and Sbah) for their love and support.

My wife Yasmin, my true love, thanks for all your support, encouragement and pearing me away from you during four years. Really, you helped me a lot and words are not enough to express how thankful I am.

I would like to thank my colleagues Mohammed Moaid, Hitham Elashry, Dr. Fouad and Dr. Ihab for the friendship they have shown me during these four years.

RESUMEN

Las composiciones ferroeléctricas (1-x)$Pb(Mg_{1/3}Nb_{2/3})O_3$ - $xPbTiO_3$ (PMNT), cercanas a la frontera de fase morfotrópica (MPB del inglés Morphotropic Phase Boundary) en x=0.35, tienen coeficientes piezoeléctricos excelentes en monocristales y cerámicas masivas. La progresiva miniaturización de los dispositivos impulsa la preparación de PMNT en forma de lámina delgada para su integración en dispositivos microelectrónicos. Sin embargo, se ha reportado que las propiedades remanentes en lamina delgada de PMNT quedan reducidas comparadas con las de los materials masivos, lo que se ha atribuido a efectos del tamaño de grano. En cualquier caso, en los ciclos de histéresis ferroeléctricos los valores de la polarización de saturación permanecen próximos a los de las cerámicas masivas, lo que implica que el problema reside en la disminución de los valores de la polarización remanente en las láminas delgadas.

En esta tesis doctoral se siguen los principios tradicionalmente usados en composites en volumen. La combinación de capas con composiciones ferroeléctricas diferentes en una configuración de composite multicapa (MLC, del inglés multilayer composite) se ha probado que mejora con éxito las propiedades dieléctricas y ferroeléctricas (remanentes), comparadas con las de las capas individuales. Basado en en esta idea, esta tesis explora la preparación y caracterización de laminas delgadas composite multicapa basados en $Pb(Mg_{1/3}Nb_{2/3})O_3$–$PbTiO_3$, con el objetivo de encontrar una solución a las limitaciones encontradas con los coeficientes piezoeléctricos remanentes en láminas delgadas.

El método de depósito de disoluciones (CSD, del inglés Chemical Solution Deposition) se utiliza en esta tesis doctoral para la fabricación de láminas sobre substratos basados en el silicio con electrodos de platino. Los diagramas de difracción de rayos X y el estudio de la evolución de la permitividad dieléctrica con la temperatura de las laminas MLC indica que no hay interdifusión significativa entre las capas de PT y PMNT, lo que confirma que CSD es un método excelente para la preparación de estas láminas composite multicapa.

La hipótesis es que la piezoelectricidad remanente se puede mejorar si la polarización en las capas de PMNT se mantiene gracias a un campo eléctrico interno producido a partir de las capas polarizadas de $PbTiO_3$ (PT) de las láminas MLC, con

una configuración de conectividad 2-2. El ferroeléctrico PT tiene valores de polarización remanente grandes.

En esta tesis estudiamos primero laminas delgadas composite multicapa con capas alternadas muy delgadas para las que la aplicación de un campo electric debería ser altamente efectivo, debido tanto al bajo espesor de las capas, como de la interacción mejorada entre las mismas, al tener más área de intercara que para multicapas similares de sólo unas pocas capas. Sin embargo, el reducido tamaño de grano de estas capas tan delgadas hace que estas laminas MLC no presenten la mejora esperada de las propiedades: Las polarizaciones remanente y de saturación de las láminas MLC con múltiples capas son 8 $\mu C \cdot cm^{-2}$ and $15 \mu C \cdot cm^{-2}$, respectivamente, lo que no puede considerarse un gran logro.

Para evitar este efecto dañino del tamaño de grano y para conseguir establecer claramente las ventajas del acoplamiento de las fases PT y PMNT en las láminas MLC, dos configuraciones distintas de las láminas MLC con capas de mayor espesor se han preparado. La lamina MLC es la más eficiente cuando todos las capas de PMNT se encuentran entre dos capas de PT. Esto da lugar a una mejora considerable de la polarización remanente con respecto a las láminas monofásicas de PMNT. Las polarizaciones remanente y de saturación de las laminas MLC-PT son ahora mayores, 10 $\mu C \cdot cm^{-2}$ and 22 $\mu C \cdot cm^{-2}$, respectivamente. Sin embargo, debido al alto porcentaje de porosidad y a las consiguientes corrientes eléctricas de fuga, no es posible aplicar campos eléctricos suficientemente elevados, lo que es un obstáculo para poder beneficiarse de manera completa de las propiedades piezoeléctricas de estas láminas.

A consecuencia de esto, la segunda parte de esta tesis se centra en la mejora de la calidad de las láminas MLC. Capas optimizadas de PT con polarización remanente grande y estable son preparadas a temperaturas de cristalización por debajo o cercanas a la de la transición para-ferroeléctrica. Las capas de PMNT film se pueden preparar con poca porosidad eligiendo la solución precursora adecuada, en este caso diluida en etanol. La reducción de la porosidad da lugar a un incremento de la polarización de saturación de estas capas. La combinación de estas capas optimizadas en las laminas composite multicapa da lugar a una mejora significativa de sus propiedades, alcanzando valores de la polarización remanente y de saturación de 27 and 36 $\mu C \cdot cm^{-2}$, respectivamente. Lo que es más importante, esto corresponde a un coeficiente piezoeléctrico remanente $d_{33}^{eff} = 67\ pm \cdot V^{-1}$.

En resumen, para beneficiarse de la excelentes propiedades piezoeléctricas de $0.65Pb(Mg_{1/3}Nb_{2/3})O_3$-$0.35PbTiO_3$ en forma de lamina delgada policristalina e integrarla en microdispositivos, es necesario preparer composites multicapa con configuraciones bifásicas 2-2, con capas ferroeléctricas de alta polarización remanente, para generar un campo eléctrico interno en el interior de las capas de PMNT y, por tanto, inducir polarización en ellas, lo que da lugar a coeficientes piezoeléctricos grandes.

ABSTRACT

The ferroelectric composition (1-x)Pb($Mg_{1/3}Nb_{2/3}$)O_3-x$PbTiO_3$ (PMNT), close to the morphotropic phase boundary (MPB) at x=0.35, has excellent piezoelectric coefficients in single-crystals and bulk ceramics. The progressive miniaturization of the devices leads to the preparation of PMNT in thin film form for their integration in microelectronic devices. However, in thin film form, it has been reported that the remnant properties of PMNT are reduced as compared to those of the corresponding bulk materials, which has been attributed to grain size effects. Nevertheless, in the ferroelectric loops the polarization saturation values remain close to those obtained in bulk ceramics, which implies that the problem relies on the decrease of the remnant polarization values in the thin films.

In this doctoral thesis the principles traditionally used in bulk composites are followed. The combination of layers with different ferroelectric compositions in a multilayer composite (MLC) configuration has proved to be successful to improve the dielectric and ferroelectric (remnant) properties when compared to those of the individual layers. Based on this idea, this thesis explores the preparation and characterization of piezoelectric multilayer composite films based on Pb($Mg_{1/3}Nb_{2/3}$)O_3–$PbTiO_3$, with the objective of finding a solution to the limitations found in thin film form with the remnant piezoelectric coefficients.

The chemical solution deposition (CSD) method was used in this PhD thesis for the fabrication of the films on platinised silicon-based substrates. The XRD patterns and the study of the evolution of the dielectric permittivity with the temperature of the MLC films indicate that there is no significant interdiffusion between the alternating PT and PMNT layers, which confirms that CSD is an excellent method to prepare these multilayer composite films.

The hypothesis is that the remnant piezoelectric can be improve if the polarization on the PMNT layers is kept by an internal electric field produced from the neighbouring poled $PbTiO_3$ (PT) in MLC films with 2-2 connectivity configuration. The normal ferroelectric PT has large remnant polarization values.

In this thesis we firstly study multilayer composite films with very thin alternating layers for which the application of an electric field should be highly effective, both due to the small thickness of the layers, and to the enhanced interaction

among the layers, with more interface area than for similar multilayers composed of few thick layers. However, the reduced grain size in these very thin layers makes that these MLC films do not show the expected improvement of the properties: The remnant and saturation polarizations of MLC films with multiple layers are 8μC·cm^{-2} and 15μC·cm^{-2}, respectively, which cannot be considered a large achievement.

In order to avoid this harmful grain size effect and to be able to establish clearly the advantages of the coupling of the PT and PMNT phases in the MLC films, two different configurations of MLC films with thicker layers have been prepared. The MLC film is most effective, when every PMNT layer is sandwiched between two PT layers. This produces a considerable enhancement of the remnant polarization with respect to the single phase PMNT films. The remnant and saturation polarizations of MLC-PT films are now higher, 10 μC·cm^{-2} and 22 μC·cm^{-2}, respectively. However, due to the large porosity and the resulting leakage currents, it is not possible to apply large enough electric fields, which is a handicap for taking full advantage of the piezoelectric properties of these films.

Therefore, the second part of this thesis is focused on the improvement of the quality of the MLC films. Optimized PT layers with large and stable remnant polarization are obtained at crystallization temperatures close or below that of the para-ferroelectric transition. The PMNT film can be prepared with a low amount of porosity choosing the right precursor solution, in this case one diluted with ethanol. The reduction of the porosity produces an enhancement of the saturation polarization in these layers. The combination of these optimized layers in the multilayer composite films results in a significant improvement of their properties reaching remnant and saturation polarization values of 27 and 36 μC·cm^{-2}, respectively. More importantly, this corresponds to a remnant piezoelectric coefficient of d_{33}^{eff} = 67 pm·V^{-1}.

Therefore, to take full advantage of the excellent piezoelectric properties of $0.65Pb(Mg_{1/3}Nb_{2/3})O_3$-$0.35PbTiO_3$ in polycrystalline thin film form and integrate it in microdevices, it is necessary to prepare multilayers in 2-2 biphasic composite configurations that use ferroelectric layers with large remnant polarization, to generate an internal electric bias within the PMNT layers and, thus, induce polarization in them, resulting in a large piezoelectric coefficients.

TABLE OF CONTENTS

PART2: PREPARATION OF HIGH QUALITY $Pb(Mg_{1/3}Nb_{2/3})O_3$ –$PbTiO_3$ LAYERS

PART3: OPTIMIZATION OF THE LAYER COMBINATION FOR A $Pb(Mg_{1/3}Nb_{2/3})O_3$ –$PbTiO_3$ –BASED MULTILAYER COMPOSITE FILM

LIST OF FIGURES

CHAPTER I. INTRODUCTION

CHAPTER II. EXPERIMENTAL PROCEDURE

LIST OF TABLES

CHAPTER I

INTRODUCTION

1.1 Piezoelectric and ferroelectric materials

The phenomenon of piezoelectricity was discovered by Jacques and Pierre Curie in 1980. When a mechanical stress is applied, an electric charge is generated (direct piezoelectric effect). Conversely, when an electric field is applied a deformation is produced (converse piezoelectric effect). This effect has traditionally attracted much attention for the development of applications, and piezoelectric single crystals and bulk ceramics are nowadays widely used.

The coefficient that describes the piezoelectric effect is obtained from the following equations:

$$D_i = d_{im} \cdot \sigma_m + K_{ij}^{\sigma} \cdot E_j \quad (1)$$

$$S_m = s_{mn}^{E} \cdot \sigma_n + d_{mi} \cdot E_i \quad (2)$$

where i, j = 1, 2, 3 and m, n = 1-6 [1]; D_i is the dielectric displacement vector; S_m is the strain tensor in reduced notation; E_i the electric field vector; σ_n is the stress tensor in reduced notation; K_{ij}^{σ} is the dielectric permittivity coefficient under constant stress; s_{mn}^{E} is the elastic compliance under constant electric field; and d_{im} is the piezoelectric charge coefficient.

Piezoelectricity appears only in non-centrosymmetric crystals. Only some of them have spontaneous polarizations (pyroelectrics) and, among them, in a group called ferroelectrics, this polarization can be reversed by the application of an electric field. Due to this characteristic, ferroelectrics are widely used. Several subcategories can be identified in the ferroelectric oxides based on its unit cell structure [2]: oxygen octahedral (simple perovskites), layer structure (layered perovskites), tungsten bronze and pyrochlore (Figure 1.1). The good properties of the single perovskites (ABO_3) has made its used widespread in piezoelectric applications. In this PhD thesis we will focus on the study of films made of two ferroelectric perovskites: the lead titanate ($PbTiO_3$) and the solid solution $(1- x)Pb(Mg_{1/3}Nb_{2/3})O_3$-$xPbTiO_3$.

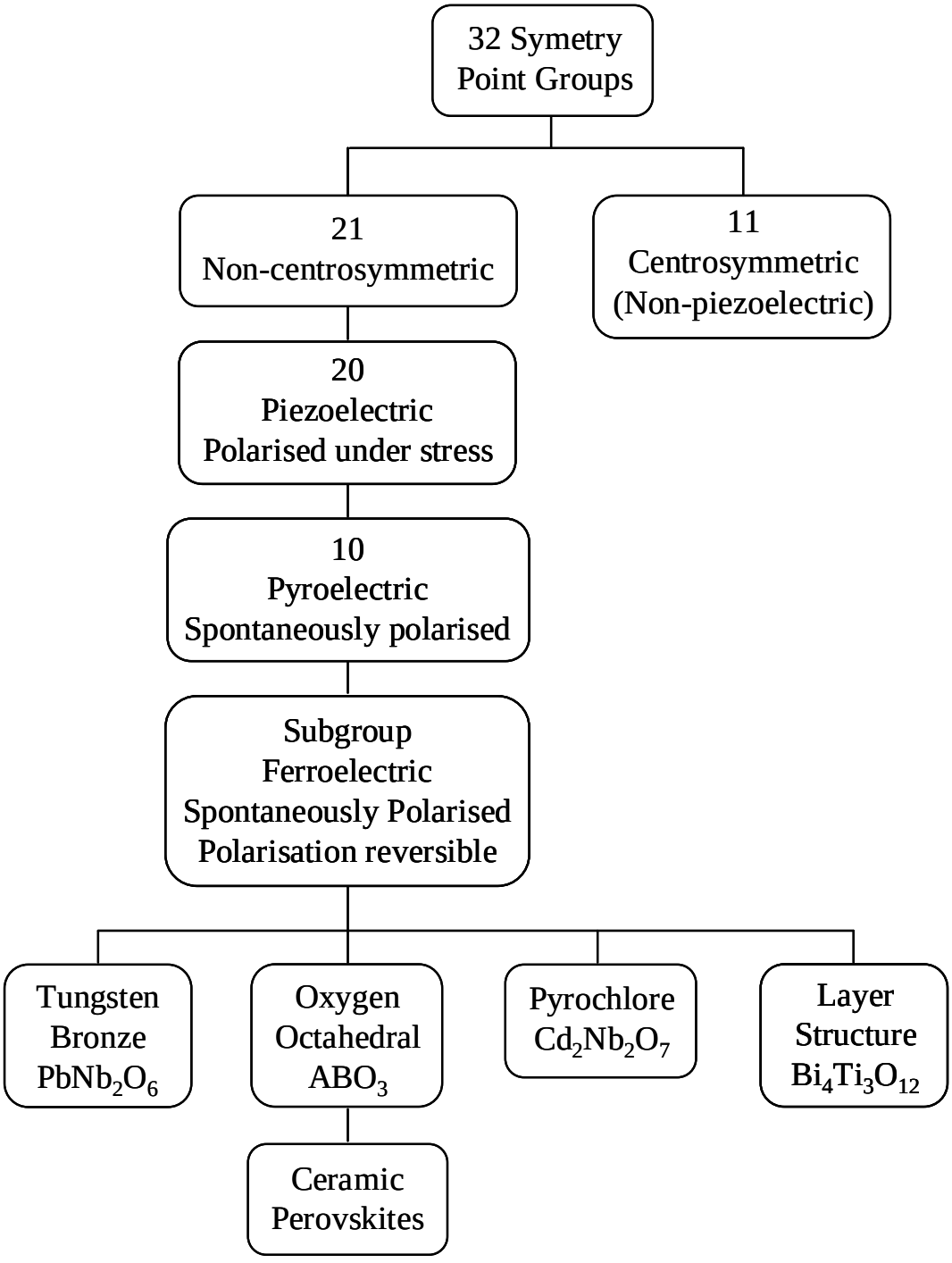

Figure 1.1. *Interrelationship of piezoelectric and subgroups on the basis of symmetry [2]*

Ferroelectrics can be defined therefore as crystallographically non-centrosymmetric dielectrics, whose spontaneous polarization can be reversed by the application of an external electric field. Typically they present a paraelectric state at high temperatures. The phase transition from this non-polar phase to the ferroelectric state takes place at the so-called Curie temperature T_C, and it is accompanied by the appearance of a dielectric anomaly (Figure 1.2).

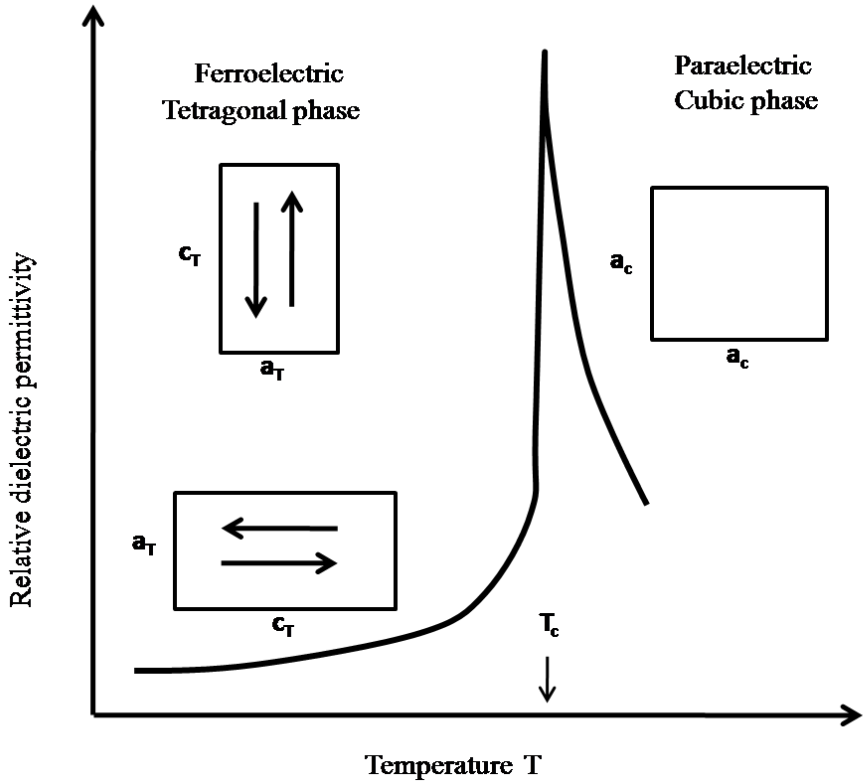

Figure 1.2. *Illustration of the typical evolution of the relative dielectric permittivity K´ of a ferroelectric material, which transforms from a paraelectric cubic phase into a ferroelectric tetragonal phase in lowering the temperature*

In order to minimise the electric and elastic energies within the crystal, ferroelectrics are structured into regions where all the electric dipoles are aligned in the same direction, called ferroelectric domains. These domains are separated by boundaries where the polarisation direction changes abruptly, known as domain walls. Domain can be classified into two categories: inversion or 180º domains and ferroelectric-ferroelastic domains. In the inversion domains the polarization in neighbouring grains is inverted, i.e., there is a rotation of 180º of the polarization across the domain wall. This

type of configuration does not cause any strain in the crystal and the domain walls do not correspond to specific crystallographic planes in the crystal, so they usually have a wavy appearance. In the ferroelectric-ferroelastic domains the polarization changes the direction from one domain to the next, producing a relaxation of the elastic energy. The domain walls in this case must correspond to twinning planes of the crystals. All this is schematically shown in Figure 1.3 for a tetragonal crystal, where the ferroelectric-ferroelastic domains correspond to 90º rotations of the polarization. The 180º domain configuration reduces the surface charge and minimise the electrostatic energy, whereas the ferroelectric-ferroelastic domains minimise the mechanical strain, and, therefore, the elastic energy of the crystal.

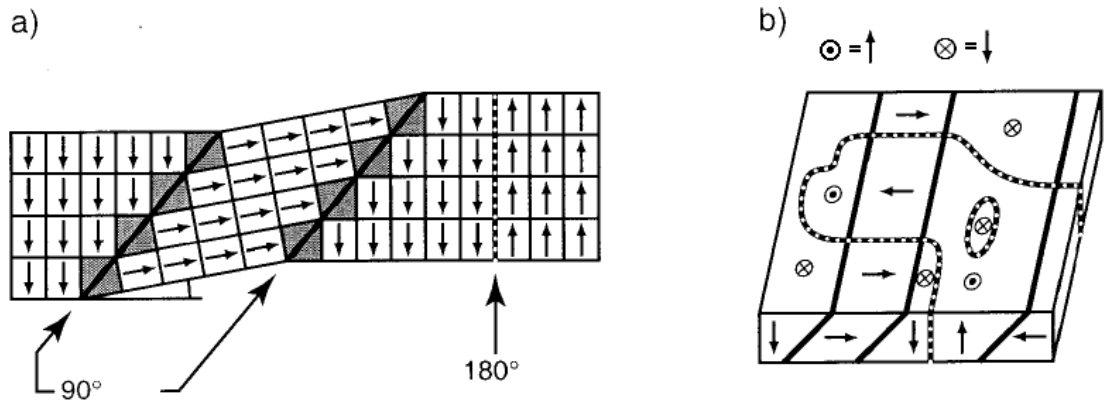

Figure 1.3. *Schematic configuration of ferroelectric domains in a tetragonal crystal: a) Detail of the domain wall with respect to the unit cells. b) Possible distribution of ferroelectric domain in a crystal [3]*

The main feature of a ferroelectric is that the sign of its spontaneous polarisation can be reversed (switched) by applying a large enough electric field giving rise to a polarization vs. electric field hysteresis loop as the one shown in Figure 1.4. The representative parameters that define the ferroelectric loop are; the remnant polarisation, P_r, the saturation polarisation, P_s, and the coercive field, E_c.

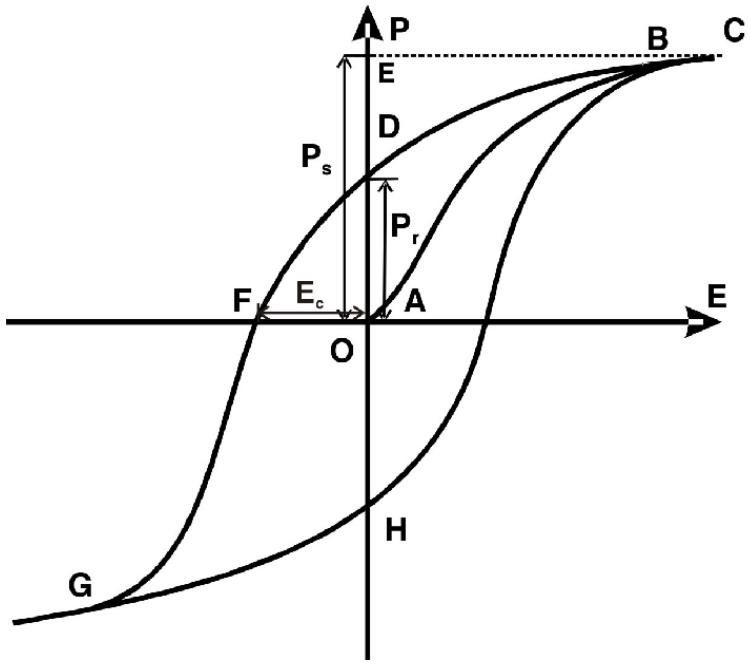

***Figure 1.4**. Ferroelectric hysteresis loop, reproduced from [4]*

The application of a low electric field generates a linear relationship between P and E, since the field is not large enough to switch any domains and the material behaves as a normal dielectric material. This behaviour corresponds to the segment OA of the P-E hysteresis loop in Fig. 1.4. As the electric field strength increases, a number of the domains with opposite polarisation direction start switching towards the field direction, producing a rapid increase in polarisation (segment AB). When all the possible domains are aligned with the electric field direction, a saturation state is reached (BC). As the field strength decreases, the polarisation will decrease (BD) but does not go back to zero. When the field is reduced to zero, some of the domains will remain aligned and the material will exhibit a remnant polarisation (P_r). The extrapolation of the linear segment BC of the hysteresis loop back to the polarisation axis (CBE) represents the value of the saturation polarisation (P_s). The remnant polarisation in a ferroelectric material cannot be removed until the applied electric field in the opposite direction reaches a certain value (at point F in Fig. 1.4). Thus, the strength of the field required to reduce the polarisation back to zero is called the coercive field strength (E_c). Further increase of the field in the negative direction will cause an alignment of the dipoles in this direction and the cycle can be completed by reversing the field direction once again.

In polycrystalline ferroelectric materials, the crystallographic directions associated to the spontaneous polarization are typically randomly oriented. This means that, prior to the application of any electric field; the net polarisation of the material is zero (see Figure 1.5). After the application of an intense electric field, in what is called poling process, a net polarisation different to zero has been induced through the mechanism of domain motion and the material exhibits ferroelectric response. This means that the poled ceramic present texture symmetry that is equivalent to noncentro symmetry and so all the physical properties will follow this symmetry.

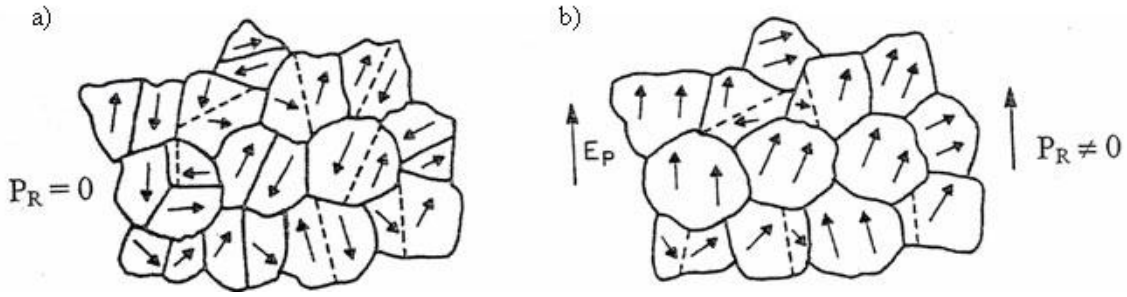

Figure 1.5. *Domain structure in a ferroelectric ceramic (a) before and (b) after the poling processs*

1.1.1. From ferroelectric bulk ceramics to thin films

By far, the largest number of applications using ferroelectric materials has been carried out in bulk ceramic form: monolithic multilayer capacitors (MLC), piezo-motors (buzzers, loud speakers, actuators), piezo-generators (accelerometers, power supplies, sensors), pressure-sensors (sonars, medical utrasounds) and resonant devices (utrasonic cleaners, surface acoustic wave filters) [5].

However, the evolution of the electronics industry towards the miniaturisation of the electronic components (Figure 1.6) led to the use of the ferroelectric oxides in thin film form to be integrated into microelectronic devices such as Micro-Electromechanical Systems – MEMS, pyroelectric microsensors and computer memories. Ferroelectric thin film devices perform the same electronic functions with only a fraction of the volume of devices based on bulk ceramics or single crystals

elements. Furthermore, films are processed at temperatures of several hundred of degree Celsius lower than those used for sintering bulk ceramics, which can be a deciding factor in their applicability. But, the quality of the film, small grain size, the substrate-film interface or the residual stresses present in thin films are responsible of the reduction of the ferroelectric properties in films [6].

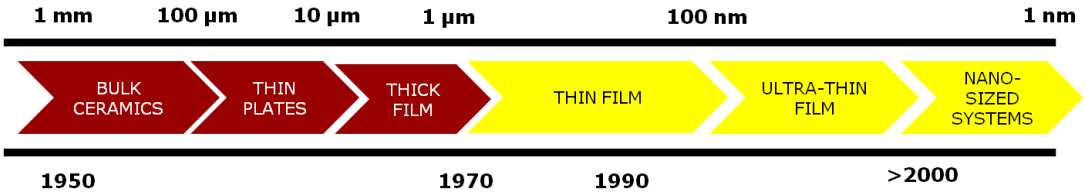

Figure 1.6. *Towards the miniaturisation of ferroelectric materials and their integration into microelectronic devices [7]*

One of the most important differences between piezoelectric films and bulk materials is the clamping of the films by the substrate, which results in a reduction of the macroscopically measured d_{33} [8,9]. The effective value of this coefficient in a film, according to the thermodynamic equation, is obtained from the following equation:

$$d_{33}^{eff} = 2K'_{33} \cdot \varepsilon_o \cdot Q_{12} \cdot P_3 \qquad (3)$$

where d_{33}^{eff} is the piezoelectric charge coefficient, K'_{33} the relative dielectric permittivity, ε_o the dielectric permittivity of vacuum, Q_{12} the electrostrictive coefficient and P_3 the polarization.

A great deal of applications have been collected under the name of MicroElectroMechanical Systems (MEMS), with typical dimensions of 1-100 microns. Some of them contain piezoelectric thin films as transducer elements, which offer a number of advantages in MEMS, due to the large motions that can be generated (typically with low hysteresis), the high energy densities available, and the low power requirements [10]. An example of integration of a ferroelectric film in MEMS is found in active microcantilevers [11] (Figure 1.7).

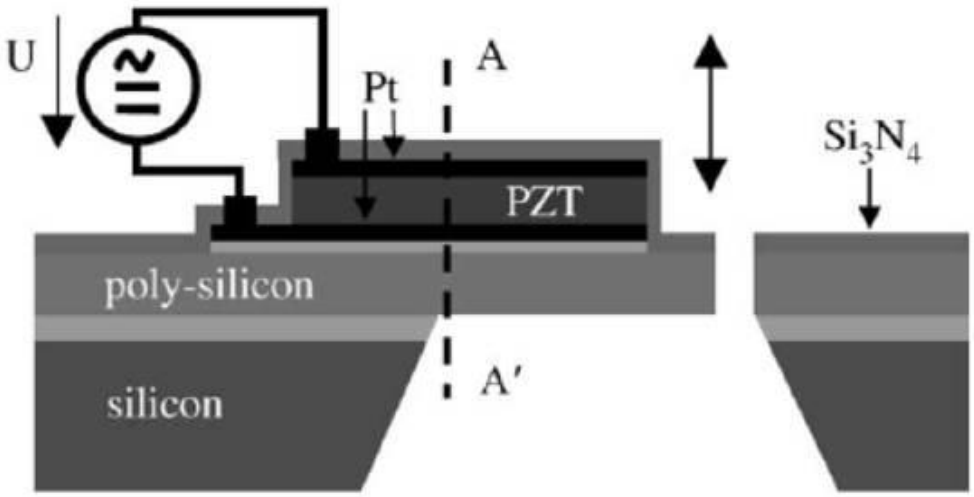

Figure 1.7. *Active microcantilever with an actuator consisting of a ferroelectric film (Pb, Zr) TiO_3 (PZT) [11]*

1.1.2. Optimized preparation methods for the preparation of ferroelectric thin films

The interest in the preparation of ferroelectric thin films began in the 60s when films of $BaTiO_3$ were prepared by hydrothermal and electrochemical methods [12]. Since then, different deposition techniques have been used for the fabrication of thin films.

Techniques used for the deposition of films can be grouped into physical and chemical methods. The former include sputtering or laser ablation as the most relevant. Chemical methods mainly include Chemical Vapour Deposition (CVD) and Chemical Solution Deposition (CSD). Table 1.1 shows the comparison of the main features of these techniques [13]. The chemical solution deposition method is included among the most convenient way to prepare films for piezoelectric applications because it offers advantages over other deposition techniques that are imperative for integration in real microelectronic devices [14], mainly its low cost, the possibility of deposition of large areas, the uniformity of the films and the high stoichiometry control, which is very important for the preparation of films of complex oxides.

Table 1.1 *Comparison of main features of common methods of ferroelectric thin film preparation*

Method	Deposition rate (Å/min)	Temperature (°C)	Stoichiometry (1-10)	Devices	Cost	Miscellaneous problems
RF sputtering	5-50	500-700	3	1-6	High	Negative ions
Magnetron sputtering	50-300	500-700	5	1-6	High	Target surface
Ion beam sputtering	20-100	500-700	8	1-6	High	Uniformity
Evaporation	100-1000	500-700	4	1-6	High	Rate control
Laser ablation	50-1000	500-700	6	1,3,5	High	Uniformity
MOCVD	50-1000	600	7	1-5	High	High substrate temperature
CSD MOD	3000 (Å/coating)	500-800	9	1,3,5	Low	High annealing temperature
Sol-gel	1000 (Å/coating)	450-750	9	1-5	Low	Multiple coating

Numerical scale for stoichiometry: 1-worst, 10-best

"Devices" number: 1-Capacitor, 2-Memory cell, 3-Actuator, 4-Electro-optic, 5-Pyroelector, 6-Surface Acoustic Wave (SAW)

Chemical solution deposition

First attempts on solution preparation of oxide-based ferroelectric thin films were carried out in 1976 by Fukushima et al. [15], reporting on the processing of $BaTiO_3$ thin films. Subsequent publications [16-18] on the preparation of $PbTiO_3$, $PbZrO_3$ and complex $Pb(Zr,Ti)O_3$ and $(Pb,La)(Zr,Ti)O_3$ perovskite thin films, show the development of Chemical Solution Deposition (CSD) methods for electronic multi-oxide thin film preparation to the early mid-80s. Since that date, the number of publications on CSD processing of ferroelectric thin films has grown exponentially. As it has been said before, the main advantages of CSD methods are the high compositional control (stoichiometry) and homogeneity of the deposits, the large surface areas deposited and the low cost associated with the materials and experimental setup.

In general, the typical CSD process involves the initial synthesis of a stable, homogeneous precursor solution that contains the multi-metal precursors dissolved in appropriate solvents with the desired molar ratio. Then, this solution is deposited onto the substrate by different coating techniques obtaining the as-deposited film, which is then dried, pyrolysed and crystallised by a thermal treatment. Thicker films can be obtained by successive deposition, drying and annealing of single coatings or layers.

The different and numerous chemical solution strategies used in the fabrication of electronic oxide films can be grouped into three main categories; Metalloorganic Decomposition (MOD), classical sol-gel processes and hybrid routes. They basically differ on the procedure followed to obtain the precursor solution and the reactions that occur during thermal annealing of the film [14].

In all the cases, the fabrication of thin films from chemical solutions (CSD) involves different steps that are detailed below. A schematic representation of these steps, for perovskite titanate solution precursors, is illustrated in Figure 1.8, according to Schwartz et al. [14]. A brief description of the main physicochemical features involved in each step will also be detailed below.

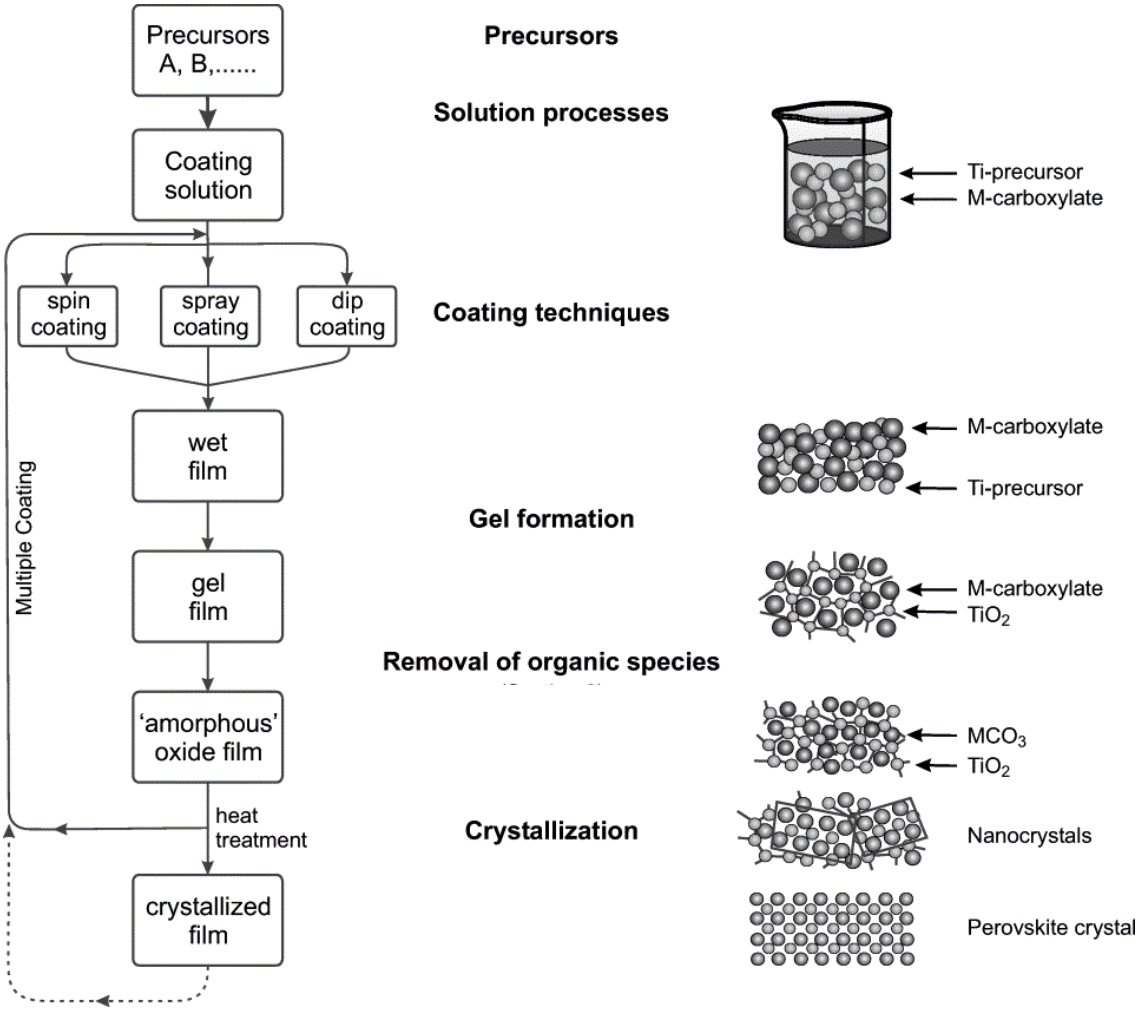

Figure 1.8. *Flow chart of a typical CSD process, with representative drawings of the structural status evolution of the metal components during the process (right-hand) Reproduced from [14]*

Since in the majority of cases pyrolysed films are typically amorphous, crystallisation into the desired oxide phase at high temperatures is accomplished by nucleation and growth phenomena producing polycrystalline films. Thus, the characteristics of these processes will define the resulting microstructure in the film. Films that display microstructures where only interface nucleation of the crystalline phase has occurred (i.e. heterogeneous nucleation), are frequently columnar in nature, whereas those in which nucleation is produced within the bulk film (i.e. homogeneous nucleation) are typically formed by equiaxed grains smaller than the total film thickness [19].

From a thermodynamic point of view, the driving forces that rule the transformation from the pyrolysed amorphous film to the crystalline ceramic material play a critical role in defining the active nucleation events and, thereby, film microstructure [20]. For example, to obtain highly oriented or epitaxial films, the film must be processed so that heterogeneous nucleation at the interface dictates the microstructure. Considering either heterogeneous or homogeneous nucleation of the film, this will depend on diverse parameters related with the free energy (ΔG) for the nucleation event of a perovskite crystal, such as its interfacial energy, the contact angle with the substrate and the driving force for crystallisation. Normally, the energy barriers for interface nucleation are lower than those expected for homogeneous nucleation [19]. As crystallisation driving force is increased (e.g. via thermal treatment) bulk nucleation becomes as probable as interface nucleation. Furthermore, films with increased densification and larger grain sizes are obtained when high crystallisation temperatures are used.

To sum up, the thermal processing conditions can significantly affect the microstructure and therefore the functional properties of the thin film. Both kinetic and thermodynamic features of the thermal treatments determine the crystallisation process of the film.

1.1.3. Challenges of ferroelectric thin films. Size and interface stress effects.

The differences of the properties of ferroelectric films and bulk ceramics have been studied widely [4,9,21]. The dielectric permittivity of thin films is generally lower than that for the corresponding bulk ceramics. Also, the ferroelectric polarization properties and the piezoelectric coefficients for films are smaller than those of bulk ceramics or single crystals with the same composition.

Size effects on ferroelectrics

The reduced grain size of thin films, due to the lower crystallization temperatures used and the reduced dimensions in one direction, causes a decrease of the

value of the ferroelectric polarization and of the piezoelectric coefficients. Grain size effects have been studied in bulk ferroelectric materials [22-25], showing the large effect of grain size on the mobility of the domain walls (important extrinsic contribution to the properties in ferroelectrics) or on the stabilization of non-pure ferroelectric phases in small crystallites. For submicron-structured 0.65PMN-0.35PT ceramic the relaxor like behavior was observed down to room temperature, as the comparison between the dielectric permittivity curves of ceramics with different grain size in Figure 1.9 shows [26]. The decrease in grain size therefore causes a strong decrease of the electrical polarization as it is shown in Fig. 1.10

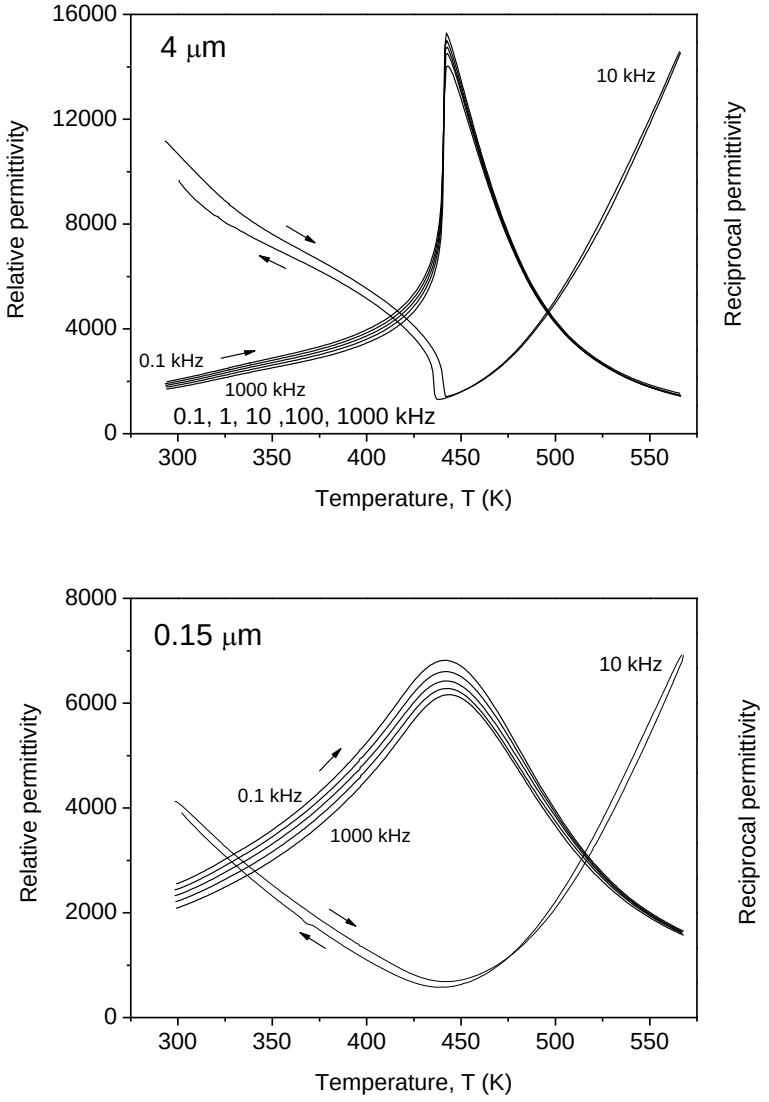

Figure1.9. *The relative dielectric permittivity K´ versus temperature for 0.65PMN–0.35PT ceramics with the average grain size of (a) 4 μm and (b) 0.15 μm [26]*

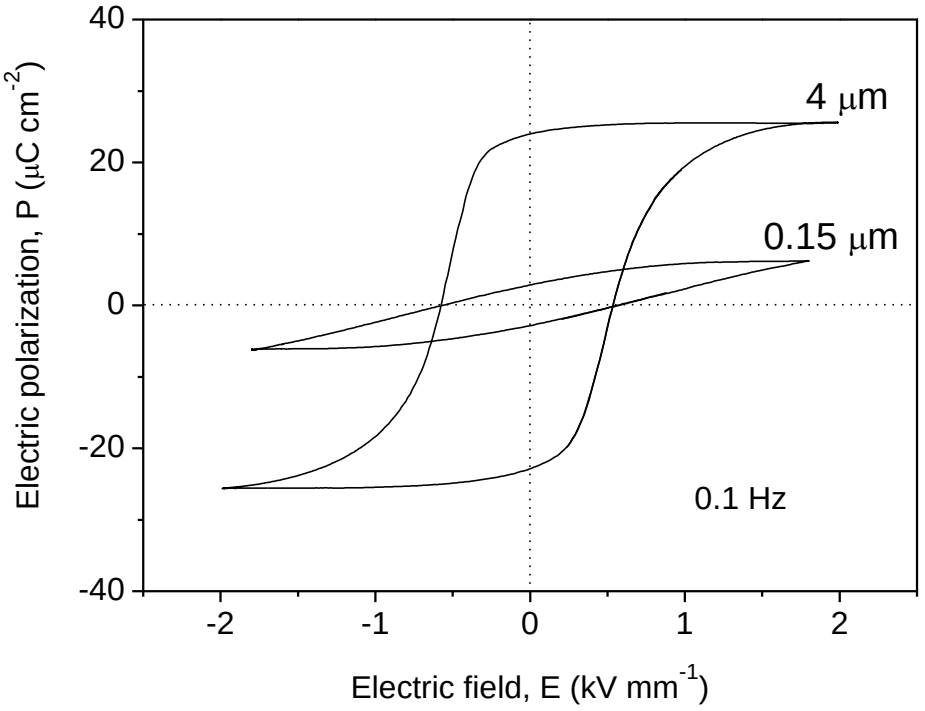

Figure 1.10. *The hysteresis loop measured at 0.1 Hz for 0.65PMN–0.35PT ceramics with the average grain size of 4 μm and 0.15 μm [26]*

Influence of the residual stresses from the substrate-film interface

Apart from the effects of drying and crystallization, with the subsequent release of organics for films prepared by CSD, the main residual stresses are the result of the usually different expansion coefficients of films and substrates [27,28]. This is schematically explained in Fig.1.11. The basic equation that rules the appearance of this stress σ_f in films is [27]:

$$\sigma_f = (\alpha_s - \alpha_f) \cdot (\Delta T) \cdot Y_f / (1 - \nu_f), \qquad (4)$$

where α_s and α_f are the thermal expansion coefficients of the substrate and the film, respectively , ΔT is the variation of temperature , Y_f is the Young´s modulus and ν_f is the Poisson´s ratio of the film. A film prepared at elevated temperatures will be under a compressive residual stress at room temperature if $\alpha_s > \alpha_f$, and under tensile stress if $\alpha_s < \alpha_f$. In Fig. 1.12 both situations are illustrated [27]. If the stresses are large enough, cracking of the films may occur.

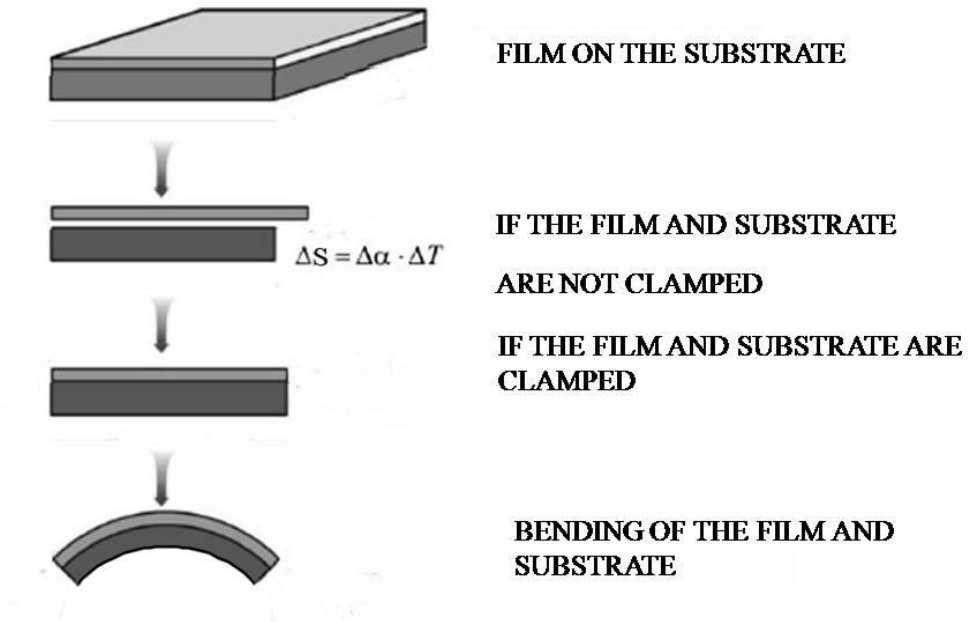

Figure 1.11. *Effect of the different deformation ΔS substrate and film in response to the temperature variations produced during film processing ΔT , which is a consequence of the different thermal expansion coefficients of both $\Delta\alpha$ [29]*

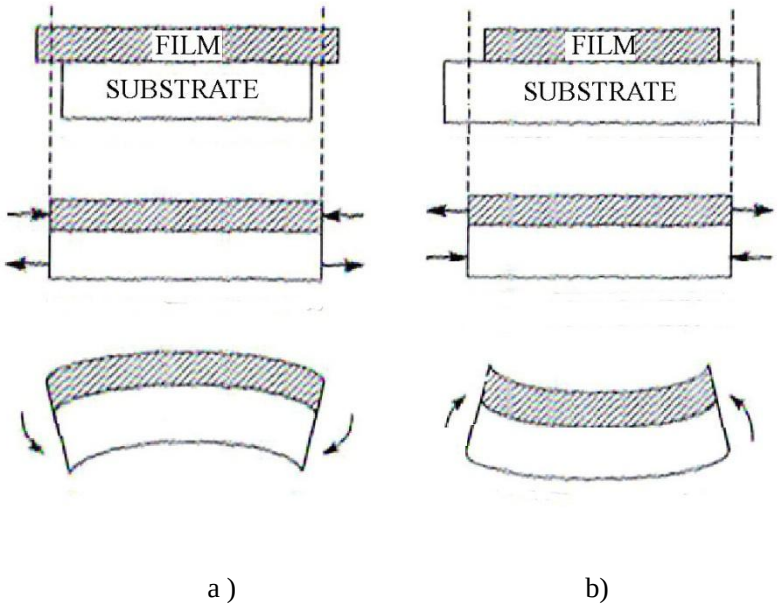

Figure 1.12. *Film under (a) compressive and (b) tensile residual stress [27]*

1.2. The solid solution $Pb(Mg_{1/3}Nb_{2/3})O_3$-$PbTiO_3$

(1-x)$Pb(Mg_{1/3}Nb_{2/3})O_3$-x$PbTiO_3$ (PMNT) is a solid solution whose end members are prototypes of a normal ferroelectric ($PbTiO_3$) and of a relaxor-ferroelectric ($Pb(Mg_{1/3}Nb_{2/3})O_3$). The interest of this solid solution for the preparation of piezoelectric films is due to the ultrahigh piezoelectric coefficients reported for single crystals [30] for compositions close to the Morphotropic Phase Boundary (MPB) between rhombohedral and tetragonal phases, which can be observed in its phase diagram, shown in Fig.1.13.

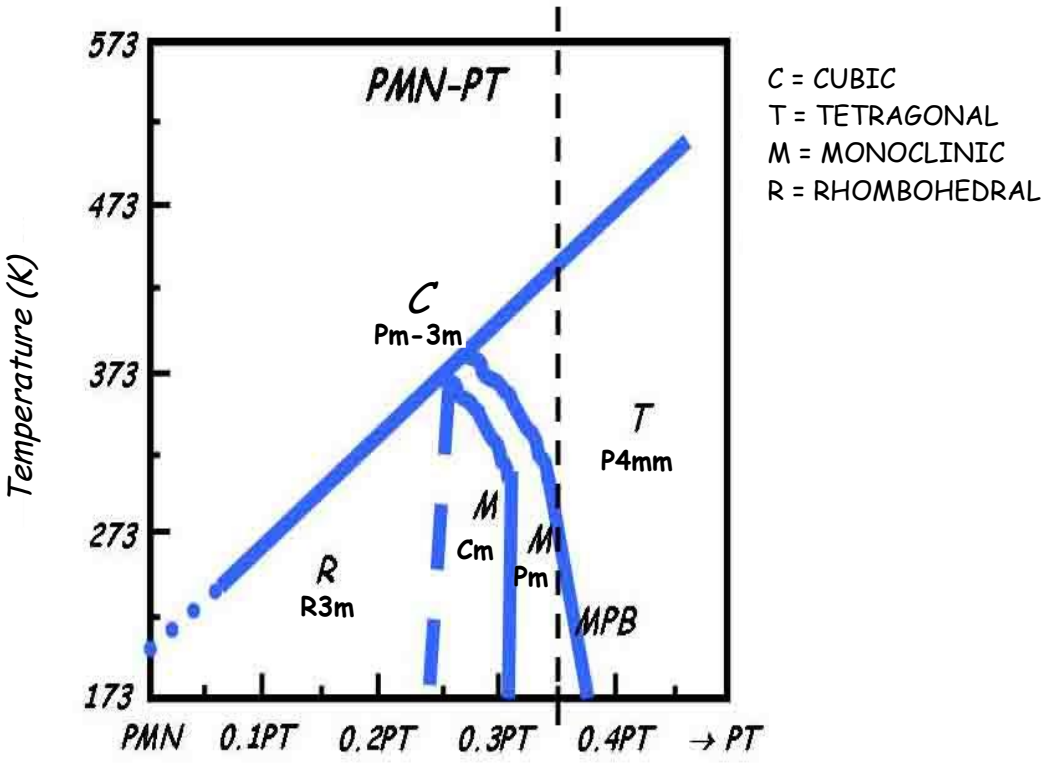

Figure 1.13. *Phase diagram of the solid solution $Pb(Mg_{1/3}Nb_{2/3})O_3$-$PbTiO_3$*

The difference between relaxor and normal ferroelectrics is based on three qualitatively different features in the temperature dependence of the dielectric permittivity. Firstly, in normal ferroelectrics the real part of the dielectric permittivity shows a Curie-Weiss law behavior at the transition temperature T_C, whereas in relaxors the dielectric permittivity shows a broad maximum (T_m). Secondly, there is strong

frequency dependence in the peak position for relaxors. And, lastly, the polarization in normal ferroelectrics goes to zero at T_C and in the relaxors the polarization extends well beyond the maximum temperature T_m [31]. The dielectric permittivity of PMN as a function of temperature shows a broad maximum of 20000 at 265K and 1 kHz, the position of which, T_m, shifts towards higher temperatures with increasing frequency within a range of 20^{o}C (between 1 KHz and 1 MHz), the so called Curie range. The addition of $PbTiO_3$ (PT) decreases the Curie range [32]. At 0.65PMN-0.35PT a morphotropic phase boundary (MPB) is observed between a rhombohedral (R3m) and a tetragonal phase (P4mm) [33,34]. After the discovery of the monoclinic phase (Cm space group) in a similar MPB of ferroelectric (Pb,Zr)TiO_3 (PZT), a number of studies have reported the presence of monoclinic phases (with space groups Cm and Pm) in the MPB region of $PbTiO_3$-based solid solutions [35-39]. For ferroelectric PMN-PT, experimental evidence shows that monoclinic phases exist at the MPB around the 0.65PMN-0.35PT composition [40]. The complexity of this phase diagram is related to the exceptional properties of the materials derived from this solid solution.

The PMNT solid solution especially at x= 0.35 in the the proximity of the Morphotropic Phase Boundary (MPB), has been the subject of special interest [41], because it exhibits excellent piezoelectric properties: it has been reported ultrahigh piezoelectric activity in single crystals of these compositions, with a piezoelectric coefficient (d_{33}) of ~ 2500 pC/N [30]. The values for the piezoelectric coefficient d_{33} of bulk ceramics with the same composition range from 525 pC/N to 710 pC/N [2, 42-44]. At the MPB, the polarization vector can be along any of the six <100> directions of the tetragonal phase or along any of the eight <111> directions of the rhombohedral phase, equally favorable energetically. This allows an easy rotation of the polarization when an electric field is applied, which is accompanied by a large deformation of the crystal, which leads to the large piezoelectric coefficients found.

1.2.1. 0.65Pb($Mg_{1/3}Nb_{2/3}$)O_3-0.35$PbTiO_3$ thin films

Compared with single crystals and bulk ceramics, the PMNT thin films at the MPB have small remnant properties, including piezoelectric, and lower dielectric permittivity values [45]. It has been reported that the d_{31} coefficient measured by a modification of the wafer flexure method in a ~1500 nm thick PMNT film is ≅ 85 pC/N [45], which means an estimated d_{33} ($-d_{31}/0.43$) of ~197 pC/N. This value decreases rapidly with the reduction of the film thickness to d_{33}~42 pC/N in ~350 nm thick film [45] and d_{33}~55pC/N measured by optical interferometry in a ~300 nm thick film [46]. The loss of the piezoelectric activity is of course related to the decrease of the remnant polarization of these films compared with their bulk counterparts. However, the saturation values of the polarization are not that different from those of bulk ceramics [45, 47].

The decrease of the grain size associated to the reduced thickness of the film has been reported as the main cause of this effect [48]. The stabilization of relaxor-like domains in submicrometric grains in ceramics [26] makes that, as it happens in relaxor ferroelectric, the removal of the electric field results in the disappearance of the polarization, which reduces drastically all remnant properties of these materials with submicrometric grains.

1.3. $PbTiO_3$ thin film

$PbTiO_3$ (PT), a prototype ferroelectric, presents large tetragonal anisotropy along the c-axis, the polar direction in the crystal, which results in large spontaneous polarization. However, this large tetragonality makes difficult the use of PT in ceramic form. Since the volume variation resulting from the first order, cubic-to-tetragonal phase transition is so high, cracking of the ceramic body is produced during the cooling process after firing. In thin film form the lower crystallization temperatures required minimizes this effect, and PT maintains high spontaneous polarization at room temperature (P_s > 50 μC/cm^2). As a consequence, the reported values of the pyroelectric coefficient (γ) of the thin films of PT is as high as 250 μC·m^{-2}·K^{-1} [49]. Also, it has a wide temperature range for the stability of the ferroelectric phase and high Curie

temperature (490^{o}C). Both polarization and Curie temperature are the highest among perovskite type structure ferroelectric materials [50]. Besides, it maintains large remnant polarization values even for the thinnest layers [51]. Also, it can be prepared at very low temperatures [52,53]. All these characteristics are complementary to those of PMNT films with compositions close to the MPB, which have not high remnant polarization values but show large piezoelectric coefficients, much higher than those of PT films. It seems that a combination of the properties of both may produce excellent piezoelectric films. And the flexibility in the preparation of PT films with different thickness and at different temperatures will help the joint preparation of alternating layers of both compositions, as PMNT films require very specific crystallization temperatures to obtain high quality films with a single ferroelectric phase [46].

1.4. Piezoelectric multilayer composite thin film

Composite materials are the combination of two or more materials in which the individual components always remain separate and distinct within the finished structure. The resultant properties of composites as a result of this combination can be classified as sum properties, combination properties and product properties [54]. The coefficients of the *sum properties* of a composite depends on the corresponding coefficients in the constituent phases. For example, the dielectric permittivity, *K*, of a composite is obtained from the permittivities and volume fractions, V_i, of the constituent phases ($K^n = K_1^n \cdot V_1 + K_2^n \cdot V_2 + \ldots$). The mixing rule, in this case the value of the exponent n, varies with the geometric arrangement of the phases. In general, the coefficient of the sum property is between those of the constituent phases. This is not true for the *combination properties,* which involve two or more different coefficients of the constituent phases. For example, the Poisson's ratio, which is the ratio of two compliance coefficients, may be much smaller for a composite than for the materials used to make it. . In contrast to them, the product property utilizes different properties in the two phases of a composite to produce a new property, not present in the constituent phases, through the interaction among them. An example of a product property is magnetoelectricity, obtained in composites made from piezoelectric and magnetostrictive phases.

Not only is the choice of the constituent materials of the composites important: the physical properties in multiphase solids also depend on the manner in which connections among the different phases present are made (connectivity) [55]. A phase in a composite may be self-connected in zero (not connected), one, two or three dimensions which corresponds to 0, 1, 2 or 3 connectivity. For example in the case of a two-phase composite, there are ten possibilities: 0-0, 1-0, 2-0, 3-0, 1-1, 2-1, 3-1, 2-2, 2-3 and 3-3.

Multilayer capacitors with alternating layers of two phases is a 2-2 composite, where both phases are self-connected in the lateral directions but not perpendicularly to them. The 2-2 connectivity of the multilayer composites (MLC) is an effective configuration for producing high electric fields with the application of relatively small voltages. This is used in the combination between soft PZT (small coercive field) with hard PZT (large coercive field). We can take advantage of the large piezoelectric response of the soft PZT in a 2-2 composite, through keeping it in a poled state with the electric field induced by the poled hard PZT layers [55]. The result is a material whose piezoelectric transducer behavior is superior to that of the single-phase soft PZT. The longitudinal piezoelectric coefficient of the multilayer composite, d^{MLC}_{33}, can be calculated from the following equation that consider two layers in series connection [55]:

$$d_{33}^{MLC} = \frac{[d_{33}^{1} \cdot \varepsilon_{33}^{2} \cdot V^{1} + d_{33}^{2} \cdot \varepsilon_{33}^{1} \cdot V^{2}]}{\varepsilon_{33}^{2} \cdot V^{1} + \varepsilon_{33}^{1} \cdot V^{2}} \quad (5)$$

where 1 and 2 denotes the two phases of the composite, $V^1$and V^2 are the volume fractions, and $\varepsilon_{33}{}^1$ and $\varepsilon_{33}{}^2$ are the dielectric permittivities of the two phases.

Due to the progressive miniaturization of the devices, it is important to prepare the desired piezoelectric composite in thin film form. Based on the principles traditionally used in bulk composites, the packing of layers of different ferroelectric compositions in a multilayer composite configuration has proved to be successful for the improvement of the dielectric, ferroelectric, piezoelectric and pyroelectric properties of single phase films, as recent reviews show [56,57]. Several multilayer ferroelectric films and superlattices have been designed searching the inducement of stress or strain effects in the films not only through epitaxial relations in superlattices [58,59], with the enhancement of the polarization by strain, but also in polycrystalline films, where the enhancement of the dielectric and pyroelectric properties are attributed to the lower

residual stress found in the heterostructures [60]. In other cases, a simple combination of the properties of the constituent phases is sought. For example, in order to achieve a film with high figures of merit for a pyroelectric detector, we can combine $Pb(Zr,Ti)O_3$ and $PbTiO_3$ layers to achieve low dielectric permittivity while preserving the large pyroelectric coefficients of PZT [61]. The use of layers that differ slightly in the composition, the so-called, compositionally graded films have shown to produce improved ferroelectric behaviour [62,63]. An issue that has attracted much attention in the field of ferroelectric multilayer composite films is the reduction of the fatigue of ferroelectric films by the combination of layers with different compositions [64-67] due to its importance for the performance of Ferroelectric Random Access Memories, FeRAMs. It must be noted that in most of these works the preferred deposition methods are Chemical Solution Deposition.

However, regarding the improvement of the piezoelectric properties in multilayer composites, there is not much work reported in thin films. Among the few examples found, improved piezoelectric strains are predicted [68] and finally observed in compositionally graded $Ba_xSr_{1-x}TiO_3$ (BST) [69]. In general, it can be said that the combination of appropriate layers to enhance piezoelectricity in films has not been explored extensively yet.

1.5. Motivation and hypothesis of the work

Materials of the solid solution $(1-x)Pb(Mg_{1/3}Nb_{2/3})O_3$-$xPbTiO_3$ with compositions close to the Morphotropic Phase Boundary show a drastic reduction in the remnant properties in thin film form that does not allow to take advantage of their high piezoelectric coefficients when integrated in microdevices. In this thesis we aim at producing films based on PMNT with high piezoelectric coefficients ready for their use in applications.

It has been reported that the values of the saturation polarization, P_s, remain close to those obtained in bulk ceramics [45,47], which implies that the problem relies on the decrease of the remnance in thin films. The reduction of the ferro/piezoelectric remnant polarization, P_r, in the MPB PMNT films can be an effect of their grain size, smaller the thinner the film is, which produces a change in the domain configuration from large conventional ferroelectric domains to a configuration of fine cross hatched domains, highly movable under an electric field, but that results in low remnant values of the polarization [26]. This effect is unique for these compositions, as grain size reduction in ferroelectrics leads, among others, to the disappearance of the ferroelastic ferroelectric domains, with a reduction of both remnant and saturation polarization values. However, ferroelectric films retain reasonable remnant properties, even for thickness well below 100 nm [51]. In addition, in thin films, the substrate-film interface plays an important role on the properties that must also be considered. It has been suggested that the appearance of an internal electric field at this interface is able to stabilize a thin layer of large ferroelectric domains on MPB PMNT thin films [48], which explains the self-polarization found in these films, and shows again the large effect that the application of an electric field has on the response of fine-grained PMNT crystals at the MPB.

As mentioned before, couplings among the components in a composite produce product properties that can be very attractive, like the coupling of the polarization among two phases reported for a soft $(Pb,Zr)TiO_3$ (PZT) with large piezoelectric response which is kept in a poled state by a hard PZT, in a 2-2 diphasic composite [13], whose properties as piezoelectric transducer are superior to those of a single-phase ferroelectric.

Based on these observations, we propose here a composite of alternating layers of PMNT (low P_r, but large P_s) and $PbTiO_3$ (PT) (large P_r, but not large piezoelectric coefficients). Similarly to the effect of the interface with the substrate described before, the internal electric field created by the poled PT layers is expected to be able to stabilize the polarization in the PMNT, and, as a consequence, should improve the remanence in this multilayer composite with respect to the single phase PMNT films.

In this work, we demonstrate the feasibility of this approach and the improvement of the piezoelectric properties obtained in these multilayer composite (MLC) films with PMNT and PT alternating layers, prepared by Chemical Solution Deposition (CSD) onto Pt-coated Si substrates. The dielectric, electrical and pyroelectric behaviour is discussed in relation with the mechanism proposed for the stabilization of the polarization. Besides, films with different combinations and number of layers are studied in order to optimize the response of the composite, as well as the use of the right processing parameters to fabricate high quality films.

1.6 References

[1] J. F. Nye, Physical properties of crystals (Oxford University Press, 2000)

[2] G.H. Haertling. J. Am. Ceram. Soc. 82, 797 (1999)

[3] M. Abplanalp, M. Zgonik, P. Günter, "Chapter 7 – Scanning Probe Microscopy of ferroelectric domains near phase transitions" p. 195 en "Nanoscale Characterisation of Ferroelectric Materials: Scanning Probe Microscopy Approach" (Ed. A. Gruverman, M. Alexe, Springer - Verlag, 2004)

[4] D. Damjanovic. Rep. Prog. Phys. 61, 1267 (1998)

[5] N. Setter, R. Waser, Acta Mater. 48, 151 (2000)

[6] F. Xu, S. Trolier- Mckinstry, W. Ren, B. Xu, Z. L. Xie, K. J. Hemker, J. Appl. Phys. 89, 1336 (2001)

[7] I. Bretos, "Low-toxic chemical solution deposition methods for the preparation of multifunctional $(Pb_{1-x}Ca_x)TiO_3$ thin films", PhD Thesis. Universidad Autónoma de Madrid (2006)

[8] K. Lefki, G. J. M. Dormans, J. Appl. Phys. 76, 1764 (1994)

[9] M. Dawber, K.M. Rabe, J.F. Scott, Rev. Mod. Phys. 77, 1083 (2005)

[10] S. Trolier-McKinstry, P. Muralt, J. Electroceram., 12, 7 (2004)

[11] H. Kueppers, T. Leuerer, U. Schnakenberg, W. Mokwa, M. Hoffmann, T. Schneller, U. Boettger, R. Waser, Sens. Actuat. A 97, 680 (2002)

[12] A.E. Feuersanger, A.K. Hagenlocher, A.L. Solonon, J. Electrochem. Soc. 111, 1387 (1964)

[13] R.A. Roy, K.F. Etzold, J.J. Cuomo. "Ferroelectric film synthesis, past and present. A select review". In Ferroelectric Thin Films, ed. by E.R. Myers and A.I. Kingon (Materials Research Society, San Francisco, 1990).

[14] R.W. Schwartz, T. Schneller, R. Waser, C. R. Chimie 7, 433 (2004)

[15] J. Fukushima, Am. Ceram. Soc. Bull. 55, 1064 (1976)

[16] J. Fukushima, K. Kodaira, T. Marsushita, J. Mater. Sci.19, 595 (1984)

[17] K.D. Budd, S.K. Dey, D.A. Payne, Brit. Ceram. Proc. 36, 107 (1985)

[18] S.K. Dey, K.D. Budd, D.A. Payne, IEEE T. Ultrason. Ferr. 35, 80 (1988)

[19] R.W. Schwartz, Chem. Mater. 9, 2325 (1997)

[20] A. Wu, P.M. Vilarinho, I. Reaney, I.M.M. Salvado, Chem. Mater. 15, 1147 (2003)

[21] N. Setter, D. Damjanovic, L. Eng, G. Fox, S. Gevorgian, S. Hong, A. Kingon, H. Kohlstedt, N. Y. Prak, G. B. Stephenson, I. Stolitchnov, A. K. Taganstev, D. V. Taylor, T. Yamada, S. Streiffer, J. Appl. Phys. 100, 051606 (2006)

[22] C.A. Randall, N. Kim, J.P. Kucera, W. Cao, T.R. Shrout, J. Am. Ceram. Soc. 81, 677 (1998)

[23] J. Carreaud, J. M. Kiat, B. Dkhil, M. Algueró, J. Ricote, R. Jimenez, J. Holc, M. Kosec, Appl. Phys. Lett. 89, 252906 (2006)

[24] X. Deng, X. Wang, H. Wen, L. Chen, L. Chen, L. Li, Appl. Phys. Lett. 88, 252905 (2006)

[25] A.M. Bratkovsky, A.P. Levanyuk, Phys. Rev. Lett., 94, 107601 (2005)

[26] M. Algueró, J. Ricote, R. Jiménez, P. Ramos, J. Carreaud, B. Dkhil, J. M. Kiat, J. Holc, M. Kosec, Appl. Phys. Lett. 91, 112905 (2007).

[27] M. Ohring, The material science of thin films (Academic Press, San Diego, 1992)

[28] S. Lu, C. Zuo, H. Zeng, H. Wen, H. Ji, Mater. Lett. 60, 255 (2006)

[29] K. Šimunov, M. Franz, G. Marić, Metalurgija 47, 93 (2008)

[30] S.E. Park, T.R. Shrout, J. Appl. Phys. 82, 1804 (1997)

[31] Z.G. Ye, Y. Bing, J. Gao, A.A. Bokov, P. Stephens, B. Noheda, G. Shirane, Phys. Rev. B 67, 104104 (2003)

[32] S.L. Swartz, T.R. Shrout, W.A. Schulze, L.E. Cross, J. Am. Ceram. Soc. 67, 311 (1984)

[33] S.W. Choi, T.R. Shrout, S.J. Jang, A.S. Bhalla, Ferroelectrics 100, 29 (1989)

[34] O. Noblanc, P. Gaucher, G. Calvarin, J. Appl. Phys. 79, 4291 (1996)

[35] Z.G. Ye, B. Noheda, M. Dong, D. Cox, G. Shirane, Phys. Rev. B. 64, 184114 (2001)

[36] B. Noheda, D. Cox, G. Shirane, J. Gao, Z.G. Ye, Phys. Rev. B. 66, 054104 (2002)

[37] J. M. Kiat, Y. Uesu, B. Dkhil, M. Matsuda, C. Malibert, G. Calvarin, Phys. Rev. B. 65, 064106 (2002)

[38] A.K. Singh, D. Pandey, Phys. Rev. B. 67, 064102 (2003)

[39] R. Haumont, B. Dkhil, J.M. Kiat, H. Al-Barakaty, H. Dammak, L. Bellaiche, Phys. Rev. B. 68, 082110 (2003)

[40] A.K. Singh, D. Pandey, O. Zaharko, J. Appl. Phys. 99, 076105 (2006)

[41] Z.G. Ye, MRS Bull. 34, 277(2009)

[42] J. Kelly, M. Leonard, C. Tantigate, A. Safari, J. Am. Ceram. Soc. 80, 957 (1997)

[43] T.Y. Koo, S.W. Cheong, Appl. Phys. Lett. 80, 4205 (2002)

[44] Z. Xia, L. Wang, W. Yan, Q. Li, Y. Zhang, Materials Research Bulletin 42, 1715 (2007)

[45] J.H. Park, F. Xu, S. Trolier-Mckinstry, J. Appl. Phys. 89, 568 (2001)

[46] M.L. Calzada, M. Algueró, A. Santos, M. Stewart, M.G. Cain, L. Pardo, J. Mater. Res. 24, 526 (2009)

[47] J. H. Park, S. Trolier-Mckinstry, J. Mater. Res. 16, 268 (2001)

[48] M. Algueró, M. Stewart, M.G. Cain, P. Ramos, J. Ricote, M.L. Calzada, J. Phys. D: Appl. Phys. 43, 205401 (2010)

[49] V.P. Palkar, S.C. Purandare, R. Pinto, J. Phys. D: Appl. Phys. 32, R1 (1999)

[50] B.A. Tuttle, D.A. Payne, J.L. Mukherjee, MRS Bulletin 20, 19 (1994)

[51] J. Ricote, S. Holgado, Z. Huang, P. Ramos, R. Fernández, M. L. Calzada, J. Mater. Res. 23, 2787 (2008)

[52] M. Kosec, B. Malic, M. Mandeljc, Mater. Sci. Semicond. Process. 5, 97 (2002)

[53] C. de Dobbelaere, M.L. Calzada, R. Jiménez, J. Ricote, I. Bretos, J. Mullens, A. Hardy, M. van Bael, J. Amer. Chem. Soc. 133, 12922 (2011)

[54] R.E. Newnham, Annu. Rev. Mater. Sci. 16, 47 (1986)

[55] R.E. Newnham, D. P. Skinner, L. E. Cross, Mater. Res. Bull. 13, 525 (1978)

[56] K. P. Jayadevan, T.Y. Tseng, J. Mater. Sci. Mater. Electron. 13, 439 (2002)

[57] D. Bao, Curr. Opin. Solid State Mater. Sci. 12, 55 (2008)

[58] H.N. Lee, H.M. Christen, M.F. Chisholm, C.M. Rouleau, D.H. Lowndes, Nature 433, 395 (2005)

[59] T. Shimuta, O. Nakagawara, T. Makino, S. Arai, H. Tabata, T. Kawai, J. Appl. Phys. 91, 2290 (2002)

[60] R. Poyato, M. L. Calzada, L. Pardo, Appl. Phys. Lett. 84, 4161 (2004)

[61] L.L. Sun, O.K. Tan, W.G. Zhu, J. Appl. Phys. 99, 094108 (2006)

[62] D.H. Bao, L.Y. Zhang, X. Yao, Appl. Phys. Lett. 76, 1063 (2000)

[63] X.H. Zhu, N. Chong, H.L. Chan, C.L. Choy, K.H. Wong, Z. G. Liu, N. B. Ming, Appl. Phys. Lett. 80, 3376 (2002)

[64] J. H. Jang, K.H. Yoon, Appl. Phys. Lett. 75, 130 (1999)

[65] D. Bao, N. Wakiya, K. Ahinozaki, N. Mizutani, J. Phys. D: Appl. Phys. 35, L1 (2002)

[66] N. Ortega, P. Bhattacharya, R.S. Katiyar, Mater. Sci. Eng. B 130, 36 (2006)

[67] D. Do, S. S. Kim, S. W. Yi, J. W. Kim, J. Appl. Phys. A: Mater. Science & Processing 94, 697 (2009)

[68] S. Zhong, Z.G. Ban, S.P. Alpay, J.V. Mantese, Appl. Phys. Lett. 89, 142913 (2006)

[69] R. Nath, S. Zhong, S.P. Alpay, B.D. Huey, M.W. Cole, Appl. Phys. Lett. 92, 012916 (2008)

CHAPTER II

EXPERIMENTAL PROCEDURE

In this chapter, the details of the preparation process of the single phase and multilayer composite films, as well as the explanation of the methods for the characterization of their properties are presented.

2.1. Preparation method of the multilayer composite films

The multilayer composite films were obtained by Chemical Solution Deposition (CSD) method, which was chosen because of the high compositional control achieved to prepare complex oxides as the ones proposed here, the large surface areas deposited and the low cost associated with the materials and experimental setup that makes CSD attractive for industrial applications.

2.1.1. Synthesis of the precursor sols

PMN and PT sols with nominal compositions of $Pb(Mg_{1/3}Nb_{2/3})O_3$ and $PbTiO_3$, respectively, were synthesized by a sol-gel method based on the diol route [1-3]. Air-stable and precipitate-free sol of PT were synthesised using lead (II) acetate trihydrate ($Pb(OCOCH_3)_2 \cdot 3H_2O$) and 1,3-propanediol ($HO(CH_2)_3OH$) as precursors. They were refluxed in air at ~155^oC for 1h. Then, titanium (IV) di-isopropoxide bis-acetylacetonate ($Ti(OC_3H_7)_2(CH_3COCHCOCH_3)_2$, 75 wt% solution in 2- propanol) was added to the mixture and reflux was maintained in air at ~110^oC for 8h. After this step, by-products were partially distilled off the solution. The volume of the distilled liquid was the 80 % volume of the total 2-propanol that the synthesized sol contains [1]. Figure 2.1 shows a scheme of this synthesis route.

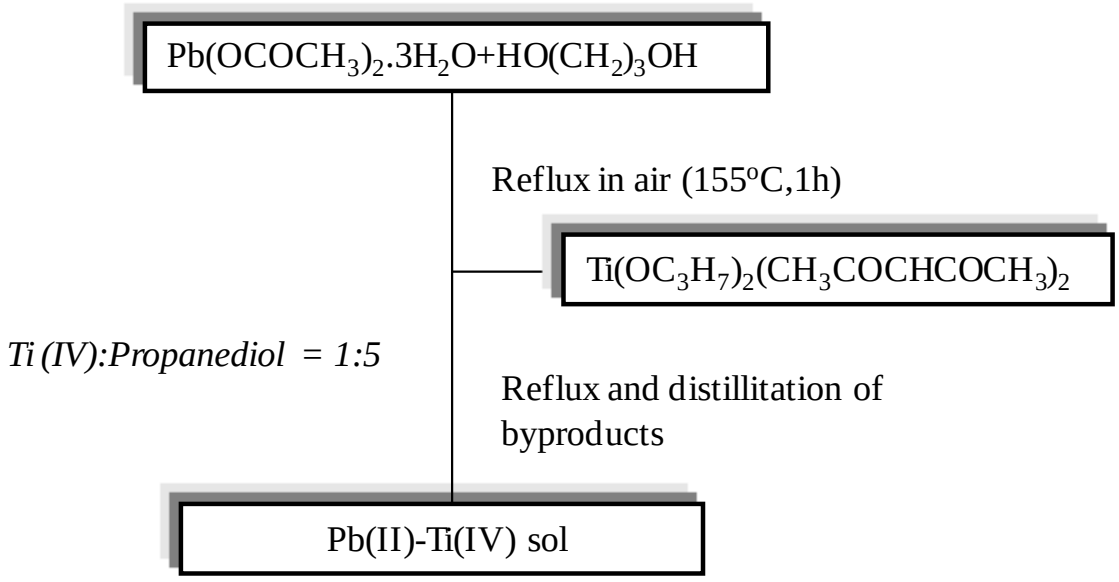

Figure 2.1. *Scheme of the synthesis of the PT sols*

Air-stable and precipitate-free PMN sols were prepared by refluxing magnesium ethoxide ($Mg(OC_2H_5)_2$) and niobium ethoxide ($Nb(OC_2H_5)_5$) in a mixture of 1,3-propanediol ($HO(CH_2)_3OH$) and acetic acid (CH_3CO_2H) acting as solvent, for 8 h in a dry nitrogen atmosphere. After distillation of byproducts, a transparent Mg(II)-Nb(V) sol was obtained. In another reaction flask, a Pb(II) solution was prepared by refluxing for 1 h in air lead acetate trihydrate ($Pb(OOCH_3)_2 \cdot 3H_2O$) with 1,3-propanediol. Distillation of the crystallization water of the acetate was carried out in vacuum. The resulting Pb(II) solution was mixed with the Mg(II)-Nb(V) sol, yielding a transparent gold- coloured PMN sol. Similarly to the preparation of the PT sols, Figure 2.2 shows a scheme of the synthesis route followed for the preparation of the sol.

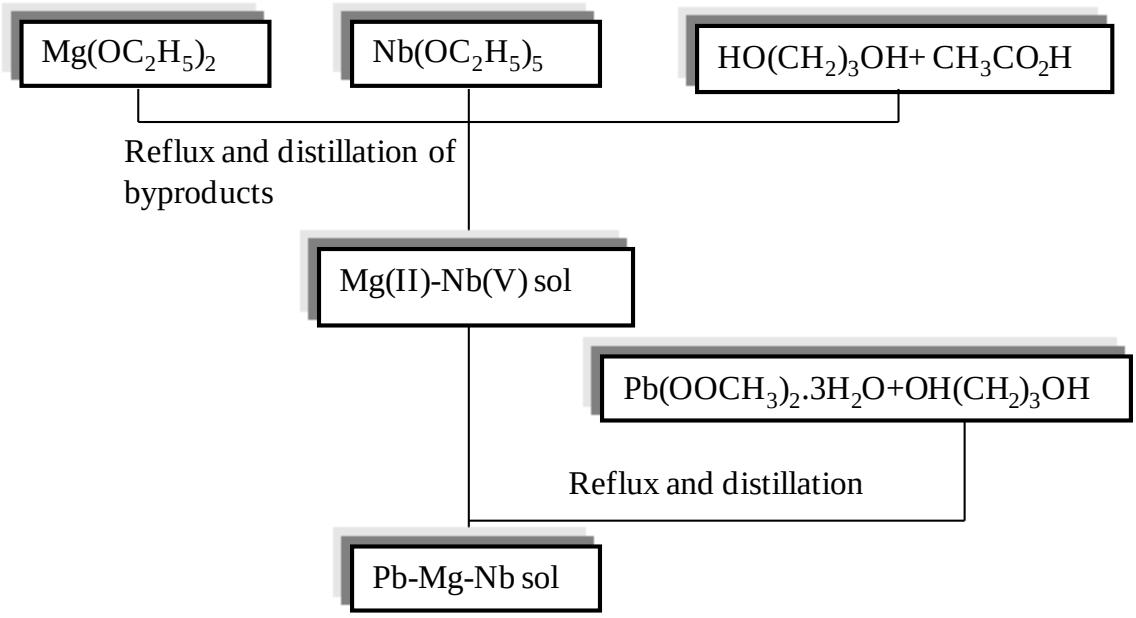

Figure 2.2. *Scheme of the synthesis route of PMN sols*

The PMN and PT sols were mixed with the appropriate ratio and stirred in air for 15 min to finally get PMN-PT sols with the nominal composition of $0.65Pb(Mg_{1/3}Nb_{2/3})O_3$-$0.35PbTiO_3$. A 10% mol of PbO excess is added to compensate for the lead loss during the thermal treatment of the film.

2.1.2. Deposition of thin layers

The precursor sols were diluted and deposited on platinized Si-based substrates by spin coating in a clean room, which includes full equipment for the cleaning of the substrates (ultrasonics bath), deposition (spinner, hot-plate) and crystallisation (rapid thermal processor) of the films, and fabrication of the capacitors (D.C. sputtering), under a laminar flux hood (CAM-1300-V) with a sterile air circulator unit (Telstar FFU).

The substrates used are: commercial $Pt/TiO_2/SiO_2/(100)Si$. Si-based substrates are chosen to facilitate the integration of the films studied in microelectronic devices. In

order to fabricate the capacitors that allow the application of an electric field and make use of the functional properties of the film, a bottom electrode is needed. Platinum is the most commonly used bottom electrode in this type of substrate because of its resistance to oxidation at the temperatures necessary for the film processing. This Pt layer, obtained by sputtering, has a thickness of ~ 50 nm. It does not adhere well directly on the Si wafer, so an adhesive layer, in this caseTiO_2 (50 nm thickness), is deposited onto the native SiO_2 (~ 20 nm thickness) layer formed on the Si surface. Pieces of 2 x 2 cm^2 of these substrates were cut and used for the depositions experiments. Prior to film deposition, substrates were cleaned with organic solvents in an ultrasonics bath. The cleaning procedure consisted in the following steps; 5 min in trichloroethylene (Cl_2CClCH, stabilised with ethanol), 4 min in acetone (CH_3COCH_3) and 3 min in 2-propanol ($CH_3CHOHCH_3$). Residual solvent as well as undesired particles on the surface were removed from the cleaned substrates with a nitrogen flow.

The deposition of the PT and PMNT layers of the multilayer composite films (MLC) of this work has been carried out with a spinner (TP 6000 gyrset system of SET-Mico- Control group model), working at 2000 rpm for 45s. This process can be divided into four stages [4]; deposition, spin-up, spin off and evaporation, as shown in Figure 2.3. During the deposition stage, a drop of the precursor solution is put onto the substrate using glass syringes equipped with non-sterile plastic nozzles and coupled with filters (Millipore) of 0.2 μm pore size to avoid the deposition of undesired particles. The liquid flows radially outwards, driven by the centrifugal force. In the spin up stage, the liquid excess flows to the perimeter of the substrate surface. This process continues during the spin off until a uniform thin layer of precursor liquid is left on the substrate. Finally, evaporation acts as the main mechanism of thinning during the last stage, without altering the uniformity of the deposited layer, showing that the viscosity of the sol is not shear dependent and stays stable over the substrate [5].

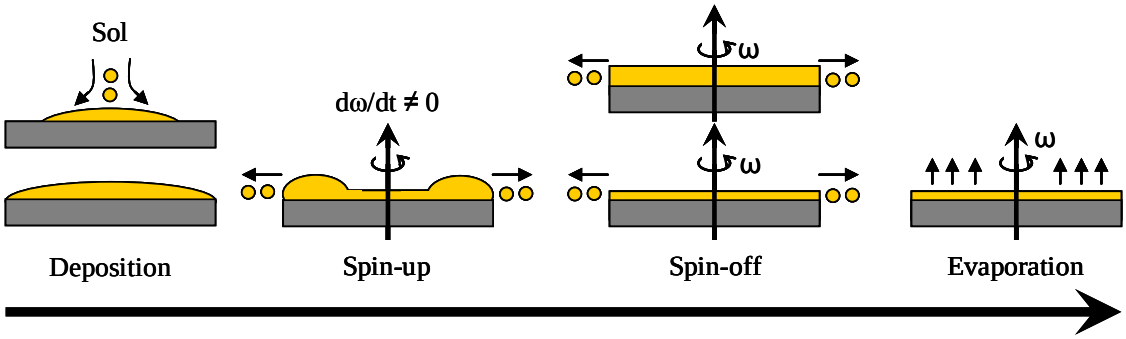

Figure 2.3. *Different steps of the spin coating deposition process*

2.1.3. Drying and crystallization

The wet films thus obtained were dried and pyrolysed in order to remove the entrapped solvent and the majority of the organic species present within the gel network. This process is carried out in hot plates stabilised at 350^{o}C.

The as-deposited PT and PMNT layers were crystallized into the desired phase by Rapid Thermal Processing (RTP). The rapid heating rates (even up to 300^{o}C/s) registered in this process produce the removal of organic species at higher temperatures [6,7], where the kinetics of the pyrolysis reactions is greatly enhanced. Furthermore, thin film densification is also promoted by RTP, since the onset of the crystallization is moved to higher temperatures. Besides, the RTP process makes difficult the stabilization of metastable, non-ferroelectric secondary phases with a crystallization temperature below that of the ferroelectric perovskite phase [6].

The crystallization of the PT and PMNT films by RTP was carried out with the Jetstar 100T JIPELEC equipment shown in Figure 2.4a. A scheme of the furnace arrangement is displayed in Fig. 2.4b. The films were placed on the sample holder plate and temperature of the process was controlled by a pyrometer and a thermocouple (with response time 10^{-3}s) in contact with the film surface [8].

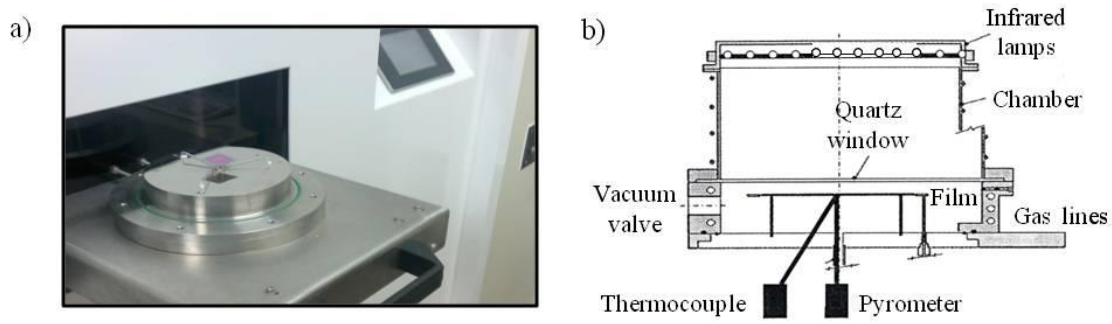

Figure 2.4. *(a) Photograph of the RTP furnace and (b) scheme of the furnace arrangement used for the crystallisation of the films*

In this work three different crystallization temperatures (400, 500 and 650^{o}C) were used for the PT layers, while all PMNT layers were crystallized at 650^{o}C.

2.1.4. Combination of layers in MLC films

The multilayer composite thin films (MLC) were fabricated by the deposition, drying and crystallization of a different number of alternating layers of PT and PMNT, starting and finishing either with a PMNT layer (MLC-PMNT) or with a PT layer (MLC-PT), in order to compare different configurations in which either every PMNT layer is sandwiched between two PT layers or, conversely, every PT layer is placed between two PMNT layers. Details of the different configurations used will be found in the following chapters.

2.2. Structural and microstructural characterization

2.2.1. Thickness measurements

The thickness of the crystalline films has been determined by profilometry, and the values were confirmed with those obtained by the direct observation of cross sections of the films by Scanning Electron Microscopy (SEM). In the profilometry, the height displacement induced in a tip in contact with the film surface is measured while the tip scans the film surface. The contact force between the tip and the film is maintained through a low elastic constant spring, whose deflection due to height slopes

is collected by an inductive transducer, and hence related to the roughness of the film. A Taylor-Hobson profilometer, Form Talysurf 50 model, was used. A carbon fibre calliper of 60 mm length, with a 60º cone-shaped diamond tip with a radius of 2 μm, allows thickness measurements with a resolution of 20 nm. In order to have a reference of the substrate, a small region of the film must be peeled-off. Thus, the thickness of the film is directly obtained by measuring the length of the step between the film surface and the naked substrate. However, after the deposition and crystallisation of the films, the scan of the surface results in a curved profile The profile is therefore fitted to parabolas or circumferences with a home-made software, from which values of thickness were calculated [9].In all cases, regression coefficients near 0.99 are obtained in the fittings.

2.2.2. Analysis of the crystalline structure

The crystalline structure of the films has been studied by X-ray Diffraction, with Bragg-Brentano (XRD) and Grazing Incidence (GIXRD) geometries.

The experimental diffraction patterns were compared with standard powder X-ray patterns of $PbTiO_3$ (JCPDSICDD 06-0452) and $Pb(Mg_{0.33}Nb_{0.67})O_3$ (JCPDSICDD 27- 1199) perovskite phases. Deconvolution and separation of reflections in the experimental patterns were carried out by using pseudo-Voigt functions in the profile program V1- 40.

The XRD measurements were carried out using a D500 powder diffractometer equipped with Cu anode ($\lambda_{CuK\alpha}$ = 1.5418 Å) working at 25 mA intensity and 40 kV voltage. Diffracted beams were collected by a scintillation detector. For the Bragg Brentano configuration, two slits of 1º for the incident beam and other two of 1º and 0.15º for the diffracted beam were used. Diffraction patterns were collected in the 2θ interval between 20 and 50º, with a step of 0.05º/3s. This configuration allowed the observation of preferred orientations in the films, since the X-ray beams impinge within the bulk of the film, as difference with the GIXRD analysis where only reflections from the layers next to the surface are observed.

The conventional Bragg-Brentano geometry (θ-2θ) may, however, not be the best configuration for the analysis of thin films, since reflections coming from the substrate could overlap those from the actual film. The grazing incidence XRD, an asymmetric Bragg geometry, is used in the analysis of thin films. In this configuration,

the incidence angle θ is fixed at a small value (α). The low incidence angles reduce the penetration of the incident X-rays within the material and, therefore, reflections coming from the substrate are minimized. In this configuration a 0.4º-Soller slit and a LiF monochromator were incorporated to the detector system. A schematic illustration of both Bragg-Brentano and grazing incidence geometries is depicted in Figure 2.5.

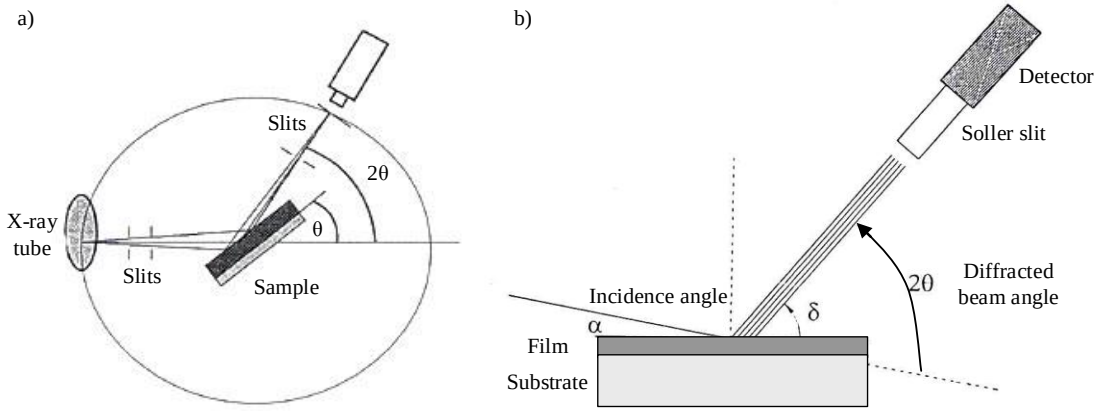

Figure 2.5. *Schematic illustration of (a) Bragg-Brentano and (b) grazing incidence geometries for X-ray diffraction*

2.2.3. Microstructural study

The microstructure of the films has been studied by optical microscopy, Scanning Electron Microscopy (SEM) and Scanning Force Microscopy (PFM).

The characterization of the microstructural features at low magnification, like residual porosity of the films, was carried out by optical microscopy. Images were obtained with a Leitz microscope, using a x22 magnification objective, which allows us to observe the overall quality of the deposit with enough resolution to study the surface defects. Calibration of the images was done with a micrometer (Leitz).

A study of the surfaces of the films with more magnifications reveals the grain size. Moreover, the analysis of the cross section of the films provides precise information on the thickness and the distribution of the layers. To this purpose we need more resolution and Scanning Electron Microscopy is used. SEM images of this work have been obtained with an ISI-DS-130 field emission gun microscope (FEG-SEM)

The analysis of the grain size is completed by the observation of the surface topography by Scanning Force Microscopy. In this work, this study is performed together with an analysis of the local piezoelectric response by the so called Piezoresponse Force Microscopy (PFM), explained in section 2.4.2. As PFM requires that the tip and the sample are in contact, the topography images shown are always obtained in contact mode (Figure 2.6), despite the wearing of the tip that is produced and that is avoided in the intermittent contact and dynamic modes. It must be considered that the lateral resolution of this technique is limited by the diameter of the tip. Special care was taken to discard images with damaged tips. The experiments were carried out with a commercial Nanotec® Electrónica scanning force microscopy, using the WSxM® software [10] for microscope control and image processing.

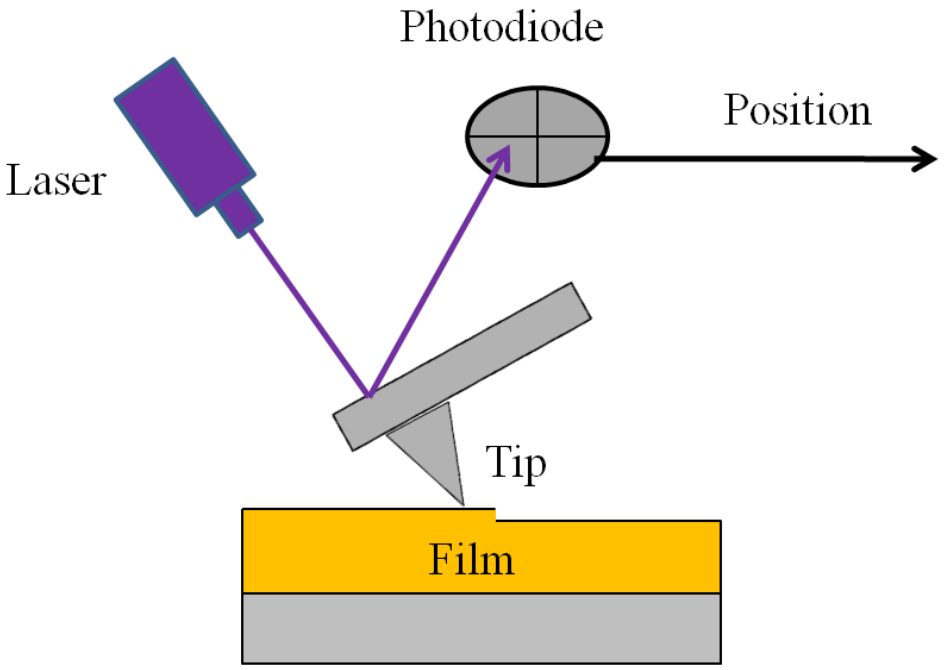

Figure 2.6. *Schematic diagram of Scanning Force Microscopy in contact mode*

2.3. Electrical characterisation

In order to perform the electrical characterisation of the films, top and bottom electrodes (capacitor configuration) are required. Top Pt electrodes of different sizes, between 0.03 and 0.4 mm^2, were deposited by cold D.C. sputtering (BAL-TEC SCD 050) using shadow masks. In order to minimize the effect of the electrical conduction

between these electrodes and the Pt coating of the substrate, firstly a deposition in conditions that reduce the damage of the film is carried out: 40mA for 200s. Then, once this first layer is deposited, more aggressive conditions are used for further Pt deposition (80mA for 100s) until the top electrode is complete. To improve the quality of the final capacitor, a post- annealing treatment was performed at 350^{o}C for 6 min. For the measurements, a contact with the Pt of the substrate is also necessary. Peeling – off one edge of the film with an acidic solution, which dissolves the film but not the Pt bottom electrode, is sufficient. This solution was prepared by mixing fluorhidric acid (HF 48%, Panreac), clorhidric acid (HCL 37%, Panreac) and deionised water in a volume ratio of HF: HCl: H_2O equal to 1:1:15. A small part of the film is immersed inside the solution until the wet part of the film is peeled-off from the substrate. An image of the top and bottom of Pt electrodes can be seen in Figure 2.7.

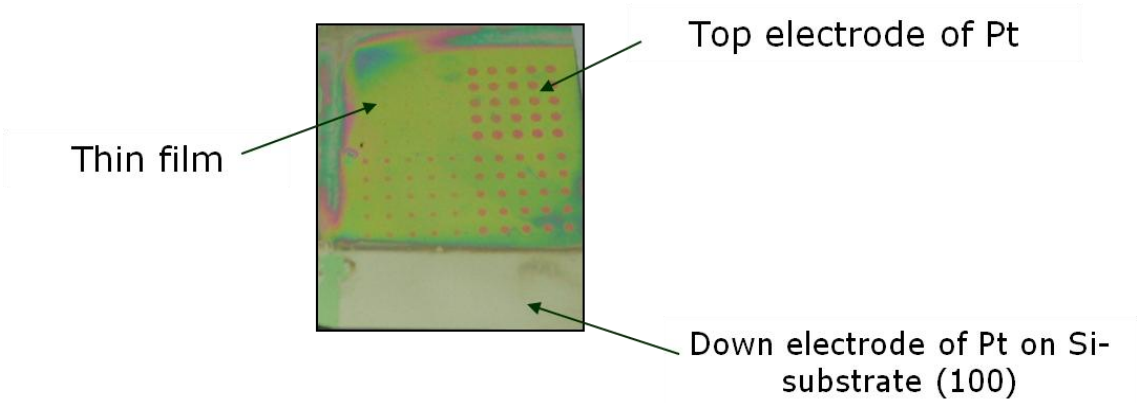

Figure 2.7. *Image of electrodes with various sizes deposited on $PbTiO_3$ film, also showing a bottom electrode area*

2.3.1. Measurement of the relative dielectric permittivity as a function of temperature

The variation of the relative dielectric permittivity (K') with temperature at several frequencies (100 Hz-1 MHz) was obtained from the measurement of the capacitance, C:

$$K' = (C\ t) / (\varepsilon_0\ S) \qquad (1)$$

where t is the thickness of the film, S is the area of the top electrode and ε_o is the vacuum permittivity .

The capacitance is measured with an impedance analyser LCR-meter HP 4284A working with the less-perturbing amplitude signal possible (10 mV), in the temperature range between room temperature and 550ºC. Thus, the temperature at which the material evolves from a ferroelectric (polar) phase to a paraelectric (non-polar) phase could be determined from the dielectric anomaly observed. In this work, the temperature at which the dielectric constant shows a maximum value (dielectric anomaly) was defined as the transition temperature ($T_m \cong T_C$) of the system, usually determined from data collected when going from the paraelectric to the ferroelectric phase (cooling run). A rate of 1.5ºC/s was used in both heating and cooling runs.

2.3.2. Measurement of ferroelectric hysteresis loops

The experimental measurement of the hysteresis loops defines the ferroelectric behaviour of the material. Ferroelectric materials behave as non-linear dielectrics, that is, their polarisation versus applied electric field (P-E) response is not linear, giving rise to the typical hysteresis loop shown in Figure 2.8a. From this measurement, the remnant polarisation ($P_r = (|+P_r| + |-P_r|)/2$) and coercive field ($E_c = (|+E_c| + |-E_c|)/2$) values can be obtained. The slight asymmetry of hysteresis loops respect to the electric field axis is usually due to the existence of internal electric fields (bias electric fields, $E_{bias} = (|+E_c| - |-E_c|)/2$) in the sample.

Another equivalent representation of the inversion of the polarisation with electric field of a ferroelectric material is the current density versus electric field (J-E) hysteresis loops. The ac electric current represents the variation of the polarisation of the material with time ($\delta P/\delta t$). The current maxima peaks depicted in Fig. 2.8b correspond to the polarisation inversion phenomena, the electric field value where the current is maximum, can be identified with the coercive field E_c. The remnant polarisation can be calculated from the areas of those peaks by integration with time. The J vs. E presentation of the hysteresis loop has the advantage of clearly demonstrating the presence of ferroelectric switching in the sample even if the contributions to the current related to conductivity and leakage are large.

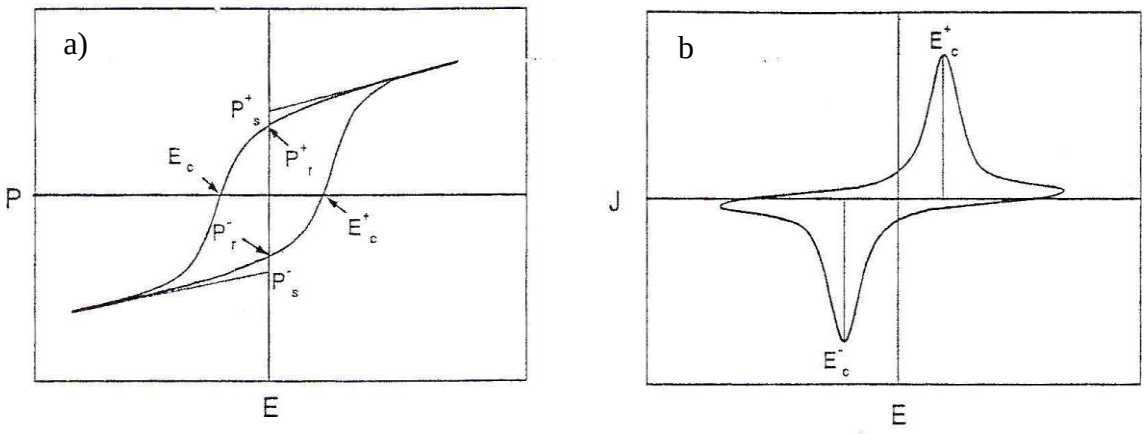

Figure 2.8. *P-E (a) and J-E (b) hysteresis loops typical of a ferroelectric*

Measurements of current density hysteresis loops have been carried out using a virtual ground circuit [11,12] shown in Figure 2.9. Experimental setup consisted of a HP 8116A pulse generator that allows the application of sinusoidal waves with electrical amplitude signals between 0.01-16 V and frequencies of 1-50 MHz. Current intensity generated values, after amplification with a Keithley 428 current amplifier, together with the voltage applied were collected with a Tektronix TDS 520 oscilloscope.

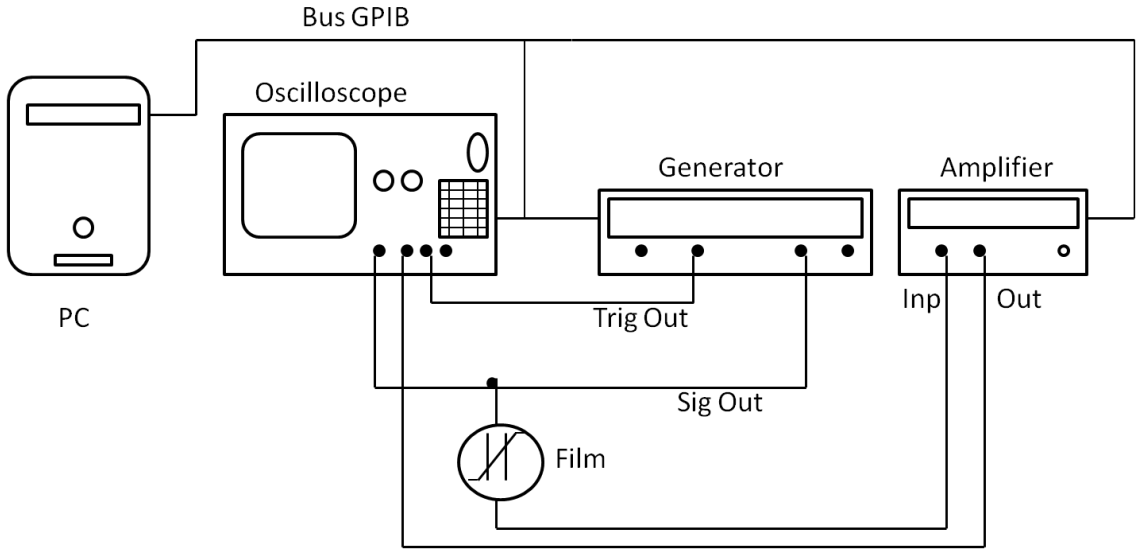

Figure 2.9. *Scheme of the experimental system for measuring current density ferroelectric loops*

Data acquisition and further processing of the data was carried out by home-made software. The integration of the current density loops obtained led to the P-E hysteresis loops. However, the integrated current was compensated by a non-perturbative method [13], since together with the charge generated from the polarisation inversion (ferroelectric current, i_F), contributions due to resistivity (ohmic current, i_R) and film capacity (capacity current, i_C) are also present. More details of these corrections are given in next section.

Additionally, a commercial RT66A standardized ferroelectric test system, the Precision Premier II system, working at a frequency of 1 kHz, was used for measuring P-E hysteresis loops, where a delay time of 1 s between the voltage conditioning and the measuring triangular waves were applied, as it represented in the Figure 2.10a. Also, with this system we used a double bipolar triangular wave (Figure 2.10b), which allows us measuring first a loop after 1s of relaxation and then another "unrelaxed" loop, without this waiting time (Figure 2.11). Note that the Precision Premier II system allows the application of triangular waves with electrical amplitude signals between 0.01-100V.The main difference with the home-made measurements is the delay time of 1 s, which allows us to observe the time relaxation of the polarization, by the comparison of the initial and final polarization values of polarization in the loops. During this time, the non-switching contributions also relax. Therefore, the measured decrease of P_r in the loop, in the case of full retention of the polarization, should be quite similar to the corrected P_r value of the home-made measurements of the hysteresis loops with sinusoidal E fields. In the case that some of the ferroelectric polarization relaxes during the 1 second delay, the relaxed P_r value obtained with the Precision Premier II system will be lower than the one obtained from the home-made measurements, and the difference should be the relaxed ferroelectric polarization.

In this work both systems have been used as the results obtained are complementary. The P_r values obtained from the loops measured with triangular waves in a commercial equipment are directly corrected from the capacitance and conductivity of the ferroelectric capacitor (since they use 1 second relaxation time for tracing the loop) while the loops obtained with sinusoidal waves (home-made system) have to be corrected from the non-switching contributions by a fitting procedure. An explanation of the correction procedure is found in the next section.

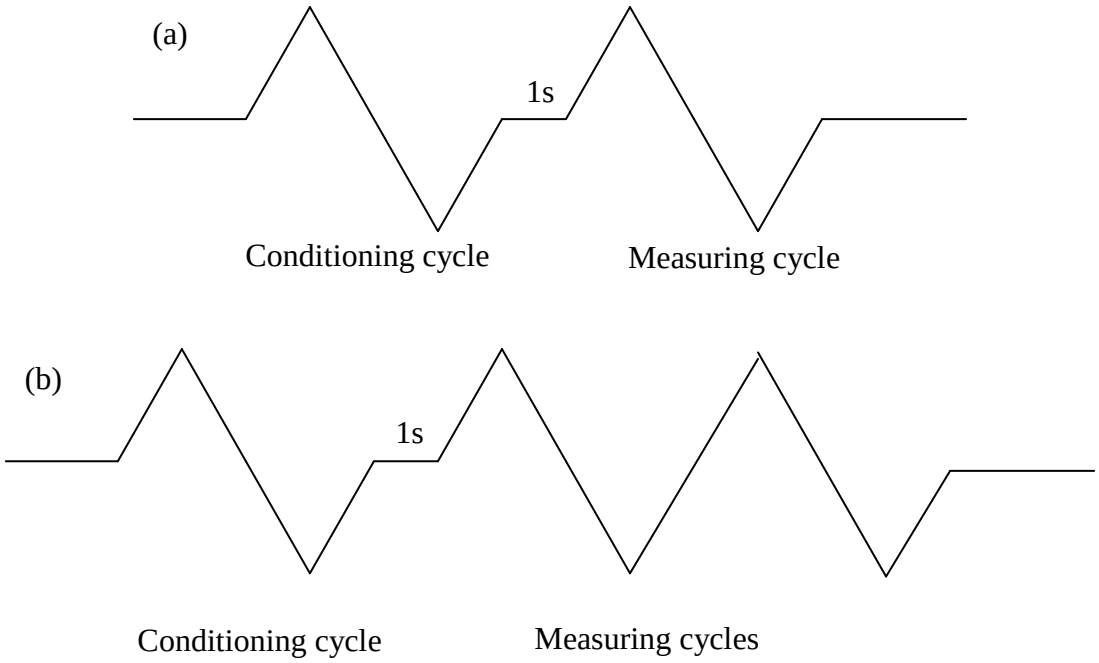

Figure 2.10. *Schematic diagram of (a) single and (b) double bipolar triangular waves used by a commercial RT66A standardized ferroelectric test system*

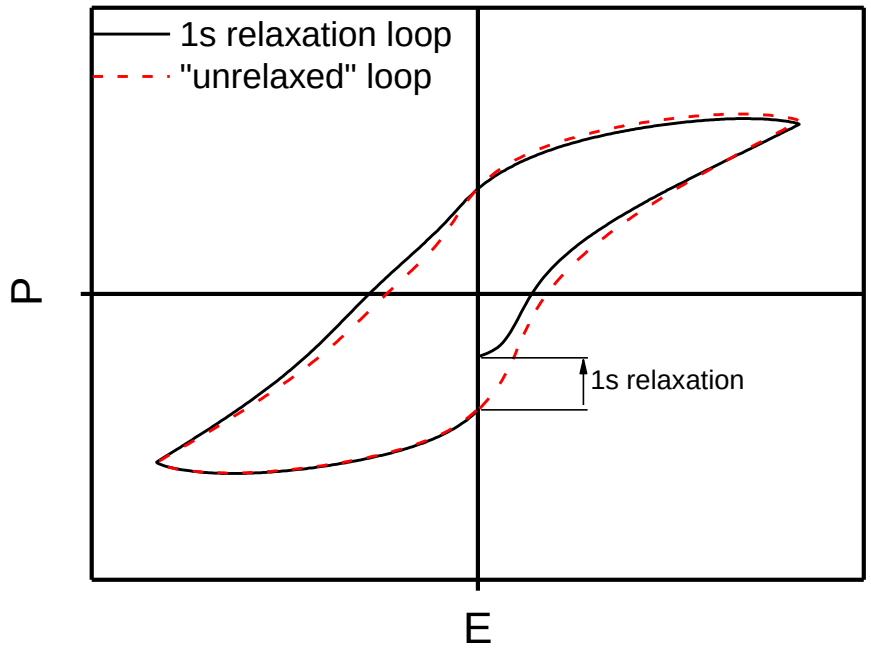

Figure 2.11. *P-E hysteresis loops obtained using the double bipolar triangular wave*

2.3.2.1 Correction method for the non-ferroelectric contributions of the experimental hysteresis loops

Due to the presence of non-ferroelectric switching contributions, the remnant polarization obtained from the experimental loop can be much larger than the real one. These contributions come from the non-relaxed and non-switching accumulated electrical charge associated with finite capacity and resistance of the film studied. In order to eliminate these contributions, the method used is based on that proposed by R. Jimenez et al. [14], in which the fitting of the experimental data to a phenomenological model allows the calculation of these non-ferroelectric contributions and then subtracting them from the experimental data. The model use a hyperbolic tangent function, which can reproduce the switched charge involved in the hysteresis loop of a ferroelectric thin film [15]. The possible asymmetry of the positive and negative switching parts of the ferroelectric hysteresis loops can also be introduced in the model [14]. This difference between the accumulated charges of different sign is attributed to an internal bias field induced by the different interfaces of both electrodes (top and bottom) with the ferroelectric film. Note that the film is deposited on the bottom electrode, and, therefore, subjected to the thermal crystallization process, while the upper electrode was deposited on the film after that. The equation used for the polarization switching, P^+, for positive voltage ramp is:

$$P^+ = P_s \tanh [(V - V_c^+)/2\delta^+] \quad (2)$$

where P_s is the spontaneous polarization, V_c^+ is the coercive voltage, V is the voltage applied and δ^+ defines the shape of the curve of hysteresis from the following equation:

$$\delta^+ = V_c^+ [\log [(1+P_r^-/P_s)/(1- P_r^-/P_s)]^{-1} \quad (3)$$

where P_r^- is the remnant polarization for negative voltage ramp.

The same equations are valid for the negative part of the loop, by changing the superscripts + and -. The non-switching contribution to the total charge Q from the finite capacitance and resistance of the sample was evaluated separately using the equation:

$$Q_{non-switching} = C_{sample} \cdot V(t) + \int_0^{1/f} \left(\frac{V(t)}{R_{sample}}\right) dt \quad (4)$$

where f is the frequency of the applied voltage signal and C_{sample} and R_{sample} are the capacitance and resistance of the sample. It is possible that C_{sample} and R_{sample} at high

fields are slightly different for the positive and negative voltages parts of the loops, which can also be considered [16].

There is another effect that must be also taken into account. This effect is the leakage current, which becomes more important as the thickness of the film decreases. The effect of these currents is important, since they produce a significant increase of the apparent polarization and coercive field to the point of hiding completely the switching phenomena in the deformed charge loops. It should be noted that leakage currents are not electrical displacement currents but real electric currents. They are associated with a continuous current phenomenon that is electronic in nature, while the contributions to the conductivity of the loops are related to ionic conductivity, electronic conductivity or mixed conductivity. The effect of the leakage currents can be large and near to the limit at which irreversible degradation occurs in the sample. In order to understand the contribution from the leakage current, we consider that the contribution of leakage currents in the experimental current loops can be represented by a non-linear almost parabolic behavior with the applied field, usually proportional to V^2. In the case of the tunneling currents or Space Charge Conduction Limited (SCLC), the exponent varies between 2 and 3.5 before entering into the degradation region [17]. Due to this behavior the leakage current can increase several orders of magnitude in a narrow range of applied fields, being the dominant contribution to the measured current at times of the order of those needed to measure the hysteresis loops in thin films (ms). Consequently, to take into account the contributions of the leakage currents in the proposed model is necessary to add a third term to the non-switching contribution. According to the leakage model of the works of Juan et al. [18].and Rose [19], the conduction current density can be of the form $J \propto V^n/t^3$, where t is the thickness of the film and n is an exponent. Due to the voltage sweep to perform the measurement of the hysteresis loop, it is also necessary to introduce a threshold voltage, above which the leakage currents are considered contributions to the current response, and below which only linear conductivity is considered. From these considerations the charge coming from the leakage current contribution to the hysteresis loop can be represented by:

$$Q_{leakage} = C_{sample} \cdot V(t) + \int_0^{1/f} B \cdot A \cdot (V(t) - V_0)^e \, dt \qquad (5)$$

where B is a constant of proportionality, A is the area of the electrode, V_0 is the threshold voltage at which leakage currents begin to dominate, and e is an exponent

with values between 2 and 3. In the proposed model a simple approximation is made, and the exponent e is fixed in the voltage range in which the leakage current is considered. This is just a necessary simplification, because the exponent may vary with the applied field [17]. Due to the fact that in ferroelectric thin films the leakage current is a phenomenon usually related to the ferroelectric / metal interfaces, in the model we can also insert asymmetry leakage contributions for positive and negative voltages [20].

It should be noted that the objective in this study is not to study the model of the leakage currents in thin films, but to correct the loops with a function that reproduces approximately the experimental leakage currents so that we can obtain ferroelectric loops with only switching contributions, which allows comparison between the single and MLC films measured in the same experimental conditions.

Taking into account the contributions from equations 4 and 5, we can use the following expression for the total charge involved in a hysteresis loop.

$$Q_{total}(V) = P^{\pm}(V) + Q^{\pm}_{non\text{-}switch}(V) + Q^{\pm}_{leakage}(V) \quad (6)$$

By using least squares algorithm to be applicable to the nonlinear fitting of the experimental data, we can obtain the spontaneous and remnant polarizations, the coercive fields, the shape factor $\delta^{\pm}_{n}$ (the higher this parameter the more slanted the loop and, thus, the lower P_r/P_s ratio is), the resistance and capacity of the sample for positive and negative voltages, as well as the parameters describing the leakage currents: e, V_0 and B.

To show graphically the corrections of the loops in Figure 2.12 there is an example of the correction of the non-switching contributions due to the capacitance and resistance in a $PbTiO_3$ film. The figure shows the J-E and the corresponding P-E loops obtained by integration. At high field we can observe the "rounding" of the experimental hysteresis loop, a consequence of the non-switching charge, which disappears when the correction is performed. In films with columnar grain growth, leakage currents begin to be important; as it can be seen in Figure 2.13. This can also be corrected to obtain hysteresis loops with only contributions coming from the polarization switching. To demonstrate the validity of the proposed model, we find that the fitted values after adjustment of capacity and resistance of the film does not differ greatly from the experimentally measured values.

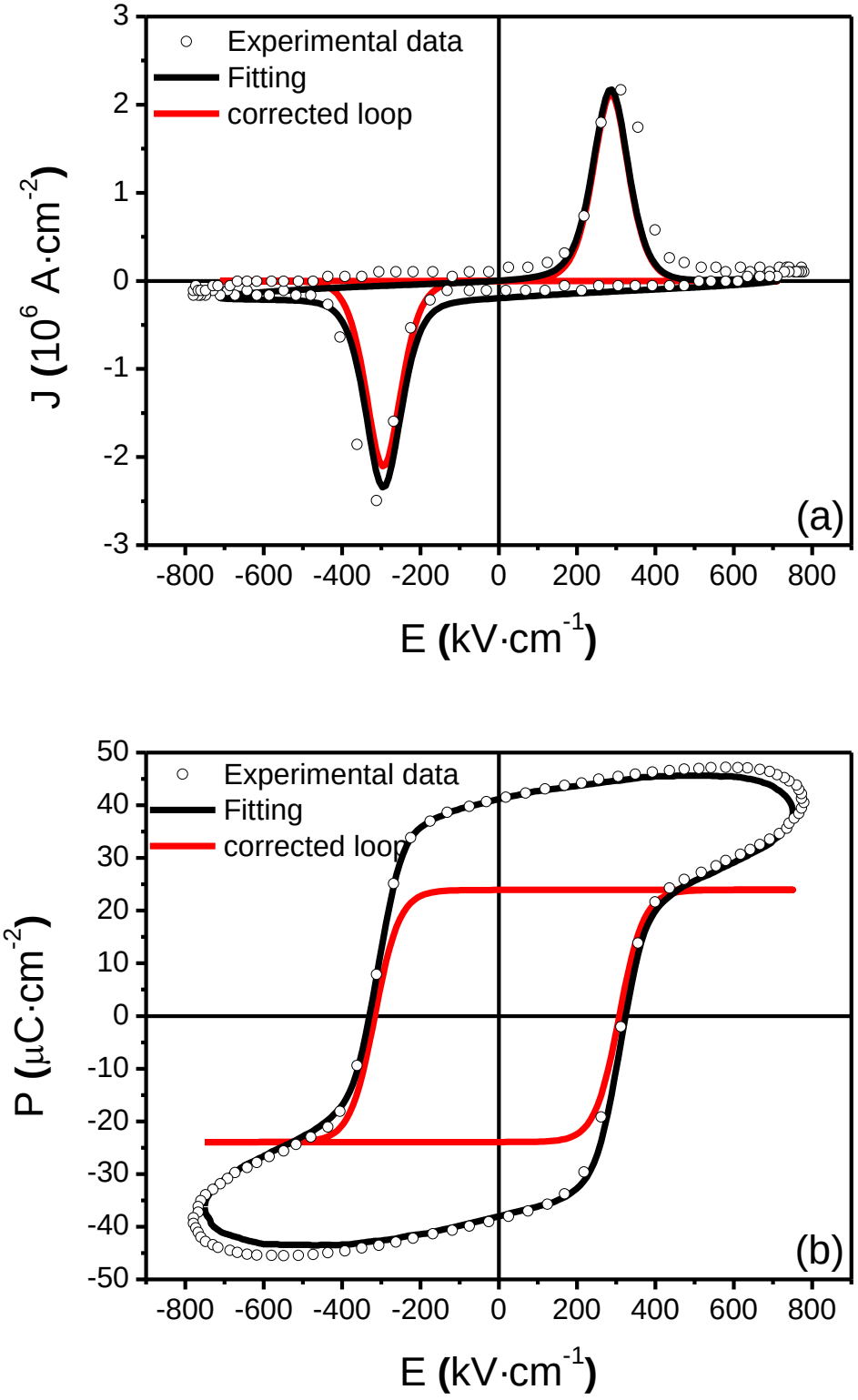

Figure 2.12. *(a) J-E experimental hysteresis loop with the fitting to the model proposed, together with the corrected ferroelectric switching loop without contributions from the capacity and the resistance of the film and (b) the corresponding P-E loops of a $PbTiO_3$ film*

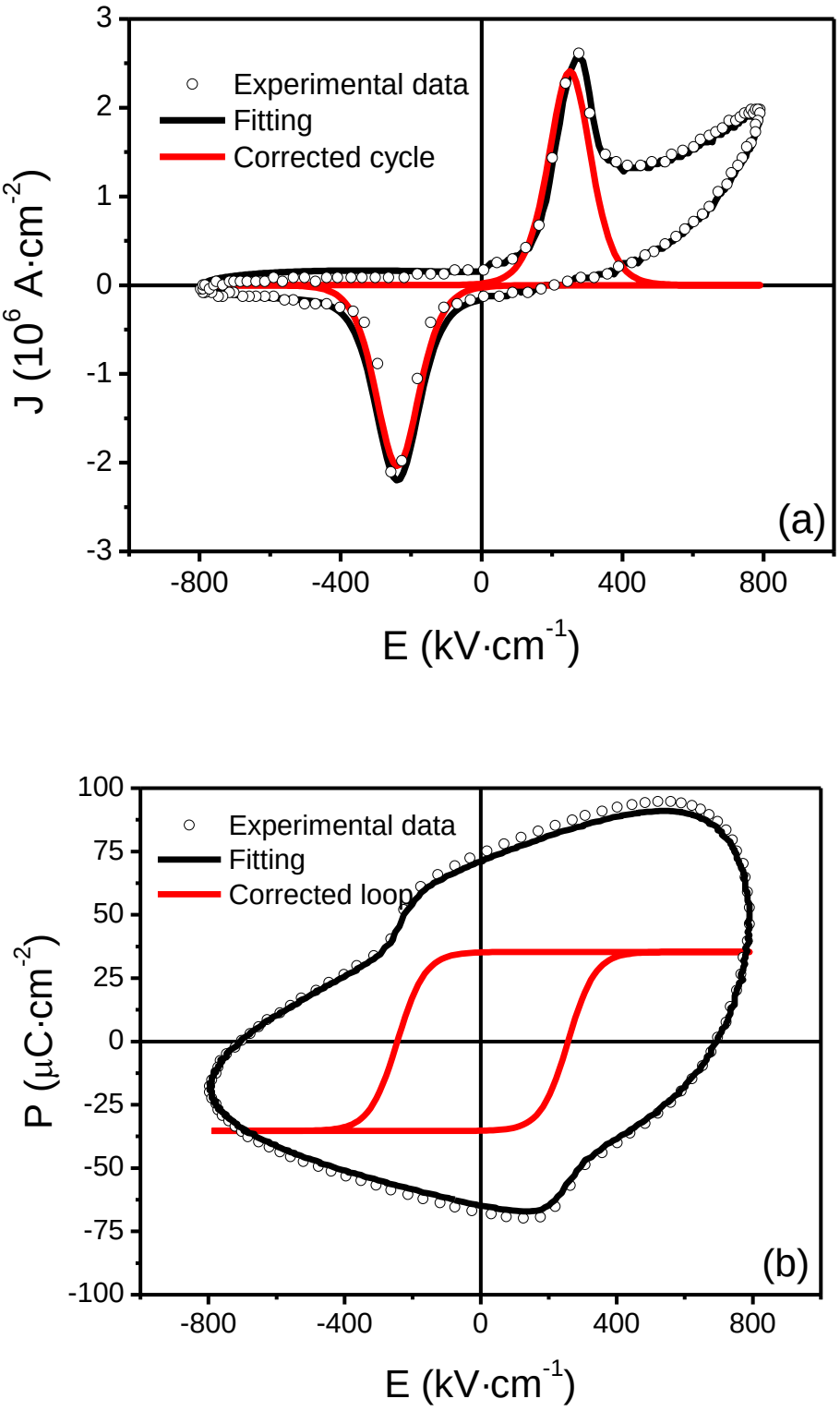

Figure 2.13. *(a) J-E experimental hysteresis loops with the fitting to the model proposed, together with the ferroelectric switching loop without contributions from non- switching and leakage current of the film and (b) the corresponding P-E loops of a $PbTiO_3$ film with columnar grain growth*

To demonstrate the validity of the approximations used in these models, the values of the remnant polarization P_r obtained from the corrected ferroelectric hysteresis loops and those deduced from measurements of switching currents (see next section for details on how to perform these measurements) are compared in Figure 2.14. It is verified that the values do not vary significantly. The ferroelectric hysteresis loop gives a corrected value of P_r of 40 μ.C·cm^{-2}, while calculating the area under the curve of the switching currents results in a value of non volatile polarization 39 μ.C·cm^{-2}, confirming the validity of the corrections made in the experimental cycles.

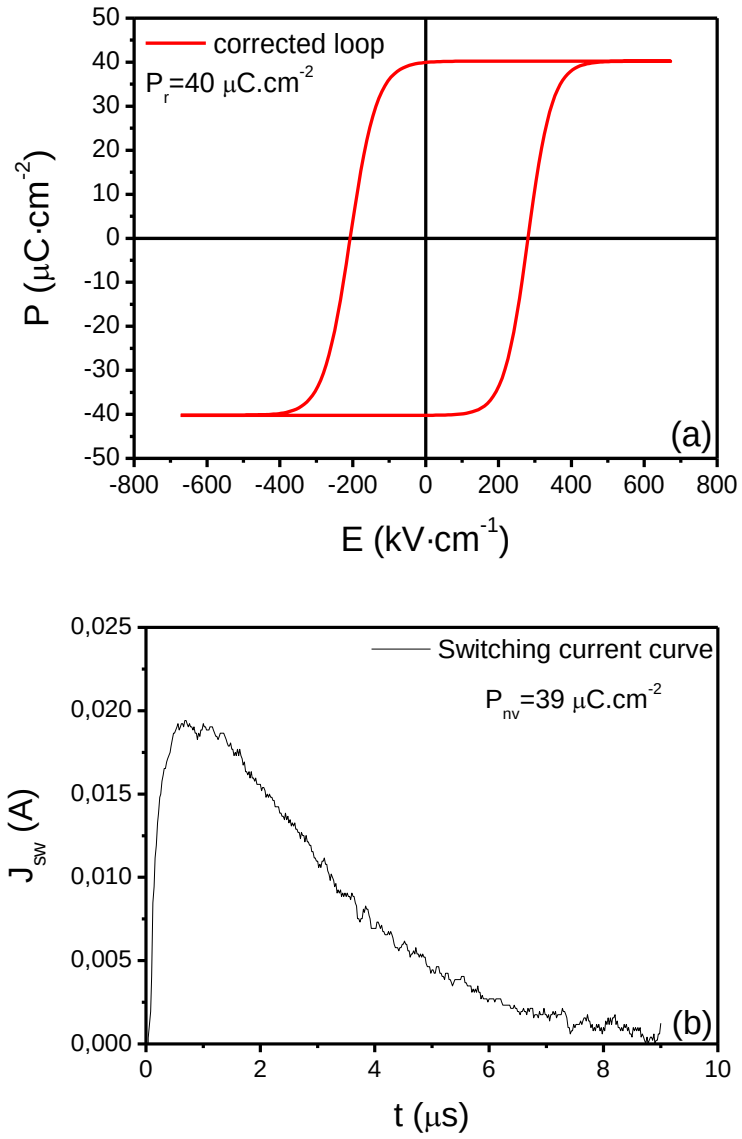

Figure 2.14. *(a) Remnant polarization P_r for a $PbTiO_3$ film obtained from a corrected hysteresis loop and (b) non-volatile P_{nv} from the integration of a switching current curve*

2.3.3. Measurement of switching current curves

During the switching process the reorientation of the polarization produces variations of the accumulated charge on the surface of the material, which results in electric currents. From the measurement of these induced currents, we can obtain information on the switching kinetics. Figure 2.15 shows the experimental set-up used for these measurements [11]. It consists basically of a HP 8116A function generator to apply electric field pulses to the film and an oscilloscope that measures the voltage drop in the resistance of 50 Ω due to the current induced by the electric pulses in the film.

For poling we used a series of pulses between 2 and 16 V with a duration of 10 μs each, and 20 μs between pulses, to get a proper poling of the film in the direction of field P_0 (Figure 2.16): "writing pulse". After waiting 300 ms the application of another pulse P_1 of opposite sign produces the switching of the polarization A second pulse P_2 with the same value and sign of the electric field leaves the polarization unchanged ("reading pulses" Figure 2.16)

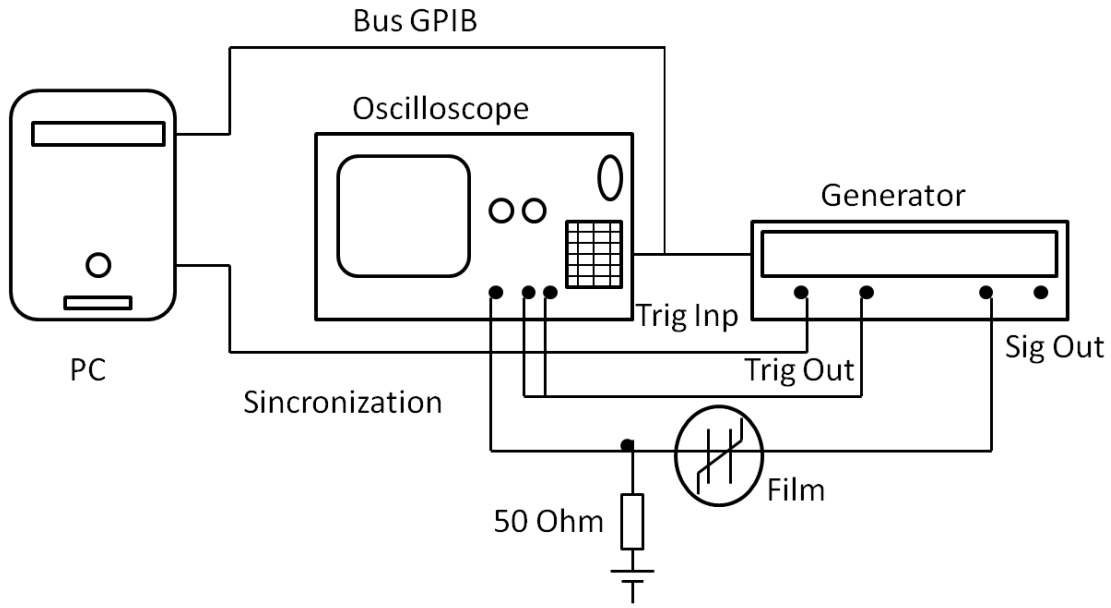

Figure 2.15. *Experimental set-up for measuring the switching current density [11]*

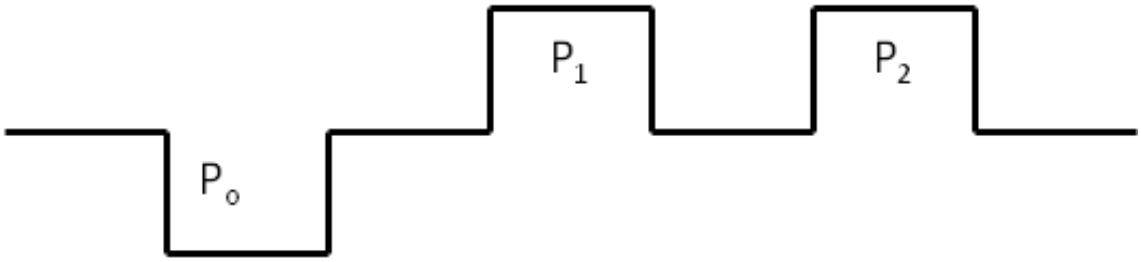

Figure 2.16. *Sequence of pulses of applying the electric field for measurement of switching currents: P_0-polarization writing pulse, P_1- first reading pulse, P_2-second reading pulse*

The currents induced for both pulses (P_1 and P_2) contain contributions associated to the capacitor discharge. Only the current obtained from the first reading pulse P_1 contains contributions coming from the polarization switching. Therefore, the difference of the currents measured in the first and second reading pulses is an estimate of the switching current density: $J_{sw} = J_1 - J_2$. An example for the experimental current curve obtained and the calculation of J_{sw} can be shown in Figure 2.17.

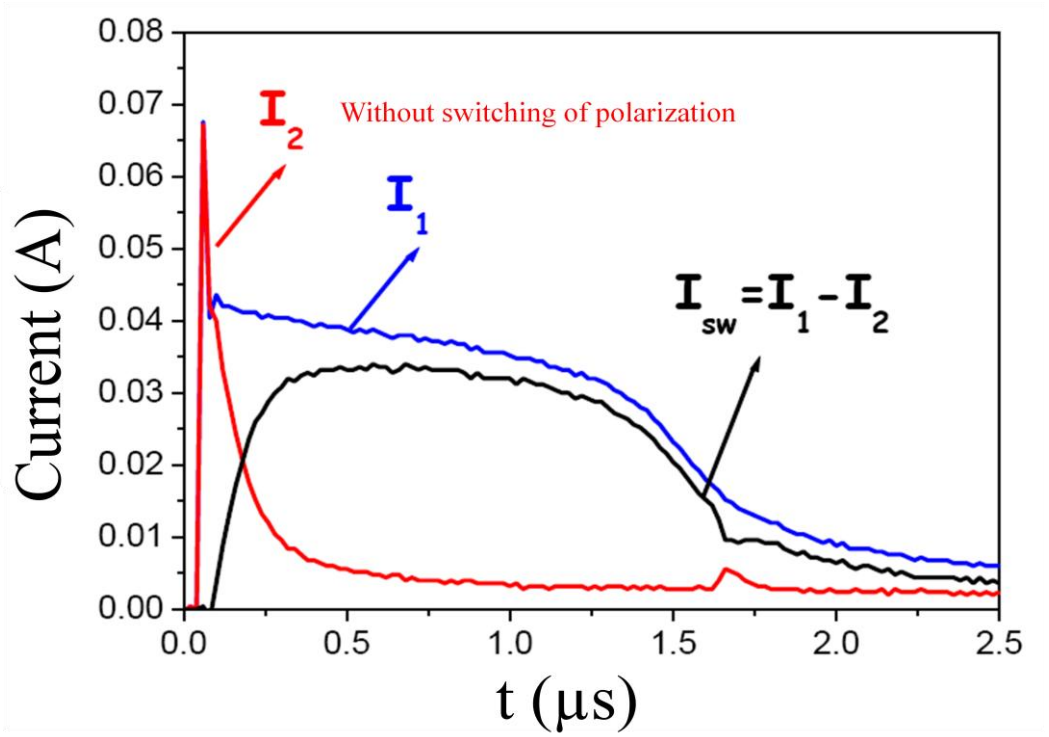

Figure 2.17. *Experimental curves of the currents obtained with polarization pulses P_1 (I_1) and P_2 (I_2) and the switching current (I_{SW}) calculated from them*

From the curve of switching current, it is possible to obtain the value of the non-volatile polarization, P_{nv} that can be defined as:

$$P_{nv} = \int_0^t J_{sw}(t)dt \,/2 \quad (7)$$

As the ferroelectric film is not ideal, during the waiting time at V=0, there is a depolarization so that the second pulse will pole again the condenser, with some degree of switching of the polarization. From these measurements, therefore, we obtain a relaxed ferroelectric polarization, i.e., the non volatile polarization, P_{nv}, which is usually smaller than the remnant polarization P_r.

2.3.4. Characterization of the polarization retention

In this thesis two different approaches have been used to characterize the retention of the polarization with time. One is based on direct polarization measurements and the other relies on the observation of the evolution with time of the pyroelectric coefficient.

2.3.4.1. Direct measurement of the polarization retention

The procedure is very similar to the one applied to measure the switching current, although the objective in this case is the determination of the switching charge and analyze its decay after the application of an electric field. The first step is the poling of the sample in a specific direction by the application of a train of electric pulses (Figure 2.18) [21]. Then, after the waiting time, t_{ret}, a second pulse is applied with amplitude equal to the poling pulses but in the opposite direction, which we call measurement or reading pulses. We measured the integrated charge from the beginning of the pulse until it reaches the maximum voltage. This charge includes the switching charge, but also other contributions, like the one corresponding to the charge of the capacitor. After 1 second, the measurement was repeated with an identical electric pulse. The measured charge this time should not include any switching contribution. The difference between the charges obtained in both pulses gives us the switching charge, i.e., the remaining switchable polarization after a time t_{ret}, which is a measurement of the retention of the polarization. After 1 s, a new poling of the sample is carried out and the experiment is repeated successively for increasing t_{ret}.

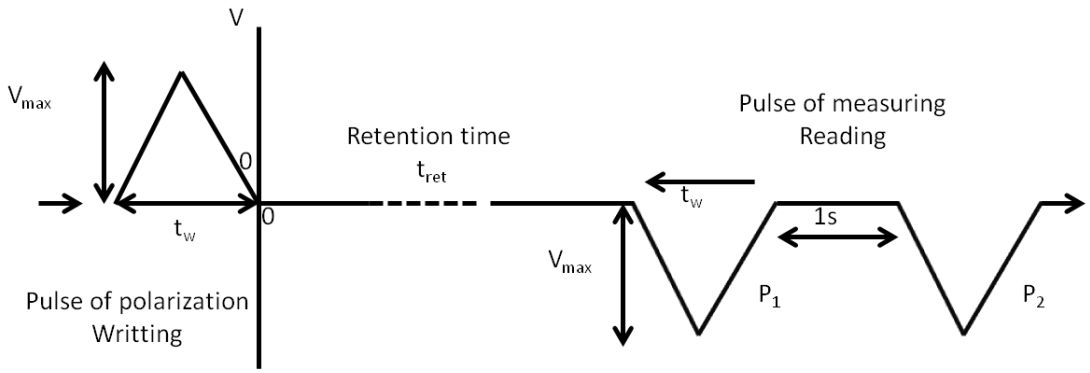

Figure 2.18. *Schematic diagram of the signal applied during the retention measurement of the ferroelectric polarization*

2.3.4.2.Evolution of the pyroelectric coefficient with time

The difficulties associated to the direct method of study of the retention of the polarization, which is very time consuming, can be avoided by an indirect method, in which the evolution with time after poling of a coefficient directly related to the polarization is used. A good choice is the pyroelectric coefficient (γ) and that is the parameter that it will be used in this thesis. The pyroelectric measurements were performed using a dynamic method [22,23]. Triangular thermal waves with 2 K of amplitude and frequency $2 \cdot 10^{-3}$ Hz are used, around a temperature of 308 K. The thermo-stimulated current obtained can be described by the equation:

$$I_{pyr} = A \cdot \gamma \cdot dT/dt \quad (8)$$

where A is the area of the capacitor and γ is the pyroelectric coefficient.

In general, it is necessary to pole the material before making pyroelectric measurements. Figure 2.19 shows the triangular thermal wave applied and the current generated in the thin film. There is a background current signal superimposed to the pyroelectric response, which usually decreases with time. The resultant current has two contributions, one resulting from the free charge generated during the polarization and the other from depolarization. Therefore, the pyroelectric coefficient is obtained from the following equation:

$$\gamma = (J_+ + J_-)/2 \; dT/dt \quad (9)$$

where dT/dt is the heating rate.

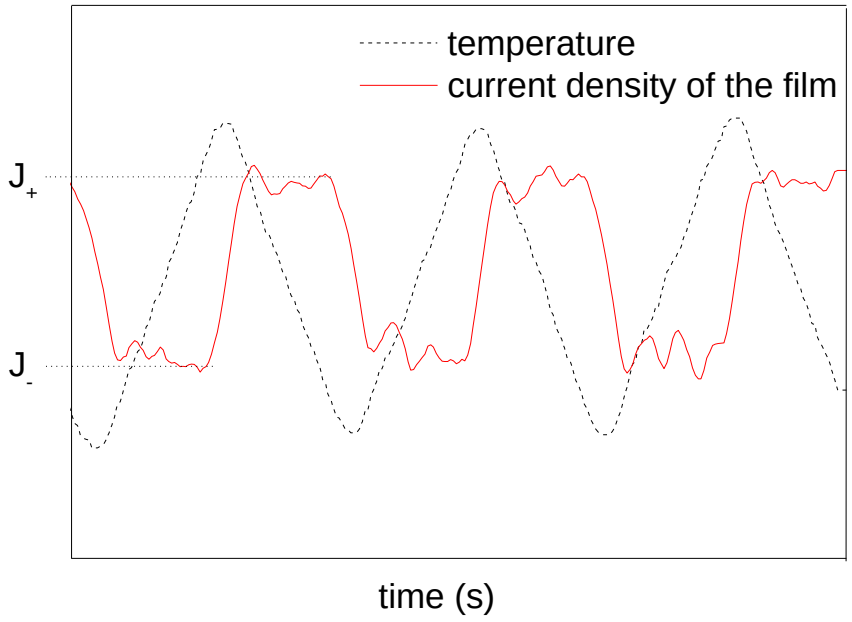

Figure 2.19. *Triangular thermal wave applied and current generated from the pyroelectric response of the thin film*

2.4. Piezoelectric characterization

2.4.1. Local piezoelectric characterization: Piezoresponse Force Microscopy

For the local characterization of the piezoelectric behavior of the films, we used Piezoresponse Force Microscopy (PFM). The PFM principle was originally demonstrated in a series of seminal works [24-27], although the term PFM was coined later [28]. It is based on the application of an electric field between a conductive tip and the piezoelectric sample, which causes a deformation in the material due to the inverse piezoelectric effect. This deformation is detected by the deflection of the cantilever holding the tip, similarly to conventional scanning force microscopy (Figure 2.20). In order to facilitate the detection of the small deformation induced by the electric field, we apply an alternating electric field: $V\cos(\omega t)$. The resulting displacement, d, experienced by the surface is detected by the photodiode, and analyzed with a lock-in amplifier:

$$d = A\cos(\omega t + \varphi) \qquad (10)$$

From here we can obtain the values of the amplitude of the deformation induced (A) and the phase (φ).

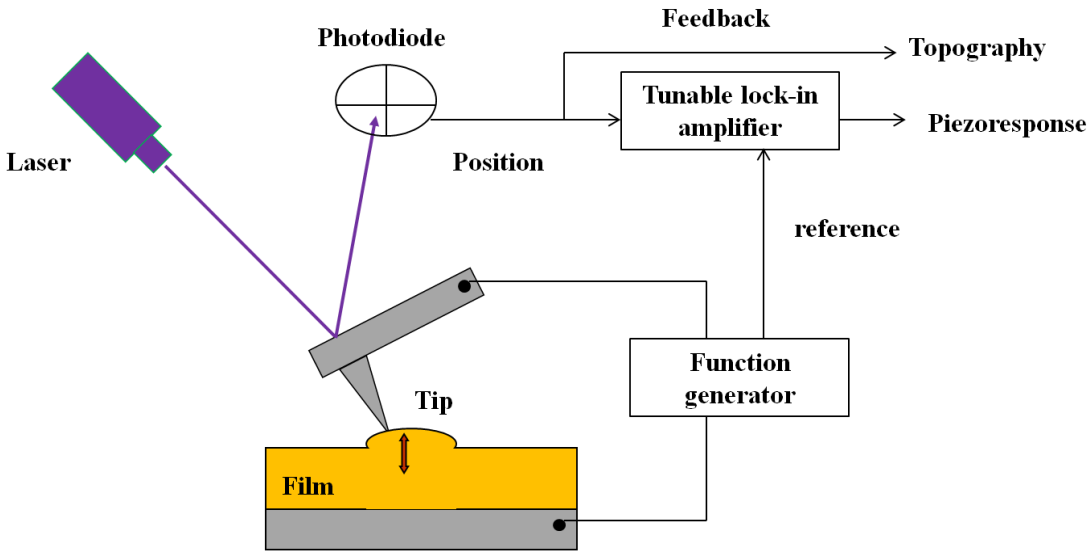

Figure 2.20. *Schematic representation of a Piezoresponse Force Microscope*

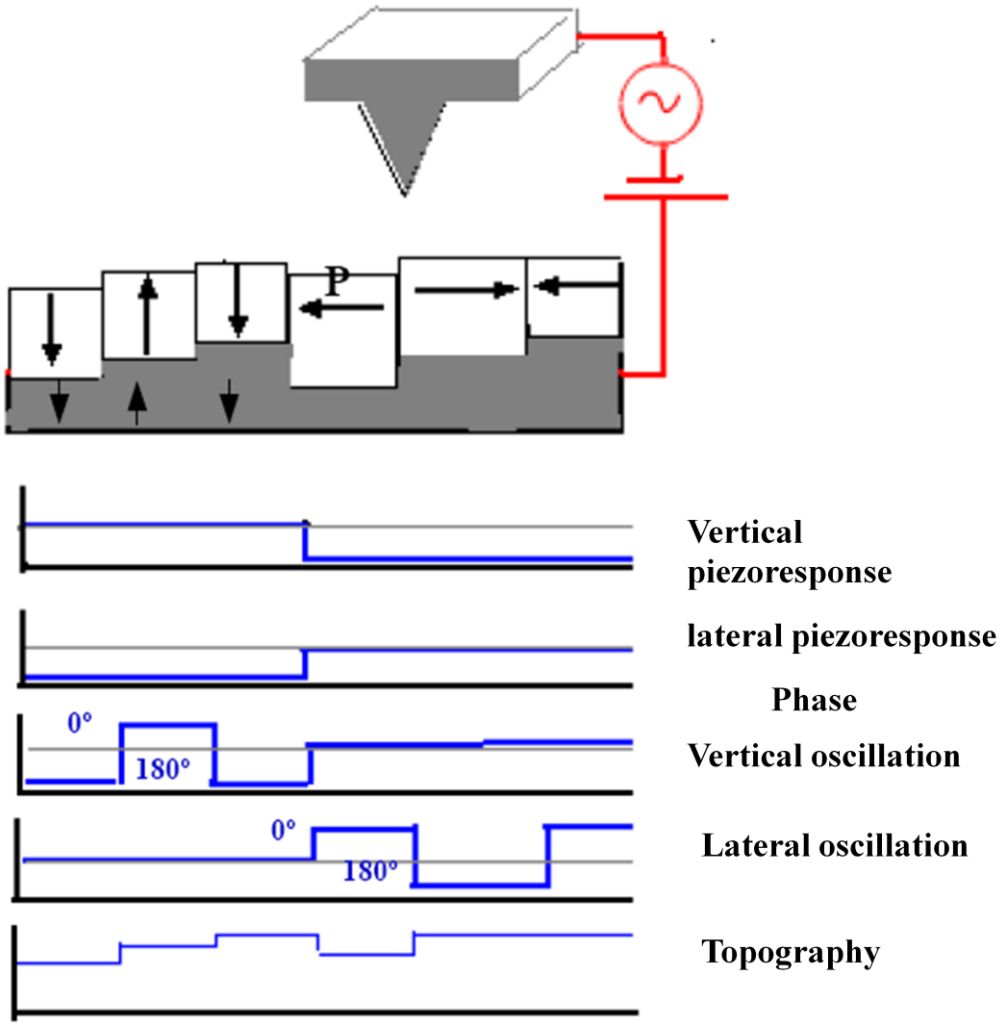

Figure 2.21. *Schematic illustration of the different responses in amplitude and phase of the piezoresponse obtained from areas with different polarization vectors P*

The amplitude A is related to the effective piezoelectric coefficient of the material. The phase φ provides information about the direction of the polarization vector. If the electric field and the component of the polarization in that direction have the same sense, the deformation of the material and the applied field are in phase, and $\varphi=0^{o}$. However, when both vectors are antiparallel, the measured displacements and the electric field are out of phase, and $\varphi=180^{o}$. We can analyze the response of the material out-of-plane or in-plane, depending on whether the measured deflections of the cantilever are normal or lateral. The variations of the piezoelectric response in different regions of the material, obtained by scanning the sample surface with the tip, allows us to obtain a map of the distribution of polarization in the material (Figure 2.21), and, therefore, the configurations of the ferroelectric domains [29].

Besides, it is possible to measure local piezoelectric hysteresis loops. They allow the study of the ferroelectric character of each individual grain in polycrystalline materials. There are two different approaches for obtaining PFM hysteresis loops [30,31], as shown in Figure 2.22: In the first one, an increasing bias is applied in a staircase way, while measuring the piezoresponse signal at every step with an AC signal. This is called in-field hysteresis loop. In the second type, the bias is applied in pulses of increasing or decreasing value, while the piezoresponse is measured between pulses. This kind of hysteresis loops is called remnant hysteresis loops, because the piezoresponse signal is measured when the ferroelectric materials is in its remnant state, at zero field.

Note that the in-field loops have an important electrostatic contribution, while remnant loops are influenced by the pulse duration and the time between the pulses. The pulse duration influences the coercive field obtained and the time interval between pulses affects the values of the coefficient d_{33}^{eff}.

Measurements are made using the tip of the cantilever as top-electrode. This implies that the applied field is not uniform with field lines resembling an umbrella. This, together with other factors related to the calibration of the piezoelectric coefficients, makes the measured values of d_{33} not quantitative [32].

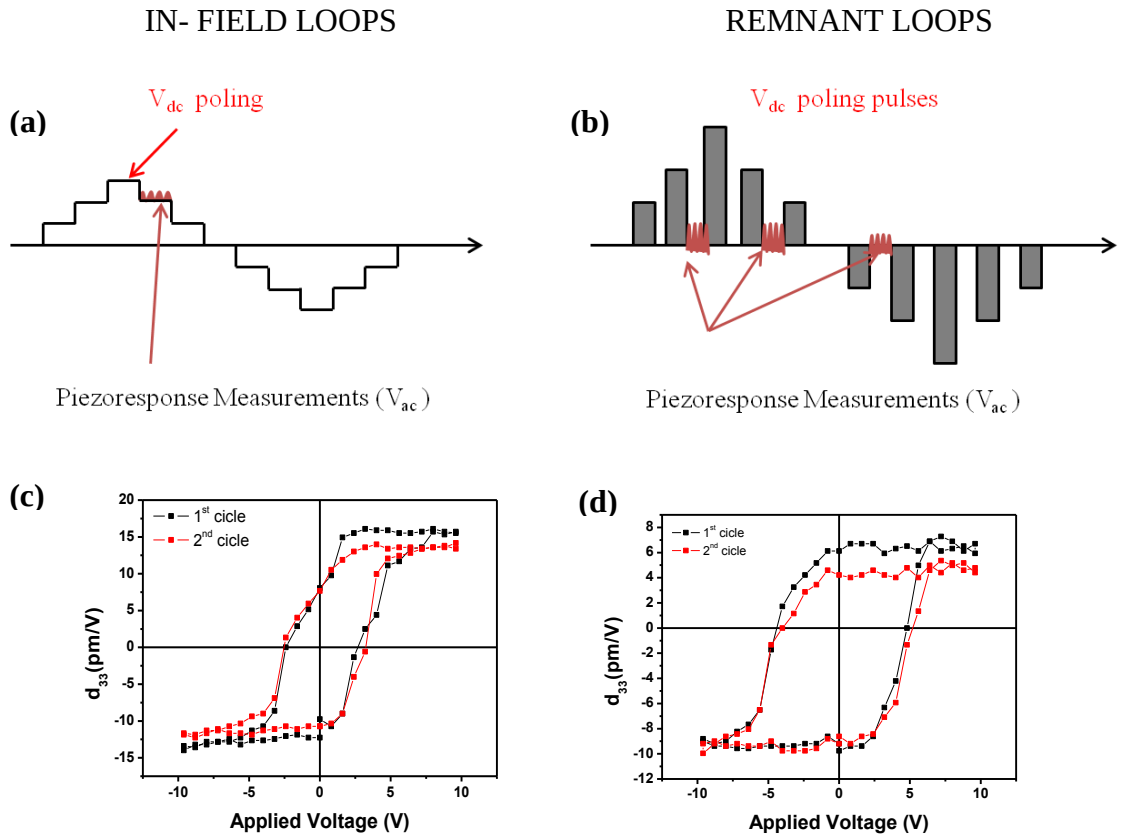

Figure 2.22. *Scheme of measuring (a) in-field and (b) remnant local piezoelectric loops and the experimental loops obtained for a ferroelectric thin film (c) in- field and (d) remnant*

The local piezoelectric characterization was carried out with a commercial scanning force microscope (Nanotec® Electrónica, controlled by WSxM® software [10]) in which Piezoresponse Force Microscopy (PFM) has been implemented with a lock-in amplifier 7265 DSP and a function generator Agilent 33120. In this work conductive Pt/Ir coated tips (Nanosensors) on cantilevers with a force constant of 42 $N \cdot m^{-1}$ and a resonance frequency of 320 kHz were used, with an applied AC voltage of 1 V at 50 kHz. In-field local piezoelectric hysteresis loops have been measured at different locations of the studied films.

2.4.2. Characterization of piezoelectric coefficients by interferometry

Macroscopic piezoelectric hysteresis loops were obtained by using a fibre optic, double-beam incidence Mach–Zehnder interferometer [33]. This is one of the best options for the measurement of piezoelectric behaviour in thin films, where the induced

displacements are small and, besides, the film is attached to a substrate. The basic schematic drawing of the interferometer is shown in Fig. 2.23. The interferometer is illuminated by a stabilized controllable laser working at λ= 1550 nm. This laser is equipped with an optical isolator and a fibre-optic plot, in order to avoid reflections and to maximize the optical input power. Afterwards, a directional coupler is used to provide the reference and signal waves.

In the reference arm of the interferometer, a length of fibre is wrapped around a piezoelectric ring with several turns under a small tension. This piezoelectric ring is used for phase modulation and also for setting the interferometer at the maximum sensitivity point.

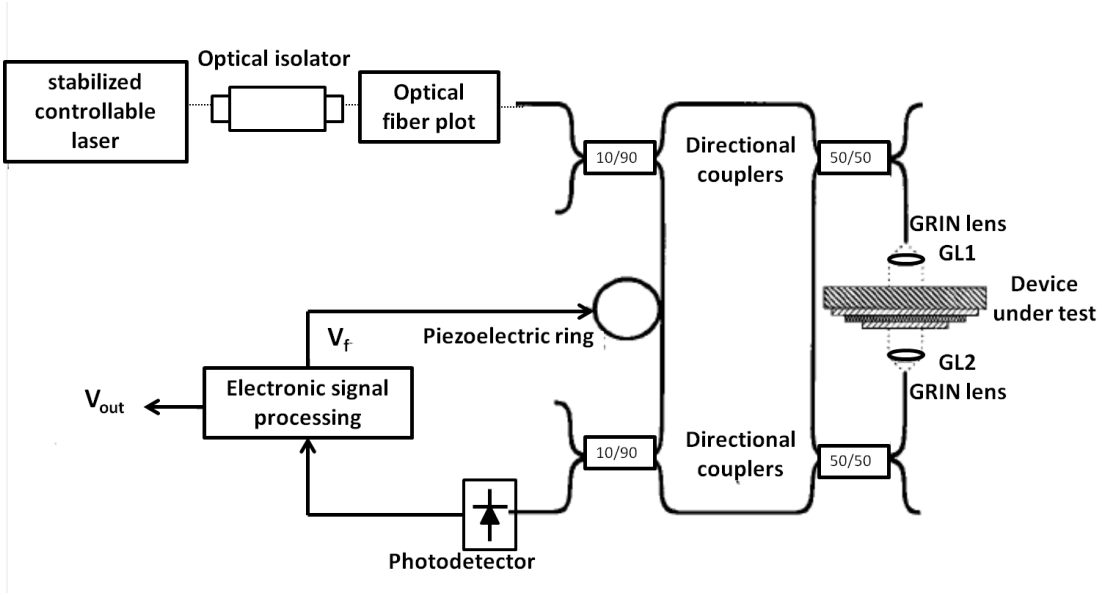

Figure 2.23. *Schematic diagram of the optical interferometer*

In the sensing arm of the interferometer, the emergent beam of the first directional coupler is collimated by a GRIN lens (GL1), reflected at the polished back face of the substrate and reinjected into the interferometer. This signal is transmitted to the second directional coupler, exits one of its output ports and another reflection occurs at the top electrode of the sample before being reinjected again into the fibre.

The waves propagated through the reference and sensing arms are combined in the output directional coupler, where they interfere. The resulting optical power is sensed by a pig tailed photodetector/low-noise amplifier combination.

The input and output directional couplers are characterized by a 90/10 coupling ratio, with 90% of the input optical power coupled to the sensing arm of the interferometer. This ratio was adopted in order to enhance the optical signal in that arm, taking into account the significant power loss in the GRIN lens-sample sections. The two other couplers have a nominal coupling ratio of 50/50, for optimizing power transmission along the sensing arm of the interferometer.

Expressing the optical path difference (OPD) between the reference arm (OP_R) and the sensing arm (OP_S) in terms of these quantities, and considering time variations, we have:

$$OPD(t) = OP_R - OP_S(t) = OPD_0 \pm 2\,\Delta L\,(t) \qquad (11)$$

where OPD_0 is the constant optical path difference between the two arms when the sample is not excited. Therefore, the optical path difference between the two arms of the interferometer is proportional to twice the thickness change of the piezoelectric thin film, and it is independent of the substrate bending effect. ΔL is the thickness change in the direction of the applied field, being L the initial thickness of the piezoelectric thin film. The deformation S_3 is, therefore, $\Delta L/L$. As the electric field is $E_3 = V_{in} / L$, where V_{in} is the applied voltage, the expression of the d_{33} coefficient is given in terms of two directly measurable quantities: ΔL and V_{in} by:

$$d_{33} = S_3/E_3 = \Delta L/V_{in} \qquad (12)$$

Note that the piezoelectric thin film is clamped to a substrate. Accordingly, the measured quantity S_3/E_3 does not represent the real d_{33} piezoelectric coefficient of the thin film (which is defined for a free sample), but in fact an effective value, which can be defined by:

$$d_{33}^{eff} = d_{33} - 2\,d_{31}\,(s_{13}^E / s_{11}^E + s_{12}^E) \qquad (13)$$

where s_{11} , s_{12} , and s_{13} are the mechanical compliances of the piezoelectric film and d_{31} is the transverse piezoelectric coefficient. It should be noted that since d_{31}, s_{12}, and s_{13} are usually negative and s_{11} positive and larger than s_{12}, d_{33}^{eff} is always smaller than d_{33}.

In this work, the macroscopic piezoelectric hysteresis loops were carried out by using a fibre optic, double-beam incidence Mach–Zehnder interferometer at INESC TEC – INESC Technology and Science, Portugal. The measurements were performed

using an AC driving voltage of 5V at 7.5 kHz, while the DC electric field was changed from 100 to 200 $kV \cdot cm^{-1}$.

2.5.References

[1] N.J. Phillips, M.L. Calzada, S.J. Milne, J. Non- Cryst. Solids 147, 285 (1992)

[2] M.L. Calzada, A. González, J. Am. Ceram. Soc. 88, 2702 (2005)

[3] M.L. Calzada, M. Algueró, A. Santos, M. Stewart, M.G. Cain, L. Pardo, J. Mater. Res. 24, 526 (2009)

[4] D.E. Bornside, C.W. Macosko, L.E. Scriven, J. Imag. Technol. 13, 122 (1987)

[5] L.E. Scriven "Physics and application of dip-coating and spin coating". In Better Ceramics Through Chemistry III, ed. C.J. Brinker, D.E. Clark, and D.R. Ulrich (Materials Research Society, Pittsburgh, 1988).

[6] R.W. Schwartz, J.A. Voigt, C.D. Buchheit, T.J. Boyle., Ceram. Trans. Ferroic Mater.: Design, Prep. Char. 43, 145 (1994)

[7] J.L. Keddie, E.P. Giannelis., J. Am. Ceram. Soc. 74, 2669 (1991)

[8] I. Bretos, "Low-toxic chemical solution deposition methods for the preparation of multifunctional $(Pb_{1-x}Ca_x)TiO_3$ thin films", PhD Thesis. Universidad Autónoma de Madrid (2006)

[9] J. Mendiola, M.L. Calzada, P. Ramos, M.J. Martín, F. Agulló-Rueda, Thin Solid Films 315, 95 (1998)

[10] I. Horcas, R. Fernández, J.M. Gómez-Rodríguez, J. Colchero, J. Gómez-Herrero, A.M. Baro, Rev. Sci. Instrum. 78, 013705 (2007)

[11] P. Ramos "Estudio de la ferroelectricidad en láminas delgadas de titanato de plomo modificados, obtenidas por sol-gel". PhD Thesis. Universidad Autónoma de Madrid (1996)

[12] D. Rivero, L. Pardo, R. Jiménez, Revista Cubana De Física 26, 169 (2009)

[13] R. Jiménez, R. Fernández, J. Ricote, "Leakage current compensation of ferroelectric hysteresis loops in ultrathin film capacitors". Piezo 2009, Electroceramics for End Users IV, Zakopane, Poland (2009)

[14] R. Jiménez, C. Alemany, M.L. Calzada, A. González, J. Ricote, J. Mendiola, Appl. Phys. A 75, 607 (2002)

[15] S.L. Millar, R.D. Nasby, J.R. Schwank, M.S. Rodgers, P.V. Dresendorfer, J. Appl. Phys. 68, 6463 (1990)

[16] R. Jiménez, C. Alemany, A. González, M.L. Calzada, J. Mendiola, Integr. Ferroel. 47, 227 (2002)

[17] H. Hu, S. B. Krupanidhf, J. Mater. Res. 9, 1484 (1994)

[18] T.P. Juan, S. Chen, J. Y. Lee, J. Appl. Phys. 95, 3120 (2004)

[19] A. Rose, Phys. Rev. 97, 1538 (1955)

[20] R. Meyer, R. Waser, K. Prume, T. Schmitz, S. Tiedke, Appl. Phys. Lett. 86, 142907 (2005)

[21] R. Jiménez, A. González, C. Alemany, M.L. Calzada, J. Mendiola, Bol. Soc. Esp. Ceram. Vidr. 41, 22 (2002)

[22] R. Jiménez, P. Ramos, M.L. Calzada, J. Mendiola, Bol. Soc. Esp. Ceram. Vidr. 37, 117 (1998)

[23] R. Jiménez, B. Jiménez, "Pyroelectricity in Polycrystalline Ferroelectrics" in Multifunctional Polycrystalline Ferroelectric Materials, L. Pardo and J. Ricote ed., Springer Series in Materials Science 140, 573 (2011)

[24] H. Birk, J. Glatz-Reichenbach, L. Jie, E. Schreck, K. Dransfeld, J. Vac. Sci. Technol. B 9, 1162 (1991)

[25] P. Güthner, K. Dransfeld, Appl. Phys. Lett. 61, 1137 (1992)

[26] K. Franke, J. Besold, W. Haessler, C. Seegenbarth, Surf. Sci. 302, L283 (1994)

[27] O. Kolosov, A. Gruverman, J. Hatano, K. Takahashi, H. Tokumoto, Phys. Rev. Lett. 74, 4309 (1995)

[28] A. Gruverman, O. Auciello, H. Tokumoto, J. Vac. Sci. Technol. B 14, 602 (1996)

[29] S.V. Kalinin, D.A. Bonnell. "Chapter 1: Nanoscale characterization of ferroelectric materials; Scanning probe microscopy approach" (Ed. A. Gruverman, M. Alexe, Springer- Verlag, 2004)

[30] T. Hidaka, T. Maruyama, M. Saitoh, N. Mikoshiba, M. Shimizu, T. Shiosaki, L.A. Wills, R. Hiskes, S. Dicarolis, J. Amano, Appl. Phys. Lett. 68, 2358 (1996)

[31] G. Zavala, J. H. Fendler, S. Trolier-Mckinstry, J. Appl. Phys. 81, 7480 (1997)

[32] C. Harnagea, A. Pignolet, M. Alexe, D. Hesse, Integr. Ferroelectr. 44, 113 (2002)

[33] J.R. Fernandes, F.A. de Sá, J.L. Santos, E. Joanni, Rev. Sci. Instrum. 73, 2073 (2002)

CHAPTER III

MULTILAYER COMPOSITE FILMS TO IMPROVE THE REMNANT PROPERTIES OF $Pb(Mg_{1/3}Nb_{2/3})O_3$-$PbTiO_3$: PROOF OF CONCEPT

PART 1

Multilayer composite films with multiple layers

We propose in this chapter the evaluation of the idea of preparing multilayer composite films composed of alternating layers of $PbTiO_3$ (PT) and $0.65Pb(Mg_{1/3}Nb_{2/3})O_3$-$0.35PbTiO_3$ (PMNT), in order to obtain films based on these compositions with an improvement of the remnant ferroelectric and piezoelectric properties. To that aim, multilayer composite films with multiple layers are analyzed. The application of an electric field on a ferroelectric multilayer with very thin multiple layers should be highly effective, both due to the small thickness of each layer, which requires in principle the application of lower electric fields, and to the enhanced interaction among the layers, with more interface area than for multilayer composed of a smaller number of layers. The reduced thickness of the ferroelectric layers, should not be a problem, as it was reported that Chemical Solution Deposition $PbTiO_3$ films maintain their remnant properties even for the thinnest layers [1]. In this part we will show the effectiveness of the mechanism proposed for the stabilization of a certain value of remnant polarization in the PMNT thin layers.

3.1.1 Thin film preparation

Multilayer composite films (MLC) were obtained by the deposition, drying and crystallization of 21 alternating layers of PT and PMNT, starting and finishing with a PT layer (top and bottom layer of the MLC film). 0.1 M solutions of $PbTiO_3$ (PT) and $0.65Pb(Mg_{1/3}Nb_{2/3})O_3$-$0.35PbTiO_3$ (PMNT) were used. A total thickness of ~230 nm is obtained, according to profilometry measurements, which is equivalent to ~ 10 nm thick for each layer. Reference films of PT and PMNT with similar total thickness were also prepared for the sake of comparison.

3.1.2 Characterization of the crystalline phases present in the films

The crystalline phases present in the films were monitored by grazing incidence X-ray diffraction (GIXRD). The two crystalline phases, $PbTiO_3$ and $0.65Pb(Mg_{1/3}Nb_{2/3})O_3$-$0.35PbTiO_3$ perovskites, are detected in the GIXRD pattern of the MLC film indicating that no significant interdiffusion between the alternating PT and PMNT layers is produced. To make this clearer, the insets of the Figure 3.1.1 show the deconvolution of the experimental data into the diffraction peaks coming from the PMNT and PT layers: in the 2θ interval between 20º-24º, the 100 peaks of PT and PMNT; between 42º and 50º the 002 and 200 peaks of PT and the 200 peak of PMNT. Deconvolution of the experimental diffraction peaks was carried out by using two pseudo-Voigt functions. The good fitting between the experimental and calculated data for MLC, confirms that no other phases different to the ones of the constituent layers of the composite are formed. Note that an intermetallic phase, $PbPt_x$, is also present due to the interface reactions usually found between the highly volatile Pb and the Pt bottom electrode [2-4]. This intermetallic formed during the thermal processing of the film is the result of a process in which some of the original lead acetate in the sol–gel coating is reduced to atomic lead at low temperatures. Then it reacts with the Pt layer to form a $PbPt_x$ intermetallic phase, before being oxidized at higher temperatures [5-7]. The decrease of the intensity of the main peaks in the MLC film, due to the mixture of two phases and the broad peaks resulting from the limited thickness of each layer, makes more visible the small contribution of this intermetallic phase. 111 Pt diffraction peak comes from the bottom Pt electrode due to the non-coated Pt region used for the

electrical contacts. It must be mentioned also that the PT and PMNT films used as a reference are single phase without any secondary phases detected.

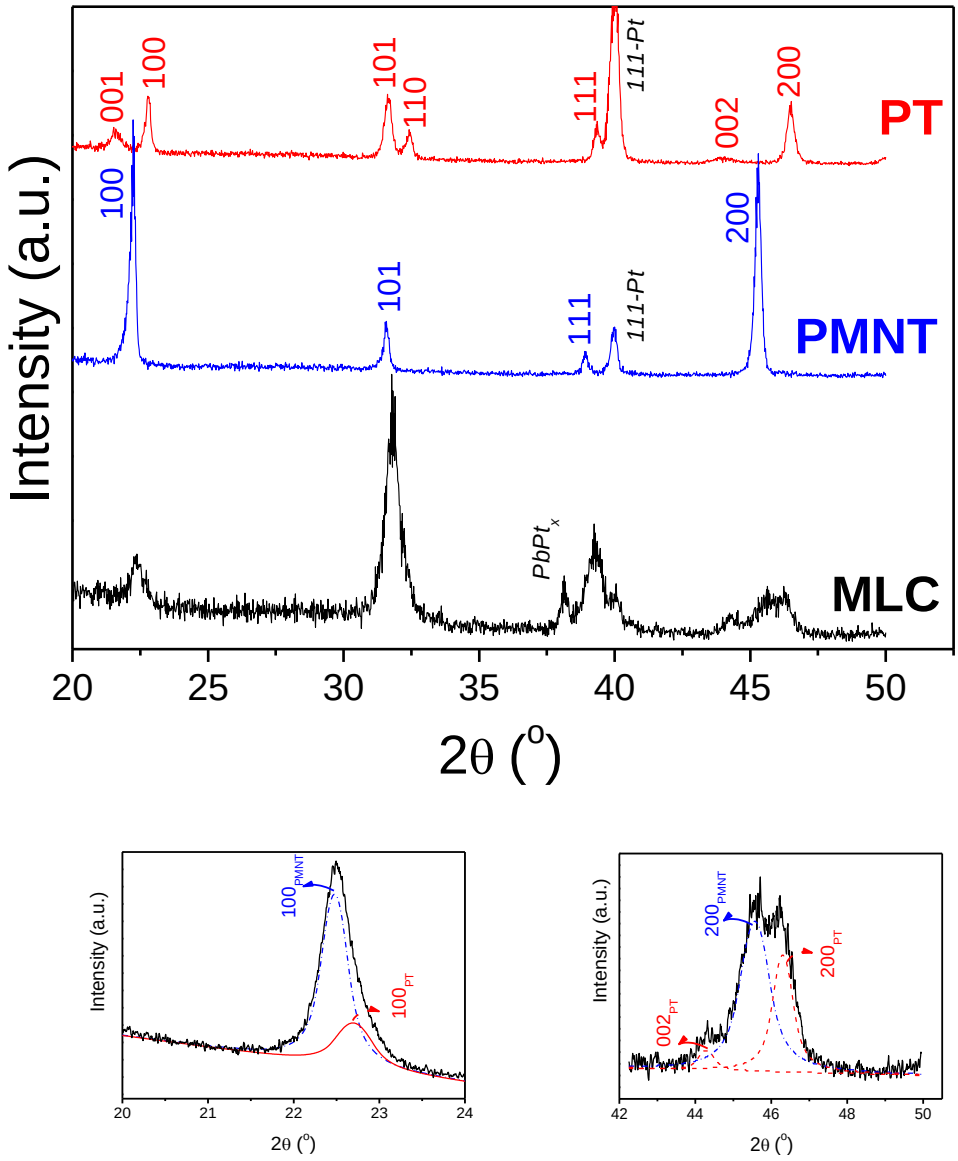

Figure 3.1.1. *GIXRD results obtained for the MLC films compared with the reference PT and PMNT films (incidence angle 1°). The insets show the deconvolution of the contributions of the PT and PMNT layers on the 100 and 200 diffraction peaks. (Pt: platinum, $PbPt_x$ intermetallic interface)*

3.1.3 Films microstructure and ferroelectric domain configuration

The optical microscopy images (Figure 3.1.2) show a uniform aspect of the films surfaces, which is a consequence of the lack of local thickness variations, indicative of the high quality of the deposition achieved. PMNT film presents fewer defects than the other two films, whose top layer is PT. This indicates the different behaviour of the complex oxide PMNT during film processing.

Figures 3.1.3, 3.1.4 and 3.1.5 show the topography (a), out-of plane (b and c) and in-plane (d and e) amplitude and phase PFM images of the PT, PMNT and MLC films. An estimation of the lateral grain size values can be obtained from the topography images. The grain size of PMNT is between 65 and 260nm, similar to PT which is 100-300 nm, while MLC grain size is much smaller (30-100 nm). The decrease of the thickness below a critical value in polycrystalline films usually leads to smaller grains, basically due to the restrictions imposed on the grain growth in the vertical direction [8]. Therefore, the deposition of very thin alternating layers in the MLC film results in a very limited growth of the grains, producing the small grains observed.

In addition, the comparison of the PFM images of the MLC film do not show any traces of ferroelastic 90º domains inside the fine grains, unlike their counterparts in the PT film, where bands of straight domain walls, typical of this type of domains, can be seen clearly. Besides, the phase PFM images show a tendency to have a large portion of the film area with the out-of-plane component of the polarization oriented towards the films surface, which indicates the presence of self polarization in all three films, stronger in the case of the PMNT film. This strong self polarization in PMNT films was observed before [9] and it has been attributed to the special characteristics of these polycrystalline films with small grain size.

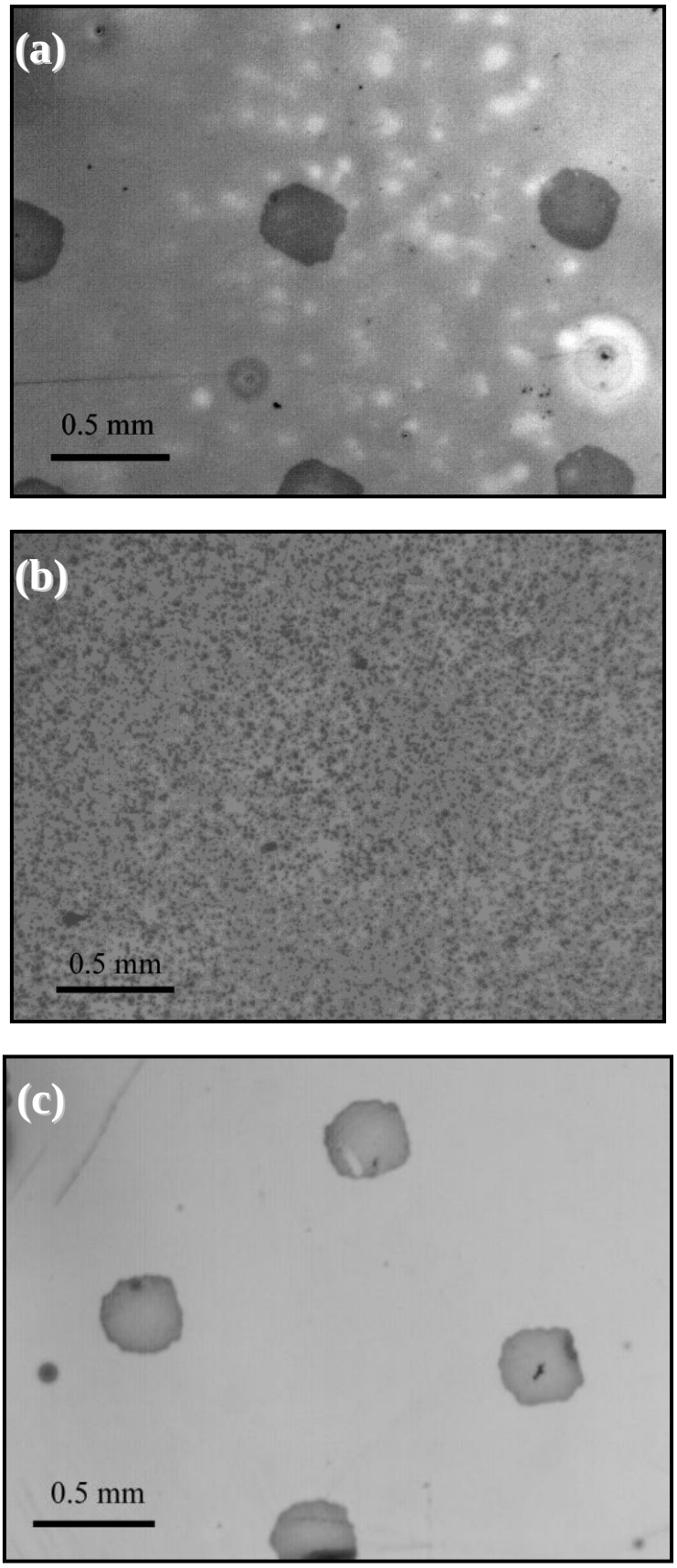

Figure 3.1.2. *Optical microscopy images of the film surfaces of (a) MLC, (b) PMNT and (c) PT films. The dark circles are the Pt top electrodes deposited for the electrical characterization*

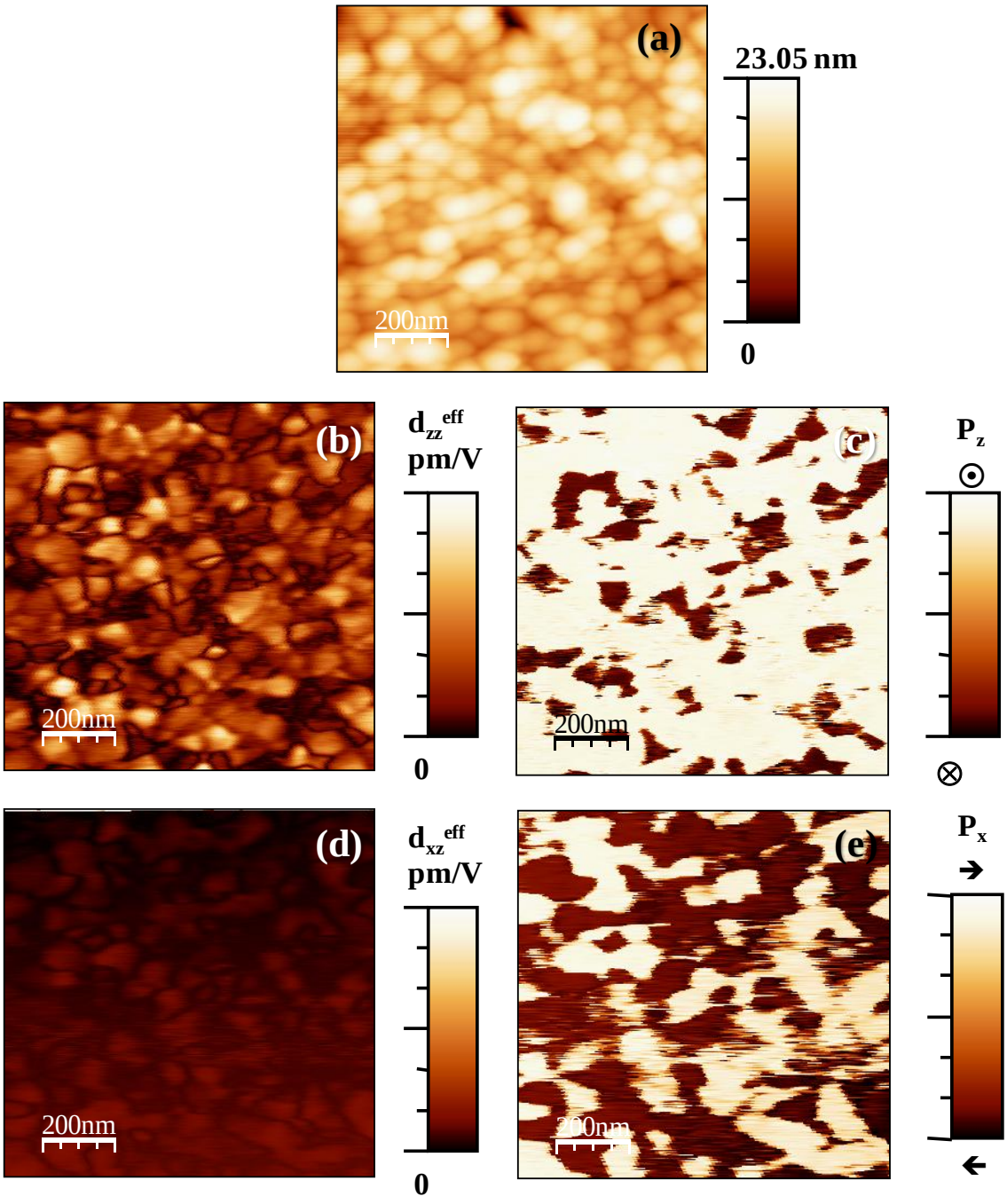

Figure 3.1.3. *SFM images of the MLC film: (a) topography; PFM out-of-plane (b) amplitude and (c) phase; in-plane (d) amplitude and (e) phase*

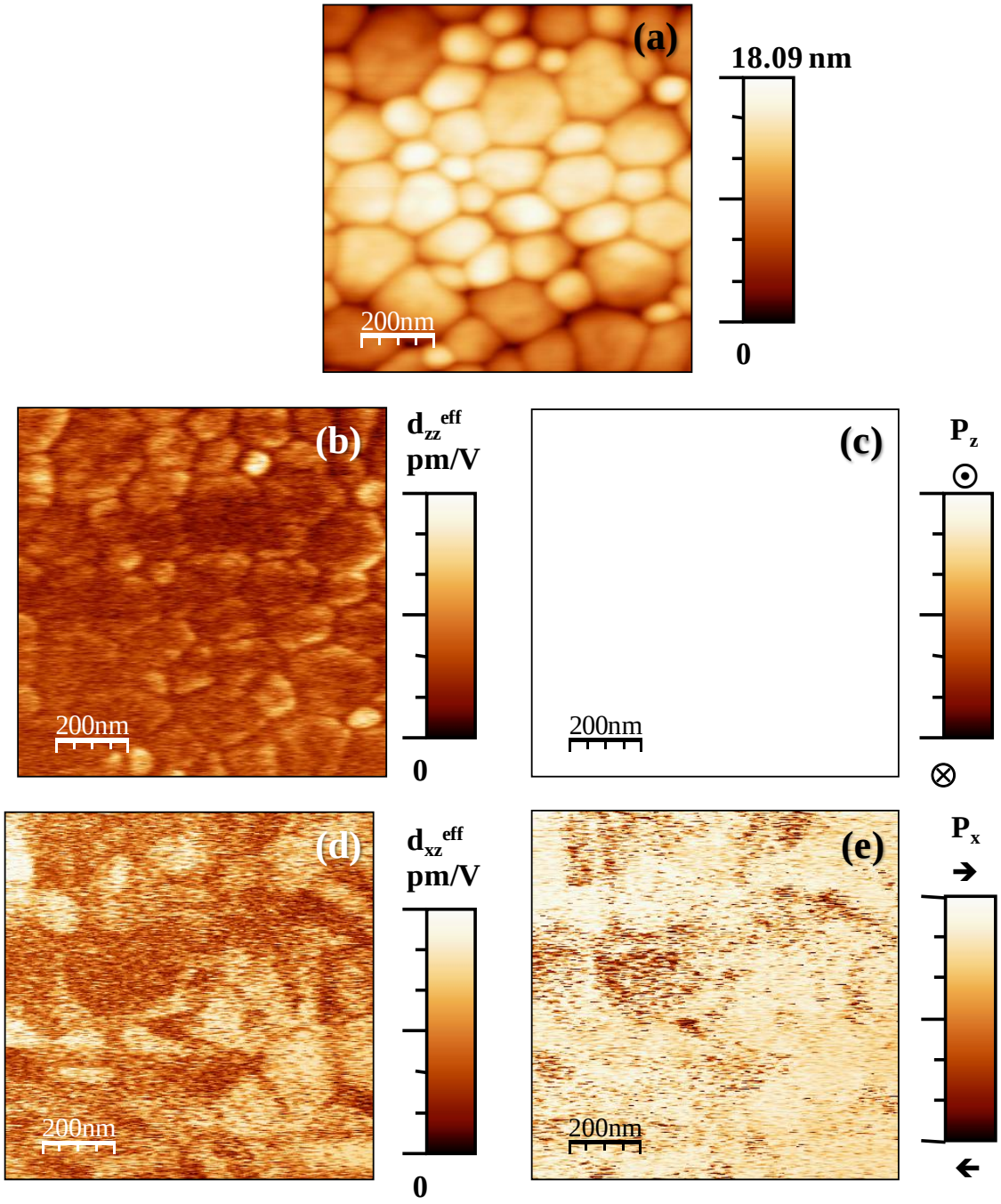

Figure 3.1.4. *SFM images of the PMNT film: (a) topography; PFM out-of-plane (b) amplitude and (c) phase; in-plane (d) amplitude and (e) phase*

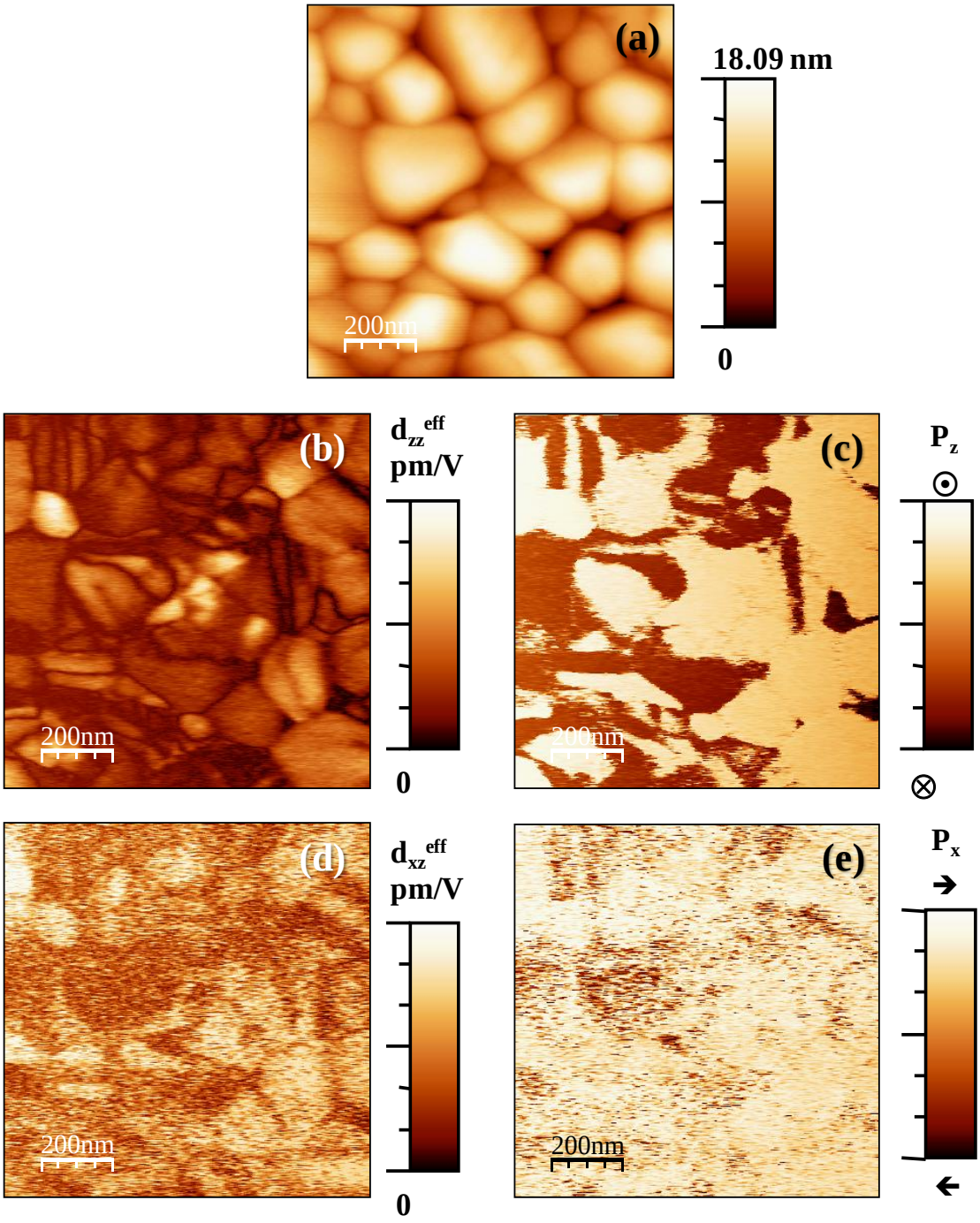

Figure 3.1.5. *SFM images of the PT film: (a) topography; PFM out-of-plane (b) amplitude and (c) phase; (d) in-plane amplitude and (e) phase*

3.1.4. Dielectric behavior

Figure 3.1.6a shows the temperature dependence of the relative dielectric permittivity of the PT, PMNT and MLC films. Measurements were carried out at different frequencies from 500 Hz to 50 kHz.

The relative dielectric permittivity of the PT film has a maximum at T_m~692 K, which corresponds to the characteristic ferro-paraelectric (FE-PE) transition of the $PbTiO_3$ perovskite. It was also observed that the relative dielectric permittivity of PT decreases with increasing frequency, i.e., it shows a large frequency dispersion of the permittivity. This can be attributed to the low quality of the interfaces between the deposited layers.

The curve corresponding to the PMNT film shows two maxima that can be related to the rhombohedric to tetragonal, ferroelectric-ferreoelectric, phase transition (~315K) and to the tetragonal to the cubic, ferroelectric-paraelectric, phase transition (~398 K) of the $0.65Pb(Mg_{1/3}Nb_{2/3})O_3$-$0.35PbTiO_3$ perovskite.

For the MLC film, the anomalies observed in the permittivity curves, shown with more detail in the inset of Figure 3.1.6a, can be ascribed to those corresponding to their PMNT and PT layers. This result gives an evidence of the existence of separate layers, as it is observed in the XRD patterns, without significant interdiffusion among them. If this is so, we should obtain a good reproduction of the K'_{MLC} behavior of the MLC film using the Maxwell-Wagner approach by assuming a stack of two in-series layers with different thickness, t; PT (t_{PT} = 92 nm) and PMNT (t_{PMNT} = 138 nm) [10]:

$$\frac{t}{K'_{MLC}} = \left(\frac{t_{PT}}{K'_{PT}} + \frac{t_{PMNT}}{K'_{PMNT}} \right) \qquad (1)$$

where K'_{PT}, K'_{PMNT} are the experimental relative dielectric permittivities obtained for the PT and PMNT films, respectively. Figure 3.1.6b presents both the calculated and the experimental permittivity curves of the MLC film, showing a good agreement. Therefore, we can conclude that not only is there no significant interdiffusion among the different layers, but also the MLC film behavior can be described as an in-series stack of PT and PMNT layers, indicating that the CSD deposition of the alternating PT and PMNT layers produces good quality multilayer composite films.

A further analysis of the permittivity curves shown in Figure 3.1.6b for the MLC film reveals not only an enhancement of the permittivity values, but also a shift of the transition temperature corresponding to the PT layers (641 K) and PMNT layers (354 K) in relation to the single phase PT and PMNT films used as a reference: 692 K and 396 K, respectively. This shift, together with the broadening of the transition peak, indicates a different stress state and a strong decrease of the grain size of the MLC compared to the single phase PT and PMNT films, corroborated by the SFM topography images of Figure 3.1.5. The decrease of the thickness below a critical value in polycrystalline films usually leads to reduced grain size, and, therefore, to a decrease of the values of the maximum relative dielectric permittivity with an associated shift to lower temperatures.

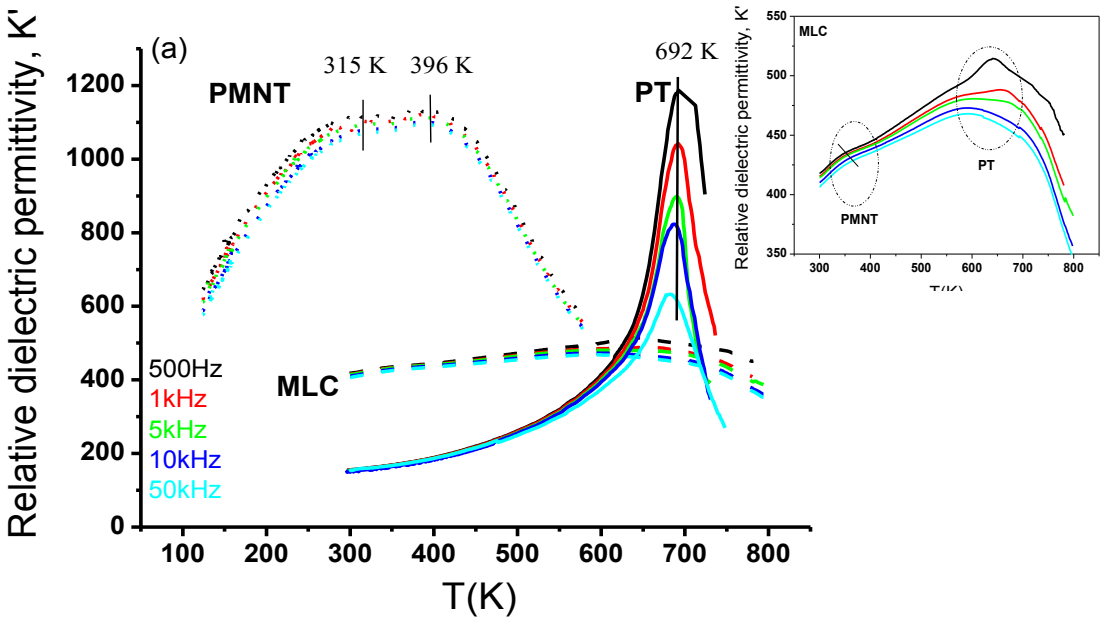

Figure 3.1.6*a. Variation of the relative dielectric permittivity (K') with the temperature for the PT, PMNT and MLC films*

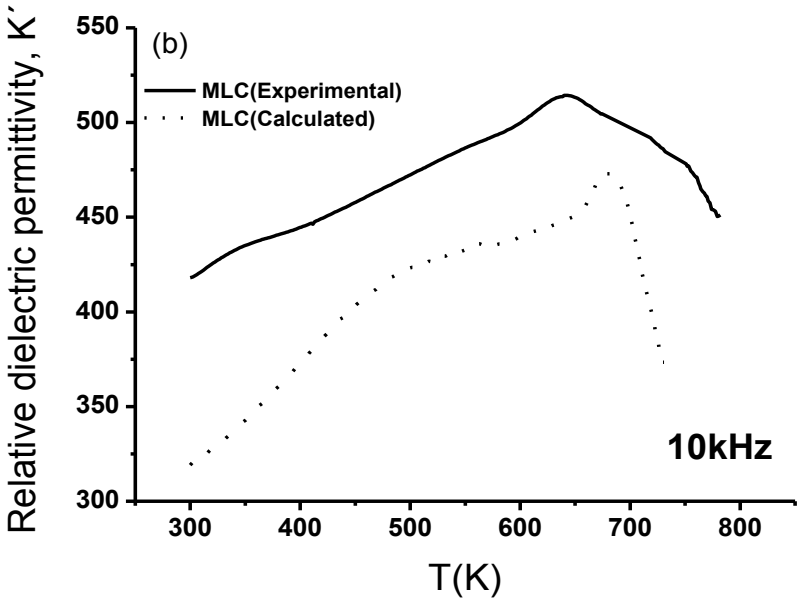

Figure 3.1.6*b. Experimental and calculated curves of the relative dielectric permittivity (K´) versus temperature at 10 kHz for the MLC film*

3.1.5. Ferroelectric properties: remnant values

Figure 3.1.7a shows the experimental current density loops at a frequency of 1 kHz for the PT, PMNT and MLC films. It must be noted that the loop corresponding to the PT film is highly asymmetric with a large increase of the current for positive values of the electric field, which is characteristic of films with large leakage currents [11]. This is not observed in the PMNT film, which indicates that any leakage problem in the MLC film may come from the PT layers. This issue will be analyzed in the next chapter, in order to find a solution. In any case, the layered structure of the MLC films, with non-leaky PMNT between PT layers, seems to largely avoid this leakage problem, as it can be seen in its current density loop. By the integration of these current loops, the corresponding P-E hysteresis loops were obtained. As explained in Chapter II, all the non-switching contributions are separated and, finally, substracted by a fitting procedure. The corrected loops are presented in Fig. 3.1.7b. The hysteresis loops show, as expected, large remnant and saturation polarization values for the PT film ($2P_r$ = 86 and $2P_s$ = 88 $\mu C \cdot cm^{-2}$) with a coercive field, E_c, of 244 $kV \cdot cm^{-1}$. In the case of the PMNT thin film, the hysteresis loop shows a slim shape and values of $2P_r$ = 8 $\mu C \cdot cm^{-2}$ and $2P_s$ = 16 $\mu C \cdot cm^{-2}$. The coercive field of this film is much lower: E_c = 109 $kV \cdot cm^{-1}$. The low remnant polarization values of the polycrystalline PMNT films of this work

have been reported previously in the literature [9,12]. The combination of both films in a multilayer composite results in larger polarizations values than the PMNT film: $2P_r$ = 16 μC·cm^{-2} and $2P_s$ = 30 μC·cm^{-2}, with an intermediate coercive field: E_c = 131 kV·cm^{-1}. One of the objectives of the fabrication of these multilayer composite films is, therefore, fulfilled, as we have obtained a film with a large amount of strong piezoelectric PMNT, but with larger remnant values of the polarization than those of the single phase film.

The results obtained prove that the use of highly remnant PT layers is able to enhance the remnant polarization of PMNT by the inducement of an internal electric field inside the PMNT layers that keeps a certain value of the polarization even when no external electric field is applied.

As the hysteresis loops have been corrected from all non-switching contributions to provide precise values of the polarization, we can compare them with values obtained by other methods. Figure 3.1.8 shows the results of the measurement of the switching currents, in the conventional experiment in which a sequence of voltage square pulses is applied (in this case of 10μs at intervals of 20μs) in order to obtain pure switching currents and observe its evolution with time. From these curves we calculate the remnant polarization values P_r or, more precisely, the non-volatile polarization P_{nv} [13]. The values are shown in the inset of the figure and it can be observed that the values are rather similar (within the error) to the ones obtained in the corrected P-E loops. Again the MLC film show larger P_{nv} values than the PMNT film. It is thus confirmed the enhancement of the remanence of PMNT layers in the multilayer composite film.

This increase of the remnant values is also confirmed when other functional properties are analyzed. The pyroelectric coefficients of the PMNT and MLC films, shown in Table 1.1, are one example. The low remanence of the PMNT film makes that the pyroelectric coefficient does not increase significantly after poling, while the MLC film reaches rather large values after poling with asymmetric values due to the presence of self polarization.

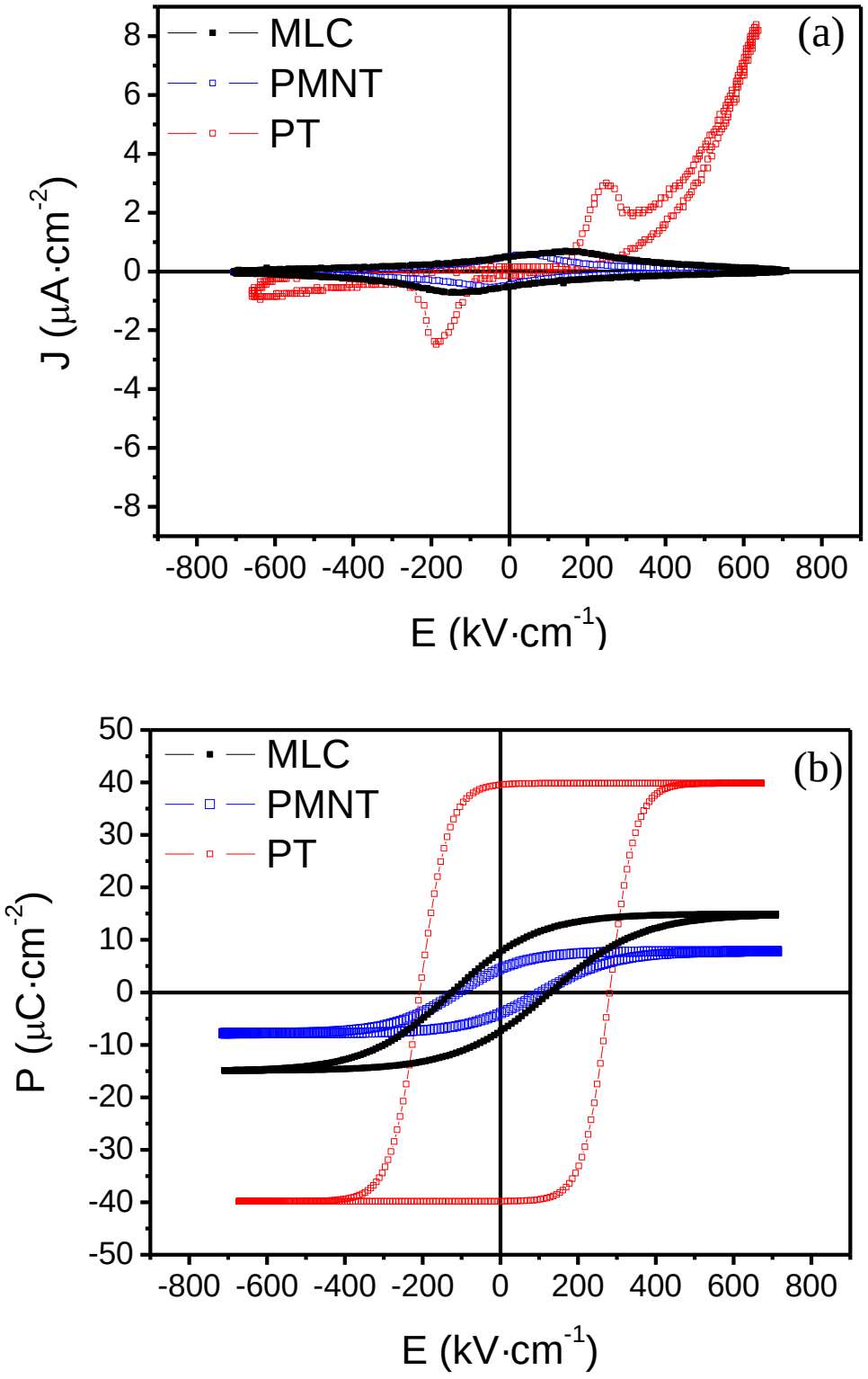

Figure 3.1.7. *(a) Experimental current loops and (b) corrected P-E hysteresis loops of the PT, PMNT and MLC films*

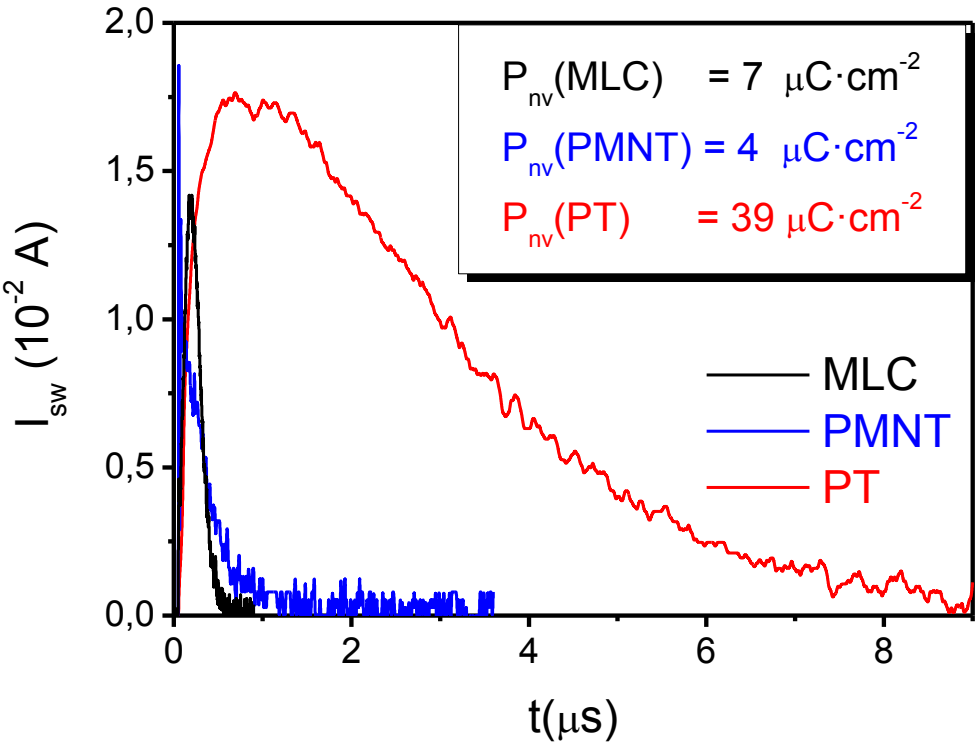

Figure 3.1.8. *Switching current transitory curves for the three films after the application of a train of pulses of amplitude 16V. In the inset the non-volatile polarization values calculated from the curves are shown*

γ / Thin film	**Before poling** (10^{-4} μC $cm^{-2}K^{-1}$)	**After poling with V(+)** (10^{-4} μC $cm^{-2}\cdot K^{-1}$)	**After poling with V(-)** (10^{-4} μC $cm^{-2}\cdot K^{-1}$)
PMNT	-4	-9	+6
MLC	-22	-180	+130

Table 3.1.1. *Pyroelectric coefficients (γ) before and after poling at 10 V for PMNT and MLC films*

The pyroelectric coefficients (γ) after poling, $\gamma_+ \sim -1.8\times10^{-8}$ C·$cm^{-2}\cdot K^{-1}$ and $\gamma_- \sim +1.3\times10^{-8}$ C·$cm^{-2}\cdot K^{-1}$, indicate clearly polarization switching with an enhanced retention

compared with the single phase PMNT film. These coefficients are close to the values reported for other polycrystalline ferroelectric thin films on Si-based substrates [14]. It must be noted that the pyroelectricity of the PMNT system has not been studied extensively, although large values have been reported under an electric field [9,15]. In our case, the pyroelectric coefficients of the MLC film can be attributed to an effective contribution of the PMNT layers to the pyroelectric behavior of the multilayer, due to an effective inducement of remnant polarization in these layers by the internal field created in the MLC.

However the remnant values measured are obtained shortly after the application of the electric field. For applications we must also analyze the retention with time of these values in the MLC film. Figure 3.1.9 shows the ferroelectric hysteresis loops of the PMNT and MLC thin films measured at 1 kHz and ~ 800 $kV \cdot cm^{-1}$, but with a delay time of 1 s between the conditioning and measuring voltage. This delay time allows the relaxation of the polarization after the conditioning wave. The hysteresis loop of the PMNT film has the expected slim shape, and the value of the P_r is reduced ~ 24% after 1s, as the difference between the starting and final values at zero field shows. This difference is reduced to less than 10% for the MLC film. This result shows that the relaxation of polarization at short times is much higher for the PMNT than for the MLC film. Therefore, we can argue that not only we achieve an increase of the remnant values of the polarization of the PMNT layers, but also they are retained at relatively short times.

Finally, to establish the functional reliability of the films, the retention of the polarization is measured for longer periods of time. Results, obtained both after the application of positive and negative electric fields (upward and downward) are shown in figure 3.1.10. After the initial decrease of the values for short times, already studied in the P-E hysteresis loops of Figure 3.1.9, values keep the remnant values quite stable for longer times. It is clear that the MLC film presents larger remnant values, which decrease less at short times than the single phase PMNT film, and keep these values for long times, similarly to the behavior of PMNT films, which are able also to maintain stable polarization values after the sharp decrease of these values at short times.

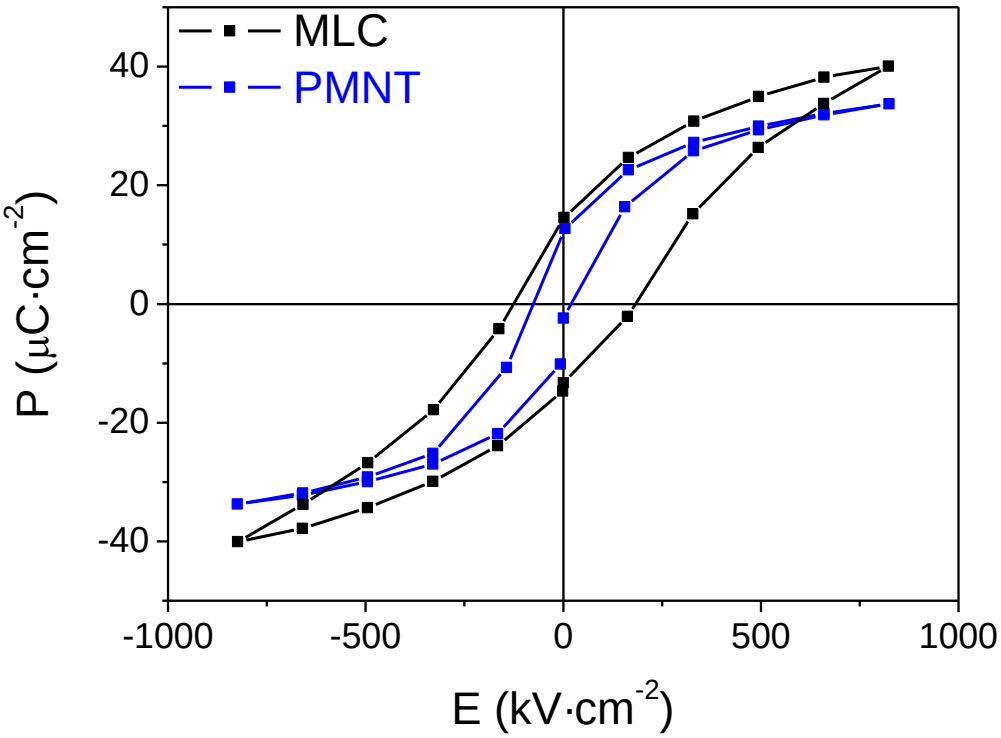

Figure 3.1.9. *P-E hysteresis loops measured at 1 kHz with 1 s of delay time*

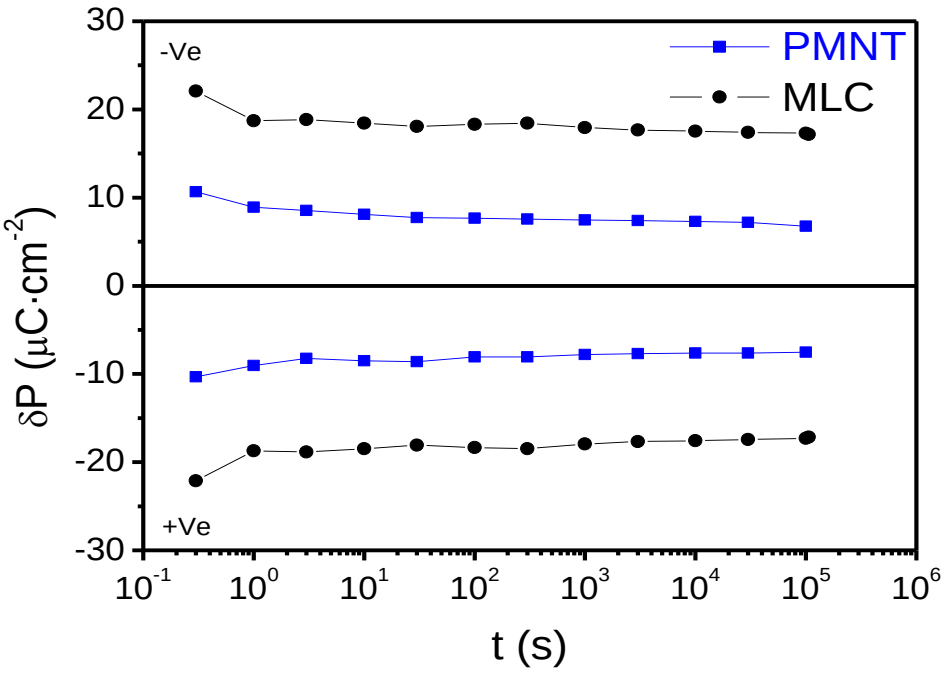

Figure 3.1.10. *Retention of the polarization of PMNT and MLC films*

The local piezoelectric hysteresis loops of the PT, PMNT and MLC films shown in Figure 3.1.11 indicate that an increase of the remnant polarization in the MLC film seems to result in an enhancement of the piezoelectric coefficients. Although quantitative values of the piezoelectric coefficients cannot be obtained from these experiments, they are an evidence of that we are able to take advantage of the high piezoelectric coefficients of the PMNT films with a multilayer composite configuration.

Also we can see that, although there is a small increase of the remanence in the MLC film compared to the PMNT, the values of the piezoelectric coefficients are not much improved. This may be associated with the small grain size of MLC film (Fig.6a), as this reduction of grain size usually results in a decrease of the piezoelectric coefficients. The absence of ferroelastic domain walls in the MLC film, when compared with the PT film, is also a consequence of the reduction of the grain size. This is a factor that may contribute to the fast switching times measured for the MLC film.

The smaller grain size of the MLC film, added to the presence of small porosity of the PMNT layers as revealed in the optical micrographs, are factors that contribute to the broad maximum observed in the dielectric curves, accompanied by a decrease of the values of the relative dielectric permittivity. This affects also the values of the piezoelectric coefficients, according to the thermodynamic equation:

$$d_{33} = 2K'_{33} \cdot \varepsilon_o \cdot Q_{12} \cdot P_3 \qquad (2)$$

where d_{33} is the piezoelectric charge coefficient, K'_{33} the relative dielectric permittivity, ε_o the dielectric permittivity of vacuum, Q_{12} the electrostrictive coefficient and P_3 the polarization. Therefore, the appearance of very small grains should be avoided in order to obtain improved piezoelectric properties in these multilayer composite films.

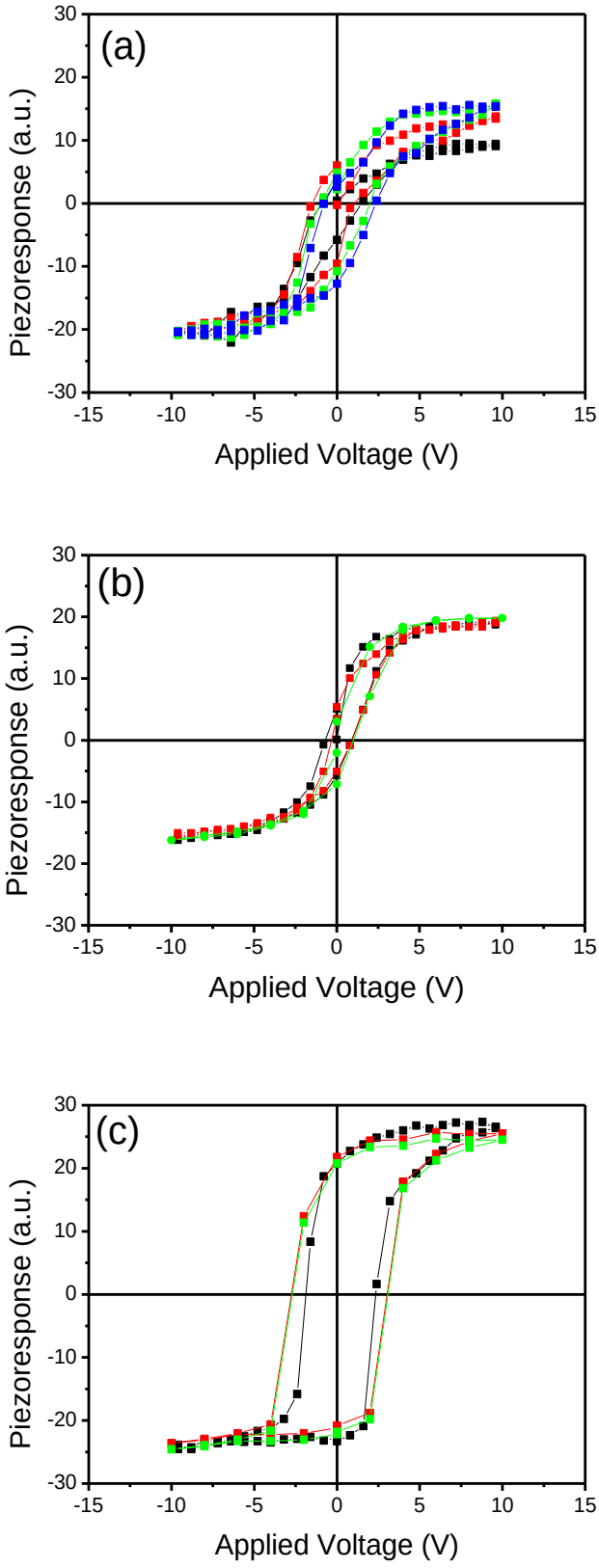

Figure 3.1.11. *Local piezoelectric in field hysteresis loops of (a) MLC, (b) PMNT and(c) PT films*

3.1.6. Remarks

- We successfully prepare multilayer composite films of PT and PMNT without significant interdifussion, according to X-ray diffraction data and relative dielectric permittivity curves. Therefore CSD seems to be an appropriate processing method to prepare ferroelectric multilayer composite films
- The MLC film makes possible the development of an internal field across the PMNT layers induced by the large remnant polarization of the PT layers, obtained after poling. This gives place to an increase of the remanence of the properties of the MLC films compared with those of the single $0.65Pb(Mg_{1/3}Nb_{2/3})O_3$-$0.35PbTiO_3$ films. Therefore, the results prove that this strategy can be used for improving the properties of thin films with low remnant polarization values.
- However, the improvement of properties is not as significant as they could be. The small grain size obtained for the MLC, due to the reduced thickness of the layers deposited, has a detrimental effect on the piezoelectric properties, which must be avoided.
- Therefore, we propose the preparation of MLC films composed of thick PT and PMNT layers, to avoid these detrimental grain size effects. This can be done by the deposition of solutions of larger molar concentration, and it will be the subject of next part.

3.1.7. References

[1] J. Ricote, S. Holgado, Z. Huang, P. Ramos, R. Fernández, M. L. Calzada, J. Mater. Res. 23, 2787 (2008)

[2] S.Y. Chen, I-W. Chen, J. Am. Ceram. Soc., 77, 2332 (1994)

[3] Z. Huang, Q. Zhang, R.W. Whatmore, J. Appl. Phys. 86, 1662 (1999)

[4] X. Guitang, H. Lai Wahchan, J. Am. Ceram. Soc. 87, 1588 (2004)

[5] Y. L. Tu, S. J. Milne, J. Mater. Res. 10, 3222 (1995)

[6] Z. Huang, Q. Zang, R.W. Whatmore, J. Appl. Phys. 85, 7355 (1999)

[7] R. Lbibb, R. Castanet, A. Rais, J. Alloys Compd., 302, 155 (2000)

[8] K.T. Miller, F.F. Lange, J. Mater. Res. 5, 151 (1990)

[9] M. Algueró, M. Stewart, M.G. Cain, P. Ramos, J. Ricote, M.L. Calzada, J. Phys. D: Appl. Phys. 43, 205401 (2010)

[10] A. Von Hippel, "Dielectric and waves" (London: Artech House) (1995)

[11] R. Meyer, R. Waser, K. Prume, T. Schmitz, S. Tiedke, Appl. Phys. Lett. 86, 142907 (2005)

[12] J. H. Park, S. Trolier-Mckinstry, J. Mater. Res. 16, 268 (2001)

[13] D. Rivero, L. Pardo, R. Jiménez. Rev. Cub. Física, 26 (2009)

[14] P. Muralt, Rep. Prog. Phys. 64, 1339 (2001)

[15] S.I. Raevskaya, Y.N. Zakharov, A.G. Lutokhin, A.S. Emelyanov, I.P. Raevski, M.S. Panchelyuga, V.V. Titov, S.A. Prosandeev. Appl. Phys. Lett. 93, 042903 (2008)

PART 2

Multilayer composite films with combinations of small number of layers

The results obtained in the multilayer composite film with multiple layers of the previous part demonstrate that the mechanism proposed for the enhancement of the remnant properties of PMNT films in a multilayer composite is effective, thus pointing at new directions for the tailoring of the functional properties of PMNT-based films. However, there are important factors that play a role in the properties of the MLC films and must be considered in order to optimize their response. The small grain size obtained due to the reduced thickness of the individual layers deposited was a handicap due to the development of significant detrimental size effects on the ferroelectric behavior of the layers. In this part we analyze MLC films where the thickness of the layers has been increased compared to the MLC films studied in the previous section by reducing the number of layers. Another important issue in order to establish the coupling among phases as the origin of the improved P_r values is the existence of a direct correlation between the relative amount of phases and the net polarization of the composite film that must be discarded. Therefore, in this section we compare MLC films with similar volume ratios of PT/PMNT phases, but with two different configurations of the alternating layers: one of them with all PMNT layers sandwiched between two PT layers and another with the opposite configuration. If the inducement of an electrical bias in the PMNT layers to maintain some polarization is not effective when the external electric field is removed, the composite effect should produce the same results for these MLC regardless the configuration used.

3.2.1 Thin film preparation

Multilayer composite films (MLC) were obtained by the deposition, drying and crystallization of 5 or 7 alternating layers of PT and PMNT, starting and finishing either with a PT layer (MLC-PT) or with a PMNT layer (MLC-PMNT), in order to compare two configurations in which either every PMNT layer is sandwiched between two PT layers or, conversely, every PT layer is placed between two PMNT layers. 0.3 M solutions of $PbTiO_3$ (PT) and 0.65Pb $(Mg_{1/3}Nb_{2/3})O_3$-0.35$PbTiO_3$ (PMNT) were used. Reference films of PT and PMNT with similar total thickness were also prepared for the sake of comparison.

Finally, we have four multilayer composite films with different configurations (see Figure 3.2.1) but similar PMNT volume fractions (V_{PMNT}):

Film	V_{PMNT}
MLC-PT5	0.40
MLC-PT7	0.43
MLC-PMNT5	0.60
MLC-PMNT7	0.57

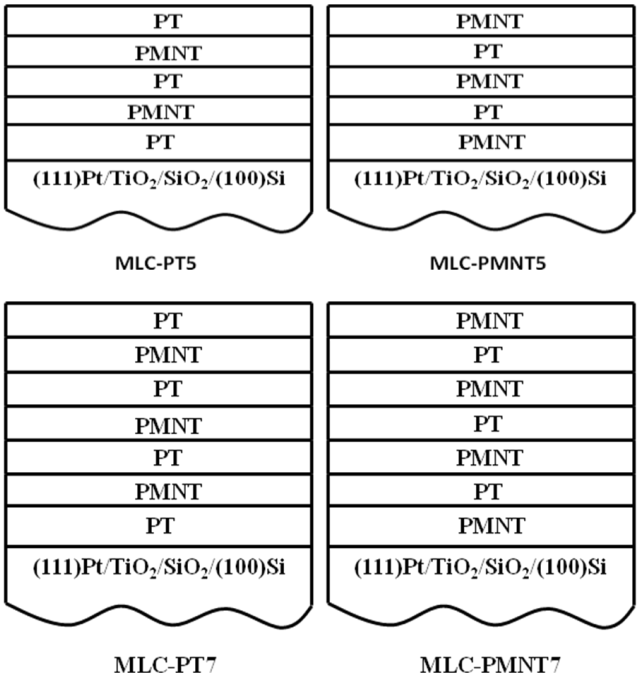

Figure 3.2.1. *Schematic diagram of the configuration of the layers for the different MLC thin films*

3.2.2 Characterization of the crystalline phases present in the MLC films

The crystalline phases of the films were studied by means of X- ray Diffraction, with Bragg-Brentano (XRD) geometry. Figures 3.2.2 and 3.2.3 show the XRD patterns of the polycrystalline PT, PMNT, MLC-PT and MLC-PMNT thin films with 5 and 7 layers, respectively. The patterns indicate that the PT and PMNT perovskite films are single phases without secondary phases detected, but some peaks from the (111)Pt/TiO_2/SiO_2/(100)Si substrate are detected. The two crystalline phases, $PbTiO_3$ and 0.65Pb($Mg_{1/3}Nb_{2/3}$)O_3-0.35$PbTiO_3$ perovskites, are the only ones present in the XRD pattern of the MLC-PT and MLC-PMNT films indicating that no significant interdiffusion between the alternating PT and PMNT layers is produced. As the diffraction peaks of these two phases are usually too close, details of the patterns are shown in the inset of the Figures 3.2.2 and 3.2.3 for 100, 110 and 200: experimental data (solid lines) with their corresponding deconvolution into the diffraction peaks from the PT and PMNT layers (dash-black and red lines). Deconvolution of the experimental diffraction peaks was carried out by using two pseudo-Voigt functions. The good fitting between the experimental and calculated data for both MLC-PMNT and MLC-PT films with 5 or 7 layers, confirms that no other phases different to the ones of the composites constituent layers are formed and, therefore, providing additional evidence that no significant interdiffusion between the PT and PMNT layers is produced. This confirms the high quality of the multilayer composite films obtained by Chemical Solution Deposition. Besides, in addition to the 111 diffraction peak from the bottom electrode of Pt, an intermetallic interface $PbPt_x$ between the films and the substrate appears in the diffraction pattern. This type of intermetallic phases are common for Pb based films deposited on Pt [1] and it can be seen that is present for all the MLC films analyzed.

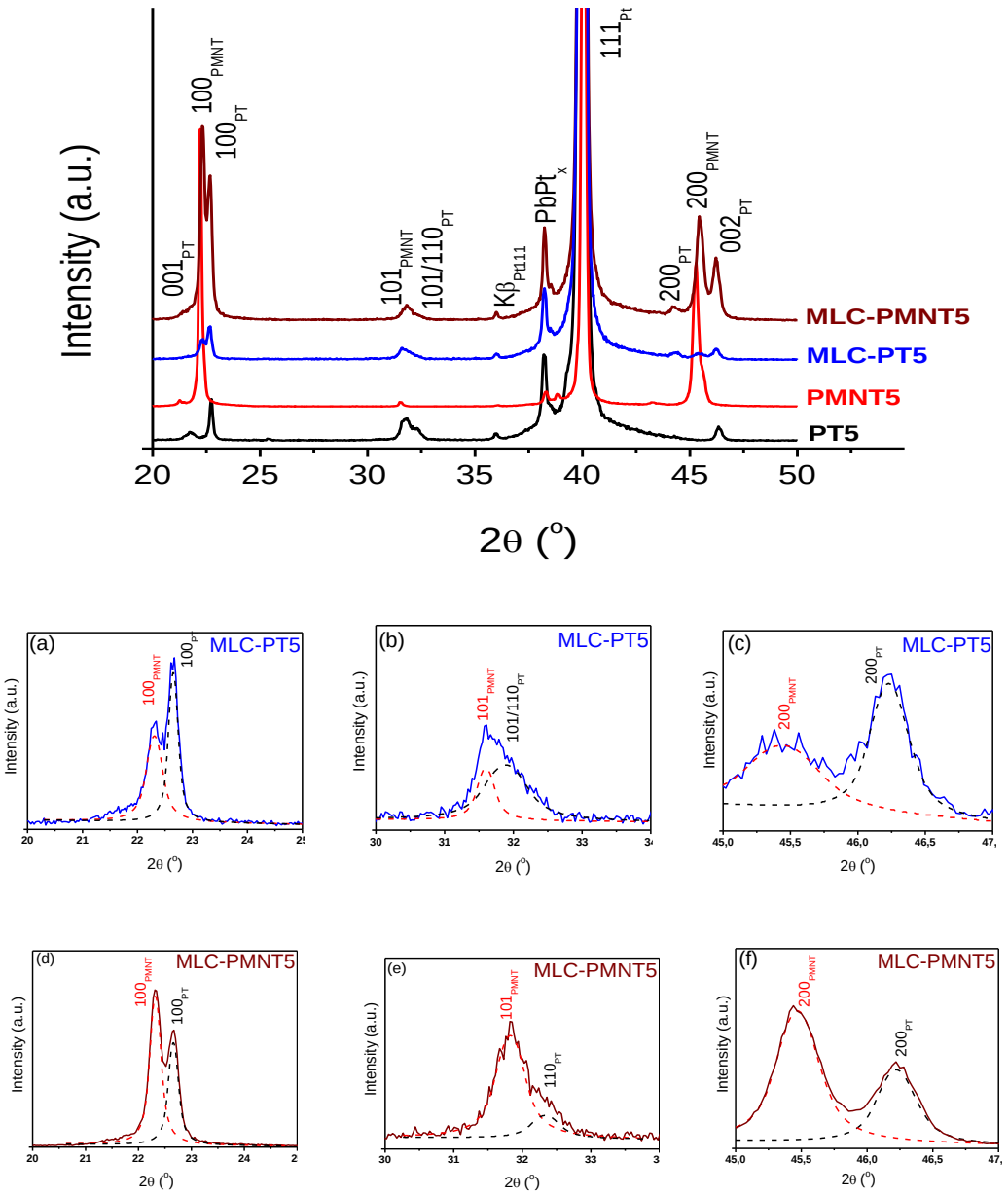

Figure 3.2.2. *XRD patterns of the PT5, PMNT5, MLC-PT5 and MLC-PMNT5 films*

Insets: Details of 100, 110 and 200 diffraction peaks (solid lines) with the calculated contributions from PT and PMNT phases (dash lines) for (a to c) MLC-PT5 and (d to f)MLC-PMNT5

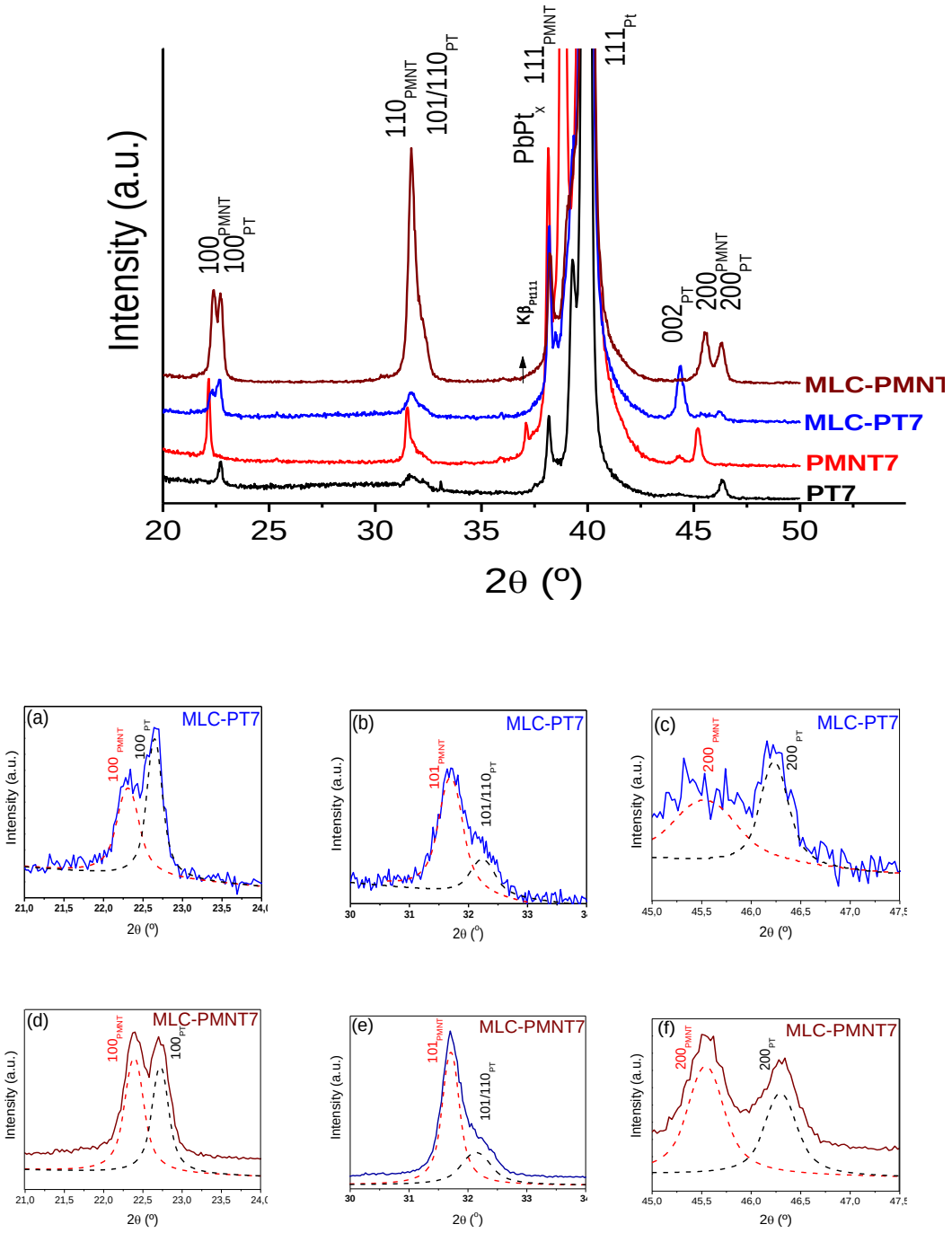

Figure 3.2.3. *XRD patterns of the PT7, PMNT7, MLC-PT7 and MLC-PMNT7 films*

Insets: Details of 100, 110 and 200 diffraction peaks (solid lines) with the calculated contributions from PT and PMNT phases (dash lines) for (a to c) MLC-PT7 and (d to f) MLC-PMNT7

3.2.3 Films microstructure and ferroelectric domain configuration

An analysis of the films by Scanning Electron Microscopy (Figure 3.2.4) reveals that the grain size of the top PMNT layer of the MLC-PMNT films (90-130 nm) is smaller than the one corresponding of the PMNT single phase film (180-270 nm). When cross sections are studied, it can be seen that single phase films develop a columnar growth that it is not possible in the MLC films, due to the grain growth limitation imposed by the alternating layers of PT and PMNT phases in the MLC films. Also, the total thicknesses of the films can be seen in the cross section images.

Regarding the porosity of the films, the plane view images show large pores in the PT7 and MLC-PT7 films that are not visible in MLC-PMNT7 and PMNT7 which have much amount of porosity with smaller size.

Figures 3.2.5 and 6 show the scanning force microscopy topography images and corresponding piezoresponse force microscopy images of the MLC films and corresponding reference single phase films. Thus, it is observed in both 7 and 5 layer films that the top PMNT layer of the MLC-PMNT films contains smaller grains (100-150 nm) than the single phase PMNT (450-500 nm for PMNT5 and 200-290 nm for PMNT7), corroborating the observations made by SEM for the 7 layer films. Also the smaller grain size of the top layer of the MLC-PT (80-150 nm) than the PT single phase (140-180) is observed. The consequence of this grain size reduction of the MLC films is the fact that PFM images do not show any bands of ferroelastic domains, which are still visible in the images of PT5. The phase images show a tendency to have large regions with the out-of-plane component of the polarization towards the film surface, which is more evident in the 7 layer films. This is an indication of the presence of self polarization in the films, which it will be studied in the analysis of the functional properties of these films.

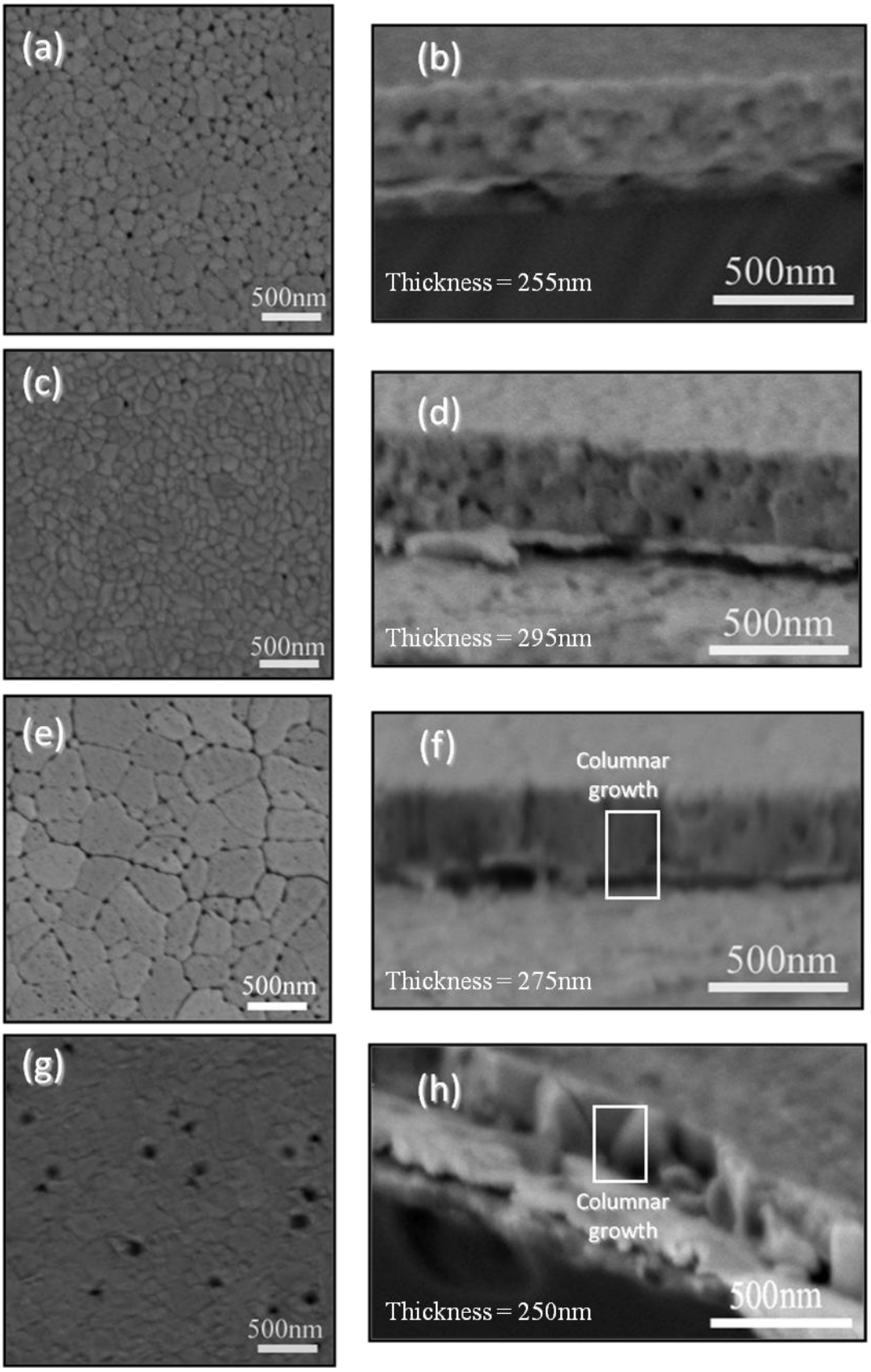

Figure 3.2.4. *Plan view and cross-section FEG-SEM images of: (a, b) MLC-PMNT7; (c, d) MLC-PT7; (e, f) PMNT7; (g, h) PT7 films*

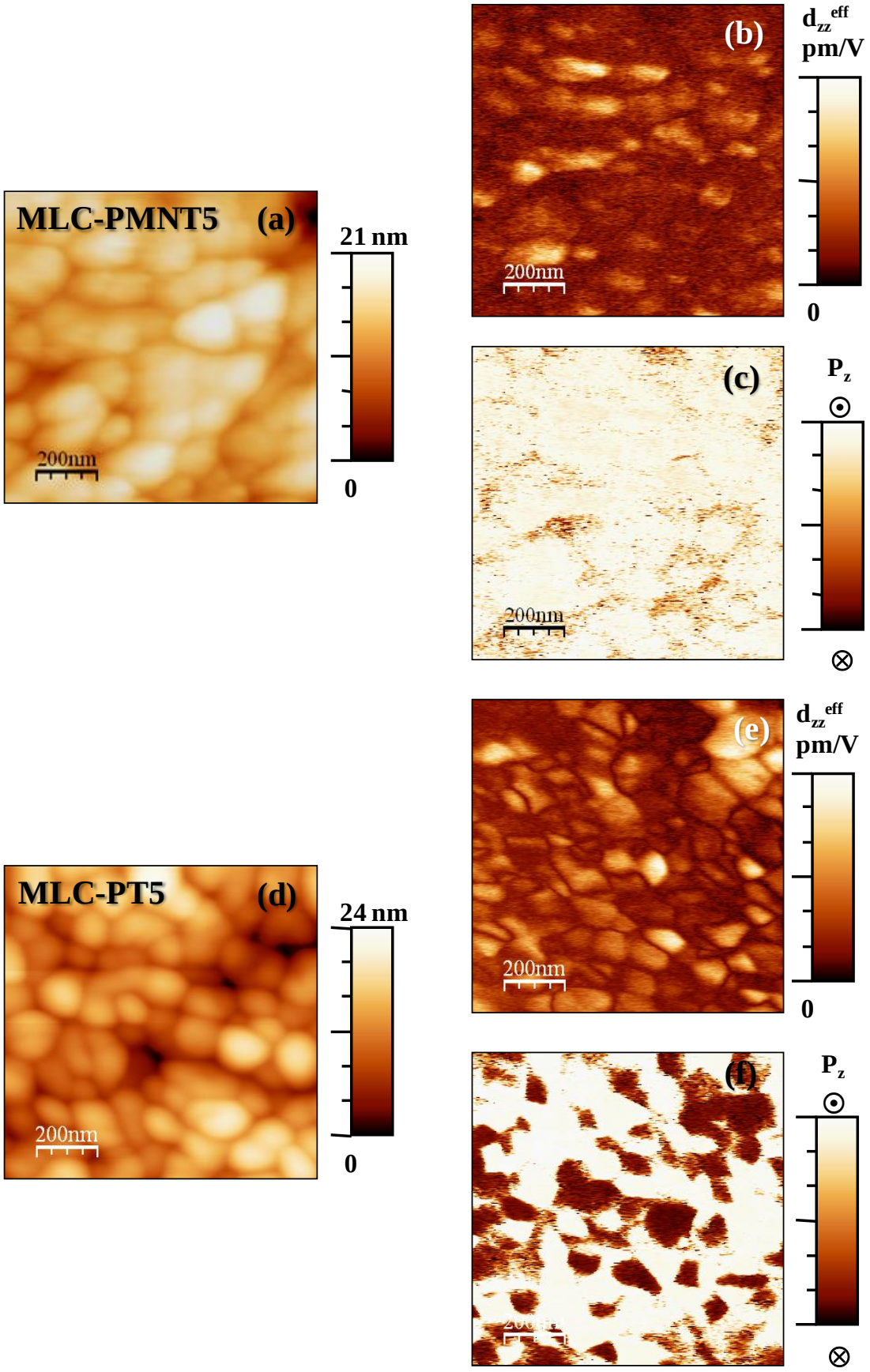

Figure 3.2.5. *SFM images of (a,d) topography; out-of-plane PFM (b,e) amplitude and (c,f) phase for the MLC-PMNT5 and MLC-PT5*

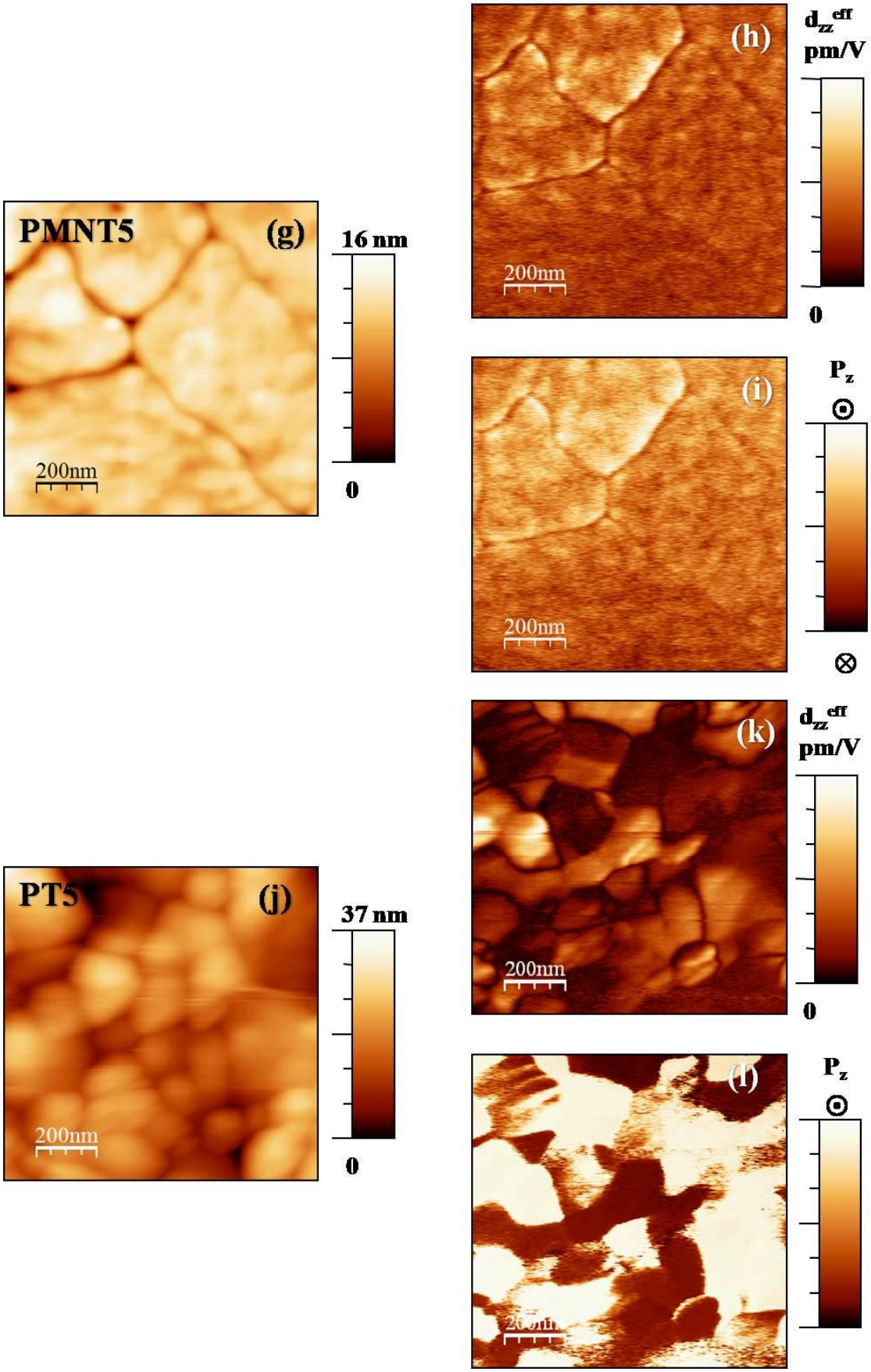

Figure 3.2.5. *SFM images of (g,j) topography; out-of-plane PFM (h,k) amplitude and (i, l) phase for the PMNT5 and PT5*

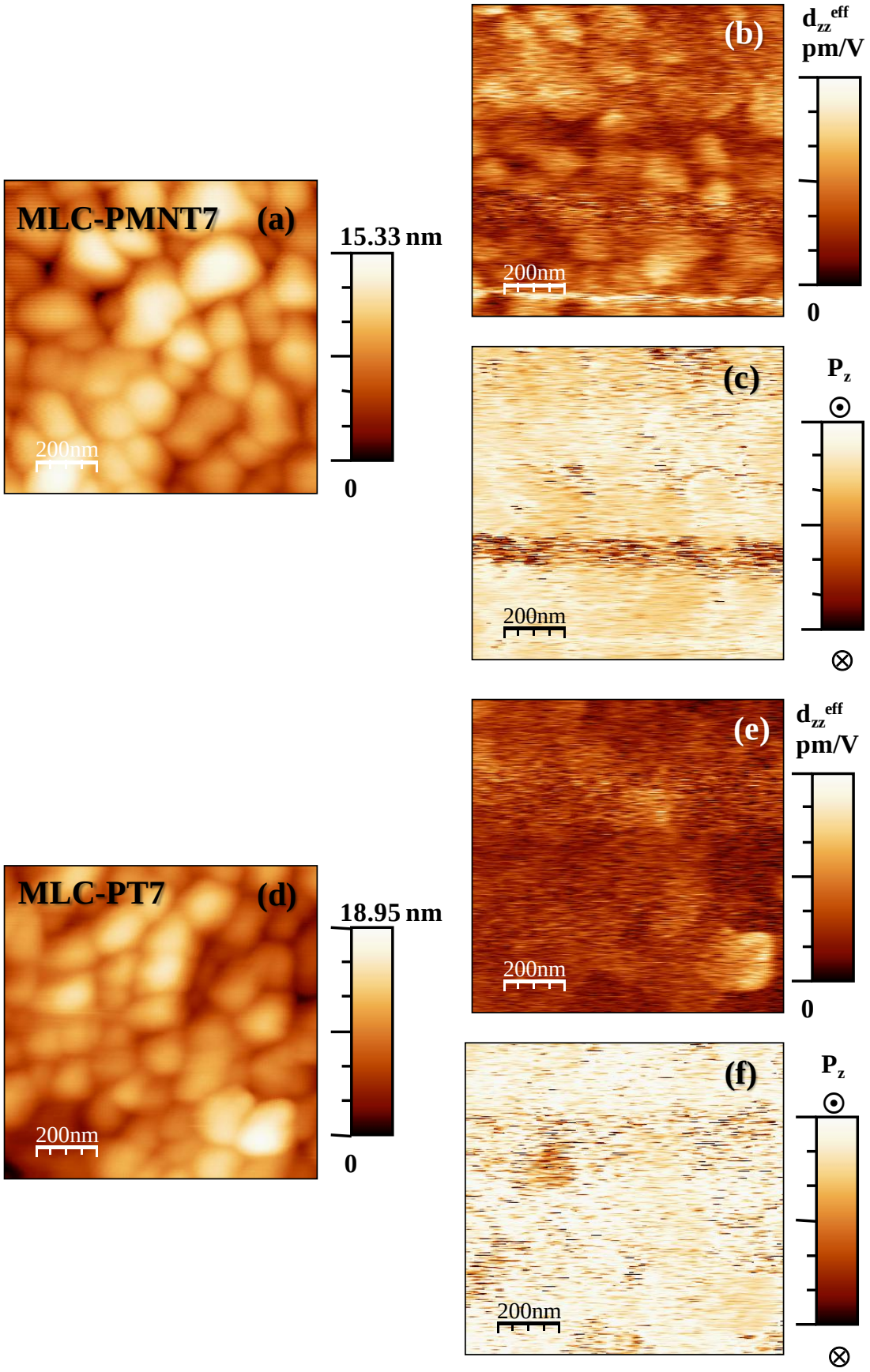

Figure 3.2.6. *SFM images of (a,d) topography; out-of-plane PFM (b,e) amplitude and (c,f) phase for the MLC-PMNT7 and MLC-PT7*

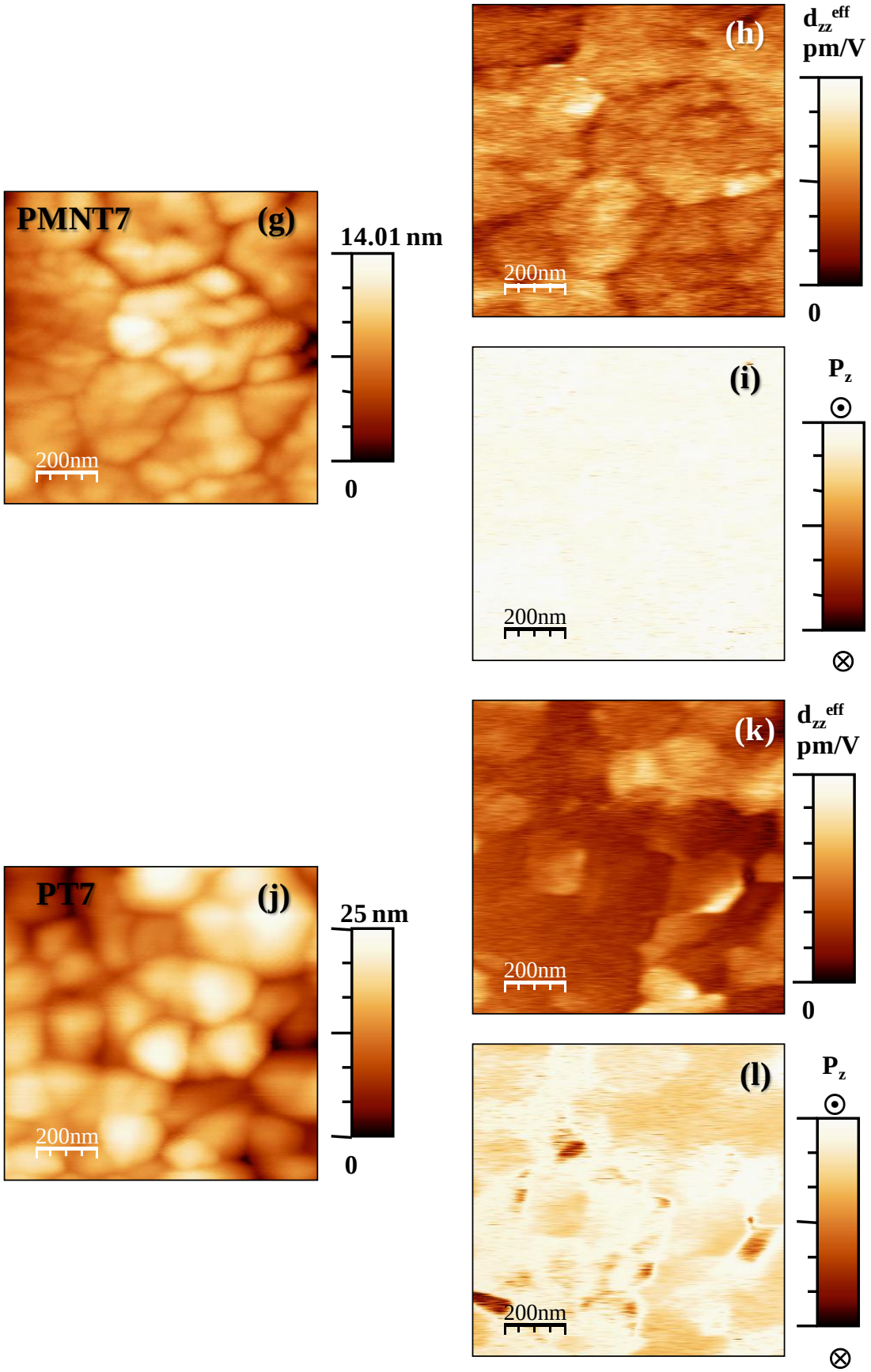

Figure 3.2.6. *SFM images of (g,j) topography; out-of-plane PFM (h,k) amplitude and (i,l) phase for the PMNT7 and PT7*

3.2.4. Dielectric behavior

Figures 3.2.7 and 8 show the variation of the relative dielectric permittivity with the temperature for the 5 and 7 layer films, respectively. Measurements were carried out at different frequencies from 500 Hz to 100 kHz.

The dielectric behavior of the single layer films of PMNT and PT presents differences for 5 and 7 layers. In the case of the PMNT5 (Figure 3.2.7), the relative dielectric permittivity shows a maximum at 403 K. For The PMNT7 film the maximum is at 386 K with a larger value of the dielectric permittivity.

The case of the PT layer is almost the opposite. The PT5 layer presents the maximum at 542 K, a temperature much lower than expected, if the value for the "bulk" material is considered, and then the permittivity decreases gradually down to a value close to zero at 600 K. The PT7 sample presents a maximum at an even lower temperature than PT5, 512 K, but with a larger permittivity of 1000. In this case it drops sharply and at 545 K the value is close to zero, which is accompanied by a similar drop of the dielectric losses. This behavior may be related to problems with the stability of the electrodes that deteriorates at high temperatures.

For the MLC films, two anomalies are observed in their permittivity curves. They correspond to those of the PMNT and PT layers. This result gives an evidence of the existence of separate layers, which is in agreement with the absence of other phases, as it is observed in the XRD patterns. This means that there is not significant interdiffusion among the layers. The two anomalies of the dielectric permittivity occur at different temperatures to those observed for the corresponding single phase films. In fact, these temperatures are closer to those observed in $PbTiO_3$ and $0.65Pb(Mg_{1/3}Nb_{2/3})O_3$-$0.35PbTiO_3$ bulk materials [2,3].

For the MLC-PMNT5 and MLC-PT5 films, the two anomalies are corresponding to the PMNT and PT layers at (428K, 454K) and (580K, 607K), respectively. The increase in the transition temperature of the PMNT layers (larger for the MLC-PT5 film) can be related to a more ferroelectric character of these layer in the MLC composite in relation with the pure PMNT film.

For the MLC7 films the results are qualitatively different. The MLC-PMNT7 response is quite similar to the MLC-PMNT5 one but with larger temperature for the maximum of the PT layers, even the dielectric permittivity values at T_m are close. The

case of the MLC-PT7 sample is quite different, with larger value for the maximum temperature of the PMNT layer (522K) and much lower value for the PT layer (611K). Transition temperature shifts as the ones observed here are related to different stress states and grain sizes of the films. The multilayer composite configuration surely have a different stress state to that of the single phase films, which show columnar growth and grain size differences that have been shown in Figure 3.2.4. The sharp drop in the permittivity observed in the PT7 and MLC-PT7 films seems related to the stability of the electrodes on increasing the temperature. This may be due to the observed columnar microstructure of the PT samples and the large volume changes on increasing temperature expected for the PT and MLC-PT films that affect the electrode behavior.

In any case, this different behavior with the temperature of the MLC films does not prevent them from showing high relative dielectric permittivity and excellent ferroelectric properties at room temperature. These results show evidences of the necessity to improve the quality of the individual layers of the multilayer composite films in order to obtain a more uniform behavior close to the various phase transitions.

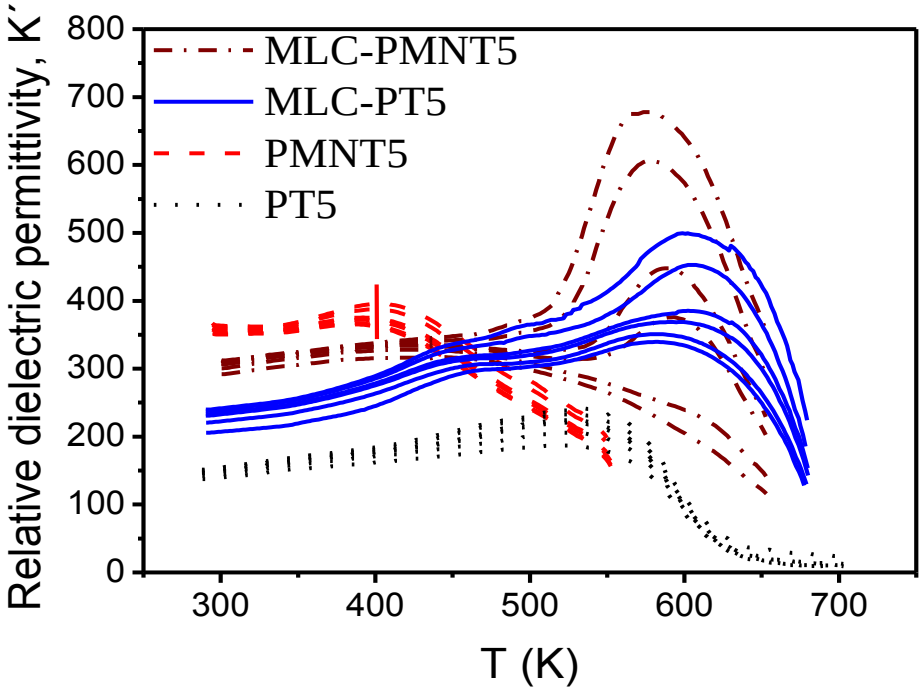

Figure 3.2.7. *Variation of the relative dielectric permittivity with temperature for the five layer PT, PMNT, MLC-PMNT and MLC-PT films*

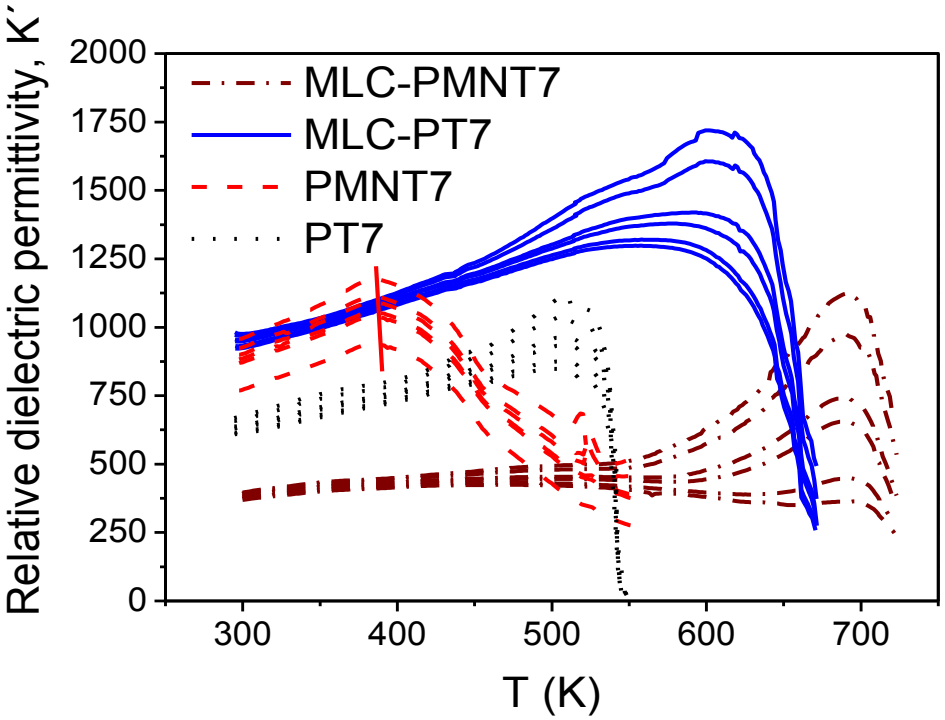

Figure 3.2.8. *Variation of the relative dielectric permittivity with temperature for the seven layer PT, PMNT, MLC-PMNT and MLC-PT films*

3.2.5. Ferroelectric properties of the MLC films: remnant values

Figures 3.2.9 and 3.2.10 show the experimental current loops and the corresponding corrected P-E hysteresis loops, measured at 1 kHz of the 5 and 7 layer films, respectively.

The current loops show that the MLC films do not present the asymmetric leakage currents that we can observe in the single phase PT films and that are common in these films. This can be the consequence of the appearance of conductivity paths along the grain boundaries of the observed columnar microstructure.

Regarding the P-E loops, MLC-PMNT films present slanted loops similar to those of the single phase PMNT films, with large differences between the remnant and saturation values: MLC-PMNT5, $2P_s = 23\ \mu C\cdot cm^{-2}$ and $2P_r = 7\ \mu C\cdot cm^{-2}$; MLC-PMNT7, $2P_s = 28\ \mu C\cdot cm^{-2}$ and $2P_r = 11\ \mu C\cdot cm^{-2}$. In the MLC-PT films, where all the PMNT layers are sandwiched between two poled PT layers, both saturation and remnant polarizations are higher, with smaller differences between them: MLC-PT5 $2P_s = 31\ \mu C\cdot cm^{-2}$ and $2P_r = 14\ \mu C\cdot cm^{-2}$; MLC-PT7, $2P_s = 45\ \mu C\cdot cm^{-2}$ and $2P_r = 20\ \mu C\cdot cm^{-2}$. There is an increment of the coercive field in the MLC-PT films compared with the PMNT single phase and MLC-PMNT which may be related to the presence of the larger number of PT layers. However, the increase of the polarization cannot only be explained by the linear additive effect of the properties of a biphasic layer composite [4]. Based on this, the remnant polarization of the MLC films P_r^{MLC} is calculated from the following equation:

$$P_r^{MLC} = (V_{PT})^{MLC} \cdot P_r^{PT} + (V_{PMNT})^{MLC} \cdot P_r^{PMNT} \qquad (1)$$

where V_{PT}, V_{PMNT} are the volume fractions, and P_r^{PT}, P_r^{PMNT} the remnant polarizations of the PT and PMNT layers present in the MLC films. Using the experimental P_r values of the single phase PT and PMNT films we obtain the calculated values for the remnant polarization of the MLC films of table 3.2.1.

It is observed that the calculated $2P_r$ values are larger than the experimental ones. It must be taken into account that in this simple approximation the differences between the characteristics of the reference PMNT single phase film and the layers in MLC films are not considered. The PMNT films have coarse, columnar grains, whereas the layers in the MLC films show small, single domain crystals, which is the origin of strong differences in the properties of them. Unfortunately we do not have reference

single phase films with similar microstructural features to those of the corresponding layers in the MLC films. Taking into account the much higher values of P_r^{PT} than P_r^{PMNT}, the PT phase should dominate the P_r^{MLC} values in the multilayer composite films, being the $P_r^{MLC-PT}/ P_r^{MLC-PMNT}$ ratio close to the volume fraction of PT for each composite as shown in table 3.2.2.

	Ref. PMNT $2P_r$ ($\mu C\ cm^{-2}$)	**Ref. PT $2P_r$** ($\mu C\ cm^{-2}$)	**Calculated $2P_r$** ($\mu C\ cm^{-2}$)	**Experimental $2P_r$** ($\mu C\ cm^{-2}$)
MLC-PMNT5	4	40	18	7
MLC-PMNT7	8	70	34	11
MLC-PT5	4	40	26	14
MLC-PT7	8	70	43	20

Table 3.2.1. *Comparison between calculated remnant polarization and experimental values for MLC films, together with the reference values of the single phase PMNT and PT used in the calculations*

MLC film	**$(V_{PT})^{MLC-PT}/ (V_{PT})^{MLC-PMNT}$**	**Calculated $P_r^{MLC-PT}/ P_r^{MLC-PMNT}$**	**Experimental $P_r^{MLC-PT}/ P_r^{MLC-PMNT}$**
5 layer MLC	1.50	1.49	2.10
7 layer MLC	1.33	1.26	1.82

Table 3.2.2. *Comparison between the ratios of the calculated and experimental remnant polarization values of the MLC films with different layer configurations, together with the corresponding PT volume ratio*

Indeed, the calculated ($P_r^{MLC-PT}/ P_r^{MLC-PMNT}$) ratios are close to the PT volume ratios for both the 5 and 7 layer MLC films. The ratios obtained from the experimental values are different. This indicates that other mechanisms, different from the linear addition of the properties of the constituent phases; have to be considered in these MLC films.

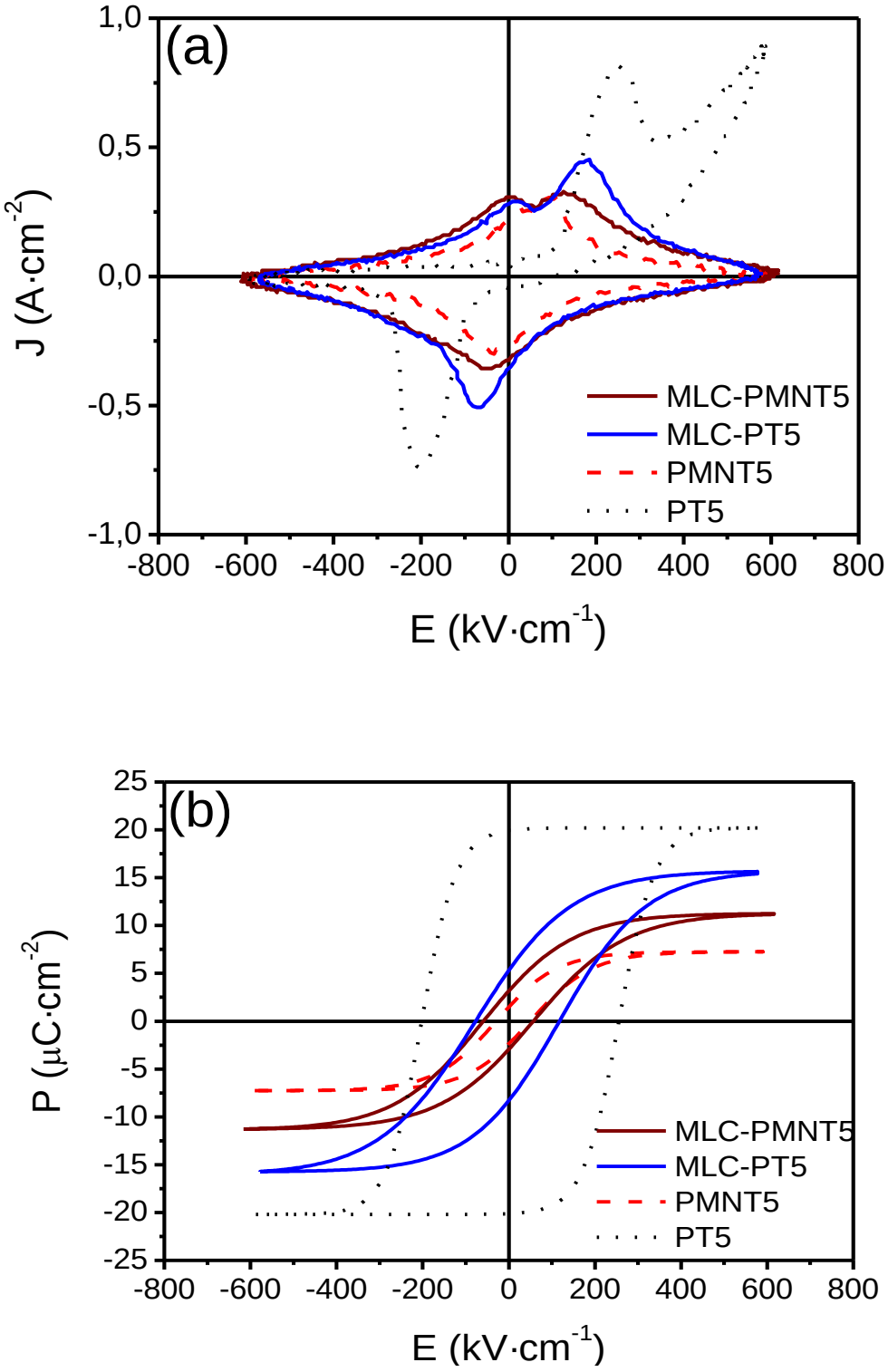

Figure 3.2.9. *(a) Experimental current loops and (b) corrected P-E hysteresis loops of the 5 layer films*

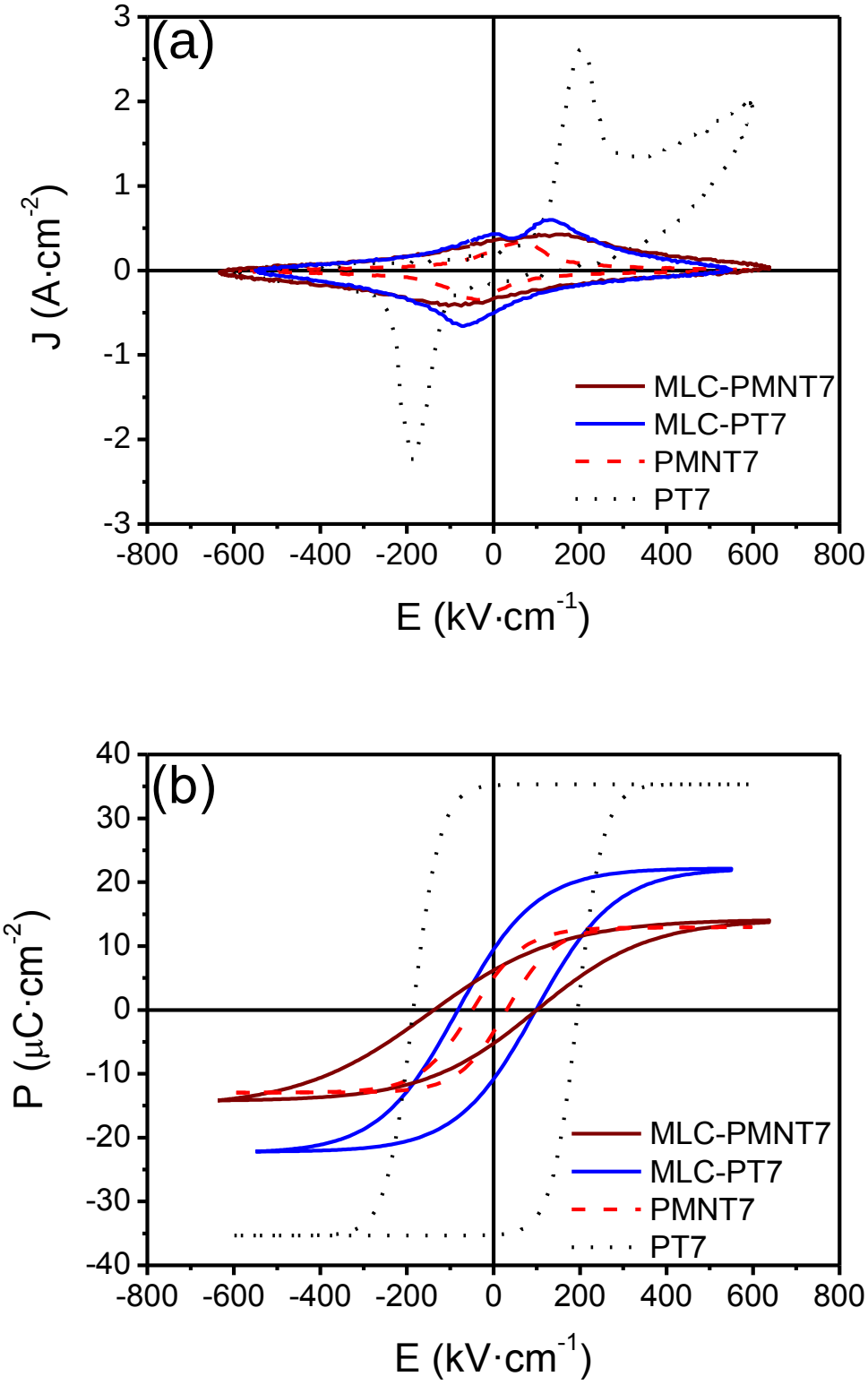

Figure 3.2.10. *(a) Experimental current loops and (b) corrected P-E hysteresis loops of the 7 layer films*

It must be remarked that under the conditions used to obtain the P-E hysteresis loops of Figure 3.2.9 and 10 (1 kHz), there is not time to reach a stable value of the polarization, i.e., full poling. This is especially important if the mechanism used for the enhancement of the polarization of the PMNT layers is based in the poling of the PT layers. Therefore, the low remnant polarization in the MLC-PMNT film can be attributed to the incomplete switching of the PT layers in these measurements. A more favorable situation (with longer switching times) will produce much higher values of the remnant polarization of the MLC films.

P-E hysteresis loops with a delay time of 1 s are shown in Figure 3.2.11 in order to analyze the relaxation at short times of the remnant polarization. It must be remembered that single phase PMNT films loses up to 84% of the remnant polarization after 1 s: PMNT5 film from 6 to 1 $\mu C \cdot cm^{-2}$ (Figure 3.2.11a); PMNT7 film from 2 to 0.5 $\mu C \cdot cm^{-2}$) (Figure 3.2.11b). This lack of polarization retention is still present for the MLC-PMNT films: 60 % loss (from 5 to 2 $\mu C \cdot cm^{-2}$) for MLC-PMNT5 and 45 % loss (from 10 to 5.5 $\mu C \cdot cm^{-2}$) for MLC-PMNT7. This fast relaxation almost disappears for the MLC-PT films, showing the effectiveness of this configuration to retain the polarization: 15% loss (from 7 to 6 $\mu C \cdot cm^{-2}$) for MLC-PT5 and 5% (from 11.5 to 11 $\mu C \cdot cm^{-2}$) for MLC-PT7. These results show that a relatively large and fast relaxation of the polarization is observed in the MLC-PMNT film, while this is negligible for the MLC-PT film. This supports the good retention of the polarization of the MLC-PT film, indicating that the induced polarization in the PMNT layers by the poled PT layers is effective.

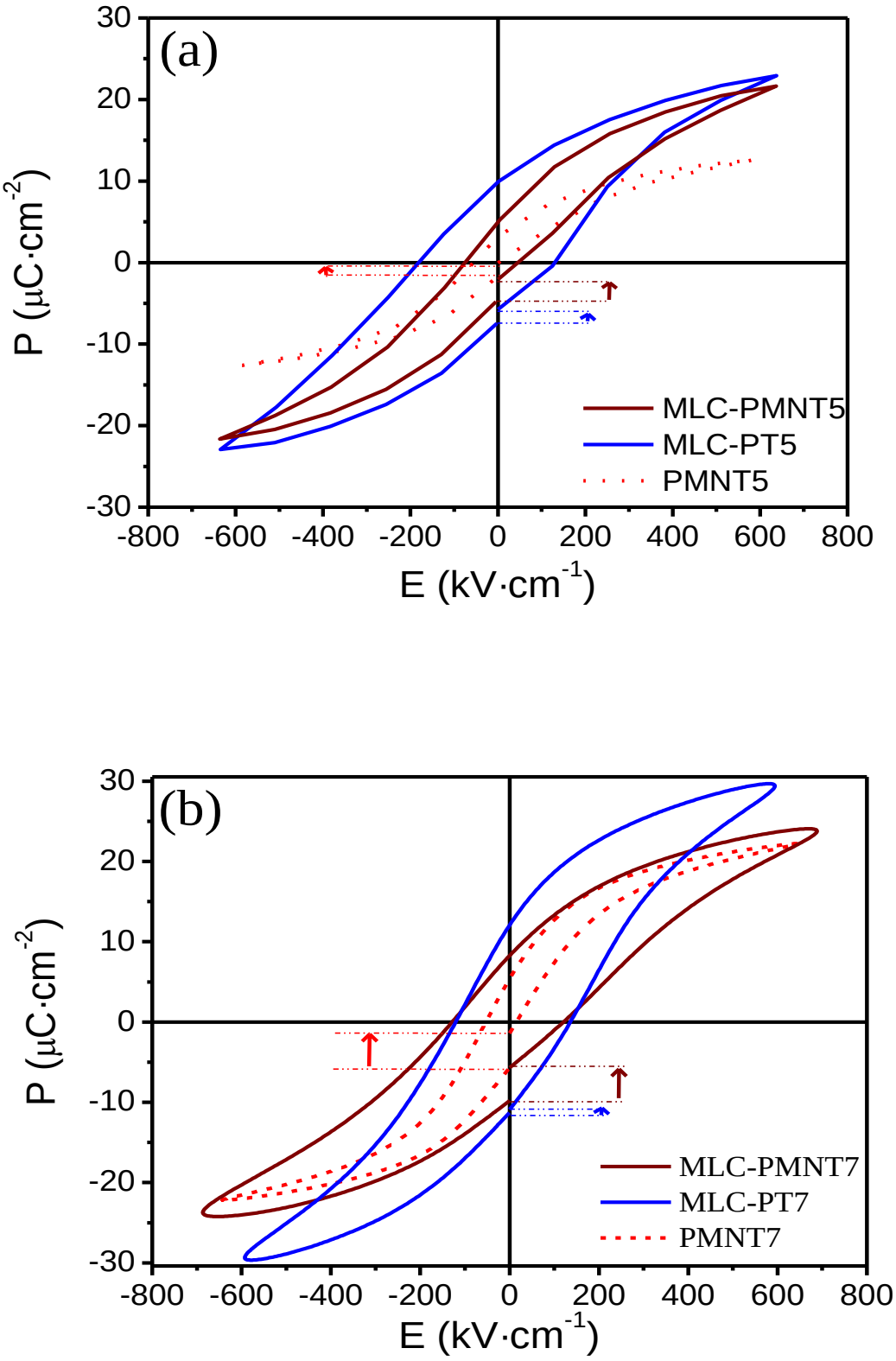

Figure 3.2.11. *P-E hysteresis loops of the (a) 5 and (b) 7layer PMNT and MLC films measured at 1 kHz with 1 s delay time*

The retention of the remnant polarization for long times is an important factor to demonstrate the functional reliability of the MLC films. There are many ways to perform this characterization; however, one of the less time consuming is the measurement of the evolution of the pyroelectric coefficient (γ) with time, before and after poling. The evolution with time of the pyroelectric coefficient for unpoled and poled films (poling field of 300 $kV \cdot cm^{-1}$) is shown in Figures 3.2.12 and 13. Poling is carried out at room temperature with a train of square pulses of 10-15 μs of duration and 300 $kV \cdot cm^{-1}$ of amplitude, both upwards (i.e. towards the film surface, positive sign) and downwards (i.e. towards the film surface, negative sign). The non-zero values of γ obtained for all the films before the poling process indicate that all of them show some degree of self-polarization, which corroborates the observations made on the PFM images. The occurrence of self-polarization is common in ferroelectric films [5] and has its origin in the interface between the film and the substrate. This self polarization can be associated to a Schottky- type electric contact between the film and bottom electrode [6] or to strain gradients and the flexoelectric effect [7]. For MLC-PMNT films, up to 40% of the initial pyroelectric coefficient value is lost after 12 h. Similarly, the pyroelectric coefficient of the MLC-PT films decreases down to a ~48% of the initial γ value after the same time. The largest percentages of losses of the coefficients with long times are obtained when the film is poled against its self-polarization. These results show that the MLC films have higher values of the pyroelectric coefficient than the PMNT film, an improvement that is associated with the enhancement of the remnant polarization in the composite multilayer configuration, as discussed above.

For MLC-PMNT5 film, the poling process produces rather stable values of the pyroelectric coefficient with time (Figure 3.2.12(a)), besides a significant increase of the overall values. The pyroelectric coefficient of the MLC-PT7 film only decreases a ~27% after long times (Figure 3.2.13(d)). These results indicates that the 7L-MLC films have higher values of the pyroelectric coefficient than the PMNT7 film, which is associated with the enhancement of the polarization in the composite multilayer configuration discussed above. In addition, the asymmetry in the polarization disappears. The MLC-PMNT7 film shows stable values of the pyroelectric coefficient with time, after the initial decrease after a short period of time, observed in the P-E loops of Figure 3.2.11(b). The MLC-PT7 film has a slow relaxation of the coefficient values with time (Figure 3.2.13(d)).

It is observed that the PMNT5 and PT5 films suffer a ~35 and 15 % loss of the initial γ value after withdraw of the poling field and 12 hours, when it is poled against its self-polarization (Figure 3.2.12(a) and (b)), respectively. Polarization is more stable in the case of PMNT5 when the electric field is applied in the same sense as its self-polarization that it suffers a ~25% loss after 12 hours.

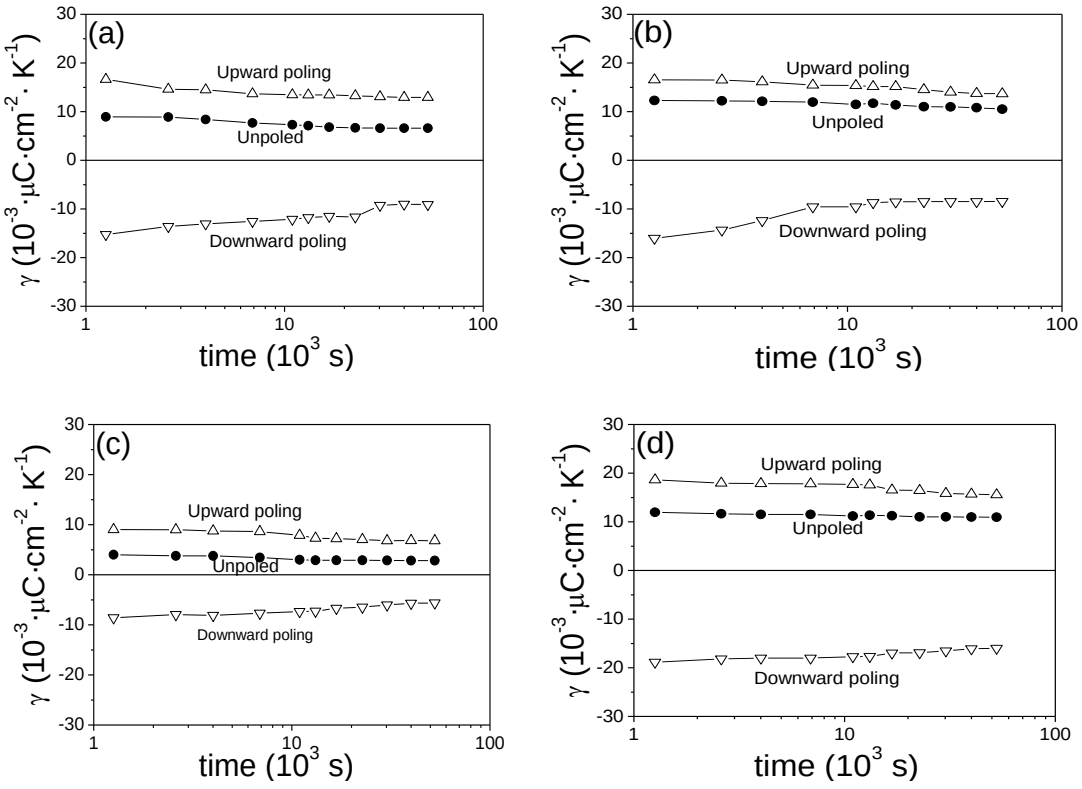

Figure 3.2.12. *Evolution with time of the pyroelectric coefficient (γ) before and after poling: (a) MLC-PMNT5, (b) MLC-PT5, (c) PMNT5and (d) PT5 films*

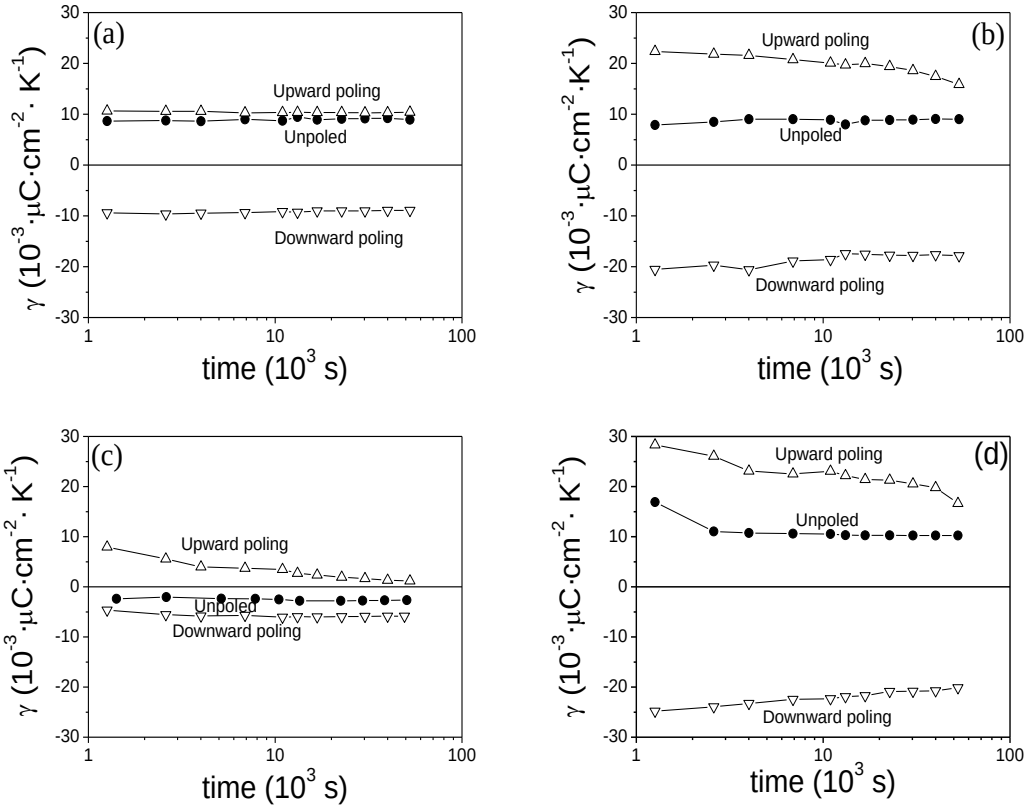

Figure 3.2.13. *Evolution with time of the pyroelectric coefficient (γ): (a) MLC-PMNT7, (b) MLC-PT7, (c) PMNT7 and (d) PT7 films*

3.2.6. Piezoelectric properties of the MLC films

The macroscopic piezoelectric behavior of the films can be studied by using a double-beam interferometer. Figure 3.2.14 shows the results obtained. Although the piezoelectric loops of the reference PMNT7 film is saturated with the maximum electric field applied (the coercive field of this film is lower, see Figure 3.2.10), the rest of the hysteresis loops for the PT and MLC films seem to be non-saturated, producing sub-coercive loops. They need the application of higher electric fields. However, the application of large electric fields for long times, required due to the stepwise application of the DC field in this type of measurements, leads to the appearance of leakage currents in these films. This is most probably due to a problem in the quality of the MLC films that will be analyzed in the next chapter. As a consequence, the piezoelectric behavior of the MLC films cannot be properly compared with that of the PMNT7 film.

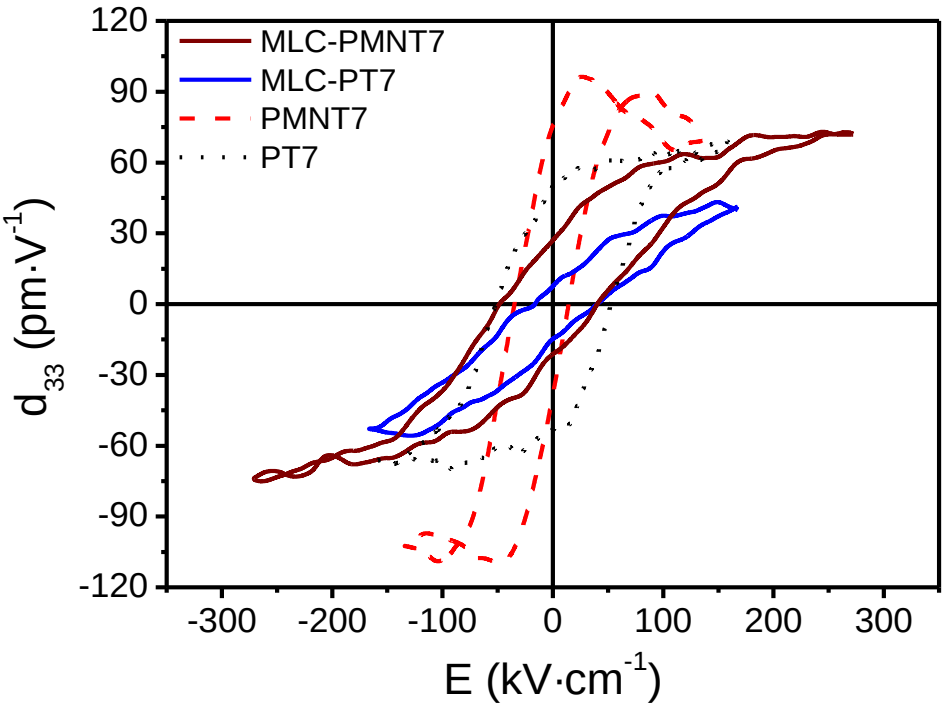

Figure 3.2.14. *Macroscopic piezoelectric responses of 7 layer films*

Local piezoelectric characterization with a Piezoresponse Force Microscope is not affected by this problem, and locally we can apply large enough electric fields to test the piezoelectric behavior of the films. Figure 3.2.15a and b shows the comparison among the local piezoelectric hysteresis loops. Regions in the film with the largest piezoelectric response are selected for measurement and representative loops are shown. This allows us to perform a qualitative analysis of the piezoelectric response of the MLC films with respect to the reference films. The results suggest that the largest remnant piezoelectric coefficients seems to be obtained for the MLC-PT films, in which, according to the previous results shown in this chapter, the enhancement of the remanence of the high piezoelectric PMNT films is more efficient. Every PMNT layer is located between two PT layers that induce a stable electrical bias in them. The single phase PT films show large remnant piezoelectric coefficients, although their intrinsic d_{33} values are not large. This may be related to the presence of 90^{o} ferroelastic domains in these films (see the PFM results of Figure 3.2.5) due to their large grain size in comparison with the MLC films. Note that the initial and final values of the loops are different for all the films, similarly to the hysteresis loops of Figure 3.2.11. This is

because both measurements are carried out, with a lapse of time under a short circuit condition among the successive measurements.

As a conclusion, these results (although local and non quantitative) can be considered evidence that MLC films achieve improved piezoelectric behavior, presenting improved remnant coefficients with respect to single phase PMNT, and without any trace of the fast relaxation characteristic observed for it, which indicates again the appearance of stable induced polarization in the PMNT layers. Therefore, it can be concluded that the configuration of MLC-PT in which every PMNT layer is sandwiched between poled normal ferroelectric layers is the most appropriate to obtain optimized piezoelectric films based on MPB PMNT.

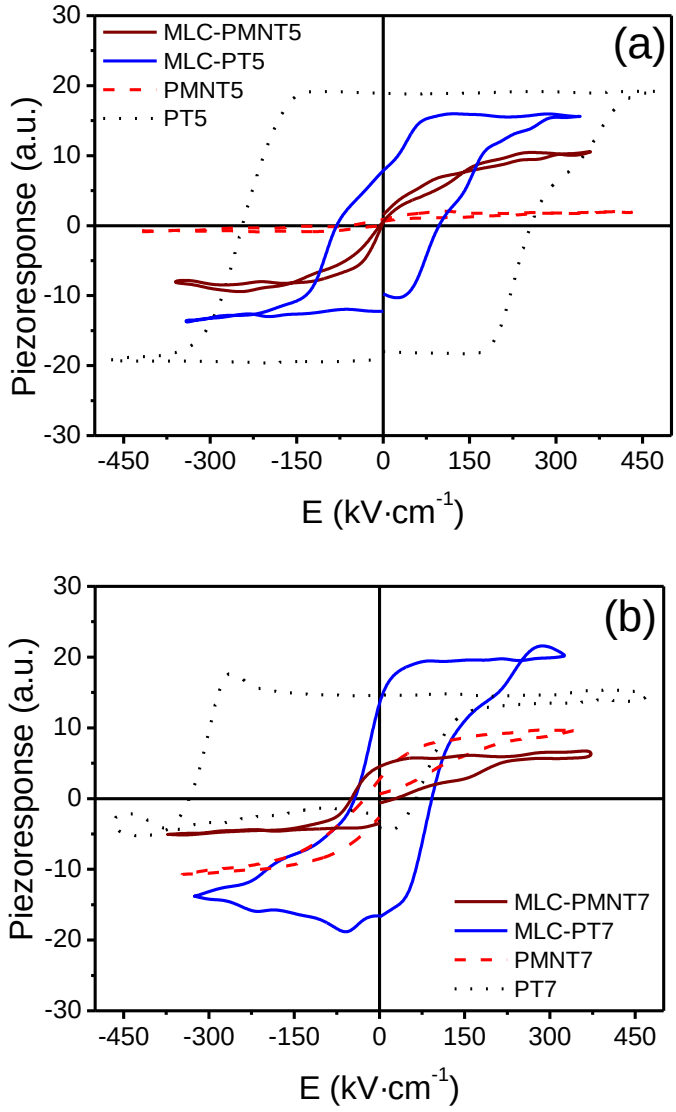

Figure 3.2.15. *Local piezoelectric hysteresis loops of (a) 5 and (b) 7 layer films*

3.2.7. Remarks

- The study of the properties of 2-2 biphasic multilayer composite thin films based on $Pb(Mg_{1/3}Nb_{2/3})O_3$-$PbTiO_3$ (PMNT), with compositions close to the Morphotropic Phase Boundary (MPB), shows that stable polarization can be induced in PMNT layers by neighbouring poled ferroelectric layers, like $PbTiO_3$ (PT). This multilayer film configuration is very effective when every PMNT layer is sandwiched between two PT layers (MLC-PT).
- The MLC-PT films produces an enhancement of the remnant polarization with respect to the single phase PMNT films
- The increase of the layer thickness, and thus the grain size, in the multilayer composite films makes easier the observation of the increase of the remanence, which if compared with the PMNT single phase film the increase of the remnant polarization reaches now 70 % (from 4 to 14 $\mu C \cdot cm^{-2}$), compared to the 50% of the multilayer composite with multiple thin layers.
- The quality of the multilayer composite films can be improved so the application of large enough electric fields is possible. Otherwise, we will not be able to take advantage of the good piezoelectric properties of these multilayer composite films.
- The relative amount of PMNT in the MLC-PT films was fixed in the examples shown in this chapter, keeping always the same thickness for the PT and PMNT layers. In order to obtain the highest piezoelectric coefficients possible, the relative amount of the PMNT layers must be increased. The improvement of the multilayer composite films will be the focus of Chapter IV.

3.2.8. References

[1] X. Guitang, H.L. Wahchan, J. Am. Ceram. Soc. 87, 1588 (2004)

[2] V.P. Palkar, S.C. Purandare, R. Pinto, J. Phys. D: Appl. Phys. 32, R1 (1999)

[3] Z. Xia, L.Wang, W. Yan, Q. Li, Y. Zhang, Materials Research Bulletin 42, 1715 (2007)

[4] R.E. Newnham, D.P. Skinner, L.E. Cross, Mat. Res. Bull. 13, 525 (1978)

[5] V.P. Afanasjev, A.A. Petrov, I.P. Pronin, E.A. Tarakanov, E. Ju Kaptelov, J. Graul, J. Phys. Condens. Matter. 13, 8755 (2001)

[6] A.L. Kholkin, K.G. Brooks, D.V. Taylor, S. Hiboux, N. Setter, Integr. Ferroelectr. 22, 1045 (1998)

[7] A. Gruverman, B.J. Rodriguez, A.I. Kingon, R.J. Nemanich, A.K. Tagantsev, J.S. Cross, M. Tsukada, Appl. Phys. Lett. 83, 728 (2003)

CHAPTER IV

IMPROVEMENT OF THE QUALITY OF THE MULTILAYER COMPOSITE FILMS

PART 1

Preparation of high quality $PbTiO_3$ layers

In the previous chapter of this work it was shown that the role of $PbTiO_3$ layers in the MLC films is the induction of an internal bias field in the $Pb(Mg_{1/3}Nb_{2/3})O_3$-$PbTiO_3$ (PMNT) layers, so these layers can have more polarization after the removal of the electric field. To do that, the $PbTiO_3$ layers must have large polarizations, only achieved when they are fully poled after the application of a large electric field. Unfortunately, it has been observed that the $PbTiO_3$ films present large leakage currents that prevent the effective application of large electric fields. This can be attributed, among other causes, to the appearance of cracks in the film. They can be produced by the stress accumulated during the preparation of the films, which are crystallized at high temperatures. On cooling from those temperatures, a phase transition at ~470^{o}C from the high temperature cubic phase to the largely asymmetric tetragonal phase of $PbTiO_3$ at room temperature takes place.

In order to avoid that, it has been reported that the temperatures necessary for the formation of the perovskite $PbTiO_3$ films can be much reduced, and even at temperatures as low as 400^{o}C, high quality films have been prepared [1]. Therefore, thin film crystallization below the transition temperature is possible, which will avoid the formation of large stresses on cooling to the room temperature. In this chapter the influence of the crystallization temperature on the properties and microstructure of $PbTiO_3$ films will be studied, in order to find the optimum preparation conditions of high quality $PbTiO_3$ layers to be incorporated in improved multilayer composite films.

4.1.1 Thin film preparation

Four layers of 0.1 M $PbTiO_3$ solution were spin coated and crystallized at three different temperatures: 400°C (PT400) which is the lowest temperatures reported for the crystallization of lead titanate based perovskites [2-4], 500°C (PT500) which is closer to the $PbTiO_3$ ferro-paraelectric transition temperature (490°C) and 650°C (PT650) which is the temperature normally used for obtaining good crystalline films of lead titanate based compositions, without the appearance of any secondary phase.

4.1.2 Characterization of the crystalline structure and the residual stress

Figure 4.1.1 shows the X-Ray Diffraction (XRD) patterns, with Bragg-Brentano geometry (θ-2θ), of the PT400, PT500 and PT650 thin films. All the PT films are single perovskite phase, without any secondary crystalline phases.

The lattice parameters a and c of the $PbTiO_3$ films were calculated from the position of the 001 and 100 diffraction peaks, and are summarized in Table 4.1.1. The diffraction peaks were deconvoluted with pseudo-Voigt functions. The tetragonality (c/a) for each crystallized film is smaller than the one obtained for single crystal $PbTiO_3$ (1.065(1)) which corresponds to lattice parameters c = 4.153(2) Å and a = 3.899(0) Å [5-7]. Besides, it can be observed that the tetragonality of these films is even smaller when the crystallization temperature is above the Curie temperature.

Another important parameter that can be deduced from the X ray diffraction data is the crystallographic preferential orientation, or texture. The preparation of highly oriented $PbTiO_3$ films with their polar axis <001> perpendicular to the film surface increases their net polarization [8]. From the relative intensity of the diffraction peaks the appearance of crystallographic preferential orientations in the PT films can be studied. We use the Lotgering factor (f_{hkl}) [9] for the <100> and <001> directions:

$$f_{hkl} = (P_{hkl} - P_0) / (1 - P_0)$$

$$P_{hkl} = I_{hkl} / \sum I_{hkl},$$

$$P_0 = I_{0\,hkl} / \sum I_{0\,hkl} \qquad (1)$$

where I_{hkl} and $I_{0\,hkl}$ are the intensities of the hkl diffraction peaks of the film and of the reference $PbTiO_3$ (JCPDS-ICDD 6-452), respectively.

The Lotgering factor goes from 0 (random orientation) to 1 (full oriented). Results are collected in table 4.1.1 and show that the films crystallized at temperatures below the transition temperature have a larger tendency to have the <001> polar direction perpendicular to the film substrate, while when the films are crystallized at 650ºC this is lost and <100> is the preferred crystallographic direction.

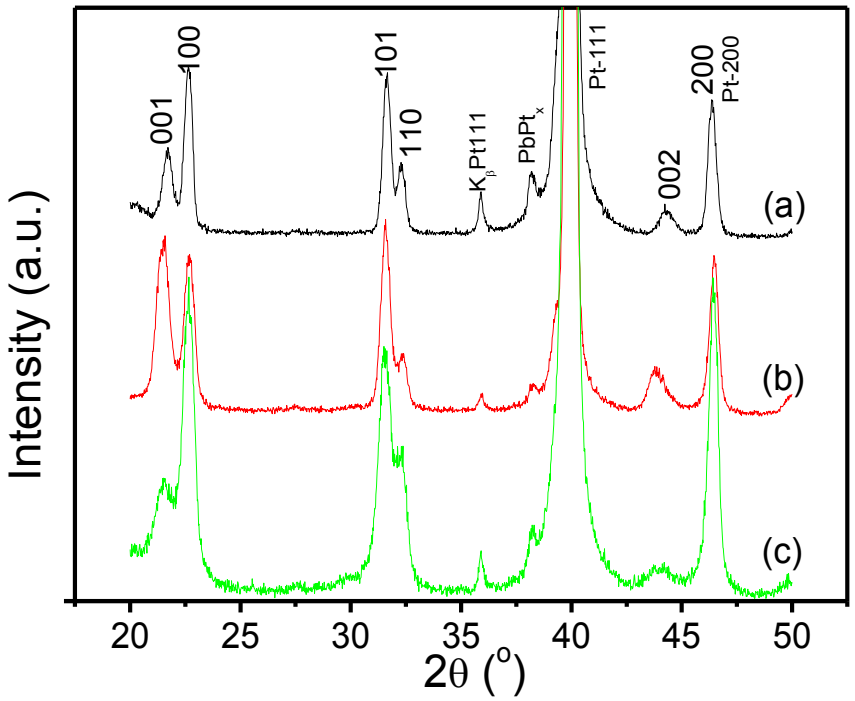

Figure 4.1.1. *XRD patterns of the (a) PT400, (b) PT500 and (c) PT650 films (Pt: platinum, $PbPt_x$: intermetallic interface)*

Film	a (Å) (± 0.005Å)	c (Å) (± 0.005Å)	c/a	Lotgering factor	
				f_{001}	f_{100}
PT400	3.926	4.131	1.052	0.3	0.1
PT500	3.919	4.137	1.056	0.4	0.1
PT650	3.927	4.098	1.044	0.1	0.3

Table 4.1.1. *Lattice parameters of the PT films together with their Lotgering factors*

The differences found in the lattice parameters and preferential orientation of the PT films when they are crystallized at temperatures above or below the Curie temperature can be attributed to the different processes that take place in both cases. When the film is crystallized in the cubic phase, the transition to the tetragonal phase is limited by the substrate to which the film is attached. Therefore, the resulting tetragonality cannot be as high as when the film is crystallized directly into the tetragonal phase as it happens in PT400 and PT500. The tensile stress of the Si-based substrate on the film during the phase transition makes that the long axis of the crystals lay preferably in the plane of the film and not perpendicular to it, so the Lotgering factor $f_{001} < f_{100}$. These restraints are not present when the crystallization takes place directly into the tetragonal phase. Therefore, in this case it is more favorable to have the long axis of crystals in the direction of free growth, perpendicular to the film surface, resulting in $f_{001} > f_{100}$ for PT400 and PT500.

These different processes are bound to produce different residual stress, which largely determine the properties of the films. There are mainly three different sources of residual stress in thin films: the lattice mismatch between substrate and film, the different thermal expansion coefficients of both and the occurrence of phase transformations from the crystallization temperature to room temperature. In our case, the deposition on a polycrystalline Pt electrode discards the occurrence of any lattice matching between film and substrate. The different thermal expansion coefficients of the PT film and the Si-based substrate are shown to result in tensile stresses [10]. Regarding the phase transition on cooling, this factor only appears for PT650. Therefore, it is worthy the analysis of this parameter.

In order to quantify the residual stress we compare the curvature radii of the substrate before deposition (R_s) and the film (R_f). The residual stress σ is calculated using the modified Stoney equation [11]:

$$\sigma = \left[\frac{E_s}{6(1-\upsilon_s)}\right]\left[\frac{t_s^2}{t_f}\right]\left[\frac{1}{R_f}-\frac{1}{R_s}\right] \qquad (2)$$

where E_s is the Young's modulus of the substrate, υ_s is the Poison ratio for the substrate, t_s and t_f are the thicknesses of the substrate and the film, respectively. The curvature radii for the three films, obtained by profilometry, are shown in Figure 4.1.2 and their values and the results of the calculations are collected in table 4.1.2. To obtain the

curvature radii, the experimental scans were fitted to circumferences or parabolas with coefficients of determination of $R^2 > 0.99$. We use for the silicon-based substrate: $E_s = 130 \cdot 10^9$ Pa, $\upsilon_s = 0.3$ and $t_s = 0.5 \cdot 10^{-3}$ m. The film thickness (t_f) is measured on Scanning Electron Microscopy images of cross-sections of the films.

The films crystallized at temperatures below the ferro-paraelectric transition temperature show, as expected for the difference in the thermal expansion coefficients of film and substrate, tensile stress (positive). However, when the crystallization occurs at 650ºC, we obtain a negative value of the stress for the PT650 film, that in principle should be attributed to a change from the expected tensile to a compressive stress state, which is in disagreement with the preferential orientation along the <100> direction perpendicular to the film surface, typical of a film under tensile stress [10]. Due to the fact that $PbTiO_3$ suffers a large transformation from a cubic to a tetragonal phase with a large c/a, the reason for this discrepancy may be attributed to a partial detachment of the film from the substrate, unable to withstand the large stress accumulated, and that invalidates the comparison of the curvature radii before and after the deposition, and, therefore, the calculation of the residual stress.

Film	R_s (m)	R_f (m)	t_f (nm)	σ_{sf} (100 MPa)
PT400	29.32	27.15	240	+0.9
PT500	27.25	25.64	260	+0.7
PT650	19.23	35.04	190	-9.8

Table 4.1.2. *Residual **s**tress of the PT films calculated from curvature radii of the substrate before film deposition (R_s) and of the films (R_f)*

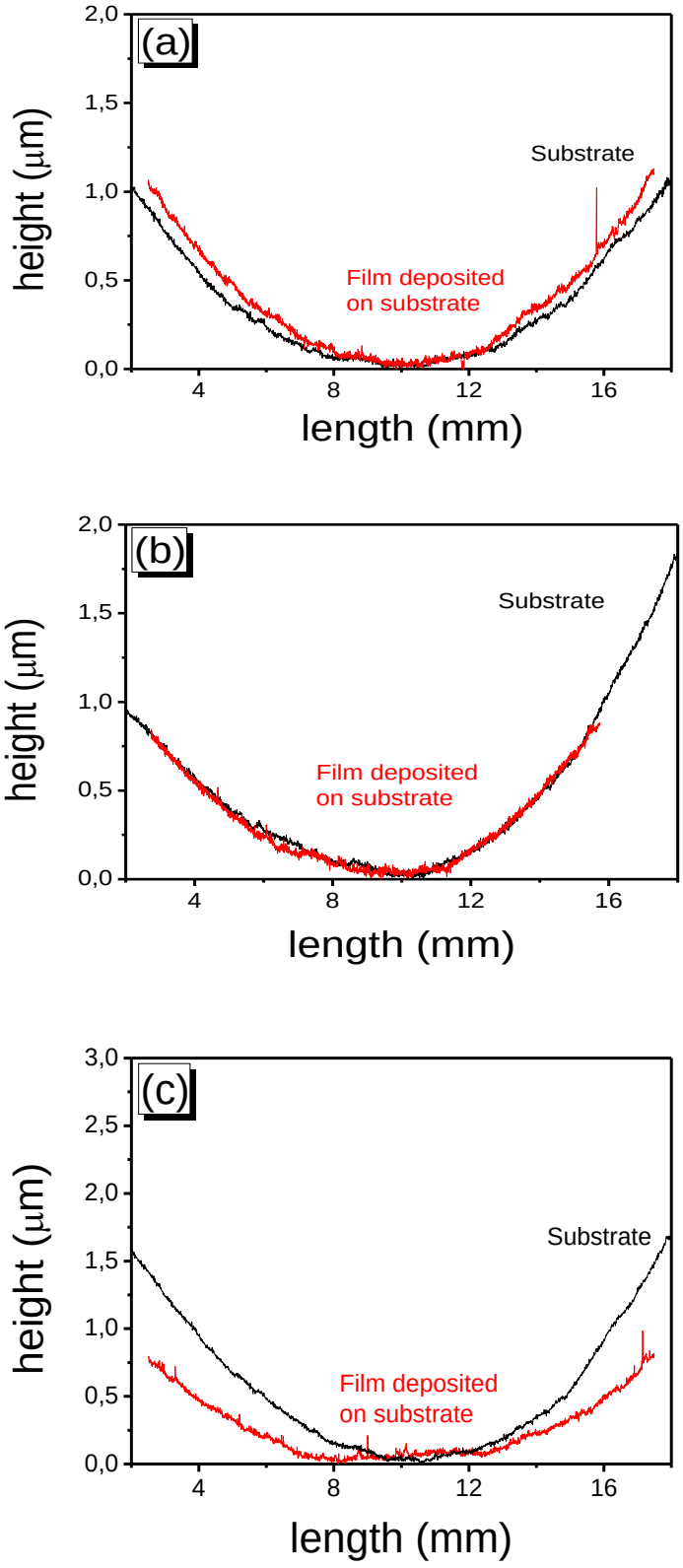

Figure 4.1.2. *Sample deflections through the top surfaces of the Si-based substrate before and after the deposition of the film: (a) PT400, (b) PT500 and (c) PT650*

4.1.3 Characterization of the films microstructure and ferroelectric domain configuration

The optical microscopy images (Figure 4.1.3) show that in the film crystallized at 650^{o}C there is a larger amount of macroscopic defects than in PT400 and PT500. This means that the probability for an electrode deposited onto the surface of the film prepared at 650ºC to cover a defect, and produce a short circuit, is much larger than for a film prepared at lower temperatures. This increase in the number of macroscopic defects of the film surface can result in large leakage currents in these capacitors as compared with those of the films prepared at lower temperatures. As a result, the electric fields used for poling these PT650 layers are less effective, requiring the application of very high fields that results in a dielectric breakdown of the film, which renders it useless for their use in multilayer composite films. .

The SEM micrographs of the surfaces of the films are shown in Figure 4.1.4. The images show fine grains for PT400 and PT500 films (100-125 nm), while the size of grains increases up to approximately 300 nm for PT650 film. The plane view images show also a large amount of small pores for PT400 film. The cross section images show that the PT650 film develop a columnar grain growth, which is not observed in the PT400 and PT500 films. The columnar microstructure of the PT650 film can also contribute to its larger leakage currents preventing the effective poling of the capacitors.

The Figures 4.1.6, 4.1.7 and 4.1.8 show SFM topography, PFM out-of-plane and in-plane images of the PT400, PT500 and PT650 thin films. The PFM images do not show any traces of ferroelastic 90º domains inside the grains, even for the largest grains of PT650 film. This can be attributed to the fact that the film thickness is not large enough for the formation of these domains. Besides, the PFM phase images show a tendency to have a large portion of the film area with the out-of-plane component of the polarization oriented towards the films surface, which indicates the presence of self polarization in all three films, stronger in the case of PT400 and PT500.

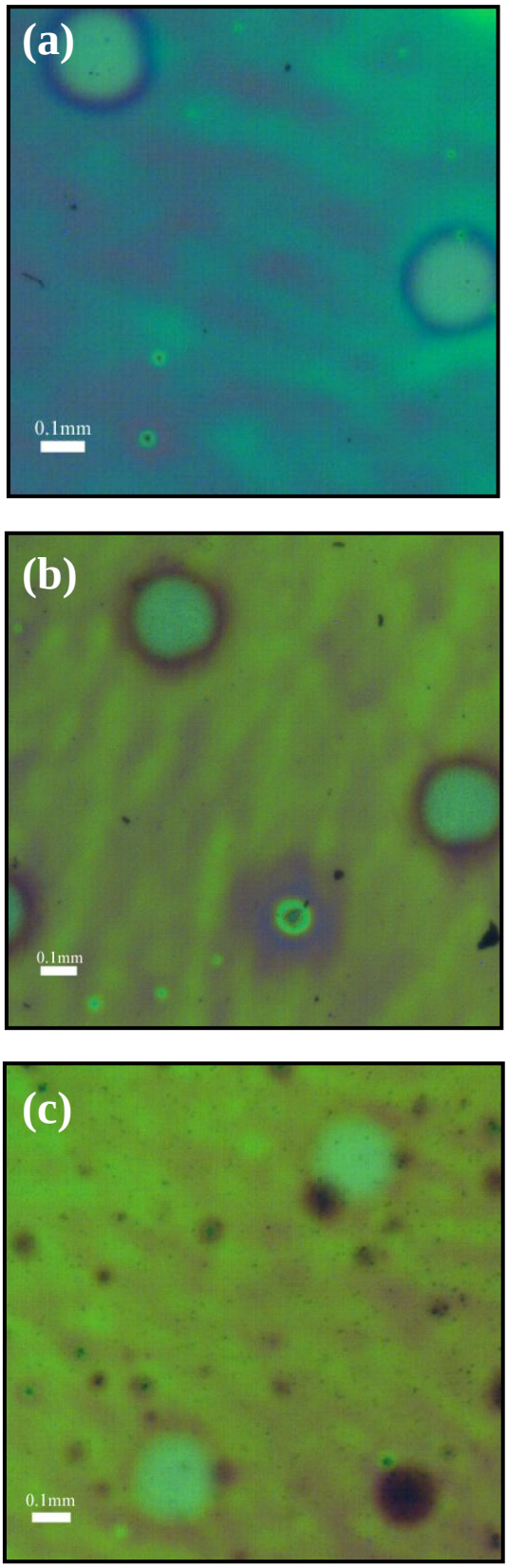

Figure 4.1.3. *Optical microscopy images of the film surfaces of (a) PT400, (b) PT500 and (c) PT650 films. Note that the bright circles are the Pt upper electrodes deposited on the film surface*

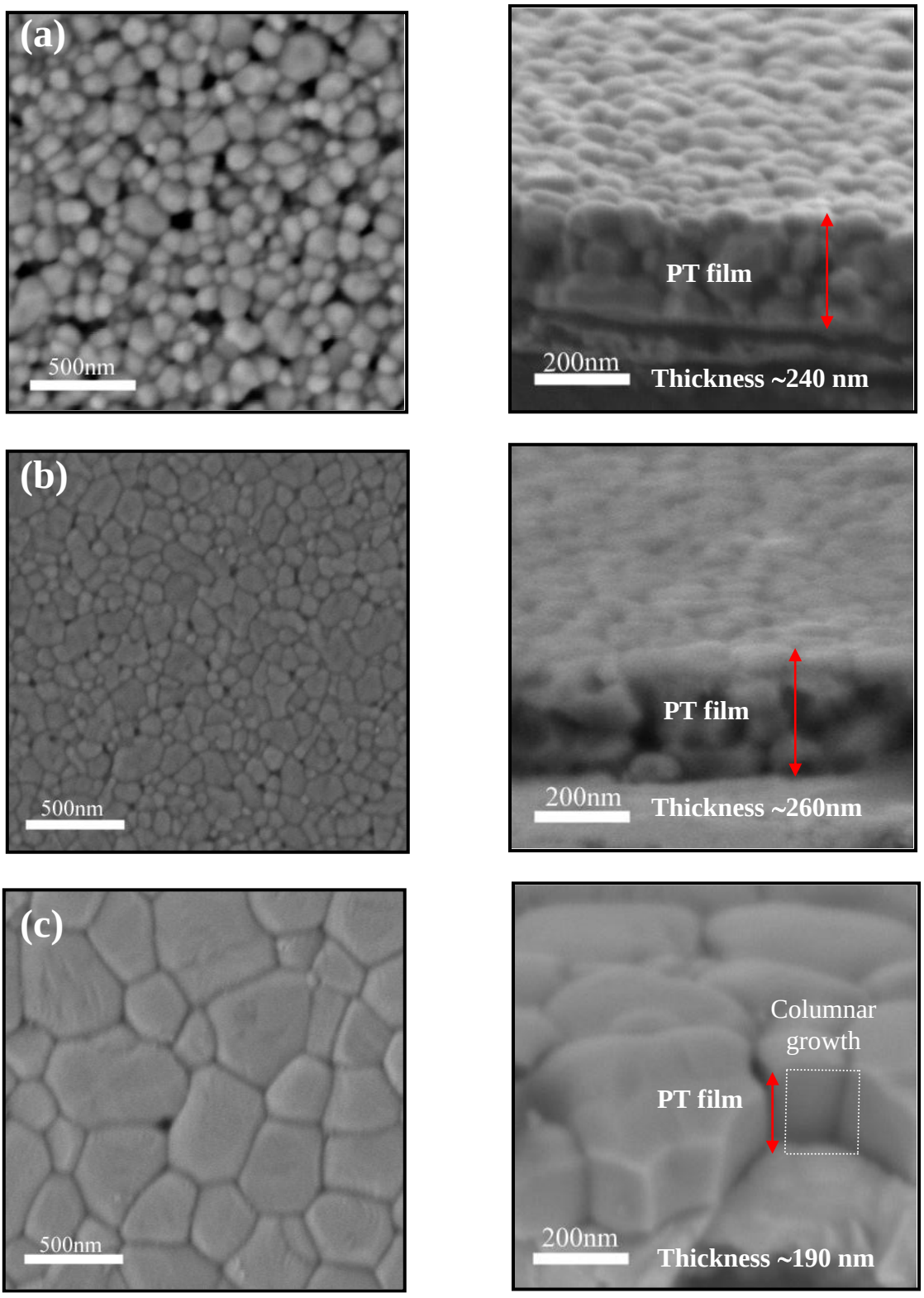

Figure 4.1.4. *SEM micrographs of plan view and cross-sections of the (a) PT400, (b) PT500 and (c) PT650 films*

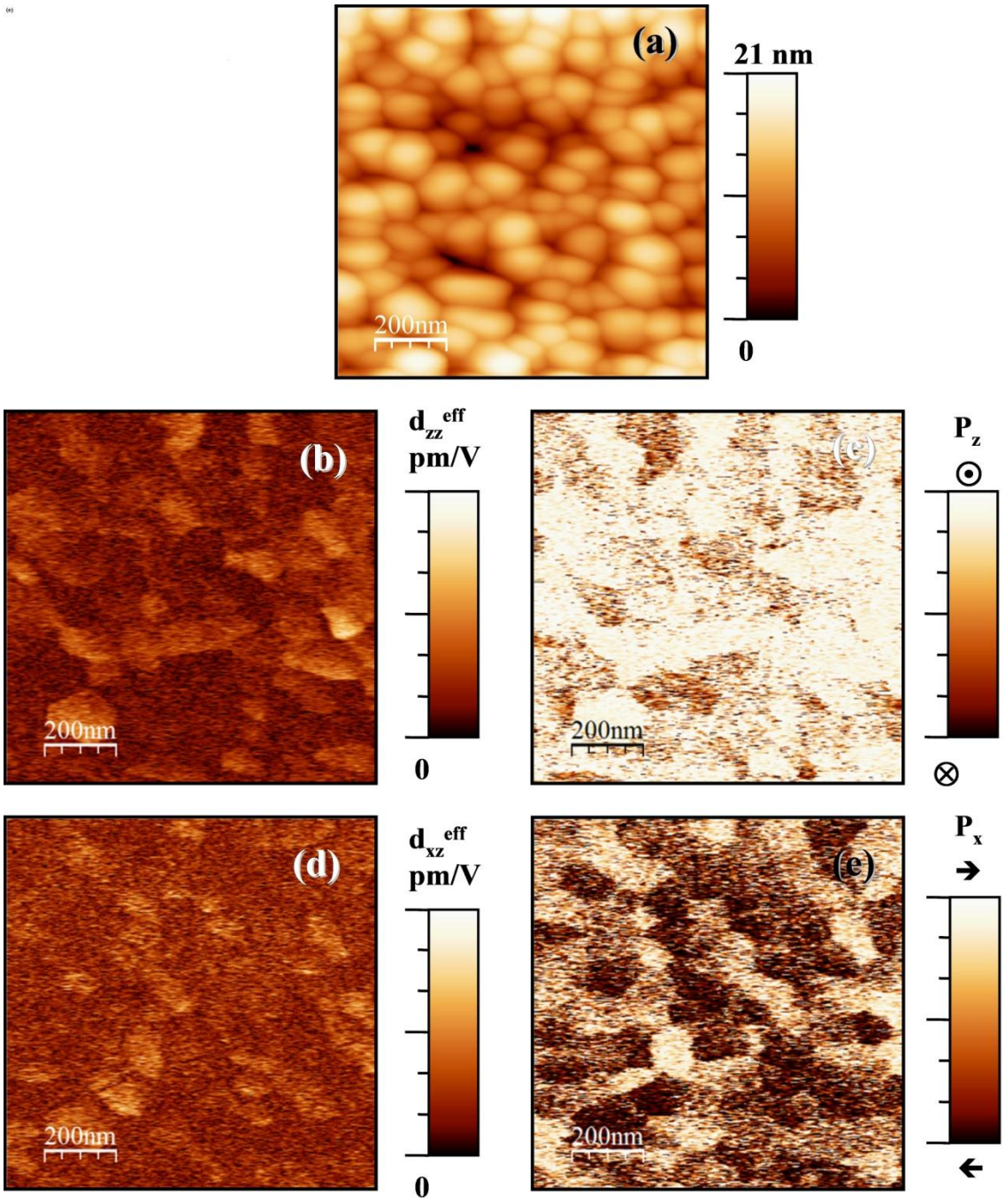

Figure 4.1.5. *SFM images of the PT400 film: (a) topography; PFM out-of-plane (b) amplitude and (c) phase piezoresponse; PFM in-plane (d) amplitude and (e) phase piezoresponse*

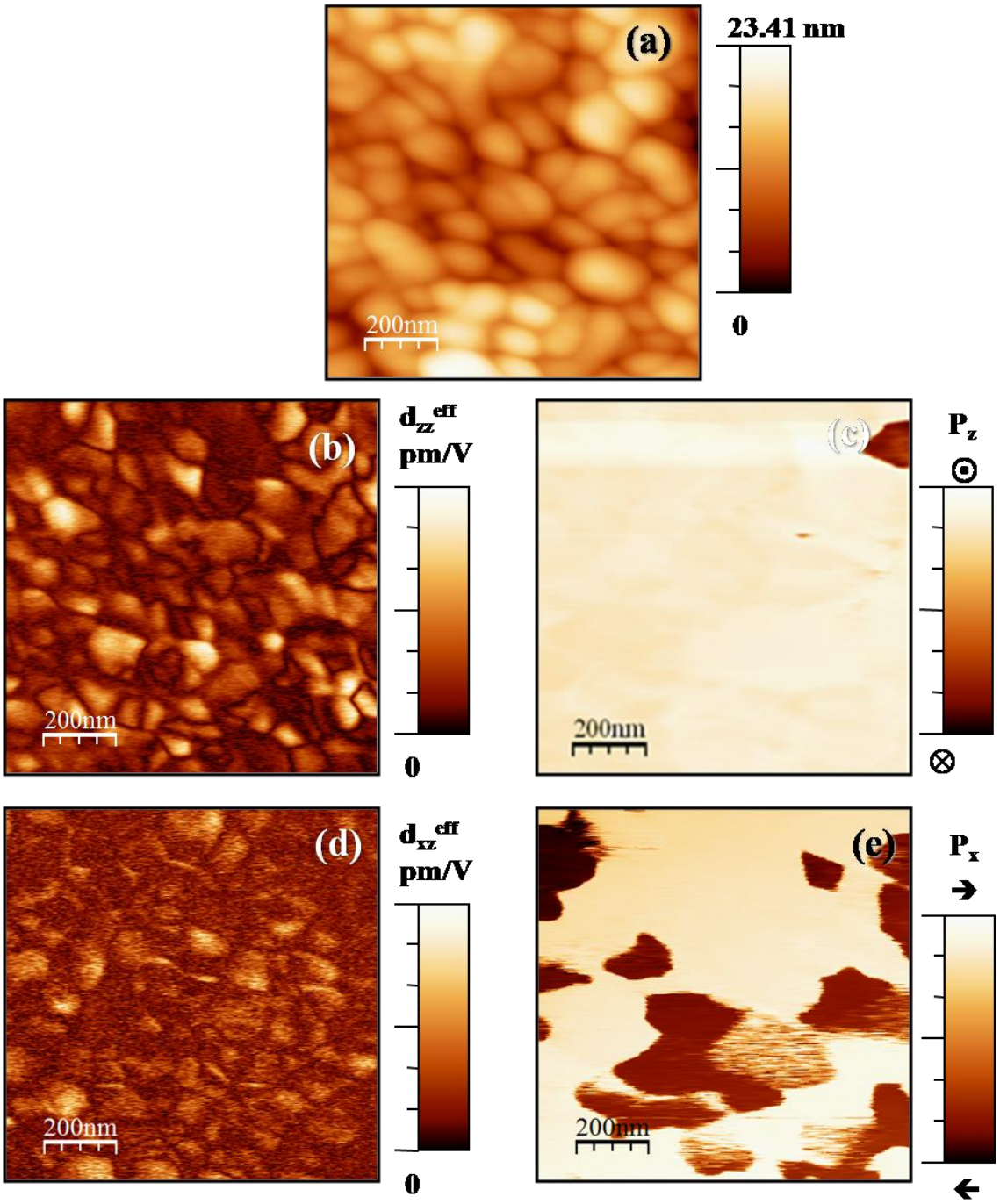

Figure 4.1..6 *SFM images of the PT500 film: (a) topography PFM; out-of-plane (b) amplitude and (c) phase piezoresponse; PFM in-plane (d) amplitude and (e) phase piezoresponse*

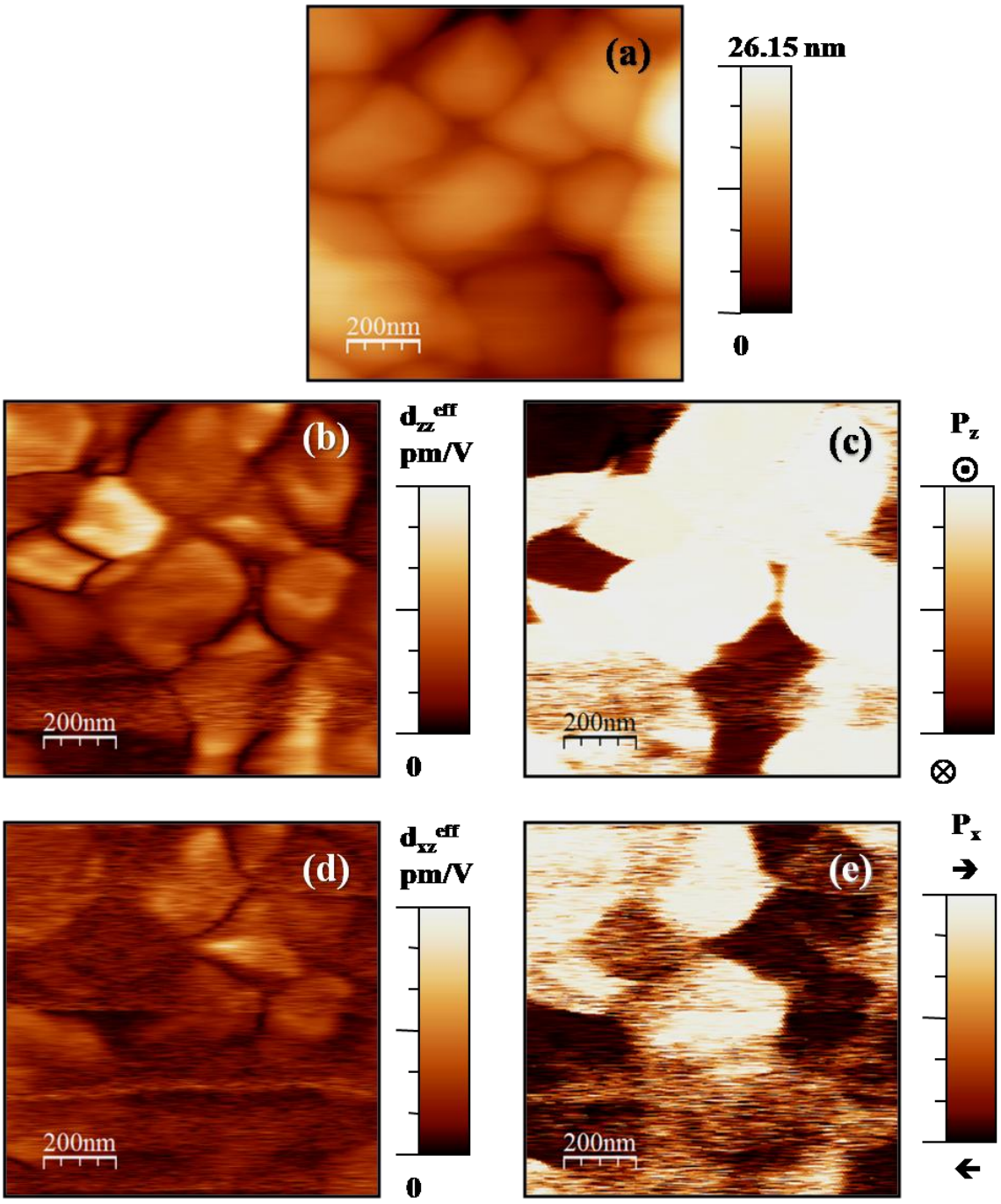

Figure 4.1.7 *SFM images of the PT650 film: (a) topography; PFM out-of-plane (b) amplitude and (c) phase piezoresponse; PFM in-plane (d) amplitude and (e) phase piezoresponse*

4.1.4. Dielectric and ferroelectric properties of the PT films

The dielectric and ferroelectric responses of the PT films prepared at different temperatures were analyzed. Firstly, in order to see the effect of the crystallization temperature on the para-ferroelectric transition of the PT films, the relative dielectric permittivity (K') vs. temperature at different frequencies for the PT400, PT500 and PT650 films are measured (Figure 4.1.8).

The PT400 film shows two maxima, at 400ºC and at 490ºC, presenting large frequency dispersion. The temperature of the maximum of the relative dielectric permittivity at 490ºC matches the temperature of the ferroelectric-to paraelectric phase transition in bulk $PbTiO_3$ materials, which is evidence that this film is almost stress free. The large frequency dispersion can be attributed to a core-shell configuration of the grains, typical of these very low crystallization temperatures, where the core is crystalline but the shell presents a defective crystallization. This shell may be the responsible of the peak appearing at a lower temperature. If this is so, the core of well crystallized $PbTiO_3$ is stress free, thanks to this shell. As the temperature of crystallization increases, the large frequency dispersion and the small peak start to disappear, as it can be seen for PT500 In figure 4.1.8.b. The temperature of the maximum of the dielectric curve decreases to 418ºC, which suggests that with the crystallization at temperatures close to the phase transition, the resulting film has some strain. This strain increases for the PT650 film, crystallized at a much higher temperature, and that shows the maximum of the relative dielectric permittivity at an even lower temperature.

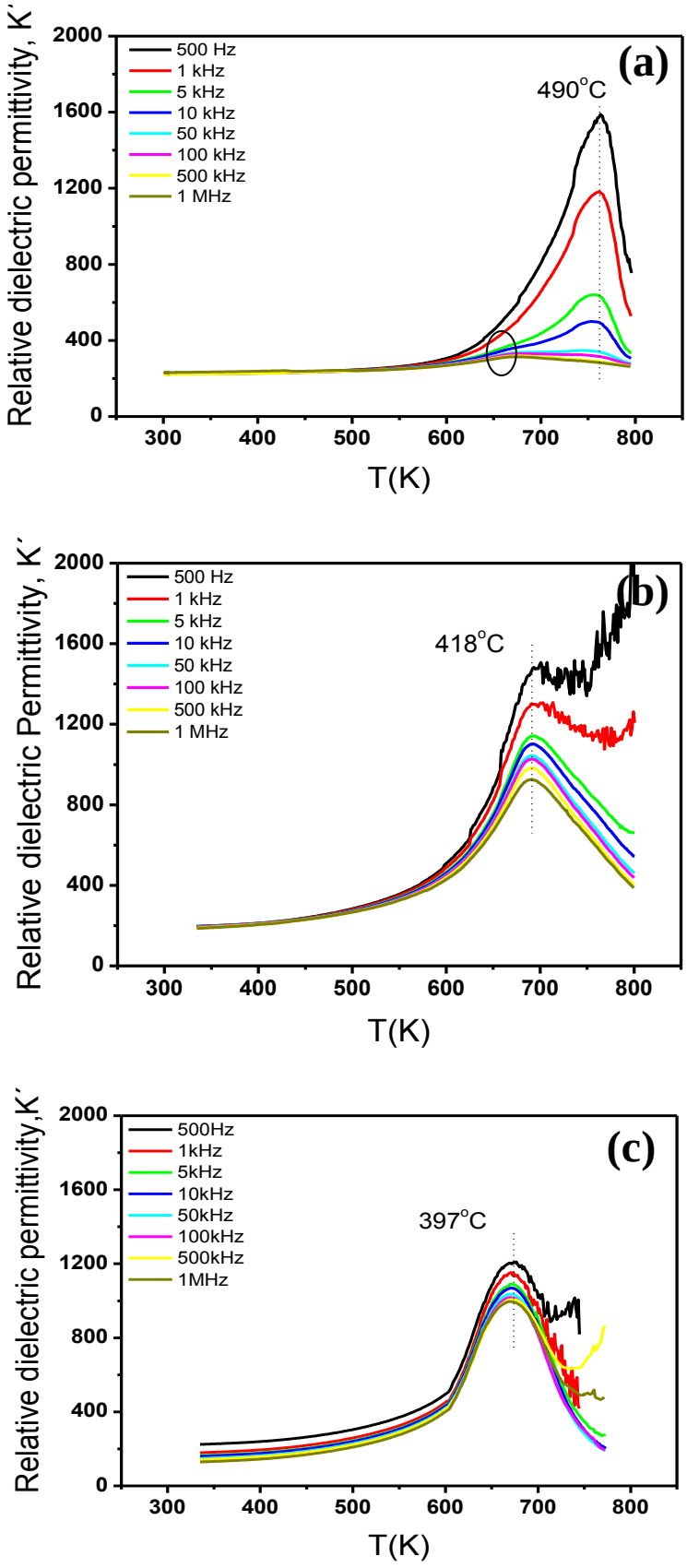

Figure 4.1.8. *Variation of the relative dielectric permittivity with temperature for the (a) PT400, (b) PT500 and (c) PT650 films, measured at various frequencies*

Figure 4.1.9a shows the current density loops measured at a frequency of 1 kHz for the three films. PT400 and PT500 films show conventional loops presenting well defined switching current maxima and rather low conductivity contribution. The PT650 film presents different characteristics. For these films two loops are presented, one obtained with relatively low fields (< 300 kV cm^{-1}) and the other with high fields (up to 1MV cm^{-1}). The first one presents small switching current peaks, indicating some quantity of easy switchable charge in the film, which disappears completely when large electric fields are applied. The loops do not present clear switching current maxima and just lossy capacitor behavior is observed. On increasing the field above 1MV·cm^{-1} high leakage currents appears, until irreversible dielectric breakdown of the capacitor occurs. This can be attributed to the present of large residual stress in this film. Crystallization above the ferro-paraelectric phase transition makes that the PT650 film must transform from a cubic to a tetragonal phase with a large c/a on cooling. This transformation may be the origin of the large residual stress of the films. Therefore, when large electric fields are applied, the switching of the large domains may produce cracking at the film-electrode bottom interface. This cracking detaches partially the film and the bottom electrode, which makes the application of the electric field very ineffective, and impedes to obtain the switching of the polarization.

Besides, the non switching contributions are reduced in the PT400 and PT500 films, which contain small losses. Figure 4.1.9b shows the corrected P-E hysteresis loops of the PT400 and PT500 films at 1 kHz. The remnant polarization of the PT400 and PT500 films are 24 and 27 μC·cm^{-2}, respectively. The larger P_r values of PT500 are indicative of the larger amount of switchable ferroelectric phase than for PT 400. The coercive field of PT500 film (E_c = 251 kV·cm^{-1}) is smaller than that of PT400 film (365 kV.cm^{-1}). This difference can be attributed to the better crystallinity of the PT500 film thanks to its higher crystallization temperature, which may also avoid the appearance of possible non-ferroelectric interfacial phases between grains.

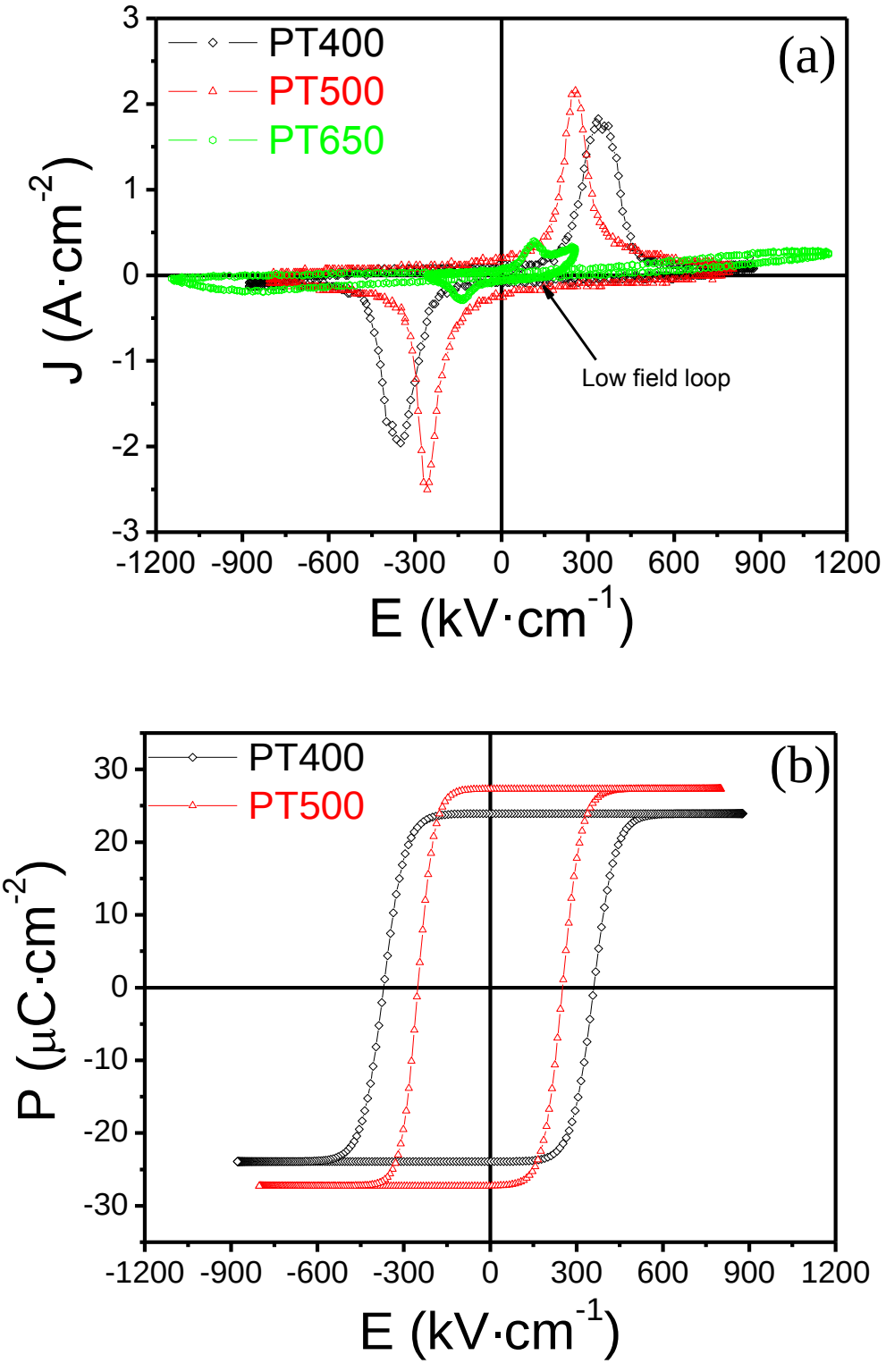

Figure.4.1.*9. (a) experimental current loops of the PT films at different temperatures (400°C, 500°C and 650°C). (b) Corrected P-E hysteresis loops obtained for the same films*

The main problem of the PT650 film is the efficient application of large enough fields, necessary to characterize its functional properties to compare with the other two films. This is not an issue for local measurements carried out with a conductive tip, as a large electric field is concentrated in a small volume of the film. Moreover, the field distribution coming from a small tip on the surface of a large grain makes that the largest effect of the film take place close to the grain surface and so, in the case of columnar grain the observed loop response is more related to the grain close to the tip than to the grain close to the bottom electrode. This last part of the grain attached to the bottom electrode, where the stress effect is more important. Therefore, the local piezoelectric loops show, to a large extent, the response of the more relaxed region of the films. Figure 4.1.10 shows local in-field piezoelectric loops for the three films studied. Regions in the film with the largest piezoelectric response are selected for measurement and representative loops are shown. It can be observed that the individual grains show comparable functional properties in all films.

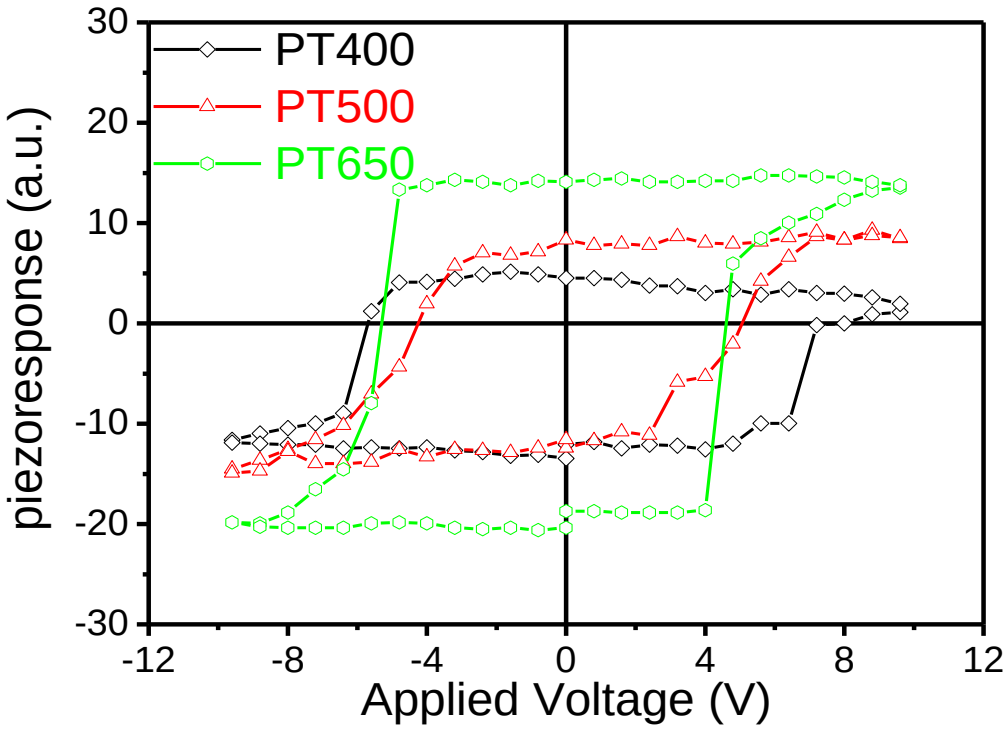

Figure.4.1.10. *Local piezoelectric hysteresis loops of PT samples at different temperatures*

Another important parameter to establish the functional reliability of the films is the retention of the remnant polarization for long periods of time. This was studied by the observation of the evolution of the pyroelectric coefficient (γ) with time. Moreover the measurement of the pyroelectric coefficient in as-prepared capacitors without poling gives important information about the initial polarization state of the capacitor. Figure 4.1.11 shows γ vs. log (time) for the three PT films, without poling and after downward and upward poling. The non-zero values of this coefficient for all the unpoled films indicate that all of them present self-polarization to some extent, corroborating the PFM results that indicate a tendency to have the out-of-plane component of the polarization pointing towards the films surface. When poling is carried out the pyroelectric coefficient values increase. In the case of poling in the same sense of the self polarization, the pyroelectric coefficients obtained are higher, due to the fact that we are applying the electric field in a sense that is already favored by the self-polarization. After some time, the absolute values of the pyroelectric coefficient are similar for both the films poled upward and downward. This means that, although poling in the same direction of the self polarization produce higher polarization, this is temporary, and finally the poling film reaches the same net polarization independently of the sense of the applied electric field used. The small values of γ for the PT650 film compared with PT400 and PT500 films can be related to the already discussed problems in the application of large electric fields in this film, which results in an ineffective poling and therefore small pyroelectric coefficients. As a conclusion, we can say that the $PbTiO_3$ films analyzed in this section are able to retain the polarization after long periods of time, which is an important feature to be an active layer in the PMNT-based multilayer composite films.

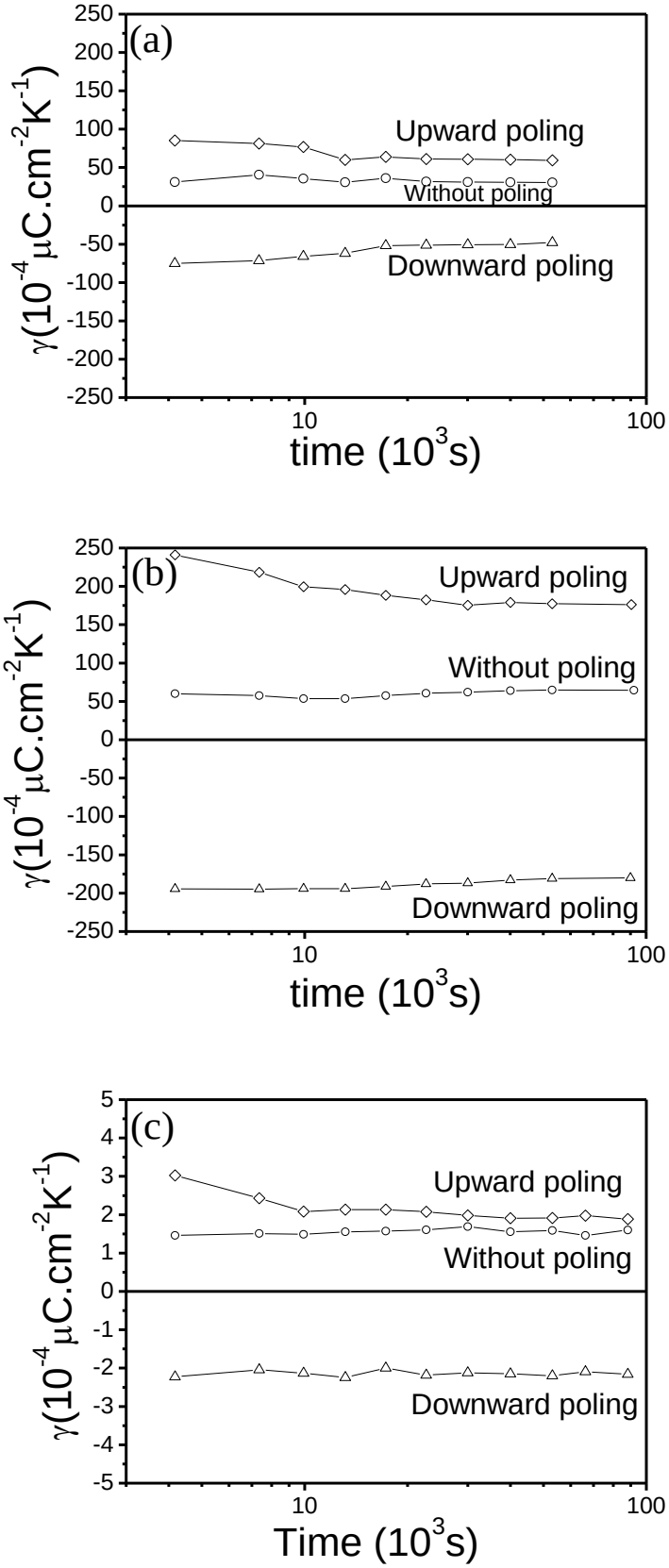

Figure 4.1.11. *Evolution with time of the pyroelectric coefficient (γ) before and after poling at 400 kV·cm^{-1}: (a) PT400; (b) PT500; (c) PT650 films*

4.1.5. Remarks

- The crystallization of $PbTiO_3$layers at low temperatures does not stabilize any secondary phases in this case.
- The crystallization of $PbTiO_3$layers at temperatures close or below the transition temperature causes an increase of the tetragonality (c/a) and of the number of the crystals with their polar axis perpendicular to the film surface. Porosity is also reduced, although for the films prepared at 400ºC there are evidences that regions of low crystallinity are present.
- The crystallization of the PT films at temperatures below and close to the ferro-paraelectric transition reduces significantly the residual stress.
- The large residual stress present in the films crystallized at 650ºC, mainly due to the contribution of the structural transformation on cooling, may produce cracking in the interface with the electrode that makes difficult the application of large electric fields, and, therefore to obtain full poling of these layers, necessary for their effective inclusion in the multilayer composite films. This is avoided if crystallization takes place at temperatures below T_C.
- The polarization values of the films crystallized at low temperatures (400 and 500^{o}C) are large and stable with time.
- Therefore, in order to obtain high quality PT films for their integration in multilayer composites, crystallization temperature must be close or below that of the para-ferroelectric transition.

4.1.6. References

[1] C. de Dobbelaere, M.L. Calzada, R. Jiménez, J. Ricote, I. Bretos, J. Mullens, A. Hardy, M. van Bael, J. Amer. Chem. Soc. 133, 12922 (2011)

[2] M. Kosec, B. Malic, M. Mandeljc, Mater. Sci. Semicond. Process. 5, 97 (2003)

[3] S.S.N. Bharadwaja, T. Dechakupt, S. Trolier-Mackinstry, H. Beratan, J. Am. Soc. 91, 1580 (2008)

[4] J. Li, H. Kameda, B.N.Q. Trinh, T. Miyasako, P.T. Tue, E. Tokumitsu, T. Mitani, T. Shimoda, Appl. Phys. Lett. 97, 102905 (2010)

[5] G. Shirane, S. Hoshino, K. Suzuki. "Phase transitions in $PbTiO_3$". Phys. Rev. 80, 1105 (1952)

[6] B. Jaffe, W.R. Cook, H. Jaffe, "Piezoelectric Ceramics" (Academic, London and New York, 1971)

[7] S.A. Mabud, A. M.Glazer, J. Appl. Cryst. 12, 49 (1979)

[8] C. Lichtensteiger, J. M. Triscone, J. Junquera, P. Ghosez, Phys. Rev. Lett., 94, 047603 (2005)

[9] F.K. Lotgering, J. Inorg. Nucl. Chem. 9, 113 (1958)

[10] R. Jiménez, A. González, M.L. Calzada, J. Mendiola, J. Mater. Res. 15, 1041 (2000)

[11] G.G. Stoney, Proc. R. Soc. London. Ser. A 82, 172 (1909)

PART 2

Preparation of high quality PMNT layers

In the multilayer composite films we aim at taking full advantage of the large piezoelectric properties of $Pb(Mg_{1/3}Nb_{2/3})TiO_3$-$PbTiO_3$. In order to do that the first step is the preparation of high quality PMNT layers. For Chemical Solution Deposition films it was reported in the literature that if the majority of the organics present in the solution are evaporated at temperatures close to those used in the drying step, the resulting film contains less residual porosity after the crystallization [1]. The evaporation temperature of the organics present in the precursor solution depends on the type of the solvent used [2], and have significant influence on the final thickness [3] and the grain size [4] of the thin film. In this part, three different solvents (Ethanol, Ethilhexanol and Propanediol) are used in the precursor solutions to fabricate PMNT layers with the best possible properties.

4.2.1 PMNT single phase thin film preparation

The PMNT precursor solutions were diluted to 0.3 M using solvents with different volatilization temperatures: Ethanol (C_2H_6O), ~78^oC; Ethilhexanol ($C_8H_{18}O$), ~185^oC and Propanediol ($C_3H_8O_2$) ~214 ^oC. After deposition and drying at 350^oC/60s, crystallization is carried out for all of them by RTP at 650^oC in oxygen, with a heating rate of 200^oC/s.

4.2.2 Characterization of the crystalline structure and residual stress

Figure 4.2.1 shows the X-Ray Diffraction (XRD) patterns, with Bragg-Brentano geometry (θ-2θ), of the PMNT thin films. No crystalline secondary phases are observed in the patterns for any of them. The comparison of the X-ray patterns of the PMNT films with those from the $0.65Pb(Mg_{1/3}Nb_{2/3})TiO_3$-$0.35PbTiO_3$ perovskite with random orientation reveals no crystallographic preferential orientation. All the diffraction peaks can be identified as coming from the $Pb(Mg_{1/3}Nb_{2/3})TiO_3$-$PbTiO_3$ perovskite (JCPDSICDD 27-1199), the Pt bottom electrode and the intermetallic $PbPt_x$ formed at the interface between the PMNT films and the substrate

Table 4.2.1 shows the curvature radii of the substrate (R_s) and the film (R_f) and the calculated residual stress, σ, for the three films. The thickness of the films is obtained from Scanning Electron Microscopy images of cross-sections of the films. The

three PMNT films obtained are under compressive stress without any significant difference in the values of σ. We can conclude that the variation of the solvent used in the precursor solution does not have any effect on the phenomena that occurs on cooling from the crystallization temperature to room temperature.

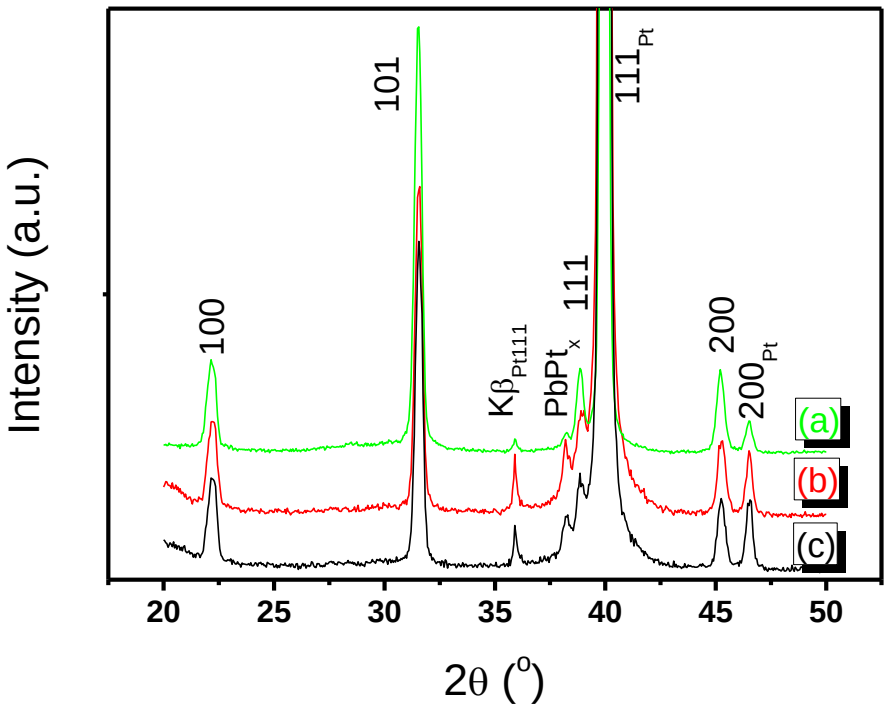

Figure 4.2.1. *XRD patterns of the PMNT films obtained from solutions diluted in (a) Ethanol, (b) Ethilhexanol and (c) Propanediol (Pt: platinum, $PbPt_x$: intermetallic interface)*

Film	R_s (m)	R_f (m)	t_f (nm)	σ (MPa)
PMNT-Ethanol	8.46	26.26	300	-206
PMNT-Ethilhexanol	11.72	38.36	230	-199
PMNT-Propanediol	10.04	27.82	246	-202

Table 4.2.1. *Residual stress of the PMNT films calculated from the curvature radii of the substrate before film deposition (R_s) and of the film (R_f)*

4.2.3 Characterization of the films microstructure and ferroelectric domain configuration

The Scanning Electron Microscopy images (Figure 4.2.2) show that the PMNT film prepared form a solution diluted with ethanol is a dense film with small grain size (40-100 nm) when compared with the other two films obtained from solutions diluted with ethilhexanol or propanediol, showing pores inside large grains (100- 425 nm). The fact that ethanol has a very low volatilization temperature results in different crystallization conditions in this film. Without organics trapped, porosity decreases, but also grain growth is affected. When cross sections are studied, it can be seen that the PMNT films obtained from solutions diluted with ethilhexanol (230 nm thick) and propanediol (250 nm thick) develop a columnar-like growth that is not seen in the PMNT film obtained from solutions diluted with ethanol, which is also thicker (300 nm).

Figures 4.2.3-5 shows the topography (a), out-of plane (b and c) and in-plane (d and e) amplitude and phase PFM images of the PMNT films. The comparison of the surface topography images of the three films shows a much smaller grain size for the PMNT film obtained from solutions diluted with ethanol (20-100 nm) than those for the films obtained from solutions diluted with ethilhexanol or propanediol, in which clusters of grains (60-200) nm are observed.

In addition, the comparison of the PFM images of the PMNT film do not show any trace of ferroelastic 90º domains due to the small grain size. The phase PFM images indicate the presence of self polarization in all three films.

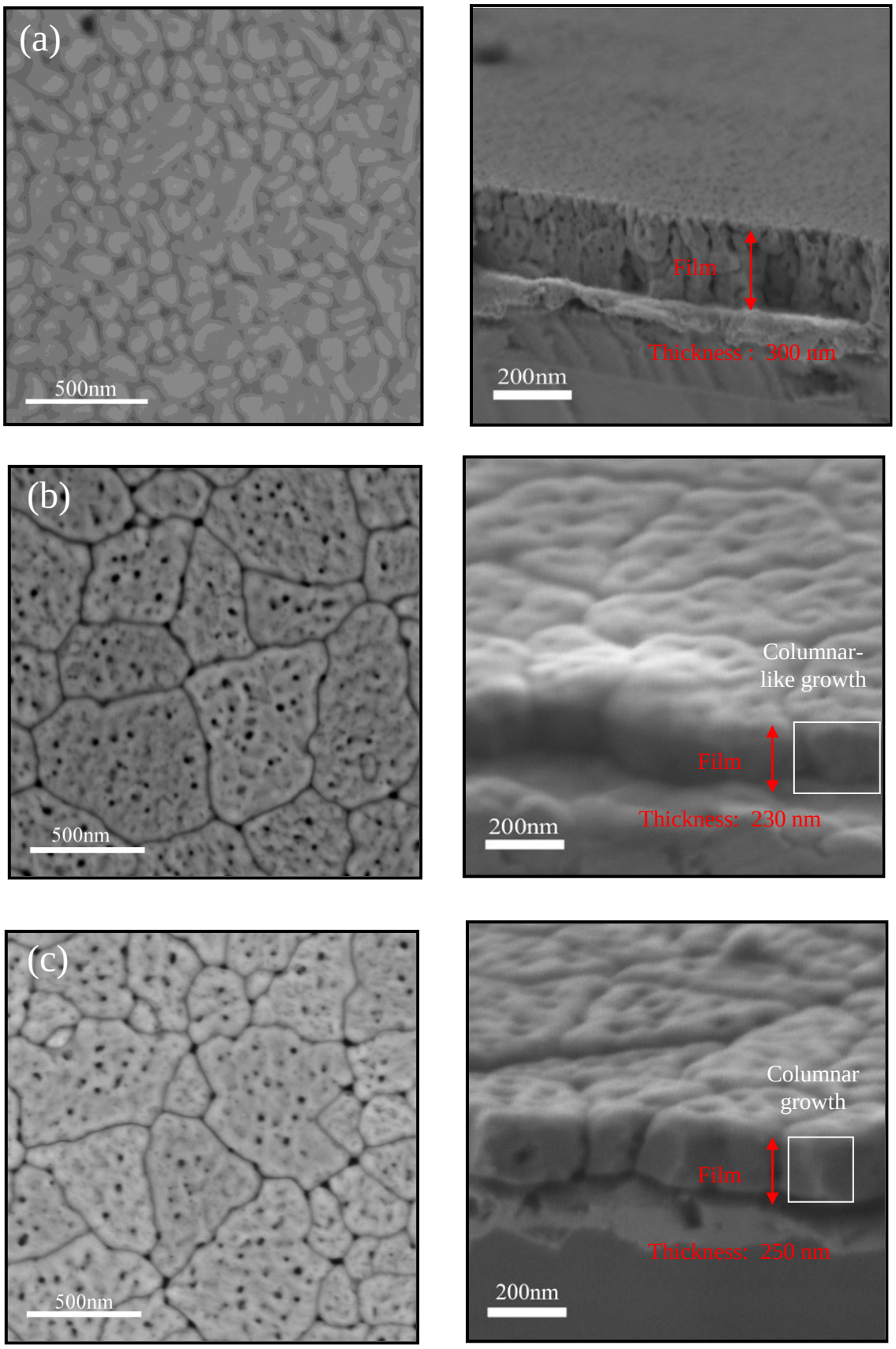

***Figure 4.2.2**. SEM micrographs of plan view and cross sections of PMNT films obtained from solutions diluted with (a) Ethanol, (b) Ethilhexanol and (c) Propanediol*

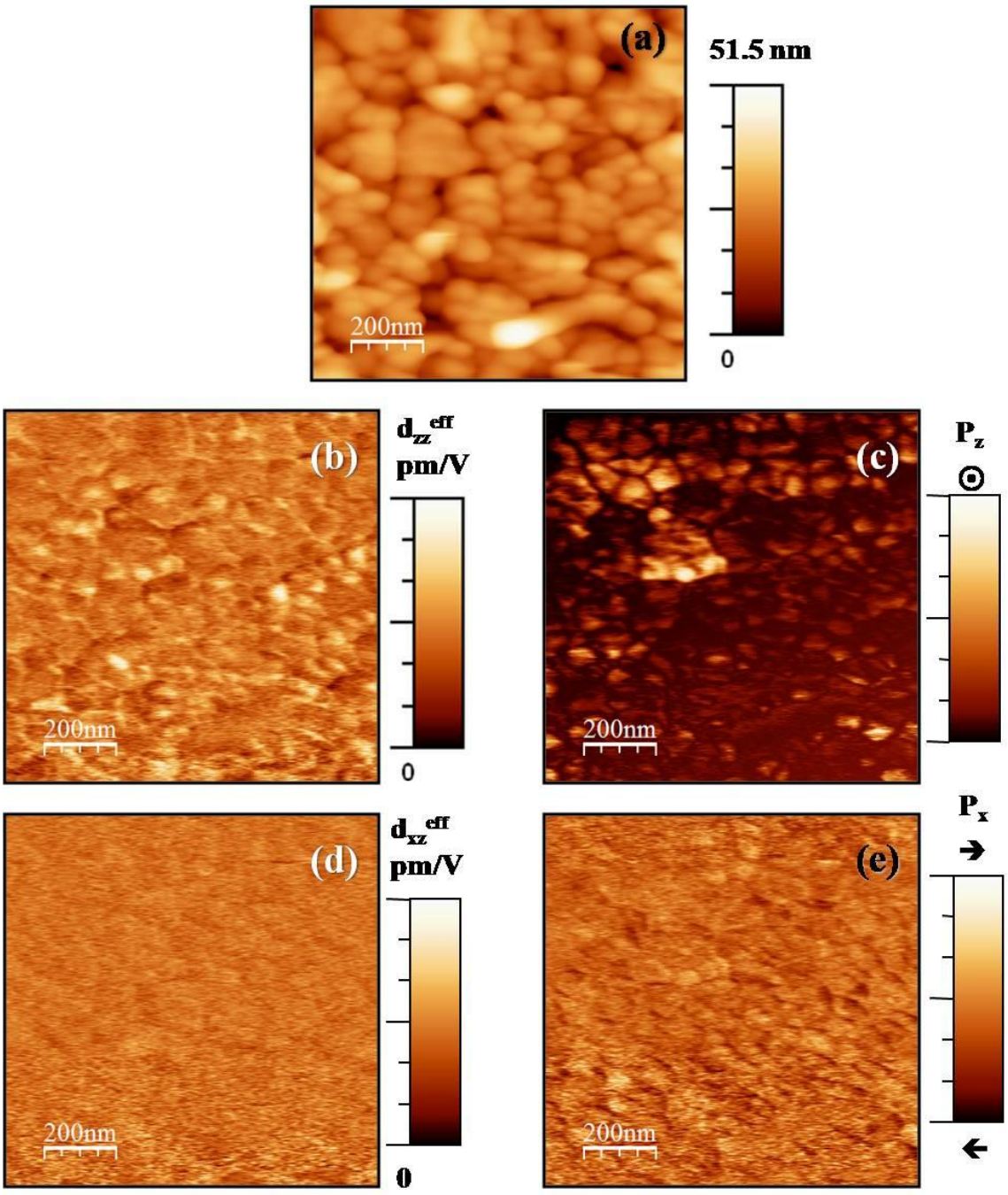

Figure 4.2.3. *(a) Topography and out-of-plane PFM (b) amplitude; (c) phase images of a PMNT film obtained from a solution diluted with ethanol*

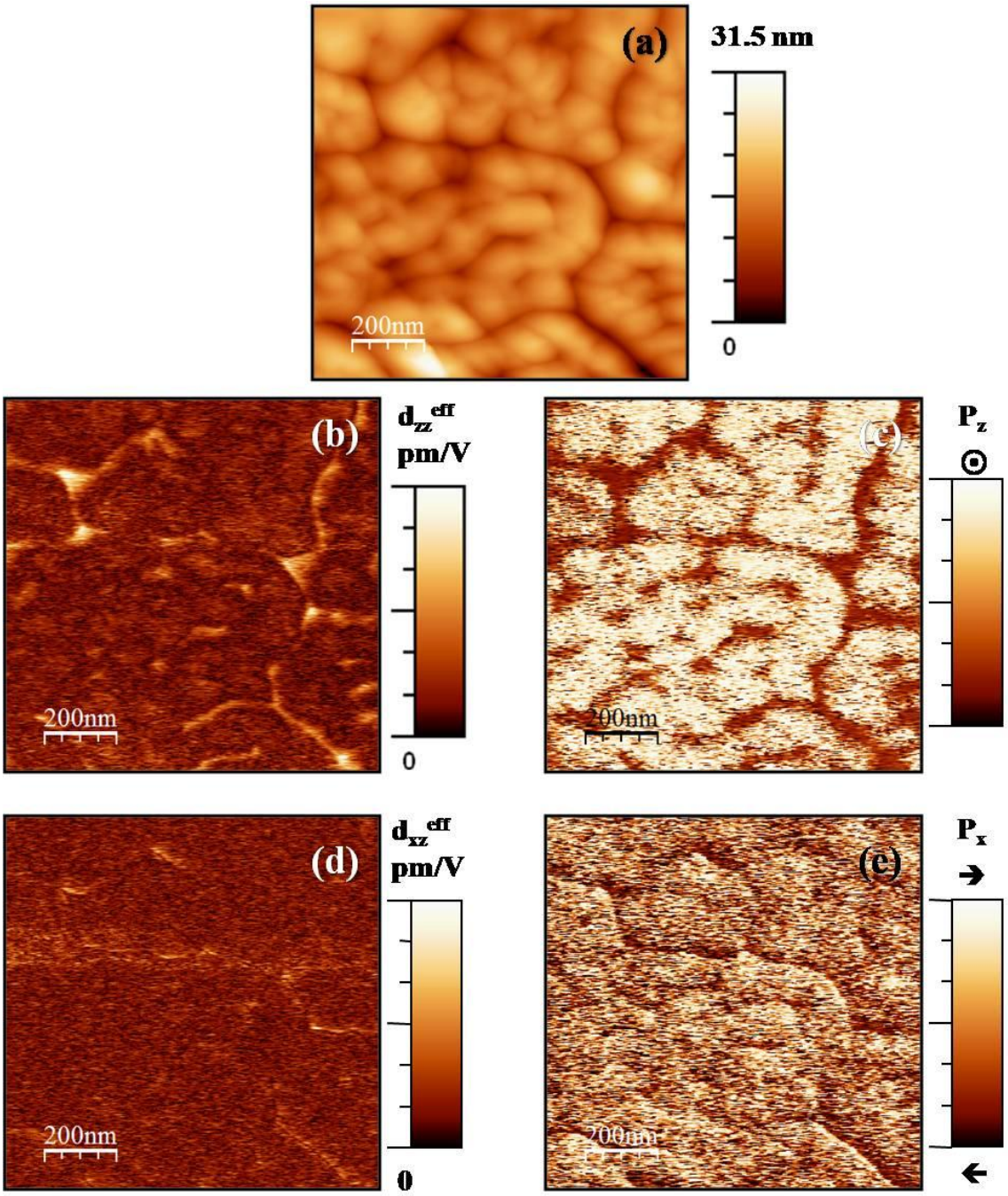

Figure 4.2.4. *(a) Topography and out-of-plane PFM (b) amplitude; (c) phase images of a PMNT film obtained from a solution diluted with ethilhexanol*

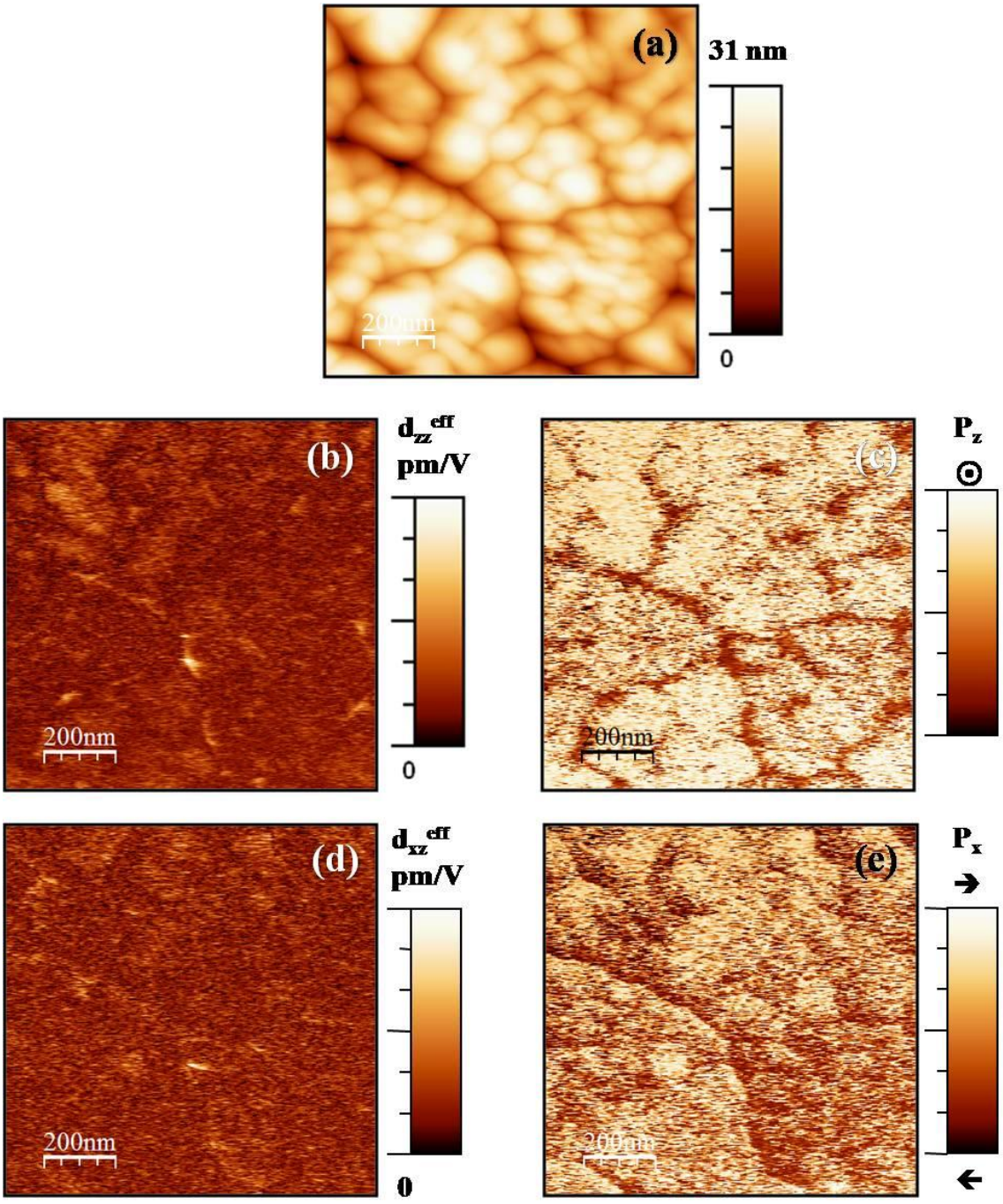

Figure 4.2.5. *(a) Topography and out-of-plane PFM (b) amplitude; (c) phase piezoresponse of a PMNT film obtained from a solution diluted with propanediol*

4.2.4 Dielectric properties of the PMNT films.

The temperature dependence of the relative permittivity and loss tangent (tanδ) for the PMNT thin films are shown in figure 4.2.6 at several frequencies. The temperatures of the maximum, T_m, for all films have lower values than those measured in similar bulk ceramics (445 K) [5]. Broadening and flattening of the dielectric anomaly associated with the ferroelectric-paraelectric phase transitions have been observed in polycrystalline films and have been associated to the small grain size and film/substrate interface effects [6,7]. Besides, the relative dielectric permittivity shows a large frequency dispersion, it decreases as frequency increases at temperatures below a broad maximum, whose position shifts towards higher temperatures with frequency, typical behavior of a relaxor-ferroelectric material [8]. This has been reported before for similar PMNT films and it has been attributed to a size effect [9]. The behavior of the PMNT films studied here is similar to that of a fine grained ceramic with similar grain size (150 nm) [10]. The relative dielectric permittivity values of the PMNT-ethanol film at room temperature and T_m are ~ 1745 and 1979 at 10 kHz, respectively, which present a larger dispersion than the PMNT-Ethilhexanol film with values of ~ 1500 and 1570 and to PMNT- Propanediol film with values of ~ 1900 and 1980. Besides, T_m for PMNT-ethanol (357-372 K) is higher than the T_m of the two other films (PMNT-ethilhexanol: 327-344; PMNT-propanediol: 334-347 K). It was observed also that there is a significant increase in the loss tangent (tanδ) above 400 K (for PMNT-Ethanol) and 450 K (for PMNT-Ethilhexanol and PMNT- Propanediol films), which is only accompanied by an increase of the permittivity for PMNT-Ethanol. This can be attributed to the different nature of the losses in this film. They are associated to grain conductivity, which may be more ionic in nature (oxygen vacancies) for PMNT-Ethanol. This means that there are more bound charges, which produces the observed increase in the relative dielectric permittivity, due to a large universal dielectric response (UDR). But the behavior of the other two films indicates that the charge carriers are free to move, so the response is coloser to a pure d.c. conductivity. Therefore, these losses can be related to currents electronic in nature along the grain boundaries of the columnar structure (see Figure 4.2.2).

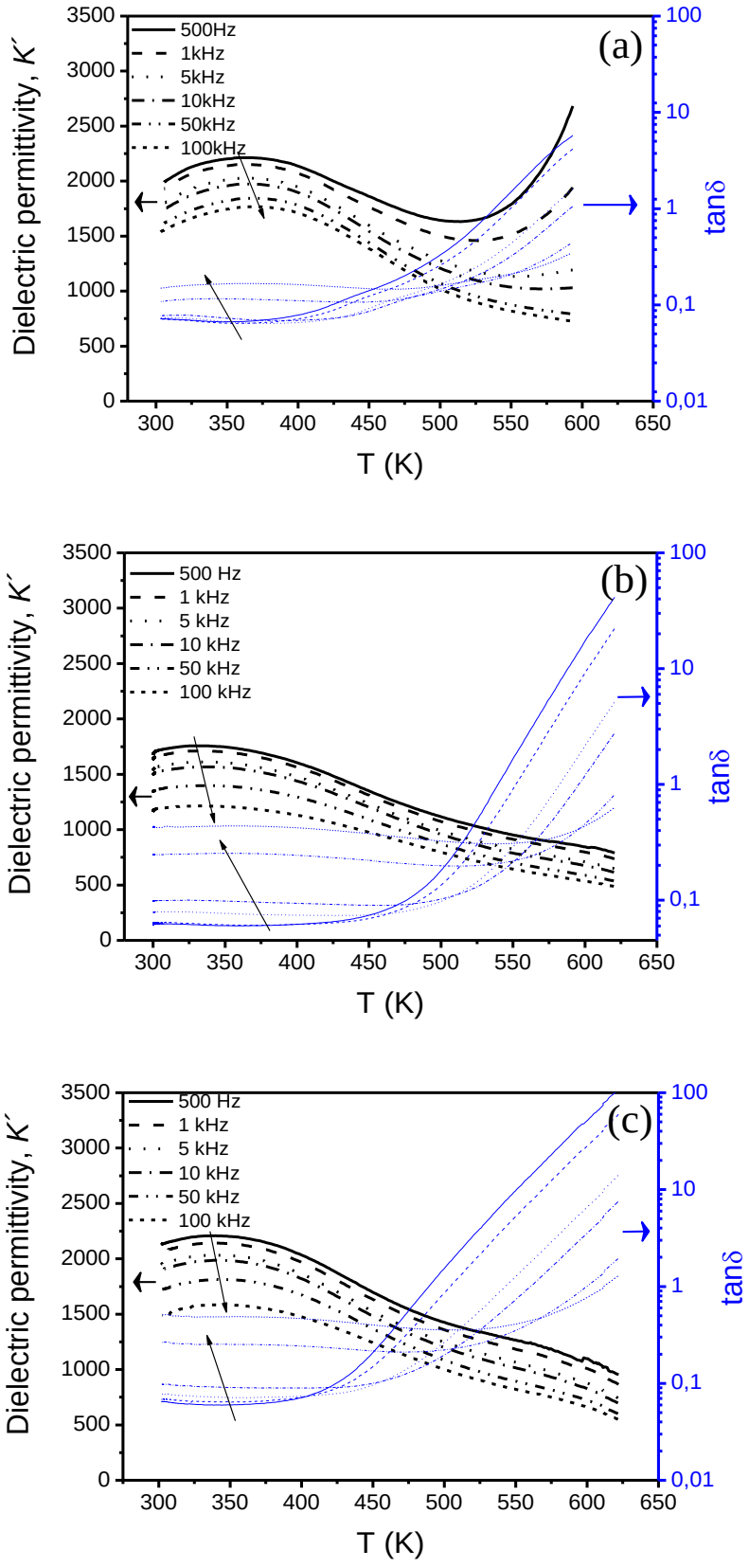

Figure 4.2.6. *Variation of the relative dielectric permittivity (K´)and loss tangent (tan δ) with the temperature, measured at various frequencies, of PMNT films obtained from solutions diluted with (a) Ethanol, (b) Ethilhexanol and (c) Propanediol*

4.2.5. Ferroelectric properties of the PMNT films

Figure 4.2.7a shows the current density loops measured at 1 kHz for the three PMNT films. It must be noted that the non-switching contributions are higher in the loop corresponding to the PMNT-propanediol film. These contributions are lower in the PMNT-ethanol film most probably due to its lower porosity and absence of columnar growth and, thus, of grain boundaries that run from top to bottom. By the integration of these current loops, the corresponding P-E hysteresis loops were obtained and corrected (Figure 4.2.7b). As expected, all the PMNT films have slanted loops with large differences between saturation and remnant polarizations. These results are associated to the relaxor character of these films. The highest saturation value is for the PMNT film obtained from a solution diluted with ethanol ($2P_s$ = 44 $\mu C \cdot cm^{-2}$), although the remnant polarization is similar to those of the PMNT film obtained from a solution diluted with propanediol ($2P_r$ = 8 $\mu C \cdot cm^{-2}$) and higher than PMNT film obtained from a solution diluted with ethilhexanol ($2P_r$ = 5 $\mu C \cdot cm^{-2}$). It seems that the application of an electric field is less efficient when columnar grains are involved.

As we have mentioned before, it is also important to study the relaxation of the polarization in short times, and this can be done in the P-E hysteresis loops obtained with a relaxation time of 1s (Figure 4.2.8). A relatively large relaxation of the polarization (50%: from 8 to 4 $\mu C \cdot cm^{-2}$) is observed in the case of PMNT film obtained from a solution diluted in propanediol, similarly to the PMNT-ethilhexanol film (40%: from 5 to 3 $\mu C \cdot cm^{-2}$). Again, the smaller grains of PMNT -ethanol film produce better results, and retain more polarization after 1 s (only 13% loss: from 8 to 7 $\mu C \cdot cm^{-2}$).

Local piezoelectric in-field loops also show slanted loops without significant remnant piezoelectric response (Figure 4.2.9). The use of different solvents in the preparation seems not to affect significantly this behavior. But, in agreement with previous results, there is a higher saturation piezoelectric response for the PMNT film obtained from a solution diluted with ethanol than that obtained from the other two films.

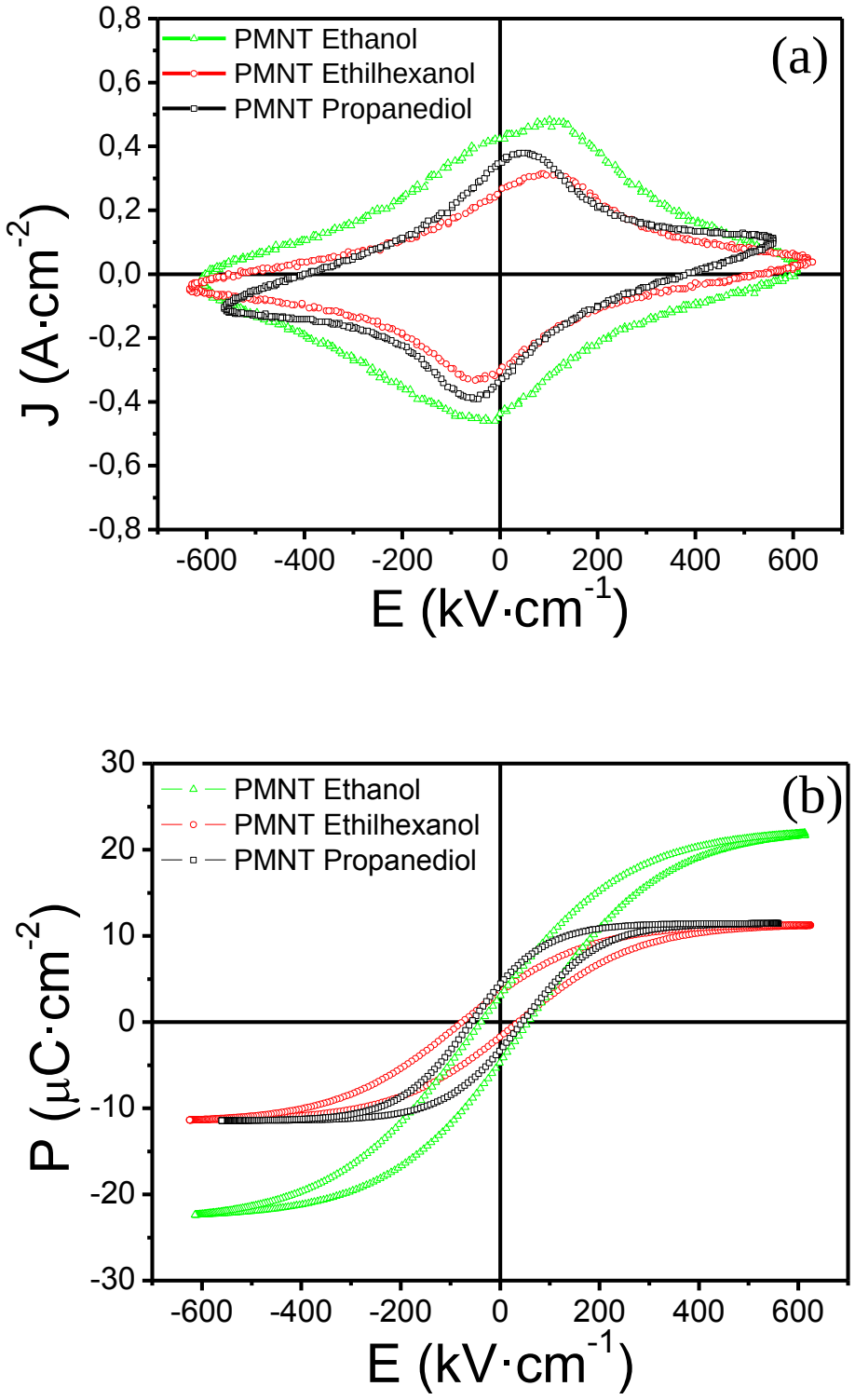

Figure 4.2.7. *(a) Experimental current loops of the PMNT films with different dilutions. (b) Corrected P-E hysteresis loops obtained for the same samples*

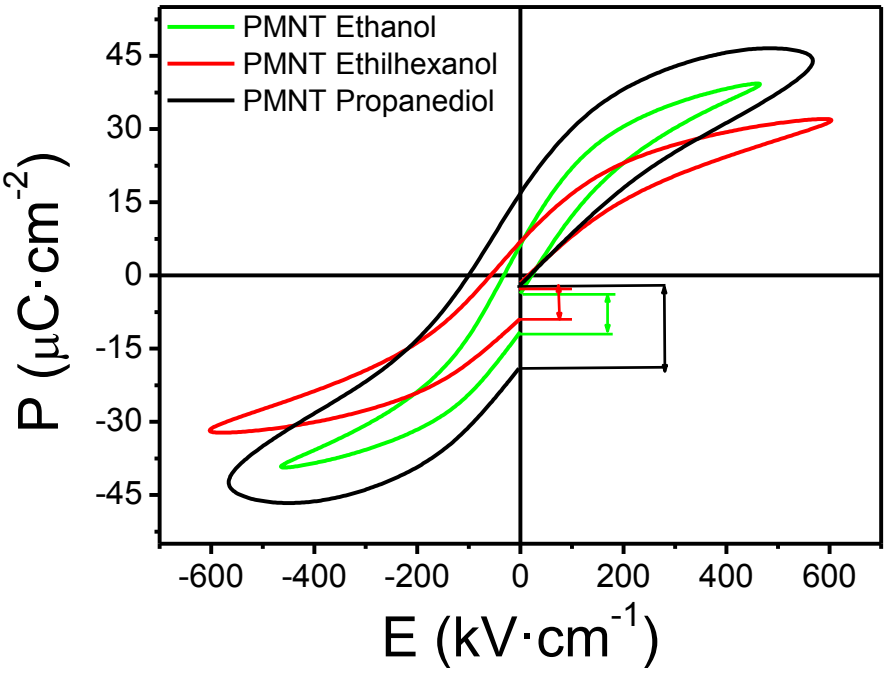

Figure 4.2.8. *Ferroelectric hysteresis loops of the PMNT films measured at 1 kHz with 1 s of relaxation*

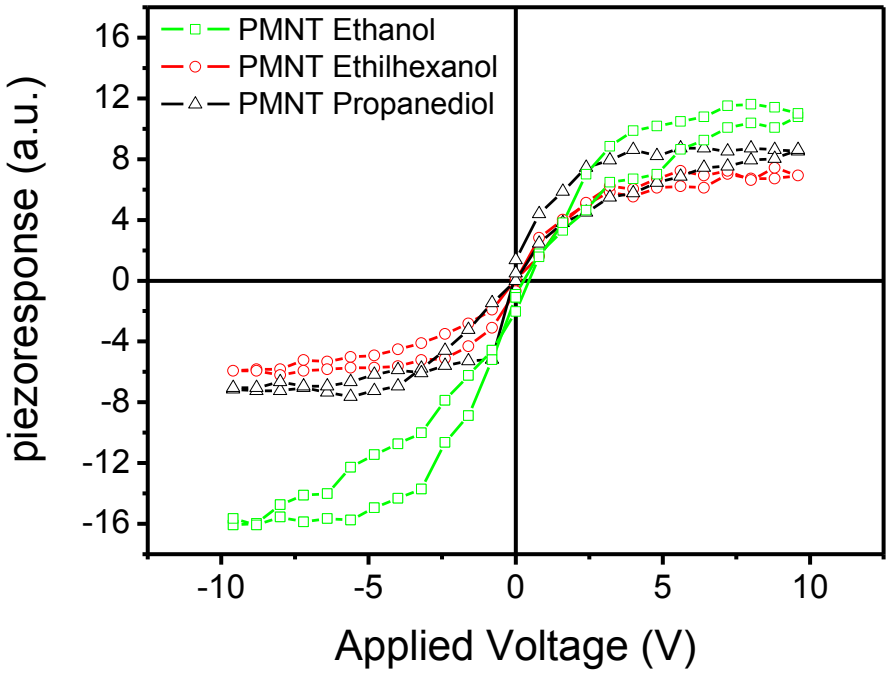

Figure.4.2.9. *Local piezoelectric hysteresis loops for the three PMNT thin films*

Finally, we study the retention of the remnant polarization for long times through the evolution with time of the pyroelectric coefficient (Figure 4.2.10). The measurement of this coefficient in as-prepared capacitors without poling gives important information about the initial polarization state of the capacitor. In this case, it indicates that all PMNT films present self-polarization that slightly decreases with time. Poling in the same direction of this self-polarization results in more stable values with time, while doing it in the opposite direction is not as effective, and pyroelectric values tend to decrease with time towards low values of the coefficient. This suggests that the factors that are the origin of the self polarization are still acting and make unstable the polarization achieved with the application of a large electric field. The existence of long lasting pyroelectric response in the as-prepared capacitors is an indication of the existence of stable ferroelectric domains in the PMNT films. This fact and the small P_r obtained in the hysteresis loops indicate that the switched polarization is not as stable as the self-polarization. This lower stability must be related to smaller size of the oriented domains that is not stable against the temperature fluctuations. All this supports the idea that it is possible to stabilize ferroelectric domains in the PMNT layers in the multilayer composites.

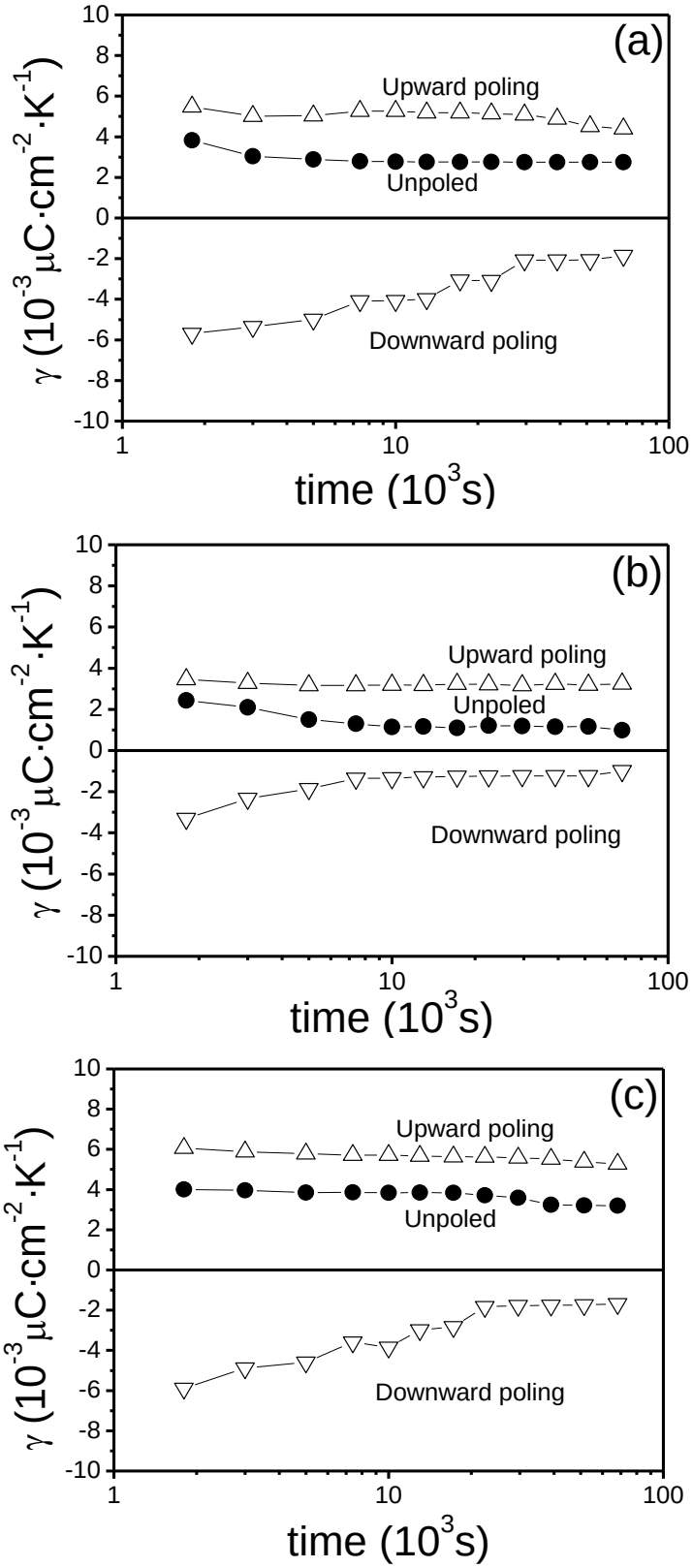

Figure 4.2.10. *Evolution with time of the pyroelectric coefficient (γ) before and after poling at 400 kV·cm*$^{-1}$*: (a) PMNT-Ethanol (b) PMNT-Ethilhexanol and (c) PMNT- Propanediol films*

4.2.6. Remarks

- The change of the solvent used for diluting the precursor solution does not influence the crystalline structure, the residual stress of the PMNT films, but it controls the porosity and the columnar growth of the grains.
- Along the grain boundaries of the columnar grains of the films obtained with solutions diluted in with ethilhexanol and propanediol, currents electronic in nature appear, which must be avoided for the effective application of large electric fields.
- The ferroelectric loops of the films prepared with ethanol (with small C chain) as a solvent present larger saturation and remnant polarization.
- Therefore, we can conclude that in order to take full advantage of the high piezoelectric coefficients of $.65Pb(Mg_{1/3}Nb_{2/3})TiO_3$-$0.35PbTiO_3$, it is necessary to use PMNT films obtained from a solution diluted with ethanol.

4.2.7. References

[1] R.W. Schwartz, T. Schneller, R. Waser, C. R. Chimie 7, 433 (2004)

[2] R. Fernández, S. Holgado, Z. Huang, M.L. Calzada, J. Ricote, J. Mater. Res. 25, 5 (2010)

[3] Y.L. Tu, M.L. Calzada, N.J. Phillips, S.J. Milne, J. Am. Ceram. Soc. 79, 441 (1996)

[4] M.L. Calzada, R. Sirera, J. Mater. Sci. 7, 39 (1996)

[5] M. Algueró, B. Jiménez, L. Pardo, Appl. Phys. Lett. 87, 082910 (2005)

[6] C.B. Parker, J.P. Maria, A.I. Kingon, Appl. Phys. Lett. 81, 340 (2002)

[7] A.M. Bratkovsky, A.P. Levanyuk, Phys. Rev. Lett. 94, 107601 (2005)

[8] L.E. Cross, Ferroelectrics 151, 305 (1994)

[9] M. Algueró, M. Stewart, M. G. Cain, P. Ramos, J. Ricote, M.L. Calzada, J. Phys. D: Appl. Phys. 43, 205401 (2010)

[10] R. Jiménez, H. Amorín, J. Ricote, J. Carreaud, J. M. Kiat, B. Dkhil, J. Holc, M. Kosec, M. Algueró, Phys. Rev. B, 78, 094103 (2008)

PART 3

Optimization of the layer combination for a $Pb(Mg_{1/3}Nb_{2/3})O_3$–$PbTiO_3$ based multilayer composite film

From the previous two parts of this chapter we conclude that for the preparation of $PbTiO_3$ layers with large and stable remnant polarization the crystallization temperature used must be below or close to the para-ferroelectric transition (490^oC). Besides, the best $0.65Pb(Mg_{1/3}Nb_{2/3})TiO_3$-$0.35PbTiO_3$ layers, with large values of the saturation polarization, are obtained from solutions diluted with ethanol. The use of these improved layers in the multilayer composite films proposed in this thesis should increase their remnant properties. In this part, we study the optimum layer combination. The volume ratio of the phases present in the composite is one factor that should be considered, and that is determinant of the dielectric and ferroelectric properties of the multilayer composites [1,2]. To analyze this, 3-layer multilayer composite films with varying thickness of the improved PT layers were prepared, searching for the best configuration for an effective induction of an internal electrical bias in the optimized PMNT layer.

4.3.1 MLC thin film preparation

Multilayer composite films (MLC) were obtained by the deposition, drying and crystallization of alternating layers of $PbTiO_3$ (PT) and $0.65(Mg_{1/3}Nb_{2/3})$ TiO_3-$0.35PbTiO_3$ (PMNT) layers. Precursor solutions were diluted to 0.1 M for PT and to 0.3 M (in ethanol) for PMNT. Crystallization is carried out in oxygen at 500^oC for the PT layers and at 650^oC for the PMNT layers. The rest of the processing conditions were not varied.

Three different MLC films were prepared. In all of them a layer of PMNT is placed between two PT layers of different thickness. Thickness of the layers is controlled by the number of successive depositions carried out. In MLC-PT1 only 1 deposited layer of PT is used, while for MLC-PT2 and 3 the thickness of the PT layer increases as 2 and 3 deposited layers are introduced. This varies the PMNT volume fraction in the multilayer (V_{PMNT}), and the total thickness of the MLC film, which can be estimated from the number of deposited layers if we assume that the thickness of each deposited layer is the same, as it is summarized in the following table:

Film	Deposited layers	V_{PMNT}
MLC-PT1	1PT/4PMNT/1PT	0.67
MLC-PT2	2PT/4PMNT/2PT	0.50
MLC-PT3	3PT/4PMNT/3PT	0.40

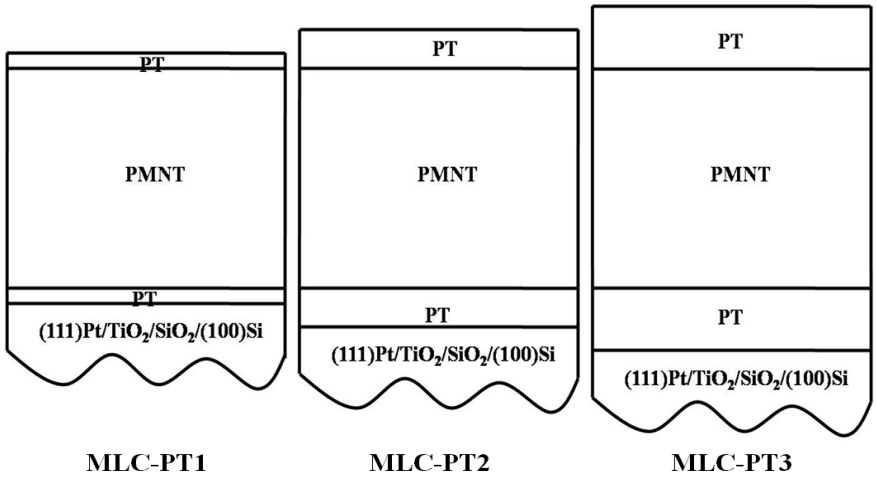

Figure 4.3.1. *Schematic diagram of the configuration of the layers for the three different MLC thin films*

4.3.2 Characterization of the crystalline phases present in the MLC films

The crystalline phases of the MLC films were studied by X- ray Diffraction, with Bragg-Brentano (XRD) geometry (Figure 4.3.2). The results indicate that no significant interdiffusion between layers is produced. As the diffraction peaks of the two phases ($PbTiO_3$ and $0.65(Mg_{1/3}Nb_{2/3})\ TiO_3$-$0.35PbTiO_3$) are usually too close, details of 100, 110 and 200 diffraction peaks are shown in the Figure 4.3.3 for all films with their corresponding deconvolution into the contributions of the two phases. This provides additional evidence of the absence of other crystalline phases other than those of the constituent layers of the composite. We can also observe diffraction peaks coming from the bottom electrode of Pt and an intermetallic $PbPt_x$ phase, commonly found in the interface between the Pb-based films and the substrate, and already reported in other MLC films in this thesis.

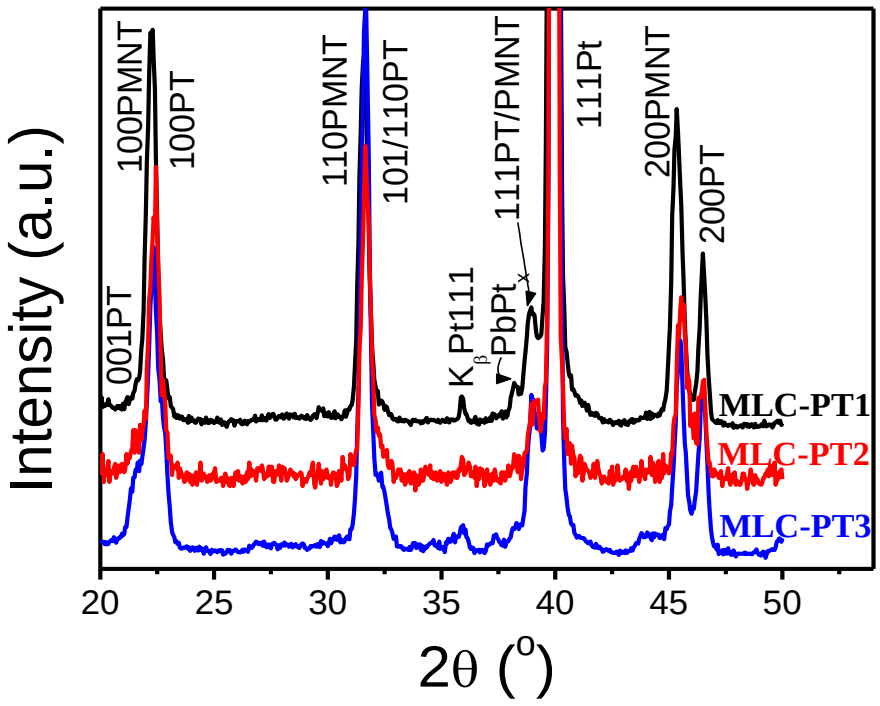

Figure 4.3.2. *XRD patterns of the MLC-PT1, MLC-PT2 and MLC-PT3 films*

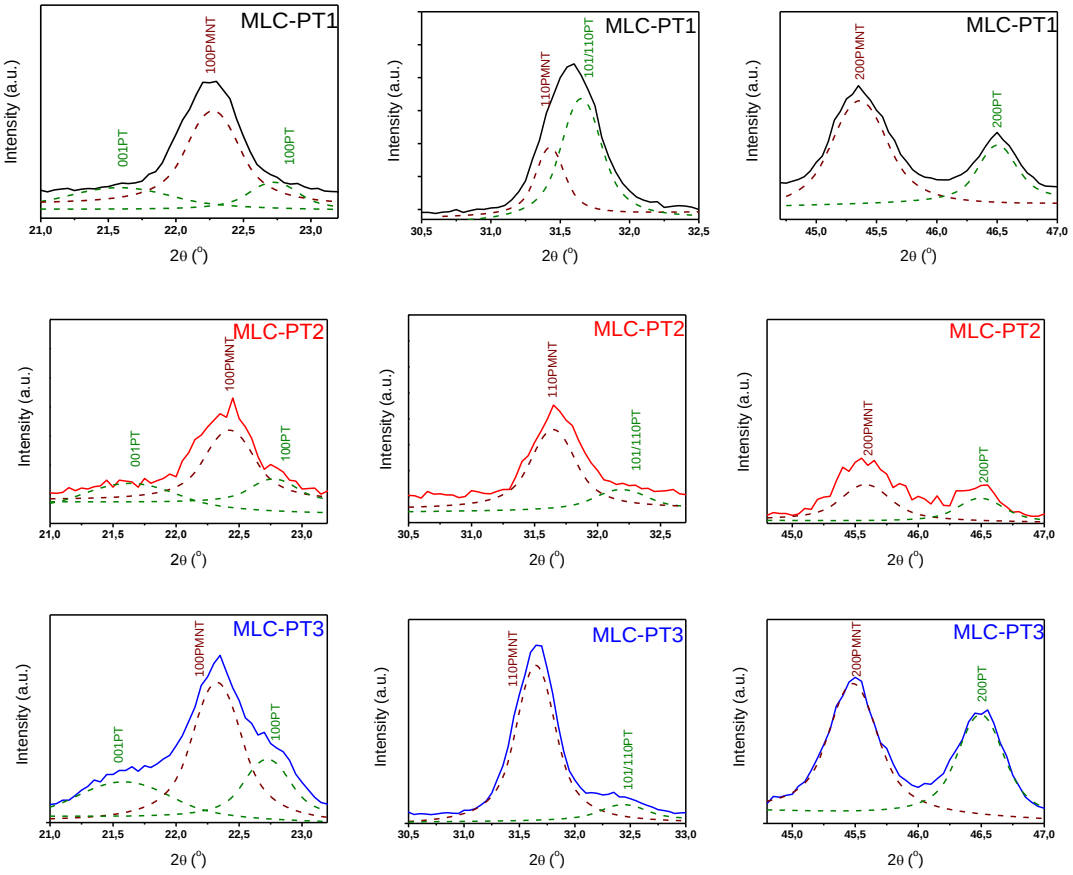

Figure 4.3.3. *Experimental diffraction data of 100, 110 and 200 peaks (solid lines) with their corresponding deconvolution (dash lines) into the contributions from the PT and PMNT layers*

4.3.3 Characterization of the films microstructure and ferroelectric domain configuration

Scanning Electron Microscopy images of the surfaces and cross sections of the MLC films are shown in Figure 4.3.4. The difference in the lateral grain size of the top PT layer is observed not to be significant for the three MLC films (160-170 nm). The variations in the thickness of the PT layer are not large enough to cause significant grain size differences, although a small increase is observed from MLC-PT1 to MLC-PT3. Observation of the cross sections reveals that the microstructure of these PT layers seems mainly formed by fine grains, while the PMNT layer is composed by columnar-like grains. The total thickness measured in the SEM cross sections of the MLC-PT1, MLC-PT2 and MLC-PT3 is 510, 782 and 970 nm, respectively. It must be noted the deteriorated state observed for this layer in MLC-PT3, with cracks and larger amount of porosity.

Figures 4.2.5-7 shows the topography, out-of-plane and in-plane PFM images of the MLC films. From the topography image we can observe in the MLC-PT1 film two different types of grain, which is a consequence of the very thin PT layer deposited in this case. The deposition of very thin layers sometimes results in an incomplete coating of the layers below [3], as in this case, and some of the larger grains of the PMNT layer are visible. The PFM amplitude images do not show any trace of ferroelectric domains inside any of the grains, which must be related to their small size. The PFM phase images show a tendency to have a large portion of the film with the out-of-plane component of the polarization oriented mostly in one direction, which indicates the presence of some self polarization in all three films.

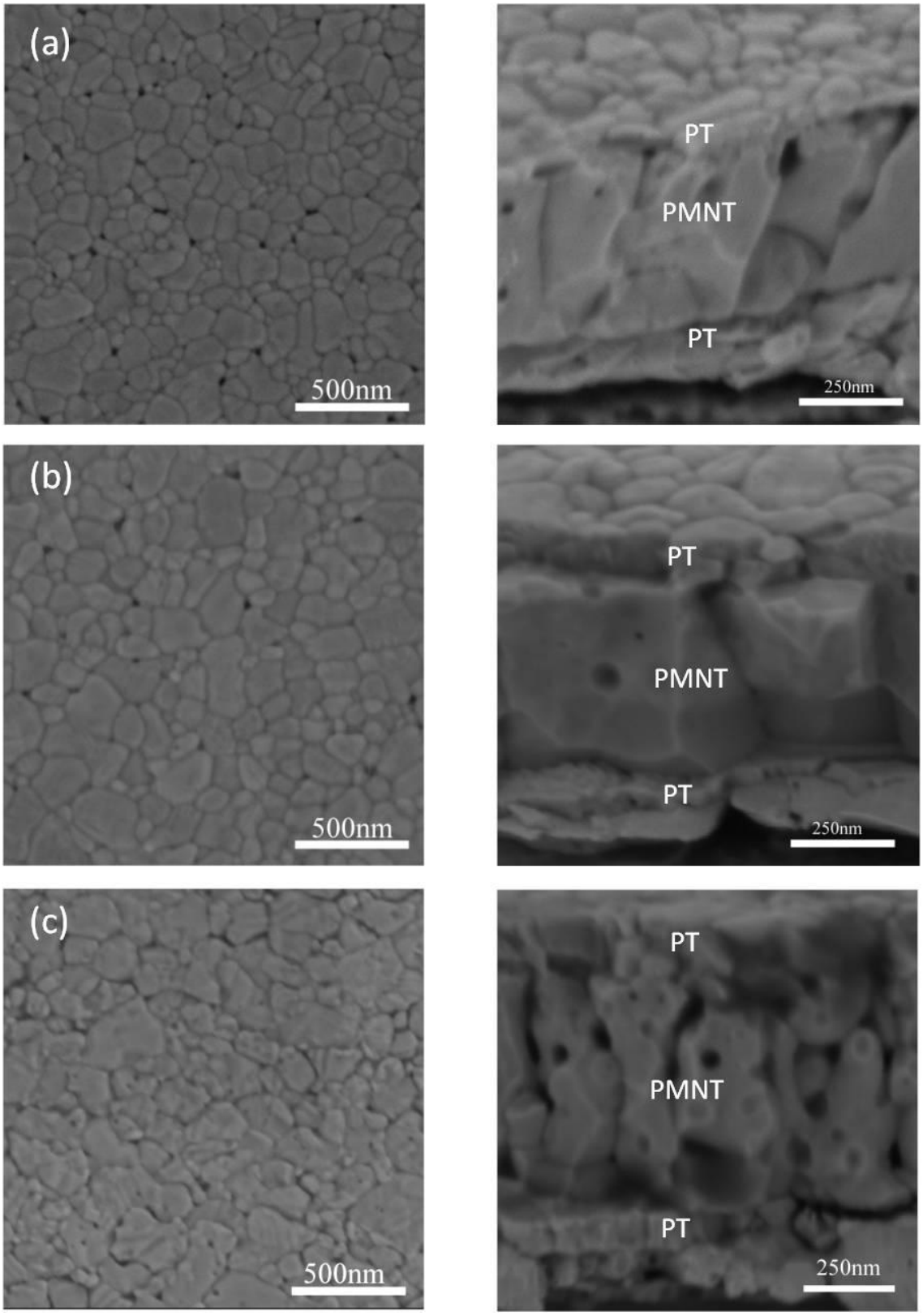

Figure 4.3.4. *Plan view and cross-section images obtained by FEG-SEM of (a) MLC-PT1, (b) MLC-PT2 and (c) MLC-PT3 films*

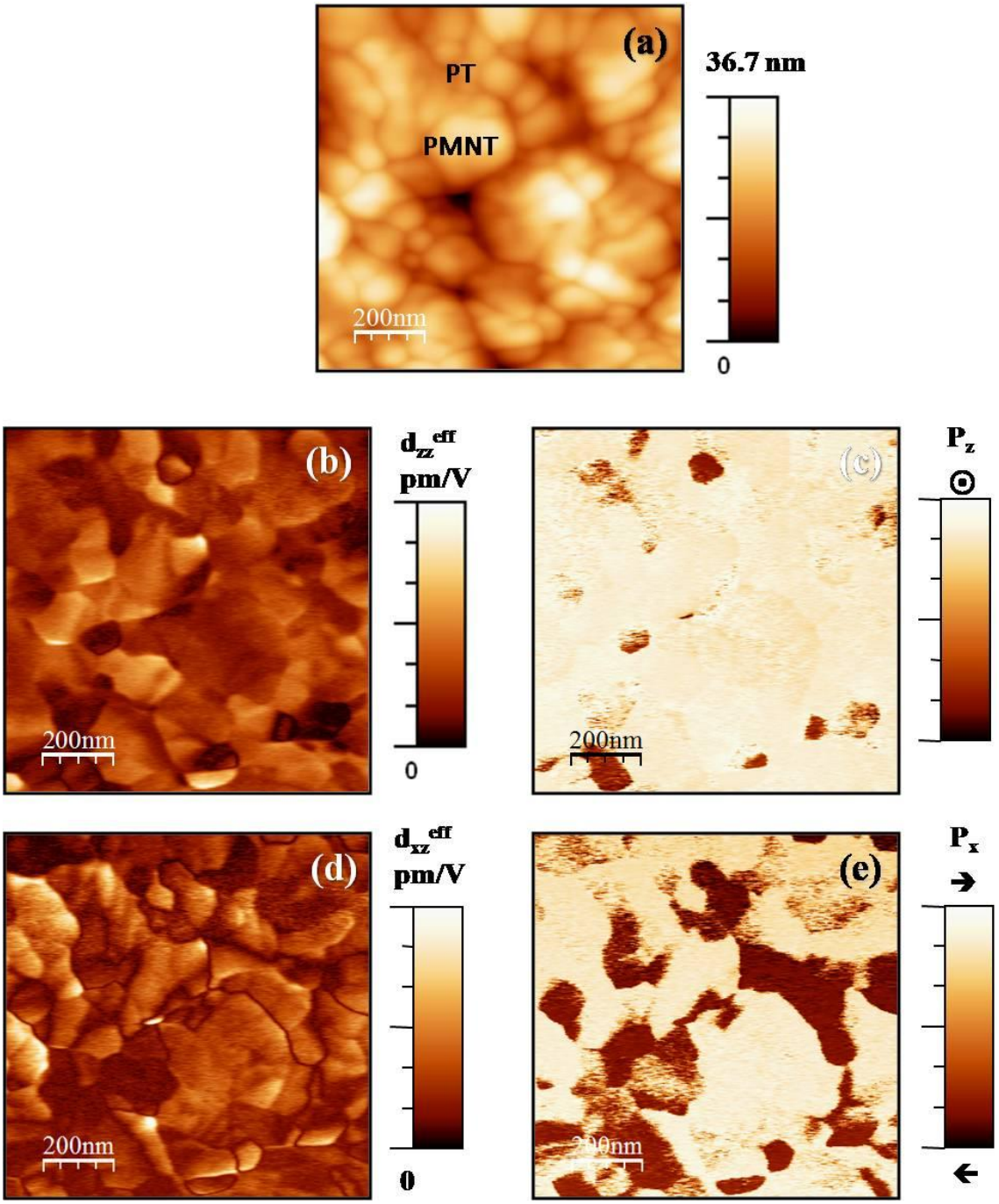

Figure 4.3.5. *(a) SFM topography ; PFM out-of-plane (b) amplitude; (c) phase; PFM in-plane (d) amplitude;(e) phase images of the MLC-PT1 film*

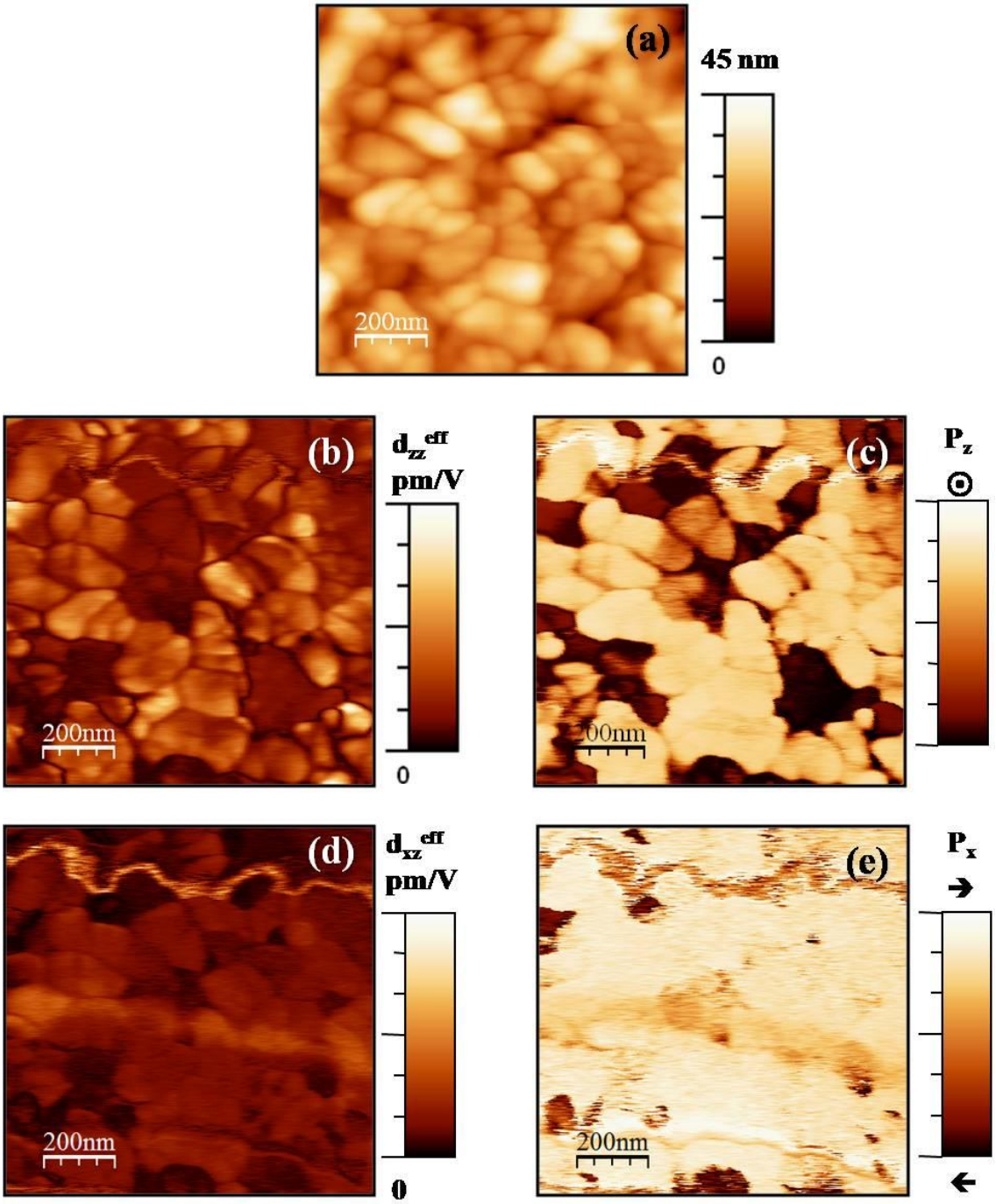

Figure 4.3.6. *(a)SFM topography; PFM out-of-plane (b) amplitude; (c) phase; PFM in-plane (d) amplitude; (e) phase images of the MLC-PT2 film*

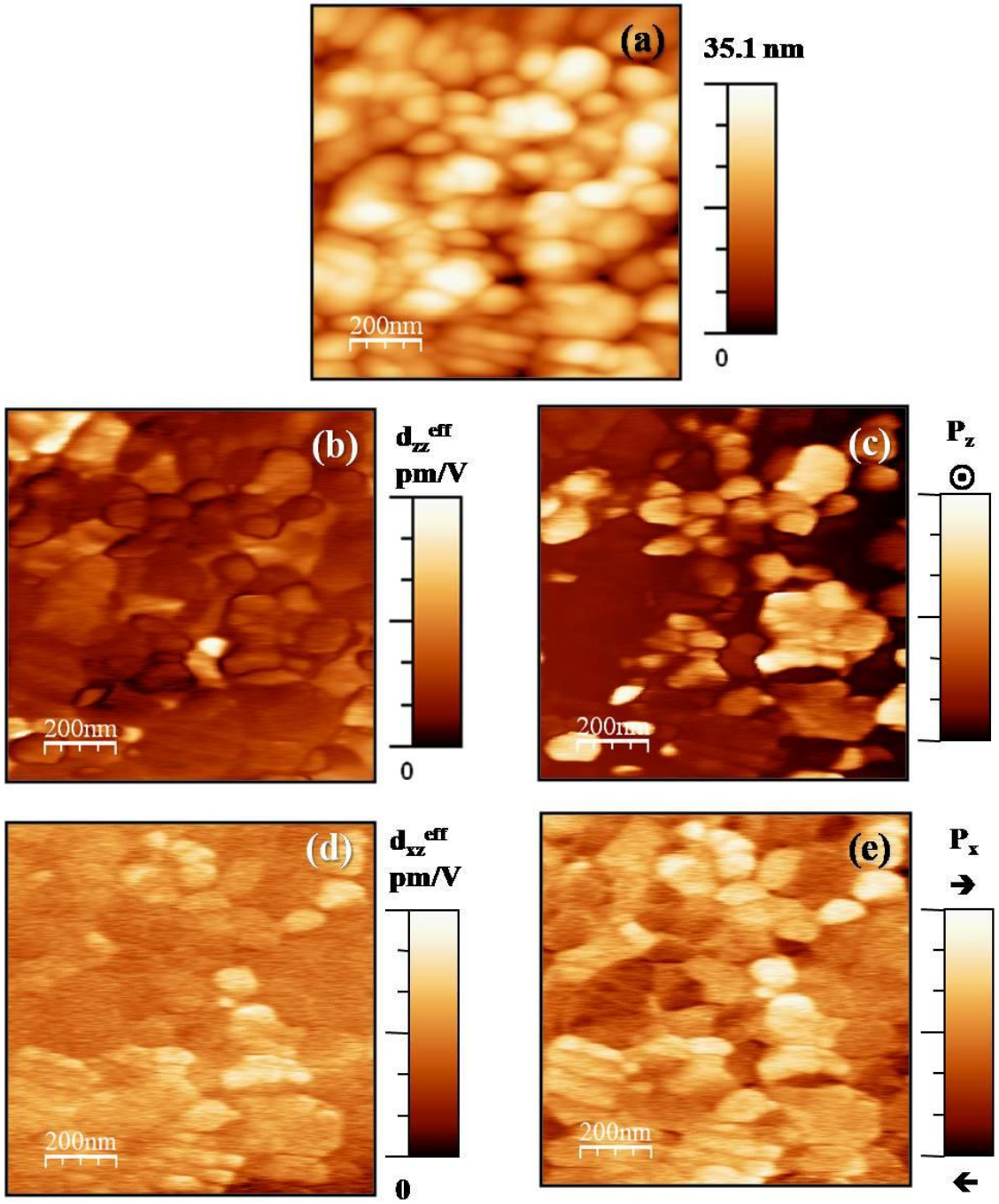

Figure 4.3.7. *(a) SFM topography; PFM out-of-plane (b) amplitude; (c) phase; PFM in-plane (d) amplitude; (e) phase images of the MLC-PT3 film*

4.3.4 Dielectric properties of the three layers MLC films.

The variation of the relative dielectric permittivity (K') with temperature was measured for the films at various frequencies. Figure 4.3.8 shows the result. We can observe the absence of the sharp drop of the relative dielectric permittivity on increasing the temperature observed in the MLC films of Chapter III. This is the consequence of the better capacitors obtained with the improved layers used for the three MLC films.

Besides, two peaks are easily identified for the three MLC thin films. One at low temperatures that can be ascribed to a phase transition corresponding to the PMNT layer and another at higher temperatures that is associated to the PT layers. This result is an evidence of the existence of separate layers, without significant interdiffusion, in agreement with the XRD results.

We can calculate the relative permittivity of the MLC films (K'_{MLC}), with a total thickness t, assuming a stack of two in-series layers of PT (t_{PT}) and PMNT (t_{PMNT}), using the Maxwell- Wagner approach:

$$\frac{t}{\kappa'_{MLC}} = \left(\frac{t_{PT}}{\kappa'_{PT}} + \frac{t_{PMNT}}{\kappa'_{PMNT}} \right) \qquad (1)$$

where K'_{PT} and K'_{PMNT} are the relative dielectric permittivities of the PT and PMNT layers, respectively. In Figure 4.3.9 both the experimental and the calculated values are compared. For the calculations we use the values obtained experimentally for the corresponding single phase films, shown in the previous two sections, and the values of the thickness measured in the SEM cross sections of Figure 4.3.3. It should be noted that only the real part of the relative permittivity is used in the model.

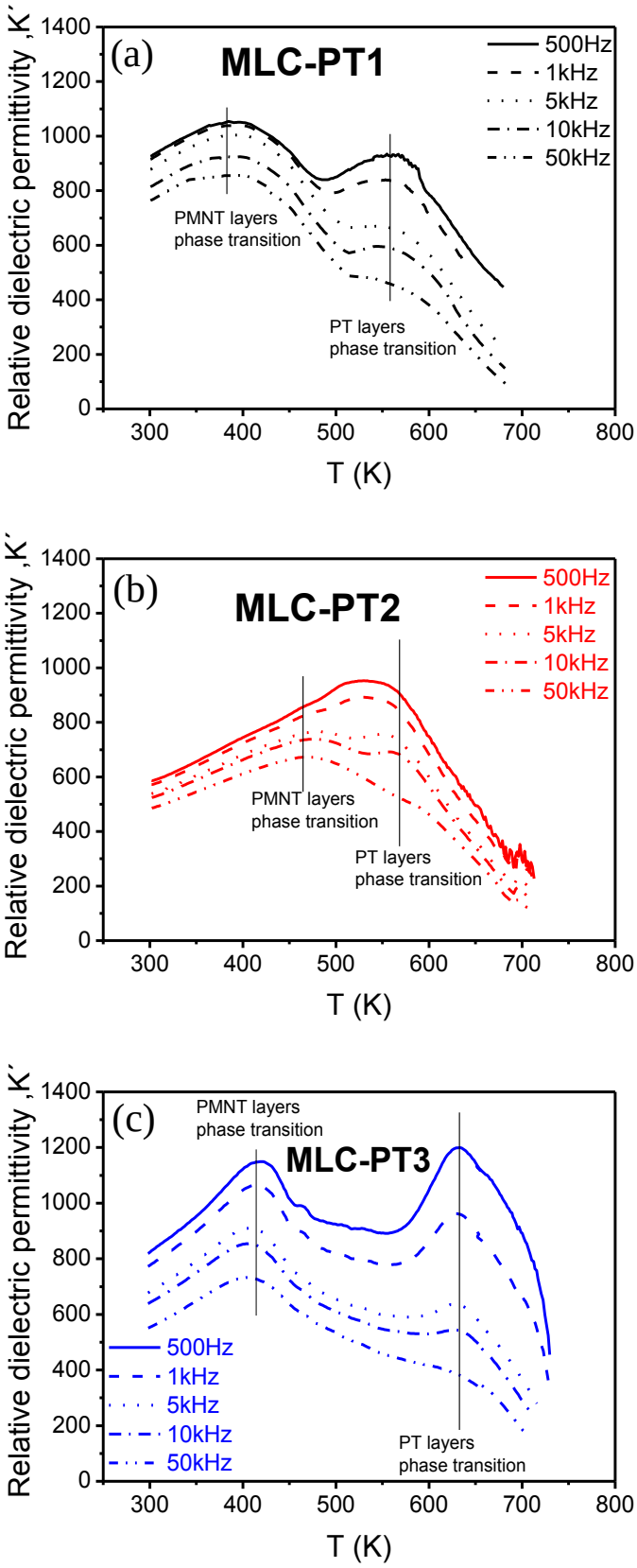

Figure 4.3.8. *Variation of the relative dielectric permittivity (K´) with temperature, measured at various frequencies, of (a) MLC-PT1, (b) MLC-PT2 and (c) MLC-PT3 films*

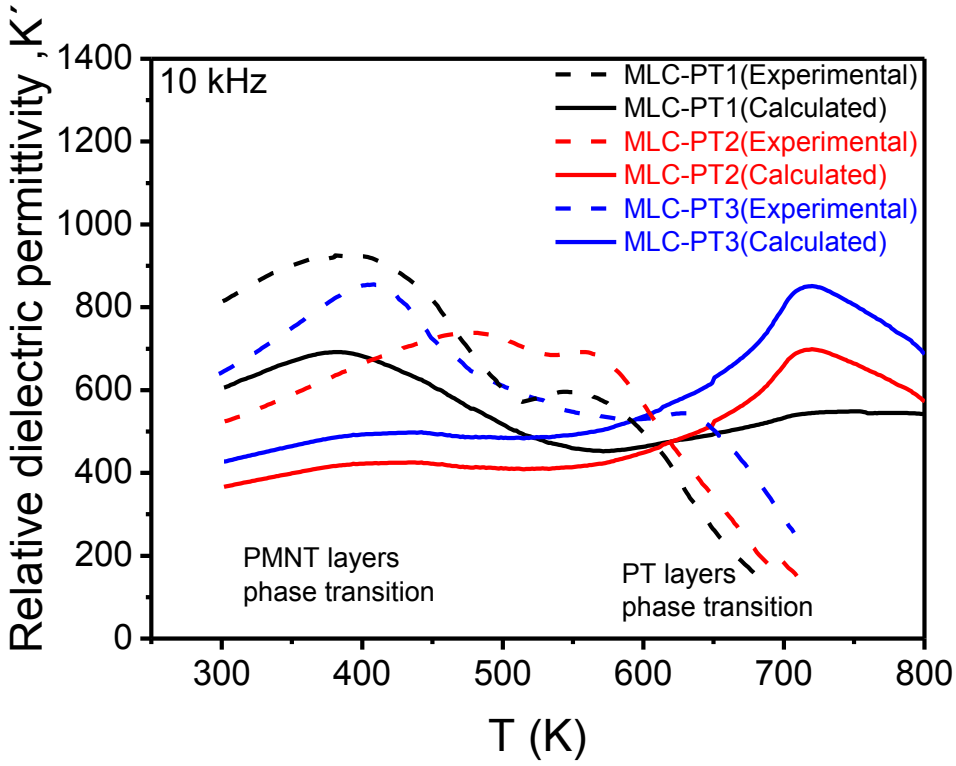

Figure 4.3.9. *Experimental and calculated curves of the relative dielectric permittivity (K') versus temperature at a frequency of 10 kHz for MLC-PT1 (black), MLC-PT2 (red) and MLC-PT3 (blue) of films*

There is no much agreement between the experimental and calculated K´ curves. The phase transitions corresponding to the PT layers are shifted to lower temperatures than those expected from the calculations, which can be attributed to the small grain size observed in these layers. An effect of the reduction of the crystal size is the decrease of the transition temperature, accompanied with a broadening of the dielectric peak [4].It can be observed that MLC-PT1, with the smallest PT grains (Figure 4.3.4a) show the lowest transition temperature for the PT layers. This temperature is higher for MLC-PT2 and 3, with increasingly larger grains.

The stress state inside the layers can also produce variations of the transition temperature [5].When the PT layers are very thin as in MLC-PT1, the stress produced in the PMNT layer is small, and therefore the transition temperature of this layer is close to the one obtained from the calculations. An increase of the thickness of the PT layers in MLC-PT2, results in larger stress on the PMNT layer, whose transition temperature increases significantly. On further increasing the PT thickness in the MLC-PT3 film, this temperature does not increase, but remains close to the calculated values for the

PMNT layer. This can be explained by a stress relaxation in this case, may be through cracks in this layer, as the ones observed in its cross section (Figure 4.3.4c).

4.3.5. Ferroelectric properties of the MLC films

Figure 4.3.10a shows the current density loops of the three MLC films measured at 1 kHz. The MLC films show conventional loops presenting well defined switching current maxima and rather low conductivity contribution in the case of MLC-PT1 and MLC-PT2 film. But there is a higher non-switching contribution (e.g. capacitance and conductivity) in the MLC-PT3 film, where a deteriorated microstructure of the PMNT layer is observed. The increase of the thickness of the PT layer produces the augment of the effective coercive field of the MLC films, as it can be observed in the corrected P-E hysteresis loops shown in Figure 4.3.10b. The hysteresis loops of the MLC films show relatively small differences between the remnant and the saturation polarization values, of around 25% for MLC-PT1 and MLC-PT3 and 34% for MLC-PT2. This is a large reduction when compared with the MLC film of Chapter 3.1 (47%) and MLC-PT5 and MLC-PT7 of Chapter 3.2 (around 55%). This improvement of the remanence of the MLC films, is also accompanied with larger polarization values: MLC-PT1 has $2P_s$= 48 $\mu C \cdot cm^{-2}$ and 2Pr = 36 $\mu C \cdot cm^{-2}$; MLC-PT2, 2Ps = 62 $\mu C \cdot cm^{-2}$ and 2Pr = 41 $\mu C \cdot cm^{-2}$; MLC-PT3, 2Ps = 71 $\mu C \cdot cm^{-2}$ and 2Pr = 53 $\mu C \cdot cm^{-2}$. These results demonstrate that the proposed mechanism of inducement of an internal electric field in the PMNT layers is more effective when we prepare MLC films with layers of improved quality.

Table 4.3.1 shows that the experimental remnant polarizations of the MLC films are higher than those calculated considering only the linear additive effect of the properties of a biphasic layer composite from the following equation (see Chapter 3.2).

$$P_r^{MLC} = (V_{PT})^{MLC} \cdot P_r^{PT} + (V_{PMNT})^{MLC} \cdot P_r^{PMNT} \qquad (2)$$

This result shows clearly that the inducement of an internal bias in the PMNT layer is more effective for these optimized multilayer films than for MLC-PT5 or 7 of Chapter 3.2, where the experimental polarization values were even below the calculated ones

.

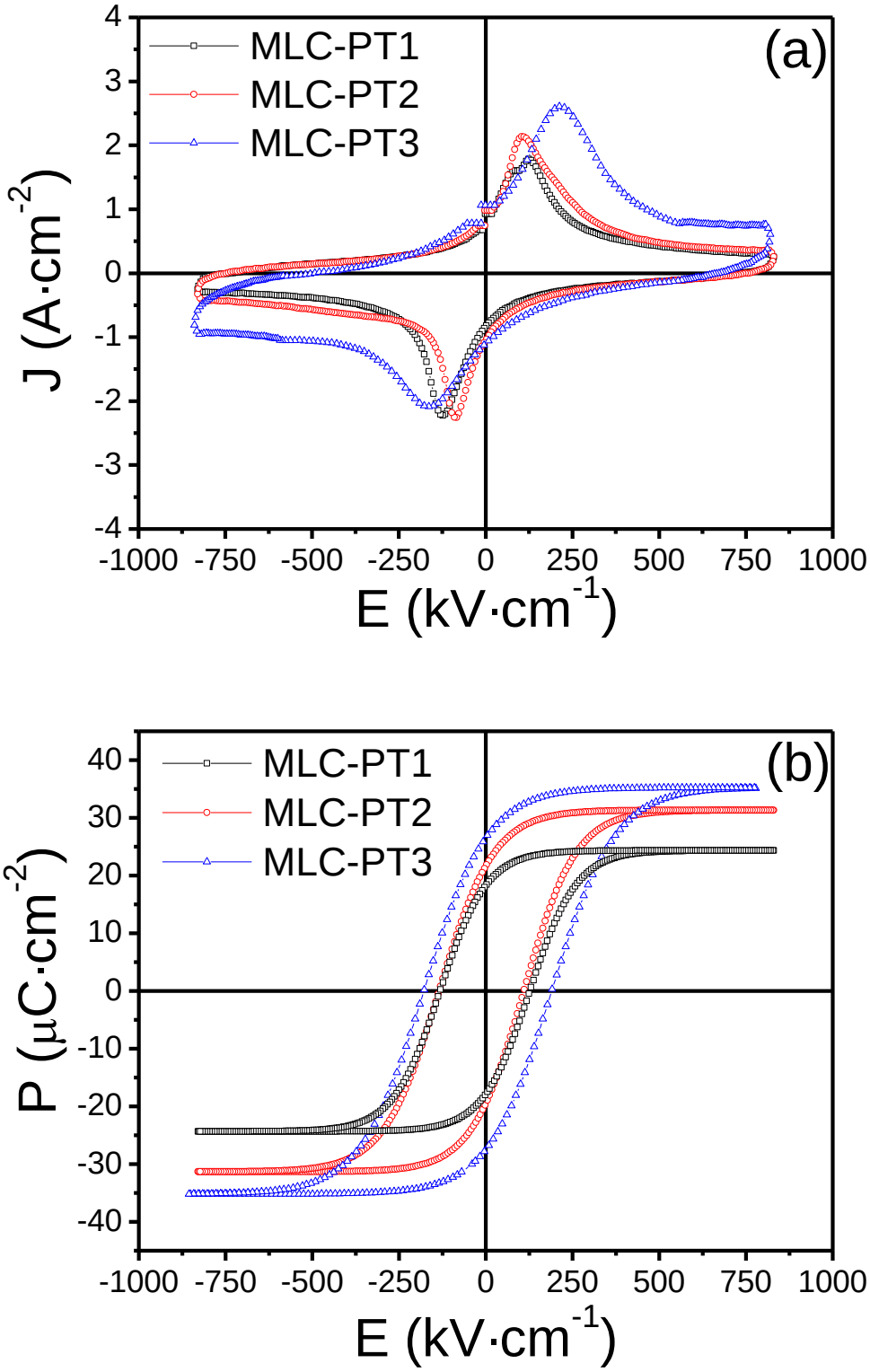

Figure 4.3.10. *(a) Experimental current loops of the MLC-PT1, MLC-PT2 and MLC-PT3 thin films. (b) Corrected P-E hysteresis loops obtained for the same films*

	V_{PT}	Ref. PMNT $2P_r$ ($\mu C\ cm^{-2}$)	Ref. PT $2P_r$ ($\mu C\ cm^{-2}$)	Calculated $2P_r$ ($\mu C\ cm^{-2}$)	Experimental $2P_r$ ($\mu C\ cm^{-2}$)
MLC-PT1	0.33	12	54	25	36
MLC-PT2	0.50	12	54	33	41
MLC-PT3	0.60	12	54	37	53

Table 4.3.1. *Comparison between calculated remnant polarization and experimental values for MLC films, together with the reference values of the single phase PMNT and PT used in the calculations*

When the volume fraction of PT increases, it can be observed that the remnant polarization increases. This is only a consequence of the additive effect and the large P_r of $PbTiO_3$: we can see almost the same rate of enhancement of the polarization for the calculated (additive composite effect only) and the experimental values. For example the ratio $(2P_r)^{MLC\text{-}PT3}/(2P_r)^{MLC\text{-}PT1}$ is 1.48 for the calculated values and 1.47 for the experimental. There is not an "extra" increase due to a more effective inducement of an electric bias in the PMNT layers. Therefore, the introduction of thicker PT layers in the MLC films does not seem to induce more remnant polarization in the PMNT layer.

In order to analyze the retention with time of the polarization values in short times, Figure 4.3.11 shows the P-E hysteresis loops measured at 1 kHz with a delay time of 1s between the conditioning and measuring voltage. This delay time allows the relaxation of the polarization after the conditioning wave which is 78% loss for MLC-PT1 film (from 18 to 4 $\mu C \cdot cm^{-2}$). It can be deduced that in the case of MLC-PT1 film, the relaxation of polarization is still dominated by the PMNT layer, so the relaxation is large. The increase of thickness of the PT layers reduces significantly this loss of the polarization at short times: 36 % for MLC-PT2 (from 31 to 20 $\mu C \cdot cm^{-2}$), and 46% loss for MLC-PT3 (from 41 to 22 $\mu C \cdot cm^{-2}$). The relaxation of the polarization is usually associated with the influence of the non-switching contributions (e.g. capacitance and conductivity), in addition to the switched back domains. The presence of some amount of leakage contribution for the MLC-PT2 and PT3 films implies that the relaxation of

the switched polarization is better than calculated from the centered loops of figure 4.3.11. If the relaxed polarization is compared with the P_r obtained from the corrected hysteresis loops (Figure 4.3.10 b) the loss of polarization is much lower 13% and 18% for the MLC-PT2 and MLC-PT3, respectively. This supports the good retention of the polarization in the MLC films, especially in the MLC-PT2 and MLC-PT3 films. This result is significant because it may be related to the existence of a threshold value below which the thickness of the PT layers does not produce an effective effect on the retention of the remnant polarization at short times.

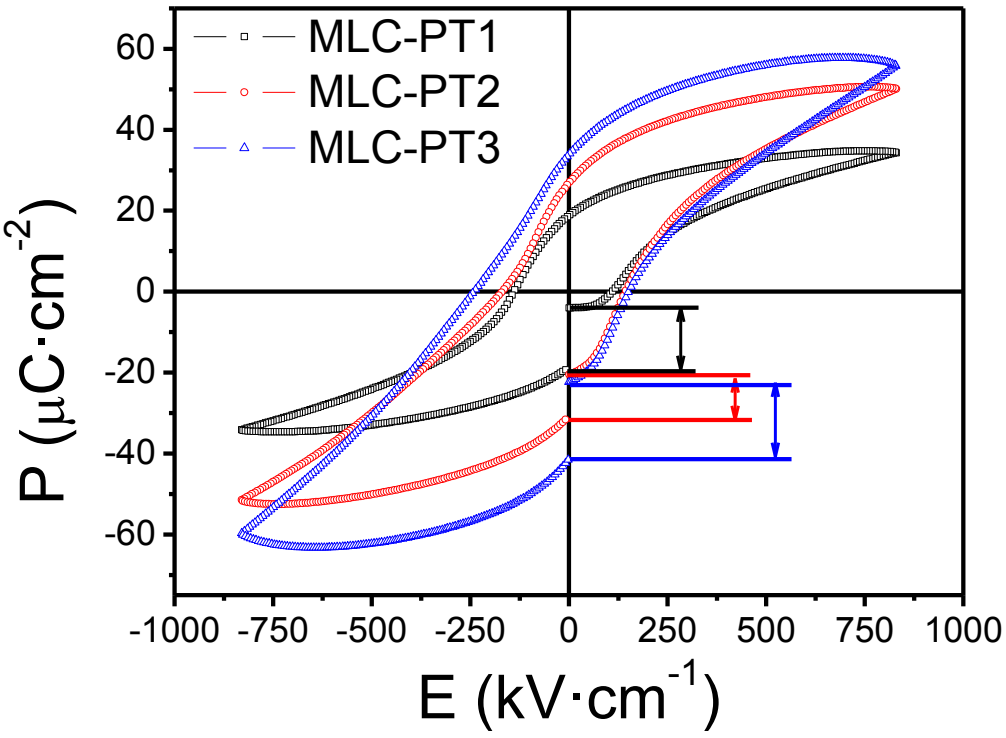

Figure 4.3.11. *Ferroelectric hysteresis loops of the MLC films measured at 1 kHz with 1 s of relaxation*

The retention of the functional properties of the MLC films for long times can be studied by measuring the evolution with time of the pyroelectric coefficient (Figure 4.3.12). As the pyroelectric coefficient in as-prepared capacitors without poling gives information about the initial polarization state, we can observe that all of them show self-polarization, similarly to that observed in the PFM images (Figure 4.3.3-5). MLC-PT1 and MLC-PT2 have strong self polarization towards the films surface, while in the MLC-PT3 film, the self polarization is towards the substrate. It is observed that the

pyroelectric coefficient is stable with time when poling is carried out against self-polarization for the MLC-PT1 film and MLC-PT2 film, while in the case of MLC-PT3 film the results show a sharp relaxation of the pyroelectric coefficient, which after 24 h goes back to the values of the unpoled film (Figure 4.3.13c). This effect can be related to the expected larger coercive field in the MLC-PT3 thin film and therefore the increase of the leakage currents when poling, preventing the correct upward poling and causing poor retention. Therefore, we can conclude that the pyroelectric coefficients are rather high and stable with time in the MLC-PT2 film, indicating that the remnant polarization achieved in these films is retained for long times.

While the thin PT layers produce problems of retention at short times(Figure 4.3.11), an increase of thickness of these layers produces sometimes retention problems at long times due to the increase in the coercive field and, thus, the difficulty to assure full poling of the thin film.

4.3.6. Piezoelectric properties of the MLC films

The effective remnant longitudinal piezoelectric coefficient of a biphasic multilayer composite, d_{33}^{MLC} can be obtained from the piezoelectric coefficients of the constituent PT and PMNT layers (d_{33}^{PT}, d_{33}^{PMNT}) with the following equation [6]:

$$\mathrm{d}_{33}^{\mathrm{MLC}} = \frac{\mathrm{d}_{33}^{\mathrm{PT}} \cdot \varepsilon_{33}^{\mathrm{PMNT}} \cdot \mathrm{V}_{\mathrm{PT}} + \mathrm{d}_{33}^{\mathrm{PMNT}} \cdot \varepsilon_{33}^{\mathrm{PT}} \cdot \mathrm{V}_{\mathrm{PMNT}}}{\varepsilon_{33}^{\mathrm{PMNT}} \cdot \mathrm{V}_{\mathrm{PT}} + \varepsilon_{33}^{\mathrm{PT}} \cdot \mathrm{V}_{\mathrm{PMNT}}} \quad (3)$$

where V_{PT} and V_{PMNT} are the volume fractions and ε_{33}^{PT} and ε_{33}^{PMNT} are the dielectric permittivity of the PT and PMNT phases.

Taking into account the usually very low remnant properties of the single phase PMNT layers, it can be considered that:

$$\mathrm{d}_{33}^{\mathrm{PT}} \cdot \varepsilon_{33}^{\mathrm{PMNT}} \cdot \mathrm{V}_{\mathrm{PT}} \gg \mathrm{d}_{33}^{\mathrm{PMNT}} \cdot \varepsilon_{33}^{\mathrm{PT}} \cdot \mathrm{V}_{\mathrm{PMNT}} \quad (4)$$

which means that d_{33}^{MLC} is mainly a function of $\mathrm{V_{PT}}$. If this is so, the remnant piezoelectric coefficient should increase as the volume fraction of PT in the MLC films increases.

But, if a large polarization is induced in the PMNT layers of the MLC films, then the d_{33}^{MLC} value measured will have an important contribution from the PMNT layer.

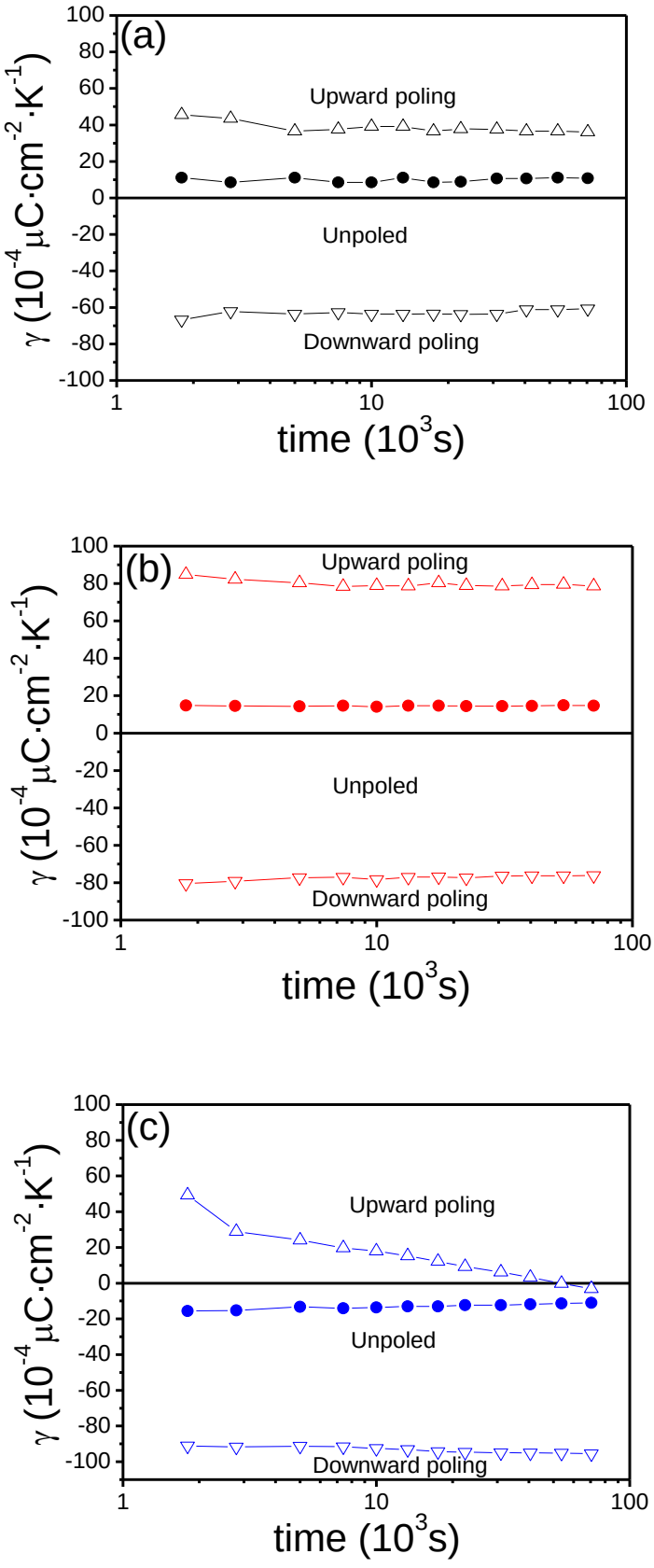

Figure 4.3.12. *Evolution with time of the pyroelectric coefficient (γ) before and after poling at 800 kV·cm^{-1}: (a) MLC-PT1; (b) MLC-PT2; (c) MLC-PT3 films*

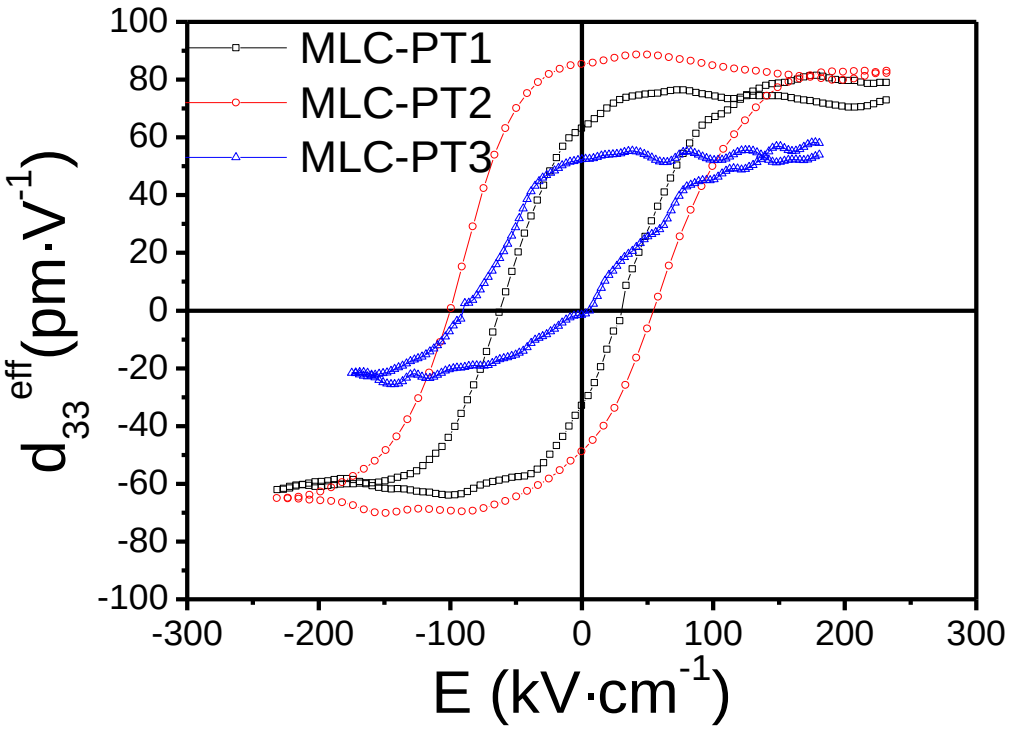

Figure.4.3.13. *Macroscopic piezoelectric responses of MLC-PT1, MLC-PT2 and MLC-PT3 thin films. Measurements were carried out with a double-beam interferometer.*

The macroscopic piezoelectric data of Fig. 4.3.13 show that for high quality MLC films, the piezoelectric response of the PMNT in MLC is improved. The measurement of saturated loops for MLC-PT1 and 2, which present remnant values that are close to the saturation values. For MLC-PT1: $(d_{33}^{eff})_r$ = 51 pm·V^{-1} and $(d_{33}^{eff})_s$ = 57 pm·V^{-1}. For MLC-PT2: $(d_{33}^{eff})_r$ = 67 pm·V^{-1} and $(d_{33}^{eff})_s$ = 74 pm·V^{-1}. Unfortunately, the values of the piezoelectric coefficients MLC-PT3 film are not reliable, because the piezoelectric loop of this film is not saturated. It has been shown that coercive fields for the MLC-PT3 film are larger than for the other MLC films. The application of large electric fields for long times, required due to the stepwise application of the DC field in this type of piezoelectric measurements, is not possible without the appearance of large leakage currents that impede the measurement.

The remnant piezoelectric coefficients obtained are much higher than the 25 pm·V^{-1} of d_{33} reported for PMNT films with similar thickness [7], whose saturation value reaches 60 pm·V^{-1}. It is remarkable that the large difference between remnant and saturation values of these films [8,9] has been brought to a minimum in the MLC films

presented here, and that the saturation values are not far of the 75 $pm \cdot V^{-1}$ reported for a highly oriented film of 800 nm thickness [10]. The piezoelectric coefficients obtained are competitive with those reported for the preferred composition in these applications, the well known piezoelectric composition (Pb,Zr)TiO_3 (PZT) at the MPB, that reaches 64 $pm \cdot V^{-1}$ for a 1.3 μm thick film [11]. The piezoelectric coefficients increase with film thickness [12], and improved piezoelectric coefficients are achieved by a careful control of microstructure and preferential orientation [13-15] or the electrodes used [16]. The control of this parameters has not been considered in this thesis, but it will be subject of future work in order to improve the piezoelectric behavior of the PMNT-based multilayer composites.

4.3.7. Remarks

- The properties of the MLC films are increased due to the improvement of the quality of the constituent layers of the multilayer composite: the optimized PT layers withstand higher electric fields without dielectric breakdown and the lower porosity of the PMNT layers produces films with larger coefficients derived from larger saturation polarization values.

- These characteristics of the optimized MLC films make more efficient the induction of polarization in the PMNT layer, and the polarization values are larger. The increased remnant polarization values result in enhanced piezoelectric functionality.

- The PT layers surrounding the PMNT cannot be too thin because the remnant polarization relaxes rapidly at short times. A very low volume content of $PbTiO_3$ produces that the behavior is dominated by the low-remnant PMNT layers.

- However, too much thick PT layers are also a problem due to the larger values of the electric voltages that are required, which may produce uncomplete poling of the PT layers, and, therefore, less effective induction of remnant polarization in the PMNT layers.

- The improved MLC films show piezoelectric coefficients that are competitive for their integration in piezoelectric microdevices.

4.3.8. References

[1] J.G. Wu, D.Q. Xiao, J.G. Zhu, J.L. Zhu, J.Z. Tan, Q.L. Zhang, Appl. Phys. Lett. 90 082902 (2007)

[2] F.C. Kartawidjaja, C.H. Sim, J. Wang, J. Appl. Phys. 102, 124102 (2007)

[3] R. Fernández, S. Holgado, Z. Huang, M.L. Calzada, J. Ricote, J. Mater. Res. 25, 890 (2010)

[4] K. Ishikawa, K. Yoshikawa, N. Okada, Phys. Rev. B. 37, 5852 (1988)

[5] G.A.C.M. Spierings, G.J.M. Dormans, W.G.J. Moors, M.J.E. Ulenaers, P.K. Larsen, J. Appl. Phys. 78, 1926 (1995)

[6] R.E. Newnham, D.P. Skinner, L.E. Cross, Mater. Res. Bull. 13, 525 (1978)

[7] M. Algueró, M. Stewart, M.G. Cain, P. Ramos, J. Ricote, M.L. Calzada, J. Phys. D: Appl. Phys. 43, 205401 (2010)

[8] J.H. Park, F. Xu, S. Trolier-Mckinstry, J. Appl. Phys. 89, 568 (2001)

[9] J.H. Park, S. Trolier-Mckinstry, J. Mater. Res. 16, 268 (2001)

[10] R. Herdier, M. Detalle, D. Jenkins, C. Soyer, D. Remiensa, Sens. Actuators A 148 122 (2008)

[11] G.S. Wang, D. Rémiens, E. Dogheche, R. Herdier, J. Am. Ceram. Soc. 89, 3417 (2006)

[12] L. Lian, N. R. Sottos, J. Appl. Phys. 87, 3941 (2000)

[13] X. Du, J. Zheng, U. Belegundu, K. Uchino, Appl. Phys. Lett. 72, 2421 (1998)

[14] D.V. Taylor, D. Damjanovic, Appl. Phys. Lett. 76, 1615 (2000)

[15] C-S. Park, S-W. Kim, G-T. Park, J-J. Choi, H-E. Kima, J. Mater. Res. 22, 1373 (2007)

[16] N. Sama, C. Soyer, D. Remiens, C. Verrue, R. Bouregba, Sens. Actuators A 158, 99 (2010)

CHAPTER V

GENERAL CONCLUSIONS

The conclusions obtained from the experimental results presented and discussed in this PhD Thesis are:

1- Ferroelectric materials with compositions that have very small remnant properties in thin film form compared to their bulk counterparts can be improved through the preparation of multilayer composite films. In the case of the present work the films of $0.65Pb(Mg_{1/3}Nb_{2/3})TiO_3$-$0.35PbTiO_3$ retain large saturation values. Therefore, the strategy followed was to keep the layers of this composition in a poled state through an internal electric field induced by poled layers of a ferroelectric with large remnant polarization.

   Based on that idea, the $Pb(Mg_{1/3}Nb_{2/3})TiO_3$-$PbTiO_3$ based multilayer composite films show a significant enhancement of the remnant polarization with respect to the single phase films. This results in enhanced remnant piezoelectric coefficients that make these multilayer composite films good candidates to be integrated in a piezoelectric microdevice.

2- The chemical solution deposition (CSD) is an effective method of fabrication of high quality multilayer composite films.

3- The preparation of films of perovskites with high tetragonality, such as $PbTiO_3$, must be done at temperatures below or closer to the transition temperature, to avoid the degradation of its functional properties. The layers crystallized at high temperatures do not allow the application of large electric fields for long times without the appearance of significant leakage currents. This makes difficult to obtain the full poling of these layers, needed for its integration in the PMNT-based multilayer composite films.

4- To obtain $0.65Pb(Mg_{1/3}Nb_{2/3})TiO_3$-$0.35PbTiO_3$ layers of high quality, with reduced porosity and large saturation polarization values, the precursor solutions must be diluted in a solvent with low volatilization temperature, as ethanol. This results in that most of the organics are evaporated during the drying step, as the temperature of crystallization used is much higher than the volatilization temperature of the solvent.

5- In order to prepare an optimized multilayer composite film, besides the improvement of the quality of the constituent layers of the multilayer composite, the volume ratio of them has influence on the properties. The layers of the phase that have large remnant polarization (such as $PbTiO_3$) must not have a very small volume content, as the remnant polarization of the composite will be dominated by the low remnant properties of the other constituent layers ($0.65Pb(Mg_{1/3}Nb_{2/3})TiO_3$-$0.35PbTiO_3$). On the other hand, the introduction of thicker layers of $PbTiO_3$ does not seem to be more effective to induce more remnant polarization in the PMNT layers. Besides, while the thin layers of $PbTiO_3$ produce problems of retention at short times, an increase of their thickness produces retention problems at long times due to the increase in the coercive electric field and, thus, the difficulty to assure full poling of these layers.

CAPÍTULO V

CONCLUSIONES GENERALES

Las conclusiones obtenidas de los resultados experimentales presentados y discutidos en esta memoria son:

1- Materiales ferroeléctricos con composiciones que tienen en forma de lámina delgada propiedades remanentes reducidas comparadas con los correspondientes materiales en volumen pueden ser mejorados a través de la preparación de un composite multicapa. En el caso del presente trabajo las láminas de $0.65Pb(Mg_{1/3}Nb_{2/3})TiO_3$-$0.35PbTiO_3$ conservan altos valores de sus coeficientes de saturación. Por tanto, la estrategia seguida ha sido mantener en un estado polarizado las capas de esta composición a través de un campo eléctrico interno inducido por las capas polarizadas de un ferroeléctrico con altos valores de polarización remanente.

   Basado en esta idea, los composites multicapa basados en $Pb(Mg_{1/3}Nb_{2/3})TiO_3$-$PbTiO_3$ presentan un incremento significativo de la polarización remanente con respecto a las láminas monofásicas. Esto da lugar al aumento de los coeficientes piezoeléctricos remanentes, lo que hace de estos composites multicapa en forma de lámina delgada buenos candidatos para ser integrados en microdispositivos piezoeléctricos.

2- El depósito de disoluciones (CSD , del inglés Chemical Solution Deposition) es un método efectivo para la fabricación de láminas delgadas composites multicapa de alta calidad.

3- La preparación de láminas de perovskitas con alta tetragonalidad, tal como $PbTiO_3$, debe ser realizado a temperaturas cercanas o por debajo de la temperatura de transición, para evitar la degradación de sus propiedades funcionales. Las capas cristalizadas a altas temperaturas no permiten la aplicación de campos eléctricos elevados durante tiempos largos sin que aparezcan corrientes eléctricas de fuga significativas. Esto dificulta la obtención de una polarización completa de estas capas, necesaria para su integración en las láminas composite multicapas basadas en PMNT.

4- Para obtener capas de alta calidad de $0.65Pb(Mg_{1/3}Nb_{2/3})TiO_3$-$0.35PbTiO_3$, con porosidad reducida y valores elevados de la polarización de saturación, las soluciones precursoras deben ser diluidas en un disolvente con temperatura de volatilización baja, como etanol. Esto da lugar a que la mayor parte de los orgánicos desaparecen durante el secado, dado que la temperatura de cristalización usada es mucho mayor que la temperatura de volatilización del disolvente.

5- Con el objetivo de preparar laminas delgadas composite multicapa optimizadas, además de la mejora de la calidad de las capas componentes del composite, el porcentaje en volumen de las fases influye en las propiedades. Las capas de la fase que tiene polarización remanente alta (como $PbTiO_3$) debe no tener un contenido en volumen muy bajo, dado que la polarización remanente del composite estará dominado por las propiedades remanentes bajas de las capas de la otra fase componente del composite ($0.65Pb(Mg_{1/3}Nb_{2/3})TiO_3$-$0.35PbTiO_3$). Por otro lado, la introducción de capas de mayor espesor de $PbTiO_3$ no parece ser más eficiente en la inducción de más polarización remanente in las capas de PMNT. Además, mientrás que las capas delgadas de $PbTiO_3$ dan lugar a problemas de retención para tiempos cortos, un aumento de su espesor produce problemas de retención para tiempos largos, debido al aumento del campo eléctrico coercitivo y, por tanto, a la dificultad de asegurar un polarizado completo de estas capas.

PUBLICATIONS DERIVED FROM THIS THESIS

Papers

H. El Hosiny Ali, R. Jiménez, J. Ricote, M. Algueró, M.L. Calzada. "Improvement of the remnant polarization of 0.65 $Pb(Mg_{1/3}Nb_{2/3})O_3$ –0.35$PbTiO_3$ thin films in a multilayer composite"

Thin Solid Films 519, 6467-6471 (2011)

H. El Hosiny Ali, R. Jiménez, J. Ricote, J. Pérez de la Cruz, J.R.A. Fernandes, M.L. Calzad. "Properties of multilayer composite thin films based on morphotropic phase boundary $Pb(Mg_{1/3}Nb_{2/3})O_3$ –$PbTiO_3$"

Thin Solid Films 520, 7205-7211 (2012)

Presentations in conferences

H. El Hosiny, J. Ricote, M. Algueró ,M.L. Calzada, R. Jiménez. "Enhanced remnant polarization in 0.65$Pb(Mg_{1/3}Nb_{2/3})O_3$-0.35$PbTiO_3$/ $PbTiO_3$ multilayer thin films"

IX Reunión Nacional de Electrocerámica, Leganés, 28-30 Junio 2009

H. El Hosiny, R. Jiménez, J. Ricote, M. Algueró, M.L. Calzada. "Enhanced functional properties in 0.65$Pb(Mg_{1/3}Nb_{2/3})O_3$-0.35$PbTiO_3$/ $PbTiO_3$ multilayer composite films"

Electroceramics XII, Trondheim, Norway, 13-16 June 2010

H. El Hosiny ali, R. Jiménez, J. Ricote, J.Pérez de la Cruz, J.R.A. Fernandes, M.L. Calzada. "Ferroelectric and piezoelectric properties of multilayer composite thin films based on MPB $Pb(Mg_{1/3}Nb_{2/3})O_3$-$PbTiO_3$"

International Symposium on Integrated Functionalities ISIF2011, Cambridge, United Kingdom, 31 July-4 August 2011

H. El Hosiny Ali, R. Jiménez, M.L. Calzada, J. Ricote. "Preparation of high quality $PbTiO_3$ thin films at temperatures close to the paraelectric-ferroelectric phase transition"

ISAF-ECAPD-PFM (International Symposium on Applications of Ferroelectrics-European Conference on the Applications of Polar Dielectrics-International Symposium Piezoresponse Force Microscopy and Nanoscale Phenomena in Polar Materials), Aveiro, Portugal, 9-13 July, 2012

UNIVERSIDAD AUTÓNOMA DE MADRID
Departamento de Física Aplicada

Madrid 2013